THE CHANGES IN CALCIUM ION ACTIVITY DURING COMMUNICATION, DEVELOPMENT, AND NORMAL FUNCTION OF THE OLFACTORY SYSTEM

by

Mavis Amity Irwin

A dissertation submitted to the faculty of
The University of Utah
in partial fulfillment of the requirements for the degree of

Doctor of Philosophy

Department of Physiology

The University of Utah

May 2014

The University of Utah Graduate School

STATEMENT OF DISSERTATION APPROVAL

The dissertation of **Mavis Amity Irwin**

has been approved by the following supervisory committee members:

Mary T. Lucero	, Chair	**3/14/14** Date Approved
Dale Matthew Wachowiak	, Member	**4/4/14** Date Approved
William C. Michel	, Member	**3/14/14** Date Approved
Michael Sanguinetti	, Member	**4/4/14** Date Approved
Karen Wilcox	, Member	**4/3/14** Date Approved

and by **Dean Li**, Chair/Dean of The Department/College/School of **Physiology**

and by David B. Kieda, Dean of The Graduate School.

ABSTRACT

The G protein-coupled receptors (GPCRs) found in the olfactory system play a key role in the modulation of Ca^{2+} activities. The complex intracellular Ca^{2+} transient and long-term Ca^{2+} oscillations affect the development, survival, response, and connection of the olfactory neurons and interneurons. The olfactory system is used as a research model because of its unique regenerative capabilities within the otherwise permanent central neuron system of adulthood. Chapter 2 looked at the Ca^{2+} activity induced by PACAP primarily through the PACAP-specific GPCRs in neonatal mouse olfactory bulb granule cell layer interneurons. The PACAP dose is recognized to be essential in the evaluation of PACAP modulation of Ca^{2+} activity. Furthermore, the numbers of PACAP responsive granule cells significantly increased between postnatal day one and five suggesting PACAP-induced Ca^{2+} activity is important in neonatal development. Chapter 3 looked at the Ca^{2+} fluxes induced by ATP through ATP specific GPCRs in olfactory epithelial (OE) sustentacular cells, which then communicate with other OE cells partially through gap junctions. The research on sustentacular cells has provided additional evidence that these cells are glial cells that coordinate the functions of neurons and basal cells in addition to fellow sustentacular cells. Chapter 4 looked at the presentation of the downstream associates of the olfactory receptors (ORs) type of GPCRs found on olfactory

sensory neurons in OE. The centrin gene, *Cetn2*, was found to have an important role in the trafficking and localization of the proteins involved in the downstream elevation of Ca^{2+} activity. In the absence of *Cetn2*, the OR downstream protein associates adenylate cyclase III and cyclic nucleotide-gated channel, which were supposed to be transported by the nonmuscle myosin II to the OSN dendritic knob, were absent. The *Cetn2* mutants show the failure to recruite the myosin in question. The resulting cilia defect disrupted the normal functions of multiple organs. All three projects have provided insights into the GCPR-inducedCa^{2+} activity modulations and the characterizations of Ca^{2+} activities in the normal functions of the olfactory system.

TABLE OF CONTENTS

ACKNOWLEDGMENTS

Dissertation Committee
Mary T. Lucero
Mike Michel
Matt Wachowiak
Michael Sanguinetti
Karen Wilcox

Coworkers who helped me
Ann Greig
Colleen Hegg
Arie Mobley
Mike Economo
Michelle Shamm
Mahendra Gradham
Shami Kanekar

Collaborators
Wolfgang Baehr
Colleen Hegg
Guoxin Ying
Mary Lucero
Houbin Zhang

Physiology Department
Vicki Skelton
Pattie O'Kane

Undergraduate students
Lara Anne Kapp
Austin Wood

Resources
Petr Tvrdik (Capecchi Lab) provided Dlx2 animals
Dudek Lab (microscope, help with animals and general support)
Seiji Shioda (PAC1R antibodies)
Ethan A. Lerner (M65 antagonist)
Christine Zabawa (Wachowiak Lab) provided mouse lines

Funding
NIH NIDCD DC002944
NIH NIDCD R01 DC02994 same as above
NIH NIDCD ARRA R01 DC02994-9
University of Utah Graduate Research Fellowship 2011
Ruth L. Kirschstein National Research Service Award #1F31DC011686-01A
NIH NIDCD Administrative Supplement to R01DC002994
Blackman Trust Fund 00253 6000 16917
AchemS Travel Awards 2009-2013

CHAPTER 1

INTRODUCTION

The Olfactory System

One of the fundamental problems in physiology is to understand the mechanisms regulating the survival and death of cells. Cell regeneration, proliferation, and apoptosis are controlled by multiple chemical and physical factors. These factors form complex pathways with multiple negative and positive feedbacks to the initial stimuli originating from multiple sources and creating changes in cell functions, which can last msecs to hours (Kandel et al., 2000). My physiological studies are centered on a system of specialty neurons, the olfactory system. Olfaction is evolutionarily one of the earliest developed senses and remains a primary, essential sense in most animal species (Leinwand and Chalasani, 2011). In mammals, the olfactory system consists of the olfactory epithelium (OE) in the nasal cavity and the main olfactory bulb (OB) in the brain, which are the regions of my research studies. The central part of the olfactory system also includes olfactory cortex regions, especially the amygdala and piriform cortex (Yokosuka, 2012). Depending on the animal family, the olfactory system may also have an auxiliary olfactory sense organ called the vomeronasal organ (VNO). The VNO connects to the accessory OB (AOB)

located adjacent to the main OB (on the posterior-dorsal side in rodents) (Yokosuka, 2012). In rodents, both the OE and VNO have sensory neurons; they are referred to as olfactory sensory neurons (OSNs) and vomeronasal sensory neurons (VSNs). The dendritic end of each OSN has between 20 and 30 ciliary processes expressing one of the 1063 known G-protein coupled odorant receptors (ORs). Each type of receptor can respond to a variety of airborne odorants (Ihara et al., 2013; Imai and Sakano, 2008). Furthermore, the OE has chemosensory receptors that respond to nonvolatile molecules, 15 known trace amine-associated receptors (TAARs), and the receptor guanylyl cyclase D (GC-D). The TAARs and GC-D are, to this date, generally believed to aid in discouraging consumption of unsafe food by being involved in the perception of unpleasant flavors (TAARs) and detecting unsafe food based on the natriuretic peptides, carbon dioxide, carbon sulfide, or uroguanylin and food-related odorant characteristics (GC-D) (Ihara et al., 2013). In contrast to the mainly ciliated neurons of the OE, VSNs are microvillar cells that have the vomeronasal receptor type 1 or 2 as well as the formyl peptide receptor on their dendritic microvilli (Ihara et al., 2013). Since my projects focused on the OE and OB of *Mus musculus*, the vomeronasal system will not be discussed any further.

The primary and first project to be discussed describes the intracellular $[Ca^{2+}]$ ($[Ca^{2+}]_i$) activity mechanisms in the granule cells (GCs) of the OB induced by a specific protein called Pituitary Adenylate Cyclase Activated Polypeptide (PACAP). The second project looks at the $[Ca^{2+}]_i$ activity in the sustentacular cells of the OE. The third study shows my electrical recordings of OSNs in the

OE as part of a collaborative work on the mechanisms of olfactory OSN signal transduction. Mice were chosen as a model because genetically these mammals closely resemble humans, and they have the ability to accept modulated specific genes of interest. All three projects involve G-protein coupled receptors (GPCRs) and their associates (downstream effectors, neurotransmitters, etc.) in the modulation of $[Ca^{2+}]_i$ response.

Function of GPCRs

GPCRs regulate a wide range of processes and are one of the essential factors in cellular function within the olfactory system. The GPCRs looked at in my projects have roles in the shaping of the olfactory system ranging from the ability to respond to odorants with the support of the surrounding sustentacular cells in the OE to the development, maturation and replacement of granule cells in the OB (Dooley et al., 2011; Hegg et al., 2009; Ogura et al., 2011; Kondo et al., 2010; Bath and Lee, 2010; Bovetti et al., 2011; Christie and Turnley, 2012). Most, if not all, GPCRs have a similar basic structure, but differ in their various binding sites, conformations for releasing G-protein, and heterotrimeric combinations of G-protein subunits (Oldham and Hamm, 2008).

The canonical GPCR protein, which is located in the plasma membrane and/or intracellular membranes of organelles and endosomes, has an N-terminus, followed by seven transmembrane (TM) domains connected by three interhelical loops on each side of the membrane, then finally a C-terminus on the opposite side of the membrane from the N-terminus (Fig. 1.1). The C-terminus has various binding sites for its specific combination(s) of G-protein subunits.

The heterotrimeric G-protein unit is comprised of three subunits referred to as α (21 subtypes), β (6 subtypes), and γ (12 subtypes). Various combinations of the subunits affect the strength and type of response (Oldham and Hamm, 2008). In the most recent classic model of GPCR function, the GPCR binds a ligand and undergoes a conformational change that activates its associated heteromeric G-protein. The Gα subunit dissociates from the tightly interacting Gβγ dimer. The G-protein dissociation process is not yet well understood, but the conserved GTPase domain on the Gα is believed to provide the binding to Gβγ dimer (Oldham and Hamm, 2008).

The binding sites on the N-terminus side of the GPCR vary, determining its affinity to specific ligands using possibly the N-terminus tail, interhelical loops, and/or TM domains. Regardless of the binding modes and type of GPCR, there is a conformational change at the C-terminus side of the membrane. If G-protein is released as a result, it may activate its effectors. In the classic example, it is supposed that the Gβγ dimer stays in the membrane and modulates membrane proteins. As for the Gα subunit, the various subtypes of this subunit can also activate (and inhibit) various pathways. The main stimulatory subtypes of Gα ($_{q}$, $_{s/olf}$) elevate the $[Ca^{2+}]_i$ through two major pathways known as the adenylate cyclase (AC) pathway and the phosphatidylinositol lipase C (PLC) pathway (Fig. 1.1). There is also a main inhibitory subtype, $G\alpha_i$, which inhibits the AC pathway (Blechman and Levkowitz, 2013). The AC pathway is activated when a $G\alpha_{s/olf}$ activates adenylyl cyclase, which uses ATP to generate cAMP. The cAMP then activates multiple downstream signals, some of them catalyzing the opening of

cyclic nucleotide gated (CNG) cation channels and voltage-gated calcium channels. The openings of especially voltage-gated calcium channels by cAMP may be direct or mediated through protein kinase A (PKA) and mitogen-activated protein kinase (MAPK). The opening of CNG channels and voltage-gated calcium channels brings extracellular Ca^{2+} into the cytoplasm, elevating the $[Ca^{2+}]_i$.

In the $G\alpha_q$/PLC pathway, PLC catalyzes the cleavage of phosphatidylinositol-4,5-biphosphate (PIP_2) into cytoplasmic inositol-1,4,5-trisphosphate (IP_3) and membrane-bound diacylglyerol (DAG). IP_3 then activates the IP_3 receptors located on the endoplasmic reticulum (ER), releasing stored Ca^{2+} into the cytoplasm, elevating the $[Ca^{2+}]_i$. DAG is believed to govern the activity of protein kinase C (PKC), an enzyme that phosphorylates various downstream proteins (Fukami et al., 2010; Kandel et al., 2000) (Fig. 1.1).

Anatomy and Functions of Cells in Olfactory System

The elevation of $[Ca^{2+}]_i$ through ion channels or by release from intracellular stores can affect enzymes, channels, and receptor potentials. If the cell membrane depolarizes past its threshold, an all-or-nothing action potential then transfers the electrical signal through the axons to neurons and interneurons. In the olfactory system, the signal response to an odorant begins in the OSNs of the OE, travels through the OB where it is processed, and from there to the olfactory cortex and other brain regions (Kandel et al., 2000).

The OE is located in the nasal cavity; the apical layer is closest to the air, just under the secreted mucus coat. It has four primary cell types: OSNs,

sustentacular cells [which function as epithelial and glial support cells (Hegg et al., 2009)], microvillar cells [MVC; act as stimulators and aid in the regeneration of olfactory cells between OE to OB, (Pfister et al., 2012)], and basal progenitor cells [which give rise to new OSNs and MVCs, (Elsaesser et al., 2005)]. The widely accepted idea is that an individual OSN contains only one OR subtype in its cilia. This seemingly single-function OR is, however, believed to perform multiple functions, starting when the OSN is immature and lacking an axon projection to the OB. The process by which a particular OR gene is activated is not well understood, but the activity of the chosen OR subtype, using $G\alpha_s$ protein (which activates the AC pathway), appears to guide the OSN axon to their determined spots in the OB. The OSN eventually expresses $G\alpha_{olf}$ protein, designed for reacting to ORs bound to odorants, also through the cAMP pathway. The $G\alpha_{olf}$-induced mechanisms appear to aid the axon targeting to become more precise and finally connect the OSN to the appropriate OB interneurons (Imai and Sakano, 2008; Fuss et al., 2013; Khan et al., 2011; Khan et al., 2013; Marcucci et al., 2011; Plessy et al., 2012).

We can follow the main olfactory signal pathway from nose to brain; it begins when odorant molecules in the environment become dissolved into the mucus coating the cilia of the OSN in the OE (Fig. 1.2). The odor ligand binds to the OR subtype of the OSN, and $G\alpha_{olf}$ protein is released, turning on downstream signals that open cyclic-adenosine monophosphate (cAMP)-gated channels. Extracellular Ca^{2+} enters and depolarizes the membrane. The responding receptor potential moves from the cilia through the OSN dendrite and soma, then

generates an action potential at the axon hillock (Kandel et al., 2000). One other OSN axon, with the same subtype of OR, joins the OSN unmyelinated axon we are following. This pair then is called an olfactory nerve filament, and it coalesces with other filaments, forming the olfactory nerve (Au et al., 2002). The olfactory nerve filaments project through a pore in the cribriform plate before reaching the OB. Each nerve filament activates what appears to be a ball of dendrites on the outermost part of the OB, known as a glomerulus. Like the nerve filaments, each glomerulus is specific to a particular OR. Each class of OSNs expressing a given subtype of OR are believed to converge their axons onto two glomeruli (Miyamichi et al., 2011; Furudono et al., 2013; Tan et al., 2010).

The signal within the glomerulus is then primarily passed on to the tufted cells deeper in the OB; these pass the signal to mitral cells, which carry the signal up the axon (De Saint et al., 2009; Gire et al., 2012). The MC axons coalesce toward the center to form the lateral olfactory tract that exits the OB and travels onward to several higher olfactory regions, especially the amygdala and piriform cortex (Yokosuka, 2012; Miyamichi et al., 2011). The stereotyped connection to the glomerulus we were following is just one of multiple signals for the same odorant. Beyond the glomerular layer, the connections became unitary and spatially represented in the OB. That said, an odorant stimulus is not broken into components, as is believed to happen for visual and auditory stimuli. Through modulation by neuropeptides and interneurons, the odorant representation becomes sparsely regional in the OB. This sparse code is

transmitted to the higher brain centers, where it is interpreted (Leinwand and Chalasani, 2011; Khan et al., 2010; Munch et al., 2013).

We have quickly traveled through the OB, following the signal from the OSN to the brain. The OB is, however, a complicated network of feedback loops between different types of interneurons (Fig. 1.2). Most of the interneurons are located in specific OB layers (Lledo et al., 2008; Parrish-Aungst et al., 2007; Au et al., 2002; Batista-Brito et al., 2008). The glomeruli are located in the outermost layer, making it a glomerular layer (GL). Some researchers, however, split this layer into the outer olfactory nerve layer and inner glomerular layer due to the olfactory nerve being reorganized extensively before the OSN axon fascicles innervate their specific glomeruli (Au et al., 2002). The GL also has periglomeruli cells and horizontal axon cells, which are believed to receive and release signals between various types of cells (Kiyokage et al., 2010). The external plexiform layer (EPL) contains uniformly positioned tufted cells (TCs) at various depths from the GL, but consists mostly of mitral cell (MC) dendrites going across the width of the EPL from the glomerular layer to the MC bodies in the mitral cell layer (MCL). The granule cell (GC) dendrites are also in the EPL. The innermost part of the MCL has short axon cells and possibly another type or types of cell that are not officially characterized and named. The internal plexiform layer (IPL) is on the innermost side of the MCL and appears to contain mainly MC axons and dendrites of GCs. The somas of these GCs are in the final main OB layer, known as the granule cell layer (GCL) (Au et al., 2002; Batista-Brito et al., 2008; Lledo et al., 2008; Parrish-Aungst et al., 2007). 99% of the

adult mouse interneuron cells in the GCL are GCs (Parrish-Aungst et al., 2007) and their primary function is to inhibit the MCs by dendrites (GCs have no axons!) extending to both the MCL and the EPL (Abraham et al., 2010; Ma et al., 2012; Shao et al., 2012). It has been believed that GCs also may inhibit TCs, but recent evidence suggests the TC inhibition comes from GL interneurons rather than GCs (Whitesell et al., 2013).

PACAP Modulation of Calicum Ion Activity

My primary research project (Chapter 2) is about the pituitary adenylate cyclase-activating polypeptide (PACAP)-induced modulation of $[Ca^{2+}]_i$ activity in the OB. For most of the experiments, I used a dynamic confocal imaging technique to track the changes in $[Ca^{2+}]_i$ activity. I applied different chemicals to an acute slice of P2-P5 neonatal mouse OB in a chamber bath using an air-pressured perfusion system. The perfusion system gently pushes the solutions through tubing onto the slice at a steady rate of 1.5–2 mL/min. The solution and experimental chemicals were steadily vacuumed away at the other side of the chamber. The focus was on the soma of the GCs, which are enriched with PACAP G-protein coupled receptors, especially PAC1 receptors (PAC1Rs) during the first neonatal mouse week.

The OB has a heterogeneous population of PAC1R isoforms that interact with either $G_{s/i}$ or G_q protein subtypes. The GCL has a higher expression of PAC1Rs than most parts of the central nervous system (CNS). Thus, PACAP is capable of activating both the AC and PLC pathways in the GCs (Blechman and Levkowitz, 2013). The PACAP response can furthermore release

neurotransmitters that turn on alternative receptors, increasing the $[Ca^{2+}]_i$ activity throughout the OB and possibly beyond. Although not investigated in this dissertation, PACAP has been widely studied for its neuroprotective effects. The PACAP-induced response generally reduces the pro-apoptosic factors such as the cleavage of caspaces (3, 8, 9,12 for example), Bax, JNK, and c-jun gene expression. PACAP furthermore generally increases the anti-apoptosic factors such as PKC, PKA, ERK, Bcl-2, and c-fos gene expression (Botia et al., 2007; Szabadfi et al., 2014; Vaudry et al., 1998; Cowan and Roskams, 2002). A good example of the mechanism of the PACAP anti-apopostic effect is its counterbalancing of the apoptotic activity induced by ceramide proteins (Aubert et al., 2006; Dejda et al., 2005; Falluel-Morel et al., 2004; Falluel-Morel et al., 2005; Falluel-Morel et al., 2006; Falluel-Morel et al., 2008; Vaudry et al., 2003; Zhokhov et al., 2008) (Fig. 1.3). Briefly, Fig. 1.3 shows how the PACAP-induced kinase activity (e.g., ERK) leads to phosphorylation of c-fos, which binds to the c-jun from the ceramide-induced pro-apoptosis route stimulated by JNK. The activator protein-1 (AP-1) binds with the anti-apoptosis c-fos/c-jun pair (builds up Bcl-2 expression) or the pro-apoptosis c-jun/c-jun pair (builds up Bax expression). Without c-fos, the gene expression elevated by c-jun alone favors apoptosis. When this happens, one or more types of caspases are cleaved by cytochrome c, which was released from mitochondria by Bax (Jin and El-Deiry, 2005). PACAP is thought to promote the anti-apoptotic pathway.

The OB being part of the CNS made it a unique research model for the anti-apoptosis and regeneration studies because unlike the majority of the CNS

neurons that stop developing by adulthood, the mature GCs (as well as other cells apart from the more permanent mitral and tufted cells) in the OB are continuously replaced throughout life (Bagley et al., 2007)! The lifetime replacement of OB interneurons was shown to be necessary for normal olfaction functions (Breton-Provencher et al., 2009; Bagley et al., 2007). PACAP is a strong candidate for contributing to the apoptosis prevention, development, regeneration, and proliferation of new cells. Studying how PACAP aids the lifetime replacement of OB interneurons will hopefully help in the treatments for CNS injuries and neurodegenerative disorders such as Alzheimer's Disease and other dementias, stroke, malformations, epilepsy, Multiple Sclerosis, and others (Atlasz et al., 2010; Ohtaki et al., 2008; Mulder et al., 1999; Delgado et al., 2003; Chen et al., 2006; Doursout et al., 2013; Dejda et al., 2005; Dejda et al., 2008; Makela et al., 2010; Ruan et al., 2012; Sherwood et al., 2007).

Calcium Store-Mediated Signaling in Sustentacular Cells

The second project (Chapter 3) used the same confocal imaging technique to track $[Ca^{2+}]_i$ activity in the OE sustentacular cells, which were historically thought to be just epithelial support cells basically keeping the electrically active OSNs separate from one another (Hegg et al., 2009). However, more recent studies suggest that sustentacular cells are glial-like. Our data of complex $[Ca^{2+}]_i$ activity in sustentacular cells further support the glial-like concept. The adenosine triphosphate (ATP) or UTP purinergics, which all living organisms use for energy (Kandel et al., 2000), were found to extremely elevate the sustentacular cell $[Ca^{2+}]_i$ levels, as compared to OSNs. The main factors

responsible for the complex calcium signaling in sustentacular cells are the extracellular purinergic-evoked release of $[Ca^{2+}]_i$ through the PLC pathway and the ability of these cells to communicate with each other, potentially through gap junctions. The ATP-induced specific calcium oscillations are suggested to integrate and coordinate multicellular functions.

Dysosmia in $Cetn^{-/-}$ Mice

The third research project (Chapter 4) uses the electro-olfactogram (EOG), a method specialized for recording from multiple OSNs using electrodes. Airborne odorants were puff-delivered to the OE surface. The amount of voltage change shows the overall strength of response through GCPRs from multiple OSNs. The project focused on centrins, which are calmodulin-related Ca^{2+} binding proteins that we suggested aid in the trafficking and localizing of ACIII and the cyclic nucleotide gated channel A2 subunit (CNGA2). I compared Cetn2ΔEx2,3 knockout mice (Cetn2 exon 2 + 3 of the centrin-2 gene deleted) with their wildtype littermates. The OEs of the knockouts have a significantly reduced olfactory response. This suggests that centrin-2 is one of the proteins needed to coordinate the transport of proteins in the cAMP pathway to the OSN cilia. Even though centrin-2 is not the sole transport coordinator for the ACIII and CNG channels, the lack of the proper localizing and trafficking causes the progressive loss of preexisting cilia in the knockouts. Furthermore, the knockouts have reduced postnatal OSN ciliogenesis/growth.

Summary

All three projects evaluating the activities of GCPRs and their induced Ca^{2+} modulating pathways elucidate how the olfactory system uses the metabotropic receptors and their complex, long-term $[Ca^{2+}]_i$ activities to support the development and function of olfactory neurons and interneurons.

Reference List

1. **Abraham NM, Egger V, Shimshek DR, Renden R, Fukunaga I, Sprengel R, Seeburg PH, Klugmann M, Margrie TW, Schaefer AT, Kuner T**. Synaptic inhibition in the olfactory bulb accelerates odor discrimination in mice. *Neuron* 65: 399–411, 2010.

2. **Atlasz T, Szabadfi K, Kiss P, Tamas A, Toth G, Reglodi D, Gabriel R**. Evaluation of the protective effects of PACAP with cell-specific markers in ischemia-induced retinal degeneration. *Brain Res Bull* 81: 497–504, 2010.

3. **Au WW, Treloar HB, Greer CA**. Sublaminar organization of the mouse olfactory bulb nerve layer. *J Comp Neurol* 446: 68–80, 2002.

4. **Aubert N, Falluel-Morel A, Vaudry D, Xifro X, Rodriguez-Alvarez J, Fisch C, de JS, Lebigot JF, Fournier A, Vaudry H, Gonzalez BJ**. PACAP and C2-ceramide generate different AP-1 complexes through a MAP-kinase-dependent pathway: involvement of c-Fos in PACAP-induced Bcl-2 expression. *J Neurochem* 99: 1237–1250, 2006.

5. **Bagley J, LaRocca G, Jimenez DA, Urban NN**. Adult neurogenesis and specific replacement of interneuron subtypes in the mouse main olfactory bulb. *BMC Neurosci* 8: 92, 2007.

6. **Bath KG, Lee FS**. Neurotrophic factor control of adult SVZ neurogenesis. *Dev Neurobiol* 70: 339–349, 2010.

7. **Batista-Brito R, Close J, Machold R, Fishell G**. The distinct temporal origins of olfactory bulb interneuron subtypes. *J Neurosci* 28: 3966–3975, 2008.

8. **Blechman J, Levkowitz G**. Alternative splicing of the pituitary adenylate cyclase-activating polypeptide receptor PAC1: mechanisms of fine tuning of brain activity. *Front Endocrinol (Lausanne)* 4: 55, 2013.

9. **Botia B, Basille M, Allais A, Raoult E, Falluel-Morel A, Galas L, Jolivel V, Wurtz O, Komuro H, Fournier A, Vaudry H, Burel D, Gonzalez BJ,**

Vaudry D. Neurotrophic effects of PACAP in the cerebellar cortex. *Peptides* 28: 1746–1752, 2007.

10. **Bovetti S, Gribaudo S, Puche AC, De MS, Fasolo A**. From progenitors to integrated neurons: role of neurotransmitters in adult olfactory neurogenesis. *J Chem Neuroanat* 42: 304–316, 2011.

11. **Breton-Provencher V, Lemasson M, Peralta MR, III, Saghatelyan A**. Interneurons produced in adulthood are required for the normal functioning of the olfactory bulb network and for the execution of selected olfactory behaviors. *J Neurosci* 29: 15245–15257, 2009.

12. **Chen Y, Samal B, Hamelink CR, Xiang CC, Chen Y, Chen M, Vaudry D, Brownstein MJ, Hallenbeck JM, Eiden LE**. Neuroprotection by endogenous and exogenous PACAP following stroke. *Regul Pept* 137: 4–19, 2006.

13. **Christie KJ, Turnley AM**. Regulation of endogenous neural stem/progenitor cells for neural repair-factors that promote neurogenesis and gliogenesis in the normal and damaged brain. *Front Cell Neurosci* 6: 70, 2012.

14. **Cowan CM, Roskams AJ**. Apoptosis in the mature and developing olfactory neuroepithelium. *Microsc Res Tech* 58: 204–215, 2002.

15. **De Saint JD, Hirnet D, Westbrook GL, Charpak S**. External tufted cells drive the output of olfactory bulb glomeruli. *J Neurosci* 29: 2043–2052, 2009.

16. **Dejda A, Jolivel V, Bourgault S, Seaborn T, Fournier A, Vaudry H, Vaudry D**. Inhibitory effect of PACAP on caspase activity in neuronal apoptosis: a better understanding towards therapeutic applications in neurodegenerative diseases. *J Mol Neurosci* 36: 26–37, 2008.

17. **Dejda A, Sokolowska P, Nowak JZ**. Neuroprotective potential of three neuropeptides PACAP, VIP and PHI. *Pharmacol Rep* 57: 307–320, 2005.

18. **Delgado M, Abad C, Martinez C, Juarranz MG, Leceta J, Ganea D, Gomariz RP**. PACAP in immunity and inflammation. *Ann NY Acad Sci* 992: 141–157, 2003.

19. **Dooley R, Mashukova A, Toetter B, Hatt H, Neuhaus EM**. Purinergic receptor antagonists inhibit odorant-mediated CREB phosphorylation in sustentacular cells of mouse olfactory epithelium. *BMC Neurosci* 12: 86, 2011.

20. **Doursout MF, Schurdell MS, Young LM, Osuagwu U, Hook DM, Poindexter BJ, Schiess MC, Bick DL, Bick RJ**. Inflammatory cells and

cytokines in the olfactory bulb of a rat model of neuroinflammation; insights into neurodegeneration? *J Interferon Cytokine Res* 33: 376–383, 2013.

21. **Elsaesser R, Montani G, Tirindelli R, Paysan J**. Phosphatidyl-inositide signalling proteins in a novel class of sensory cells in the mammalian olfactory epithelium. *Eur J Neurosci* 21: 2692–2700, 2005.

22. **Falluel-Morel A, Aubert N, Vaudry D, Basille M, Fontaine M, Fournier A, Vaudry H, Gonzalez BJ**. Opposite regulation of the mitochondrial apoptotic pathway by C2-ceramide and PACAP through a MAP-kinase-dependent mechanism in cerebellar granule cells. *J Neurochem* 91: 1231–1243, 2004.

23. **Falluel-Morel A, Aubert N, Vaudry D, Desfeux A, Allais A, Burel D, Basille M, Vaudry H, Laudenbach V, Gonzalez BJ**. Interactions of PACAP and ceramides in the control of granule cell apoptosis during cerebellar development. *J Mol Neurosci* 36: 8–15, 2008.

24. **Falluel-Morel A, Vaudry D, Aubert N, Galas L, Benard M, Basille M, Fontaine M, Fournier A, Vaudry H, Gonzalez BJ**. Pituitary adenylate cyclase-activating polypeptide prevents the effects of ceramides on migration, neurite outgrowth, and cytoskeleton remodeling. *Proc Natl Acad Sci USA* 102: 2637–2642, 2005.

25. **Falluel-Morel A, Vaudry D, Aubert N, Galas L, Benard M, Basille M, Fontaine M, Fournier A, Vaudry H, Gonzalez BJ**. PACAP and ceramides exert opposite effects on migration, neurite outgrowth, and cytoskeleton remodeling. *Ann NY Acad Sci* 1070: 265–270, 2006.

26. **Fukami K, Inanobe S, Kanemaru K, Nakamura Y**. Phospholipase C is a key enzyme regulating intracellular calcium and modulating the phosphoinositide balance. *Prog Lipid Res* 49: 429–437, 2010.

27. **Furudono Y, Cruz G, Lowe G**. Glomerular input patterns in the mouse olfactory bulb evoked by retronasal odor stimuli. *BMC Neurosci* 14: 45, 2013.

28. **Fuss SH, Zhu Y, Mombaerts P**. Odorant receptor gene choice and axonal wiring in mice with deletion mutations in the odorant receptor gene SR1. *Mol Cell Neurosci* 56: 212–224, 2013.

29. **Gire DH, Franks KM, Zak JD, Tanaka KF, Whitesell JD, Mulligan AA, Hen R, Schoppa NE**. Mitral cells in the olfactory bulb are mainly excited through a multistep signaling path. *J Neurosci* 32: 2964–2975, 2012.

30. **Hegg CC, Irwin M, Lucero MT**. Calcium store-mediated signaling in sustentacular cells of the mouse olfactory epithelium. *Glia* 57: 634–644, 2009.

31. **Ihara S, Yoshikawa K, Touhara K**. Chemosensory signals and their receptors in the olfactory neural system. *Neuroscience* 254C: 45–60, 2013.

32. **Imai T, Sakano H**. Odorant receptor-mediated signaling in the mouse. *Curr Opin Neurobiol* 18: 251–260, 2008.

33. **Jin Z, El-Deiry WS**. Overview of cell death signaling pathways. *Cancer Biol Ther* 4: 139–163, 2005.

34. **Kandel E, Schwartz J, Jessell T**. *Principles of Neural Science*. McGraw-Hill Companies, 2000.

35. **Khan AG, Parthasarathy K, Bhalla US**. Odor representations in the mammalian olfactory bulb. *Wiley Interdiscip Rev Syst Biol Med* 2: 603–611, 2010.

36. **Khan M, Vaes E, Mombaerts P**. Regulation of the probability of mouse odorant receptor gene choice. *Cell* 147: 907–921, 2011.

37. **Khan M, Vaes E, Mombaerts P**. Temporal patterns of odorant receptor gene expression in adult and aged mice. *Mol Cell Neurosci* 57: 120–129, 2013.

38. **Kiyokage E, Pan YZ, Shao Z, Kobayashi K, Szabo G, Yanagawa Y, Obata K, Okano H, Toida K, Puche AC, Shipley MT**. Molecular identity of periglomerular and short axon cells. *J Neurosci* 30: 1185–1196, 2010.

39. **Kondo K, Suzukawa K, Sakamoto T, Watanabe K, Kanaya K, Ushio M, Yamaguchi T, Nibu K, Kaga K, Yamasoba T**. Age-related changes in cell dynamics of the postnatal mouse olfactory neuroepithelium: cell proliferation, neuronal differentiation, and cell death. *J Comp Neurol* 518: 1962–1975, 2010.

40. **Leinwand SG, Chalasani SH**. Olfactory networks: from sensation to perception. *Curr Opin Genet Dev* 21: 806–811, 2011.

41. **Lledo PM, Merkle FT, Alvarez-Buylla A**. Origin and function of olfactory bulb interneuron diversity. *Trends Neurosci* 31: 392–400, 2008.

42. **Ma TF, Zhao XL, Cai L, Zhang N, Ren SQ, Ji F, Tian T, Lu W**. Regulation of spike timing-dependent plasticity of olfactory inputs in mitral cells in the rat olfactory bulb. *PLoS One* 7: e35001, 2012.

43. **Makela J, Koivuniemi R, Korhonen L, Lindholm D**. Interferon-gamma produced by microglia and the neuropeptide PACAP have opposite effects on the viability of neural progenitor cells. *PLoS One* 5: e11091, 2010.

44. **Marcucci F, Maier-Balough E, Zou DJ, Firestein S**. Exuberant growth and synapse formation of olfactory sensory neuron axonal arborizations. *J Comp Neurol* 519: 3713–3726, 2011.

45. **Miyamichi K, Amat F, Moussavi F, Wang C, Wickersham I, Wall NR, Taniguchi H, Tasic B, Huang ZJ, He Z, Callaway EM, Horowitz MA, Luo L**. Cortical representations of olfactory input by trans-synaptic tracing. *Nature* 472: 191–196, 2011.

46. **Mulder H, Jongsma H, Zhang Y, Gebre-Medhin S, Sundler F, Danielsen N**. Pituitary adenylate cyclase-activating polypeptide and islet amyloid polypeptide in primary sensory neurons: functional implications from plasticity in expression on nerve injury and inflammation. *Mol Neurobiol* 19: 229–253, 1999.

47. **Munch D, Schmeichel B, Silbering AF, Galizia CG**. Weaker ligands can dominate an odor blend due to syntopic interactions. *Chem Senses* 38: 293–304, 2013.

48. **Ogura T, Szebenyi SA, Krosnowski K, Sathyanesan A, Jackson J, Lin W**. Cholinergic microvillous cells in the mouse main olfactory epithelium and effect of acetylcholine on olfactory sensory neurons and supporting cells. *J Neurophysiol* 106: 1274–1287, 2011.

49. **Ohtaki H, Nakamachi T, Dohi K, Shioda S**. Role of PACAP in ischemic neural death. *J Mol Neurosci* 36: 16–25, 2008.

50. **Oldham WM, Hamm HE**. Heterotrimeric G protein activation by G-protein-coupled receptors. *Nat Rev Mol Cell Biol* 9: 60–71, 2008.

51. **Parrish-Aungst S, Shipley MT, Erdelyi F, Szabo G, Puche AC**. Quantitative analysis of neuronal diversity in the mouse olfactory bulb. *J Comp Neurol* 501: 825–836, 2007.

52. **Pfister S, Dietrich MG, Sidler C, Fritschy JM, Knuesel I, Elsaesser R**. Characterization and turnover of CD73/IP(3)R3-positive microvillar cells in the adult mouse olfactory epithelium. *Chem Senses* 37: 859–868, 2012.

53. **Plessy C, Pascarella G, Bertin N, Akalin A, Carrieri C, Vassalli A, Lazarevic D, Severin J, Vlachouli C, Simone R, Faulkner GJ, Kawai J, Daub CO, Zucchelli S, Hayashizaki Y, Mombaerts P, Lenhard B, Gustincich S, Carninci P**. Promoter architecture of mouse olfactory receptor genes. *Genome Res* 22: 486–497, 2012.

54. **Ruan Y, Zheng XY, Zhang HL, Zhu W, Zhu J**. Olfactory dysfunctions in neurodegenerative disorders. *J Neurosci Res* 90: 1693–1700, 2012.

55. **Shao Z, Puche AC, Liu S, Shipley MT**. Intraglomerular inhibition shapes the strength and temporal structure of glomerular output. *J Neurophysiol* 108: 782–793, 2012.

56. **Sherwood NM, Adams BA, Isaac ER, Wu S, Fradinger EA**. Knocked down and out: PACAP in development, reproduction and feeding. *Peptides* 28: 1680–1687, 2007.

57. **Szabadfi K, Szabo A, Kiss P, Reglodi D, Setalo G, Jr., Kovacs K, Tamas A, Toth G, Gabriel R**. PACAP promotes neuron survival in early experimental diabetic retinopathy. *Neurochem Int* 64: 84–91, 2014.

58. **Tan J, Savigner A, Ma M, Luo M**. Odor information processing by the olfactory bulb analyzed in gene-targeted mice. *Neuron* 65: 912–926, 2010.

59. **Vaudry D, Falluel-Morel A, Basille M, Pamantung TF, Fontaine M, Fournier A, Vaudry H, Gonzalez BJ**. Pituitary adenylate cyclase-activating polypeptide prevents C2-ceramide-induced apoptosis of cerebellar granule cells. *J Neurosci Res* 72: 303–316, 2003.

60. **Vaudry D, Gonzalez BJ, Basille M, Anouar Y, Fournier A, Vaudry H**. Pituitary adenylate cyclase-activating polypeptide stimulates both c-fos gene expression and cell survival in rat cerebellar granule neurons through activation of the protein kinase A pathway. *Neuroscience* 84: 801–812, 1998.

61. **Whitesell JD, Sorensen KA, Jarvie BC, Hentges ST, Schoppa NE**. Interglomerular lateral inhibition targeted on external tufted cells in the olfactory bulb. *J Neurosci* 33: 1552–1563, 2013.

62. **Yokosuka M**. Histological properties of the glomerular layer in the mouse accessory olfactory bulb. *Exp Anim* 61: 13–24, 2012.

63. **Zhokhov SS, Desfeux A, Aubert N, Falluel-Morel A, Fournier A, Laudenbach V, Vaudry H, Gonzalez BJ**. Bax siRNA promotes survival of cultured and allografted granule cell precursors through blockade of caspase-3 cleavage. *Cell Death Differ* 15: 1042–1053, 2008.

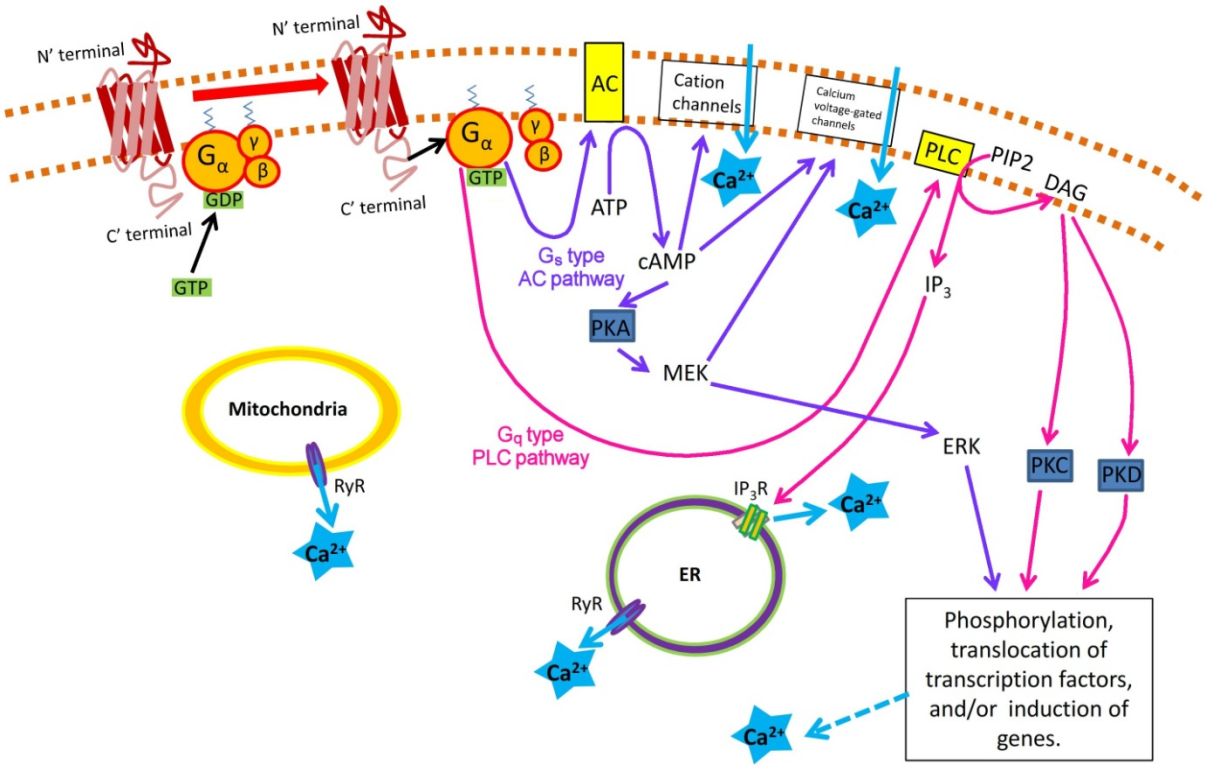

Fig. 1.1: How GCPRs activate PLC (pink arrows) and/or AC (purple arrows) pathways. Blue arrows represent Ca^{2+} (blue stars) entry into intracellular space. PLC = phosphoinositide-phospholipase C, PIP = phosphatidylinositol-4,5-bisphosphate, DAG = diacylglycerol, IP_3 = inositol triphosphate (and receptor), ER = endoplasmic reticulum, RyR = ryanodine receptor, GDP/GTP = guanosine-5'-di/triphosphate, ATP = adenosine-5'-triphosphate, AC = adenylate cyclase, cAMP = cyclic adenosine monophosphate, PKA/PKC/PKD = protein kinase A/C/D, MEK = mitogen-activated protein kinase, ERK = extracellular signal-regulated kinases.

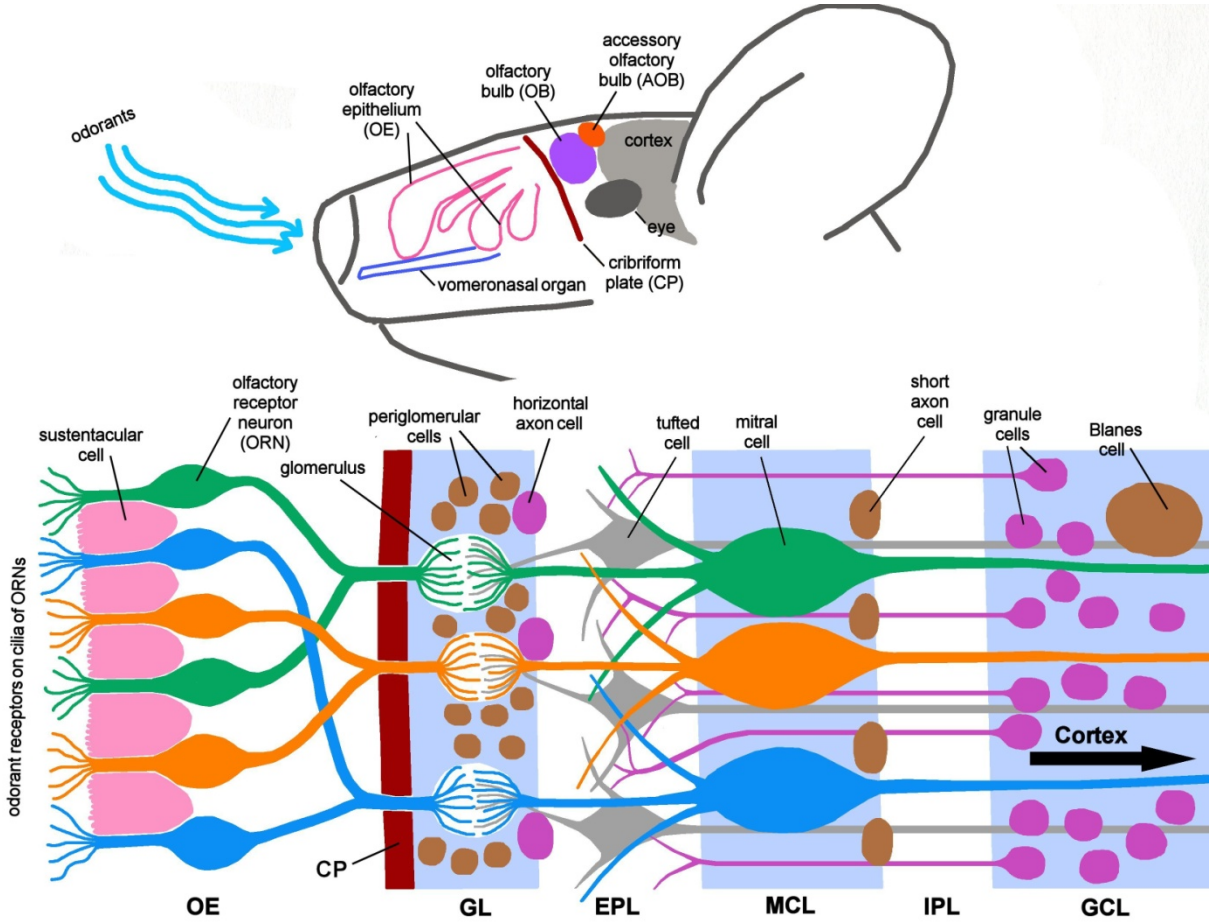

Fig. 1.2: Diaphragm of olfactory system. (GL = glomerular layer, EPL = external plexiform layer, MCL = mitral cell layer, IPL = internal plexiform layer, GCL = granule cell layer)

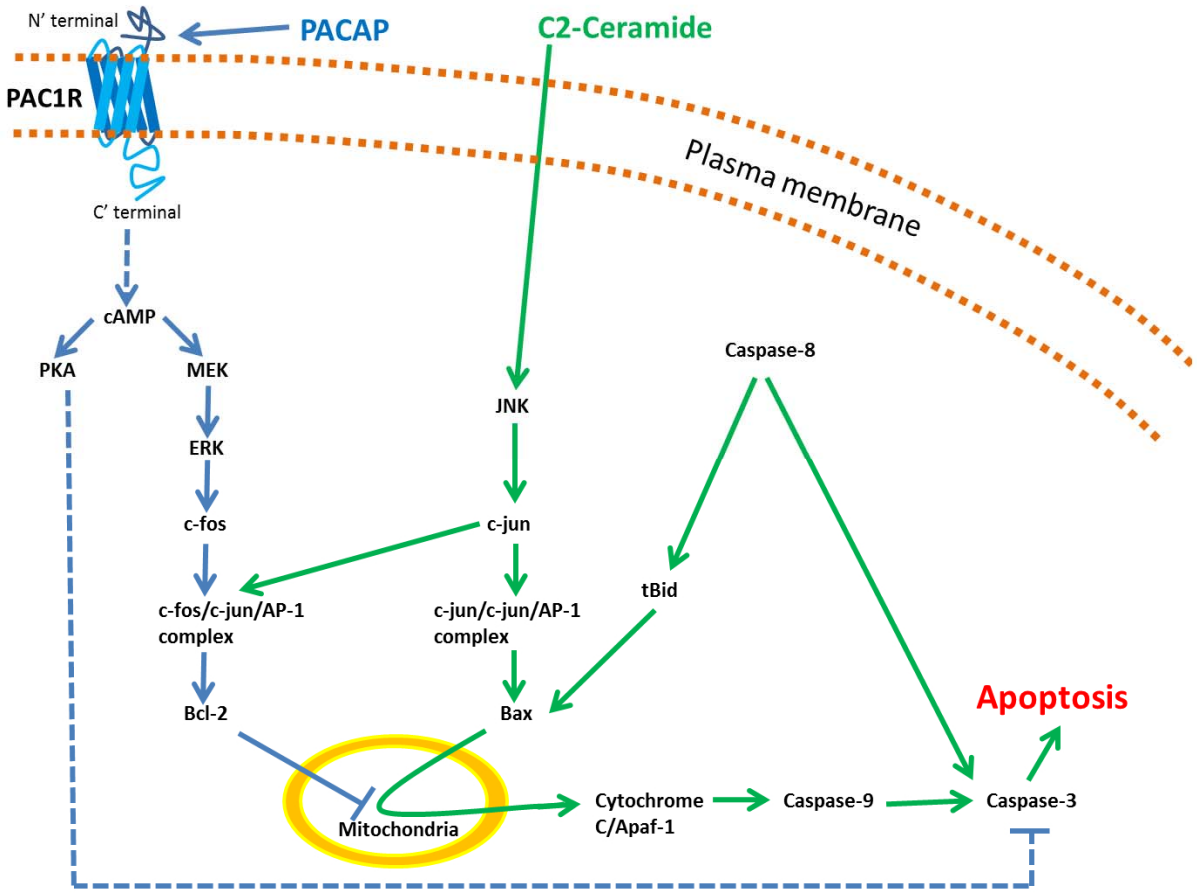

Fig. 1.3: How PACAP act as anti-apoptosis factor opposing the pro-apoptosis pathways. Blue represents PACAP-induced anti-apoptotic factors. Green represents pro-apoptotic factors which can be induced by ceramides or other insults. (PAC1R = PACAP receptor; PKA = protein kinase A; cAMP = cyclic adenosine monophosphate; MEK = Mitogen-activated protein kinase; ERK = extracellular signal-regulated kinases; AP-1 = Activator Protein-1; Bcl-2 = B-cell lymphoma 2; JNK = c-Jun N-terminal kinases; Bax = BCL2-associated X protein; tBid = truncated Bcl2 Interacting Protein; cytochrome C = cytochrome complex; Apaf-1 = Apoptotic protease activating factor-1).

CHAPTER 2

PACAP MODULATION OF CALCIUM ION ACTIVITY IN THE MOUSE OLFACTORY BULB

Introduction

Pituitary Adenylate Cyclase Activating Peptide (PACAP) is a potential candidate for neurogenesis therapy following injury or neurodegenerative disease due to its anti-apoptotic properties (Arimura, 1998; Atlasz et al., 2010; Bourgault et al., 2009; Chen et al., 2006; Cowan and Roskams, 2002; Dejda et al., 2005; Dejda et al., 2008; Delgado et al., 2003; Di et al., 2012; Doursout et al., 2013; Hansel et al., 2001; Kanekar et al., 2010; Makela et al., 2010; Mulder et al., 1999; Nakamachi et al., 2008; Ohtaki et al., 2006; Ohtaki et al., 2008; Ruan et al., 2012; Sherwood et al., 2007; Shioda et al., 2006; Szabadfi et al., 2012; Szabadfi et al., 2014; Vaudry et al., 2009; Yang, 2008). PACAP was originally discovered in 1989 by Miyata et al. and was described as a neuropeptide that stimulates cAMP formation in the pituitary cells, hence the current name (Miyata et al., 1989). Today PACAP and its PACAP-specific G protein coupled receptors (PAC1R, VPAC1R, and VPAC2R) are studied in other parts of the central nervous system (CNS) such as the cerebellum, hippocampus, and olfactory system, as well as throughout the body (16). The functions of PACAP in the CNS

are largely neurotrophic during development and neuroprotective or neuromodulatory during adulthood (Arimura, 1998; Dejda et al., 2008; Delgado et al., 2003; Ravni et al., 2006; Sherwood et al., 2007; Vaudry et al., 2002). Thus, despite its relatively recent discovery, PACAP is now considered to be one of the most important regulators of biological functions (Vaudry et al., 2000c). Our interest in the physiological functions of PACAP and PAC1Rs developed partly from the noteworthy problem of PACAP knockout mice often dying before weaning. The high mortality of PACAP knockouts suggests that PACAP is required for normal development (Raineki et al., 2010; Sherwood et al., 2007).

PACAP and PAC1R expression are highest in the CNS regions that continue to regenerate throughout adulthood such as the dentate gyrus and olfactory system (Hansel et al., 2001; Mulder et al., 1999) as well as in sensory integration areas including the retina (Atlasz et al., 2010; Delwig et al., 2013; Kiss et al., 2006; Markhotina et al., 2007; Silveira et al., 2002; Szabadfi et al., 2012; Szabadfi et al., 2014), cerebellum (Allais et al., 2007; Botia et al., 2007; Falluel-Morel et al., 2007; Falluel-Morel et al., 2008; Jozwiak-Bebenista et al., 2007; Mei et al., 2004; Vaudry et al., 1998; Vaudry et al., 1999; Vaudry et al., 2000b; Vaudry et al., 2000a; Vaudry et al., 2002; Vaudry et al., 2003; Zhokhov et al., 2008), hippocampus (Ago et al., 2011; Costa et al., 2009; Di et al., 2003; Kambe and Miyata, 2012; Liu et al., 2003; Macdonald et al., 2005; Taylor et al., 2014), and suprachiasmatic nucleus (SCN) (Dziema and Obrietan, 2002; Irwin and Allen, 2010; Kopp et al., 1999; Kopp et al., 2001; Michel et al., 2006; Webb et al., 2013). Ca^{2+} imaging studies in SCN showed that the initial PACAP-induced

response is variable, ranging from slow (sec) to rapid (msec) increases in intracellular [Ca^{2+}] ([Ca^{2+}]$_i$). Following the initial response, durations of post-PACAP Ca^{2+} fluctuations are also variable and can persist from minutes to hours (Kopp et al., 1999). It appears that the variability in PACAP response profiles mainly depends on the dominate type of PAC1R splice variant being activated (Ago et al., 2011; Blechman and Levkowitz, 2013; Nicot and Dicicco-Bloom, 2001; Yan et al., 2013; Zhou et al., 2002). Either way, it is generally agreed that PACAP has a role in directly or indirectly inducing long-term changes in Ca^{2+} activities (Baxter et al., 2011; Dziema and Obrietan, 2002; Kopp et al., 1999; Kopp et al., 2001; Michel et al., 2006; Tanaka et al., 2007).

Within the olfactory system, the constant generation of new neurons is required to maintain normal function of both olfactory epithelium and the olfactory bulb (OB) (Breton-Provencher et al., 2009). PACAP and PAC1Rs are found throughout the olfactory system with high mRNA expression in the olfactory epithelium, OB, and anterior olfactory nucleus (Allen Brain Altas, 2013; Jaworski and Proctor, 2000; Shioda et al., 1997). Our lab has been studying the physiological effects of PACAP and PAC1Rs in the olfactory epithelium (Han and Lucero, 2005; Han and Lucero, 2006; Hansel et al., 2001; Hegg et al., 2003b; Hegg et al., 2003a). However, little is known about the physiological effects of PACAP in the OB (Olianas and Onali, 1999). Here we provide the first physiological recordings of PACAP-induced [Ca^{2+}]$_i$ responses in genetically identified neurons of the neonatal mouse OB.

The mouse OB has several discrete layers containing at least seven different types of interneurons and two classes of projection neurons (tufted cells and mitral cells) (Batista-Brito et al., 2008). We limited our study of PACAP to the granule cell layer (GCL). The GCL has two main types of GABAergic interneurons, 97% of which are the small (4–8 um) granule cells (GCs), and the other 3% are the large (12–18 um), ovoid-soma Blanes cells (Potter et al., 2009). The GCL has one of the highest expression levels of PAC1R mRNA in the CNS. Although the GCL region has little to no PACAP gene expression, the GCs primarily connect with the mitral cells (MCs) and receive input from the anterior olfactory nucleus; both are areas of enriched PACAP gene expression (Batista-Brito et al., 2008; Jaworski and Proctor, 2000; Allen Brain Altas, 2013; Shioda et al., 1997).

In the following experiments, we examined the effects of PACAP on cells in the GCL of P2 to P5 mice, the time period when the majority of GCs migrate into the OB from the subventricular zone (Batista-Brito et al., 2008; Lemasson et al., 2005).

We hypothesized that the PACAP activation of GCs triggers developmentally important $[Ca^{2+}]_i$ oscillations and participates in the establishment of OB circuitry within the first postnatal week. In the first experiments, we asked whether PACAP directly or indirectly modulates $[Ca^{2+}]_i$ in the developing granule neurons within the olfactory bulb by evaluating the kinetics of PACAP responses in the presence and absence of neurotransmission. In the second study, we used functionally (based on excitatory GABA responses)

and genetically identified cell types to determine the developmental time course of PACAP responsiveness in GCL neurons in neonatal mouse OB. We evaluated both the GC cells (labeled Dlx2-tdTomato) and the GAD65 GC subtype group (labeled GAD65-tdTomato). The changes in the population of PACAP-responding cells within the 4 days evaluated, especially among the GAD67 cells, provide clues about the first week of PACAP activity in the developing OB.

Understanding the role of PACAP in modulating $[Ca^{2+}]_i$ in developing neurons may provide important insight for mechanisms mediating the maturation required for establishing sensory maps and neuronal circuits. In the future, this understanding may be critical for promoting therapeutic integration of neuroblasts during early development, following injury, or in neurodegenerative disease.

Materials and Methods

Animals

All animal procedures were approved by the University of Utah Institutional Animal Care and Use Committee and were conducted under the guidelines of the NIH Guide for Care and Use of Laboratory Animals.

The defined Cre recombinase (IRES-CRE linked) transgenic C57/BL6 mice for Dlx2-IRES-CRE (gift from Dr. Mario Capecchi Lab) was used. The Dlx2-IRES-Cre mouse line was generated in the Capecchi lab by inserting an IRES-Cre-FRT-neo-FRT cassette in the 3' untranslated region of the Dlx2 gene. The targeting vector was prepared with 129S6/SvEvTac mouse genomic DNA previously isolated from the RPCI-22 BAC library (BACPAC Resources). The

vector was electroporated in 129R1 embryonic stem (ES) cells, and successfully targeted clones were confirmed by Southern blotting. ES cells were injected in the blastocysts of C57Bl6 recipients to generate chimera founders. Positive offspring was bred to FLP delete mice to remove the neo selection marker, and the line was bred to homozygosity. Automated genotyping service for this strain is available from Transnetyx (probes: "Dlx2-1 WT" and "Dlx2-1 KO").

Additionally, the defined Cre recombinase (IRES-CRE linked) transgenic C57/BL6 mice for GAD65-IRES-CRE [JAX Stock #0101802; The Jackson Laboratory (Taniguchi et al., 2011)] and PCdh21 [The GENSAT Project; Stock #030952-UCD; Mutant Mouse Regional Resource Centers (Nagai et al., 2005)] were used. To specifically label the IRES-CRE linked genes as red, mice from each line were crossed with mice containing the Rosa-tdTomato gene (ROSA26-CAG promoter). The Swiss Webster transgenic mice for GAD67 are Green Fluorescent Protein (GFPF)-linked. The pups were checked for specific expression using ultraviolet light. Any pups with nonspecific expression, which appeared completely red from head to toe, were not used. The specific expression of Dlx2 is primarily in the head region. GAD65 and PCdh21 had expression mainly in the head, but in patterns on the body too.

Live Slices of the OB

Live coronal slices of the OB (400 μM thick) were prepared between 11 AM to 12:30 PM [due to circadian changes in PACAP (Granados-Fuentes et al., 2006)] from P2–P5 mice (Hegg et al., 2003c). Briefly, following decapitation, the jaws, skin, and eyes were removed, and then the whole skull was embedded in

carrot and sliced using a vibrotome. The slices were cut in ice cold low Na^+/high Mg^{2+} bicarbonate buffer (in mM: 220 sucrose, 3 KCl, 10 $MgSO_4.7H_2O$, 1.25 $NaH_2PO_4.H_2O$, 25 NaH_2CO_3, 25 D-glucose, and 0.2 mM $CaCl_2.2H_2O$, bubbled with 95%O_2/5%CO_2). Slices were then placed in low Ca^{2+} artificial cerebral spinal fluid (ACSF) (in mM: 125 NaCl, 3 KCl, 1.3 $MgSO_4.7H_2O$, 1.25 $NaH_2PO_4.H_2O$, 25 NaH_2CO_3, 25 D-glucose, and 0.2 mM $CaCl_2.2H_2O$, bubbled with 95%O_2/5%CO_2, pH 7.4). The slices recovered for at least 40 min at room temperature before loading with 1.3 mM Ca^{2+} ACSF containing the membrane permeant Ca^{2+} sensitive dye [37 MμM Fluo-4 AM (Invitrogen), which is prepared with 20% Pluronic F-127 (Calbiochem)] and 100 μM probenecid (Sigma) at 37ºC for an hour. The slices were used between 1 to 4 hours after cutting and experimented on for no more than 8 hours after cutting.

Confocal Calcium Imaging

Fluo-4 loaded slices were gently stabilized in a chamber under a single wire over the cartilaginous parts of nose. The gassed ACSF solution continuously flowed over the slices (1.5–3.0 ml/min). Test solutions were applied using a small volume loop injector (500 μl) in line with the bath flow. A Zeiss LSM 510 Version 3.0 SP3 confocal laser scanning system was used for data collection and analysis (488 nm excitation filter for Fluo-4 and 568 nm excitation filter for Rosa-tdTomato). Time series experiments were performed collecting 256 x 256 pixel images at 1.27 Hz. Imaging studies were performed at 50–100 μm below the surface of the slice to avoid damaged cells. A z-stack of images, about

11–13 μm apart, was collected at the end of each experiment to confirm location of recording sites that were between the middle of the GCL to the edge of the mitral cell layer (MCL).

Immunocytochemistry

The whole skulls were prepared by removing skins, jaws, and eyes then fixed in 4% paraformaldehyde overnight at 4ºC. The heads were sequentially equilibrated with 15% and 30% sucrose prior to embedding in OCT compound and were stored at –80ºC. The 12 μm thick frozen sections were captured on glass slides using a cryostat microtome and stored at –20ºC. The sections were postfixed for 5 min in 4% paraformaldehyde/0.1 M PBS and rinsed thoroughly with PBS-0.2% Tween-20. Antigen retrieval was performed by incubating the slides in citrate buffer (10 mM sodium sodium citrate, 0.05% Tween-20, pH 6.0) for 2 minutes at 96^{o}C, then cooled to room temperature and rinsed several times in PBS. Nonspecific binding was blocked with 2% horse serum in PBS for 30 min at room temperature. Sections were incubated with a rabbit anti-Pac1 antibody [kind gift of Dr. Seiji Shioda or Aviva ARP59945, both 1:200 (Matsuno et al., 2008)] overnight at 4°C. After the primary antibody was removed, the sections were rinsed several times with PBS, and incubated with a secondary antibody (goat anti-rabbit Alexa 488, Jackson ImmunoResearch Laboratory, 1:300) for 1 hour at room temperature. The slides were washed 2 x 5 minutes in PBS, once for 5 minutes in water with DAPI, and cover slipped. The tissue sections were imaged on a Zeiss Axio Imager microscope using Axiovision software. Zero primary controls were run for all mouse lines and ages.

Chemicals and Drugs

The powder form of PACAP-27 (Phoenix Pharmaceuticals) was freshly dissolved in ACSF with 0.01% BSA (Sigma) kept on ice and discarded at end of each experiment day (~4 hours.) An ACSF loop of 0.01% BSA alone was used as a control. BSA was added to all other experimental solutions apart from the elevated K^+ (HK) solution. HK (95 mM NaCl, 50 mM KCl, 1 mM $MgCl_2$, 2 mM $CaCl_2$, 10 mM HEPES, 10 mM Glucose, and 100 μM probenecid) was applied to monitor the health of the slice and identify cells with voltage-gated Ca^{2+} channels. The PAC1R-specific antagonists M65 (Kind gift from Dr. Ethan Lerner, Harvard; Bachem) and PACAP 6-38 (Phoenix Pharmaceuticals) were stored at -40^{o}C until day of use. The 50 μM GABA solution was also made fresh every experiment day and kept on ice.

The dose response curve of PACAP included 1 nM, 10 nM, 20 nM, 40 nM, 60 nM, and 100 nM PACAP-27 with increasing washing times between each PACAP application to give the slices time to recover (>10 minutes after 10 nM, >20 minutes after 20 nM, >60 minutes after 40 nM, and >80 minute after 60 nM). To determine the possibility of partial desensitization between 40 nM and 60 nM, the order was reversed in a subset of slices.

40 nM PACAP was shown to affect both Ca^{2+} release from intracellular stores through the PLC pathway (2-APB; Enzo Life Sciences) and Ca^{2+} entry from extracellular space (Ca^{2+}-free extracellular solution) through the ACIII pathway (data not shown).

An antagonist cocktail containing 5 receptor/channel blockers was designed to allow recording of PACAP responses in the absence of synaptic transmission. The antagonist cocktail included 1 μM TTX (Na^+ channels; Sigma), 50 μM APV (NMDA; Tocris), 50 μM DNQX (AMPA/kainate; Tocris), 10 μM SR95531 ($GABA_A$; Tocris), 100 μM LY341495 ($mGluR_{1a, 2, 3,4a,5a,7a,}$ and $_8$; Tocris), and 10 μM CGP52432 ($GABA_B$; Tocris). The effectiveness of the antagonists was confirmed by blocking 50 mM L-glutamate or 50 μM GABA induced $[Ca^{2+}]_i$ responses in our slice preparation (data not shown.) PPADS ($P2Y_1$ and A_{2A}; Tocris) was also originally included in the cocktail, but omitted for the present data due to its significant side effect of decreasing resting $[Ca^{2+}]_i$ levels. In addition, Doengi et al. (2008) suggested that PPADS has no effect on $[Ca^{2+}]_i$ responses in the OB. The expression of purinergic receptors in the OB is primarily in the astrocytes and olfactory ensheathing cells [personal observations using SR101 astrocyte-labeling dye (Doengi et al., 2008; Doengi et al., 2009; Rieger et al., 2007)].[1] The interneurons in the OB, especially in juvenile mice, are believed to have little to no expression of purinergic receptors (Allen Brain Altas, 2013; Thyssen et al., 2013; Doengi et al., 2008).

Analysis

PACAP, GABA, and HK responsive cells within the tdTomato expressing cell population in the GCL zone were identified by measuring changes in

[1] Fischer et al. 2011 suggested that ATP acts as neurotransmitter on the glial cells, affecting the overall principal OB neuronal performance. The expression of the purinergic receptor gene is suggested to be found in all layers of OB in all major cells, but the actual functional expression would be in only the glial cells.

fluorescence intensity compared to baseline (ΔF). The BSA control was used to identify spontaneously active cells, which were removed from further analysis. The numbers of responsive cells were analyzed by placing regions of interest (ROIs) on each PACAP-induced responsive cell and measuring the latencies, time to peak, area under curve (120 recorded seconds of response), and amplitudes (Fig. 2.1). We considered measuring response durations, but these were difficult to measure at higher PACAP concentrations due to some post-PACAP repetitive oscillations lasting tens of minutes. To correct for the lag time between the loop injection and maximal stimulus delivery to the cells, the time between the start of loop injection to HK responses was subtracted from each PACAP trace. To obtain the area under curve (Ca^{2+} flux), Origin 6.0 was used to subtract a baseline from the data. After baseline subtraction, the area under the curve of ΔF from the start of the response to 120 secs was calculated using GraphPad Prism 5.

All cells that were counted as PACAP responding cells met the following three conditions: Firstly, the PACAP-induced $[Ca^{2+}]_i$ activity showed an amplitude increase of >5% above the baseline noise and a duration of >50 secs. Secondly, the response began at or after the average latency of HK (100–120 secs). Thirdly, the PACAP response started within the range of the HK duration, which is the approximate duration the antagonists would be on the tissue. For the experiments involving antagonists, which might block PACAP responses in individual cells, one more condition was met; the HK was applied before and after each PACAP plus/minus antagonist treatment. Only the PACAP-activated

cells that showed HK responses at the start and end of the series of runs were evaluated for PACAP responsiveness in the antagonists.

For counting the total number of PACAP, GABA, control BSA, and HK-responsive cells, the series of runs from each slice was exported from the LSM files (510 LSM Version 3.0 SP3) into ImageJ (http://rsbweb.nih.gov/ij/) as TIFF image sequence files of 200 to 500 images. The first 20–40 images in the sequence were summed and used as a baseline for subtracting from the remainder of the sequence to yield a picture of fluorescence changes (a.k.a. responding cells) occurring after the baseline time range. The baseline subtracted images showing responsive cells were superimposed on an image showing the red tdTomato labeled cells. Responsive cell counts were categorized into red and nonred labeled groups for each test substance. The counts were done blind.

Results

Heterogeneous PACAP Responses

Application of 40 nM PACAP routinely elicited increases in $[Ca^{+2}]_i$ in HK-responsive cells in slices of P4 mouse OB (Fig. 2.2, *A*–*E*). The PACAP-induced responses showed variation in latency and duration with some responses lasting over 20 minutes (Fig. 2.2 and data not shown). The predominate response was a sustained increase in $[Ca^{2+}]_i$ that reached a peak within seconds and then slowly returned to baseline over the course of minutes (796/1413 cells, 56%; Fig. 2.2*C*). The second most common response to PACAP was a single transient $[Ca^{2+}]_i$ increase (simple bursts) that returned to baseline within the duration of the

HK response (305/1413 cells, 22%; Fig. 2.2, *D* and *E*). Of the remaining 22% of PACAP responsive cells, the majority developed a slow "saw tooth" post-PACAP $[Ca^{2+}]_i$ oscillation (0.01–0.04 Hz, 246/1413 cells, 17%; Fig. 2*A*) and a few cells developed a fast "saw tooth" oscillation (0.05–0.1 Hz, 66/1413 cells, 5%; Fig. 2*B*). Kopp et al. (1999) found somewhat similar percentages in cultured SCNs: simple transients (20%), $[Ca^{2+}]$ oscillations (15%) and "sustained oscillations" (called biphasic response with initial $[Ca^{2+}]$ followed by plateau phase; 65%) (Kopp et al., 1999). PACAP-induced $[Ca^{2+}]_i$ oscillations lasted between 5 to 20-plus minutes (Fig. 2.2, *A* and *B*). Although the responses to PACAP were heterogeneous with cells in close proximity showing very different response patterns from each other, repeated PACAP application produced similar responses within the same cell (Fig. 2.3*A*). To determine the basis for the heterogeneity of the responses to PACAP, we examined the PACAP dose dependence, the kinetics, the developmental time course, and identified responding cell types within the GCL region of OB.

PACAP Concentration-response Curve

Dickson et al. (2006) tested the dose response curve of PACAP, VIP, and their antagonists using the cultured CHO cell line by measuring both the intracellular cAMP and Ca^{2+} concentrations (Dickson et al., 2006). They reported the PACAP 27 EC_{50} to be 10 nM. Because it is difficult to extrapolate from cell culture to in situ, we examined the dose dependence of PACAP 27 on slices from P2 to P5 pups. Unlike most regions of the rodent CNS, PACAP and PAC1R were shown to be spatially enriched in the OB at P0 and maintained within the

OB throughout development. The GCL in particular has high expression of PAC1Rs. The MCL was shown as a mixture of PACAP and PAC1R expression (Jaworski and Proctor, 2000; , 2013). For the dose curve (Fig. 2.3*B*), concentrations of PACAP were tested at 1, 10, 20, 40, 60, and 100 nM. To minimize desensitization to repeated PACAP applications, the minimum washing/recovery time was empirically determined for each concentration. Every slice had a maximum of four PACAP exposures with appropriate washing times between applications.

The dose response curve is presented as the ratio of PACAP responsive cells divided by HK responsive cells. By normalizing to the number of HK responsive cells, we are counting the number of PACAP sensitive cells among the healthy neurons in the GCL. For a slice to be deemed "healthy" we looked for approximately 80% of the visible cells to respond to HK. Thus, the dose response curve was based on the normalized percentage of PACAP responsive cells relative to the number of HK responsive cells recorded within 10 minutes of each PACAP application. We found that the percentage of PACAP responsive cells significantly increased with concentration. Although the curve did not saturate, we did not use concentrations higher than 100 nM because the responses to 100 nM PACAP did not desensitize and were not blocked with PAC1R antagonists.

Dickson et al. (2006), who used cultured CHO cells, did dose curves for a variety of PACAPs, VIPs, and their antagonists/agonists (Dickson et al., 2006). Interestingly, even though the CHO-cells PACAP $[Ca^{2+}]_i$ EC_{50} was 3–5 nM,

blocking about 80% of the 30 nM PACAP $[Ca^{2+}]_i$ activity required 10 μM M65 [a specific PAC1R antagonist from sand flies, (Yu et al., 2008)]. We found that a cocktail of 1 μM M65 and 150 nM PACAP 6-38 [a truncated version of PACAP which competitively binds the receptor (Robberecht et al., 1992)] was able to block an average of 84 ± 4% of 40 nM PACAP responses (52/278 cells; n = 5; $p < 0.05$ paired t-test). This confirms that the majority of the 40 nM PACAP responses in slices are blocked by the well characterized PAC1R antagonists (Fig. 2.3*C*).

Kinetics of PACAP Responses

To see whether there are any age-related changes in the kinetics of the PACAP effects, the slices were age-grouped as P2, P3, P4, and P5. The slices were treated using one of the two series of PACAP concentrations. The 10-20-40-60 nM PACAP series was tested on slices from 13 pups. The 20-60-40-100 nM PACAP series was tested on slices from 5 pups. No significant age-dependent or series dependent kinetic changes were found between P2 to P5 (data not shown). Thus, the slices were pooled together regardless of age between P2 to P5 for the kinetic analyses.

We measured the kinetics and amplitude of the PACAP-induced $[Ca^{2+}]_i$ activity as outlined in Fig. 2.1. We found that on average, the latency for PACAP responses decreased with increasing concentrations (significant between 10 nM and 20 nM to all higher concentrations [$p < 0.0001$, unpaired t-test; Fig. 2.4*A*)]. In addition, the time to peak also shortened between 40 nM to 100 nM, but was not statistically significant ($p = 0.06$, unpaired t-test; Fig. 2.4*B*).

The dose-dependent changes in fluorescence intensity amplitude with PACAP application did not follow a classic dose-response curve. Figure 2.4*C* shows that the average amplitude of PACAP responses increased significantly with concentrations up to 40 nM PACAP (range from $p \leq 0.01$ to $p < 0.0001$, unpaired t-test). Both 60 nM and 100 nM PACAP concentrations elicited significantly lower average PACAP response amplitudes ($p < 0.05$ between 40 nM and 100 nM; $p < 0.001$ between P40 and P60, unpaired t-test). By comparing amplitude histograms of PACAP responses to 40 nM with 100 nM PACAP, we observed a shift towards more cells with smaller amplitudes at 100 nM PACAP (Fig. 2.4*E*). The shift suggested that 100 nM PACAP might be recruiting downstream cells or perhaps cells with low PAC1R expression. To answer whether the higher PACAP concentrations prolong the cell $[Ca^{2+}]_i$ activity, the area under curve or Ca^{2+} flux was measured for the first 120 secs after PACAP reaches the slice (as determined by HK application). Figure 2.4*D* shows an overall increase in Ca^{2+} flux with increasing PACAP concentrations. The average Ca^{2+} flux of 100 nM PACAP responses is significantly greater than 20 nM, 40 nM, and 60 nM PACAP. Additionally, the Ca^{2+} flux induced by 20 nM PACAP is significantly lower than that of 40 nM and 60 nM PACAP ($p \leq 0.0006$ or $p < 0.0001$, unpaired t-test). However, the Ca^{2+} fluxes [areas under the curves (ΔF-seconds)] were not significantly different when comparing 40 nM and 60 nM PACAP.

Direct Versus Indirect PACAP Effects

The observation of a larger response amplitude at 40 nM as compared to 60 nM PACAP, as well as the ability to effectively block 40 nM PACAP, suggested that 40 nM was the ideal concentration for physiological experiments done on live acute OB slices. Therefore we used 40 nM PACAP for evaluating PACAP responses in the remainder of the studies. Because the dose-response curve for PACAP did not appear to saturate and showed the surprising increase in low amplitude responses at 100 nM PACAP, we questioned whether PACAP-induced increases in $[Ca^{2+}]_i$ were causing downstream glutamate or GABA release, which in turn increased the number of responsive cells. To tease out the cells that were directly activated by PACAP from those responding to possibly glutamate or GABA, we applied 40 nM PACAP in the presence and absence of a series of cocktails of neurotransmitter antagonists described in the Methods. The first cocktail (Glu/GABA/Na) was designed to block all downstream neurotransmission and any other possible pathways that may elevate the $[Ca^{2+}]_i$ in interneurons.

The Glu/GABA/Na cocktail contains antagonists for blocking NMDA, AMPA, mGluR (all types), $GABA_A$, and $GABA_B$ receptors. TTX was included to reduce occasional spontaneous action potentials. [The sodium channels however may have little to no role in PACAP downstream mechanisms (Pugh et al., 2010)]. We found that on average, the Glu/GABA/Na cocktail reduced the percentage of PACAP responding cells to 32 ± 5% of the PACAP control done on the same slice, (41/139 cells; n = 4 slices; Fig. 2.5). Overall, 41 of the 139 cells

that responded to the PACAP control also responded to PACAP + Glu/GABA/Na antagonists and were therefore directly activated by PACAP. We evaluated the kinetics of those 41 cells using the same approach as for PACAP at different concentrations (Fig. 2.6*A*). Only the latency was not significantly changed. Amplitude ($p = 0.01$, paired t-test), time to peak ($p < 0.01$, paired t-test), and the area under curve ($p < 0.001$, paired t-test) were significantly reduced in the presence of the antagonist cocktail, suggesting the involvement of GluRs and GABARs in the $[Ca^{2+}]_i$ response to PACAP even within cells directly activated by PACAP (Fig. 2.6*B*).

To examine the independent effects of the downstream glutamate receptors (GluRs) versus GABA receptors (GABARs) in the presence of PACAP, the antagonist cocktail described above was separated into two groups. The groups are GluR-only antagonists (NMDA, AMPA, and mGluRs) and GABAR-only antagonists ($GABA_A$ and $GABA_B$). The antagonist for sodium channels (TTX) was not included in the individually grouped cocktails because we wanted to see whether blocking one or another group had consequences on the occasional global spontaneous action potentials (none was seen within the duration time of blockage; data not shown). Addition of GluR antagonists reduced the number of PACAP-responding cells to 26 ± 3% of PACAP control (31/118 cells, n = 3; Fig. 2.5). GABAR-only antagonists reduced PACAP responses to 54 ± 11% of the PACAP control (67/129 cells, n = 4; Fig. 2.5). This indicates that GluRs are the main contributor to the downstream $[Ca^{2+}]_i$ activity. GABARs appear to augment the activity of GluRs, by either increasing or

decreasing the $[Ca^{2+}]_i$ response intensity, depending on cell maturity. GABA is excitatory in neuroblasts and immature neurons, further increasing the post-PACAP $[Ca^{2+}]_i$ activity. In mature neurons, GABA is inhibitory and may decrease the elevation of $[Ca^{2+}]_i$ in the PACAP control. PACAP responses in mature neurons show a greater increase in $[Ca^{2+}]_i$ in the presence of GABAR antagonists due to less GABAergic inhibition. A subset of slices was tested with both blocker cocktails sequentially. PACAP-responsive cells were activated by PACAP in the presence of GABAR-only antagonists but their response to PACAP was blocked by GluR-only antagonists (24 out of 40 cells; n = 2) further supporting the conclusion that the majority of the downstream PACAP-induced effects are mediated by glutamate (Fig. 2.7).

PACAP Effects on Non-GC Cells of OB

The GCs activity within the OB network can be influenced by negative and positive feedback of other types of OB cells. The glutamatergic $PAC1R^+$ mitral cells (labeled with PCdh21 tdTomato), which release glutamate onto GCs, responded to 40 nM PACAP, typically initiating the sinusoidal-like waves shown in Fig. 2.8. Blanes cells are also $PAC1R^+$, and they release GABA neurotransmitters onto hundreds of GCs throughout the GCL (Pressler and Strowbridge, 2006). Cells of appropriate size and location to be Blanes cells responded to 40 nM PACAP with transient $[Ca^{2+}]_i$ increases (unpublished observations).

Role of PACAP in Maturation of Dlx2 and GAD65 tdTomato Expressing Cells in GCL

The connection of GCs to the OB network depends on the maturity of the cells. In the next section, we look at the rapidly developing OB between P2 to P5. It is known that the interneuron precursors (neuroblasts) take about 3 days to migrate from their origin in the subventricular zone (SVZ) to the OB, which not surprisingly correlates with the rapidly growing OB increasing from 25% of adult interneurons at P0 to 55% by the end of the first week (Lemasson et al., 2005).

In order to specifically identify PACAP responsive cells in the GCL, we primarily used two lines of IRES-CRE-linked transgenic mice: Dlx2-CRE and GAD65-CRE, which were crossed with the Rosa-tdTomato (using the ROSA26-CAG promoter) transgenic mice line to provide gene-specific red cells. The ROSA26-CAG promoter was used to label IRES-CRE-linked *Dlx2,* an essential migrating gene, at the neuroblast stage (Batista-Brito et al., 2008). The SVZ-born *Dlx2*-labeled neuroblasts, which have migrated to the olfactory bulb, become both types of GABAergic GCs (GAD65 and GAD67) as well as periglomerular cells (Plachez and Puche, 2012). Although Dlx2 is switched off in mature cells, the red fluorescence remains throughout the cell lifespan. The Dlx2-tdTomato is expected to label the majority of GCs residing in the GCL (Potter et al., 2009). Figure 2.9 shows the expression of Dlx2 tdTomato (red) in 12 µm sections of OB from P2 and P4 mice. PAC1R-specific antibody labeling (green) colocalizes with a subset of Dlx2 expressing cells in the GCL and labels mitral cells in the MCL. Compared to total cell counts using DAPI nuclear

staining, 89% (1735/1945; n = 2) of GCL cells are $Dlx2^+$ and 21 ± 1% (535/3160 cells; n = 3) are colabeled with PAC1R antibodies at P2, while in the P4 OB, the percentage of cells colabeled with both $Dlx2^+$ and PAC1R antibody increases to 34 ± 1% (836/2979 cells; n = 4). The 34 ± 1% of $PAC1R^+$ cells in the immuncytochemistry (ICC) at P4 correlates nicely with the percentage of cells that responded directly to PACAP in the presence of Glu/GABA/Na antagonists (32 ± 5%; ages P4–P6; Fig. 2.6). The second transgenic mice line was the GABAergic GAD65 tdTomato, in which the ROSA26-CAG promoter was used to label the IRES-CRE-linked *GAD65* gene. The use of the GAD65 label helps narrow the evaluation of the cells in the GCL down to two GABAergic subtypes. In 8-week old mice, about 50% of the OB GABAergic GCL cells express GAD65 (Parrish-Aungst et al., 2007). The other 50% are generally the larger GAD67 expressing cells. However, 20% of the GABAergic GCL cells are capable of expressing both GAD65 and 67 (Parrish-Aungst et al., 2007). GAD65 and GAD67 protein expression is not turned on until the cells exit the migratory pathway, but these subtypes are predetermined while still neuroblasts in the SVZ. The similar timings of protein expression suggest that both subtypes enter the OB at similar developmental stages (Plachez and Puche, 2012; De et al., 2007; Kelsch et al., 2007; Merkle et al., 2007). Figure 2.10 shows the labeling of GAD65 (red) in P2 and P4 mice. The Dlx2 and GAD65 transgenic lines were used for the identification of mature and immature neuronal cells in the PACAP versus GABA experiments.

Using GABA Responses to Identify Immature GCs

To help discern whether PACAP is activating mature or immature GCs, we used GABA to elevate the $[Ca^{2+}]_i$ in immature cells. Figure 2.11 is a diagram showing how the GABA neurotransmitter acts as an excitatory neurotransmitter in migrating neuroblasts or immature neurons. In neonatal OBs, the immature neuroblast cells elevate internal $[Ca^{2+}]_i$ in response to GABA as they migrate over long distances to their destinations (Dzhala et al., 2010; Tong et al., 2009; Darcy and Isaacson, 2009; Mejia-Gervacio et al., 2011; Wang and Kriegstein, 2008). GABA binds to ionotropic $GABA_A$ receptors and the cell will either depolarize or hyperpolarize, depending on intracellular Cl^- concentration. Immature neurons maintain high intracellular Cl^- levels via activity of highly expressed Na^+-K^+-Cl^- cotransporter 1 (NKCC1) transporting Cl^- into the cell (Dzhala et al., 2010; Takayama and Inoue, 2004; Glykys et al., 2009; Wang et al., 2005). Thus $GABA_A$ receptor activation of migrating neuroblasts and immature neurons causes Cl^- to exit the cell. The resulting Cl^- efflux depolarizes the cell and opens the voltage-gated Ca^{2+} channels (Glykys et al., 2009). In mature neurons, NKCC1 is downregulated and internal Cl^- is kept low with the increased expression of K^+- Cl^- cotransporter 2 (KCC2), so opening of $GABA_A$ channels hyperpolarizes the cell. Thus immature neurons can be physiologically distinguished from mature neurons by $[Ca^{2+}]_i$ responses to GABA (Wang and Kriegstein, 2008). Figure 2.12*A* shows an example of a functionally immature cell responding to 50 μM GABA with an increase in $[Ca^{2+}]_i$.

Based on Ca^{2+} responses to sequential application of GABA and PACAP (Fig. 2.12*B*), 3 groups of cells were identified in the GCL of neonatal OB. The first group is the "GABA-only" GCs, which respond to GABA and not PACAP (Fig. 2.12*C*). The GABA-only GCs may or may not become $PAC1R^{+}$ when mature. The 'GABA+PACAP' group in Fig. 2.12*C* includes the GCs that respond to both GABA and PACAP with increases in $[Ca^{2+}]_i$, implying that they are immature cells with either expression of PAC1Rs on the plasma membrane or some early connections formed. The "PACAP-only" group in Fig. 2.12*C* includes the presumably mature GCs that respond to PACAP but do not increase $[Ca^{2+}]_i$ in response to GABA. Both transient increases and repetitive oscillations in $[Ca^{2+}]_i$ activity are seen for PACAP-responsive cells in the GABA+PACAP and PACAP-only groups (Fig. 2.12*C*).

Age-related Increases in the Percentage of
PACAP Responsive Granule Cells

Figure 2.13*A* shows the calculated percentage of all GABA and/or PACAP responsive cells labeled red for Dlx2. The graph shows a shift in the percentage of immature GABA-only cells at P2 (n = 8 mice; 867 cells) to mature PACAP-only cells at P5 (n = 5 mice; 967 cells). This shift suggests that GCs express functional PAC1 receptors during their maturation process. The nonred cell counts in the images taken from Dlx2-dt Tomato mice made up 6% (165/2708 cells; n = 20 mice) of the GABA and/or PACAP responsive OB GCL cells across all ages evaluated. The Blanes cells, which originate in the OB and do not migrate from the SVZ (Plachez and Puche, 2012), may account for 2–3% of the

unlabeled population. The other 3–4% of unlabeled responsive cells might be other non-Blanes interneurons in the GCL.[2] (The glial cells such as astrocytes are not a factor in the analysis, please see discussion.)

Figure 2.13*B* shows the calculated percentages of all $GAD65^+$ GABA and/or PACAP responsive cells. The graph shows no significant change for all three groups within the age range studied. Figure 2.13*C* shows the percentages of the GAD65 dtTomato nonred cells ($GAD65^-$), which we assume to be GAD67 cells since all of the interneurons in the GCL are either $GAD65^+$ or $GAD67^+$ or both $GAD65^+$ and $GAD67^+$ (Batista-Brito et al., 2008; Lemasson et al., 2005; Parrish-Aungst et al., 2007). As with the Dlx2 labeled cells, the $GAD65^-$ cells shifted from mostly GABA-only cells to PACAP-only cells between P2 (n = 3 mice; 41 cells) and P5 (n = 8 mice; 67 cells). Out of all of the GABA and/or PACAP responsive $GAD65^-$ cells, those responding only to GABA (immature) made up an average of 50 ± 3% at P2 (20/41 cells) and decreased to 24 ± 6% by P5 (18/67 cells) ($p < 0.005$). Those cells responding to both GABA and PACAP (maturing) decreased from an average of 30 ± 2% at P2 (12/41 cells) to 11 ± 3% by P5 (8/67 cells) ($p = 0.001$). Conversely, although only an average of 20 ± 5% of the $GAD65^-$ cells responded to PACAP at P2 (9/41 cells), their numbers increased to 53 ± 9% by P5 (41/67 cells) (mature; $p = 0.01$).

[2] Pressler et al (2006) accumulated an informal list of GCL minority cells: Golgi cells (deep GCL), Stellate cells (deep GCL), Vertical cells of Cajal, Bitufted neurons, Short Axon cells (near MCL), and Horizontal cells (near MCL).

Discussion

In the studies described above, we found that PACAP is capable of eliciting $[Ca^{2+}]_i$ responses in cells at various stages of maturation in the GCL and ML of the olfactory bulb in P2–P5 mice. We found that the PACAP-induced $[Ca^{2+}]_i$ changes were heterogeneous and dependent on both direct activation of PAC1 receptors and on subsequent recruitment of additional cells through downstream release of glutamate and GABA. The percentage of functional PAC1R expressing cells in the GCL that were directly activated by PACAP increased over the P2–P5 time window and matched the percentage of $PAC1R^+$ cells identified by immunocytochemistry. By utilizing mouse lines that express the red tdTomato in specific cell types, we determined that the $Dlx2^+$ cells that migrate into the OB via the RMS are capable of responding to PACAP before they transition to mature GCs. The further subdivision of the migrating GC population into GAD65 and GAD67 subtypes revealed the surprising observation that the time-dependent increase in mature PAC1R expressing cells observed in the Dlx2 studies occurs as a result of maturation in the GAD67 GCs but not the GAD65 GCs. This observation supports our hypothesis that PACAP activation of immature GCs initiates developmentally important $[Ca^{2+}]_i$ oscillations during the first postnatal week of development.

The OB interneuron response to PACAP in acute slices shows that the majority of the $[Ca^{2+}]_i$ activity occurs through downstream activation of both the glutamate and GABA receptors on non-$PAC1^+$ GCs, providing a wide variety of $[Ca^{2+}]_i$ activity responses ranging from simple transients, slow to fast saw tooth

oscillations, and sustained oscillations (Fig. 2.2). Possible factors contributing to the variety of responses are the dose of PACAP (Figs. 2.3 and 2.4) and the downstream PACAP-induced activation of glutamate and/or GABA receptors (Figs. 2.5, 2.6, and 2.7). The time to peak is constant across the concentrations tested, but was shown to decrease in Glu/GABA/Na antagonists. The faster time to peak when downstream contributions to the $[Ca^{2+}]_i$ signal are blocked supports the idea that PAC1R activation initiates the $[Ca^{2+}]_i$ response, but it is the PACAP-mediated GABA and glutamate release that augments the signal in both the directly and indirectly activated cells. The increase in Ca^{2+} flux with increased concentrations of PACAP suggests an increasing glutamate and/or GABA release onto GluRs and/or GABARs. This is supported by the observation that the co-application of GluRs and/or GABARs antagonists with PACAP reduced the PACAP-induced $[Ca^{2+}]_i$ increases in the majority of cells (Fig. 2.7). Collectively, these findings suggest that PACAP may be an important modulator of glutamate and GABA release in developing mouse OB.

The factor appearing to have no significant effect on PACAP-induced Ca^{2+} kinetics and intensities during first neonatal week is age; the P2, P3, P4, and P5 age groups show similar responses in terms of latency, time to peak, amplitude and Ca^{2+} flux (data not shown). However, the percentage of PACAP-responding cells does rapidly increase during the first neonatal week (Fig. 2.13.) The day-to-day shift from immature GABA-only neuroblasts at P2 to mature PACAP-only GCs at P5 appears to be driven by the maturation of the GAD67 subtype of GCs. The increase in PACAP responsive cells correlates with the noted increase in

PAC1R$^+$ between P2 and P4 according to the ICC results [21 ± 1% in P2 (n = 3; 3160 cells); 34 ± 1% in P4 (n = 4; 2979 cells)].

Despite having the same rate of development as GAD65 cells upon entering the OB, the GAD67 cell subtype develops complicated connections to PAC1R$^+$ projection neurons such as MCs (Plachez and Puche, 2012). It is still unclear when, if actually ever, the GAD65 subtype GCs shift from mostly immature, PACAP unresponsive cells to mature PACAP-responding ones.

Dose Dependence and Block of PACAP Responses

The reported EC_{50} for PACAP responses ranges between 0.25 and 3 nM in cell culture systems, and increases to 30–50 nM PACAP in acute slices (Jozwiak-Bebenista et al., 2007; Kambe and Miyata, 2012; Nicot and Dicicco-Bloom, 2001; Dickson et al., 2006). *In vitro* experiments used as much as 100 nM PACAP (one used 200 nM) to obtain maximal neuroprotective effects (Basille-Dugay et al., 2013; Dziema and Obrietan, 2002; Kopp et al., 1999; Kopp et al., 2001; Masmoudi et al., 2003; Pugh et al., 2010; Scharf et al., 2008; Vaudry et al., 2002). At least one lab also used extremely high [PACAP] doses in slices (Sun et al., 2003). In contrast to the studies in cell lines, Jozwiak-Bebenista et al. (2007) measured a PACAP EC_{50} ~0.25 nM for both primary cultured neuron and astrocyte cells. They also tested acute cerebral cortical slices, which are PAC1R$^+$ rich compared to the majority of the CNS apart from the OB and obtained an EC_{50}~30 nM (Jozwiak-Bebenista et al., 2007). At least two different studies (Masmoudi et al., 2003; Vaudry et al., 2002) confirmed that responses to 100 nM PACAP in cultured cells are blocked using only PACAP 6-38 (PACAP 38

with first 6 peptides deleted). Other studies used between 1 to 10 nM PACAP in the cultures and showed block using only PACAP 6-38 (Kambe and Miyata, 2012; Shioda et al., 2006; Vaudry et al., 2002). The doses of PACAP 6-38 were reported to be 600 to 1000 nM. The dose-response curve for our OB slices suggested that 40 nM PACAP is ideal for our $[Ca^{2+}]_i$ imaging approach because response amplitudes decreased at higher PACAP concentrations possibly due to desensitization during the PACAP application. Unlike the previous cell culture studies, we were unable to completely block 40 nM PACAP-induced $[Ca^{2+}]_i$ activity when using as much as 1 μM PACAP 6-38 (data not shown), perhaps because we study our cells in slices. Costa et al. (2009) used hippocampus slices, and they were able to block 0.5 nM PACAP with 500 nM PACAP 6-38. However, at 10 nM, PACAP was not blockable at 500 nM PACAP 6-38 (Costa et al., 2009).

PACAP has the characteristics of other cell-penetrating peptides and was shown capable of crossing the plasma membrane through direct translocation and endocytosis, without the aid of receptors (108;109). Intracellular PACAP is able to activate the intracellular PAC1Rs N-terminal ends. PACAP also moves from cell to cell and exits back out into extracellular space (Doan et al., 2012a; Doan et al., 2012b). This is noteworthy because it may explain why responses to 100 nM PACAP are unaffected by the PAC1R antagonist cocktail used to reduce 40 nM PACAP by 84 ± 4%. Furthermore, 100 nM PACAP responses are not blocked by the cocktail of Glu/GABA/Na blockers (data not shown). Collectively, our data suggest that responses to 100 nM PACAP may be insensitive to PAC1R

antagonists because PACAP is translocated and acting intracellularly. The 16% of the 40 nM PACAP responses that are not blocked by PAC1R antagonists may also reflect intracellular PACAP activity. Studies beyond the scope of the present work will be required to confirm these observations. Other less likely explanations include activation of VPAC1/2Rs by the 100 nM PACAP as discussed below.

VPAC Receptors Are Not Mediating PACAP Responses

PACAP acts primarily through PAC1Rs. However, PACAP also can trigger Ca^{2+} increases through VPAC1/2Rs (Inglott et al., 2012). The question of whether 100 nM PACAP was not blocked by PAC1R antagonists due to the activation of VPAC1/2Rs was considered. The VPAC1/2Rs are the primary receptors for vasoactive intestinal peptide (VIP). Interestingly, no VIP-induced Ca^{2+} activity was observed when up to 1 μM VIP was applied to the slices from mice < P5 in age with (data not shown.) Concentrations of VIP higher than 1 μM were not tested because this amount has the potential of acting through the PAC1Rs (Dickson et al., 2006). At least one other lab reported no $[Ca^{2+}]_i$ activity when 100 nM VIP was applied to cultured suprachiasmatic nucleus from 1–7 neonatal day old rats (Kopp et al., 1999). The Allen Brain Atlas mRNA labeling of VPAC1/2Rs was shown in OBs of older mice. The OBs of the P4 mice however have no detectable VPAC1/2R expression (Allen Brain Altas, 2013). What may correlate to the difficulty of blocking 100 nM PACAP *in situ* was the recent finding discussed above suggesting that the PACAP peptide is membrane permeable, activating the intracellular PAC1Rs and sometimes repermeating upon exit from the cells (Dickson et al., 2006; Doan et al., 2012a).

Direct vs Indirect PACAP-induced Ca^{2+} Transients and Oscillations

PACAP binding to PAC1Rs is capable of activating numerous pathways that increase $[Ca^{2+}]_i$, including Ca^{2+}-dependent synaptic release and Ca^{2+}-induced Ca^{2+} release (Kambe and Miyata, 2012; Pugh et al., 2010; Doan et al., 2012a; Doan et al., 2012b). The black arrows in Fig. 2.7 show the initiation of a Ca^{2+} oscillation at the approximate time when the applied PACAP and the GluR + GABAR antagonists are washed out. This suggests that the directly activated $PAC1R^+$ cells increase $[Ca^{2+}]_i$ and synaptically release glutamate and/or GABA onto both immature and mature cells to prolong the oscillation (Figs. 2.2, 2.5, 2.6, and 2.7). The role of GluRs and/or GABARs on the pattern of oscillation was individual and independent. The uniqueness of each oscillation pattern likely depends on the network connections, cell maturity (GABA-induced excitation discussed below), and expression of the GluRs and/or GABARs. The PACAP-induced downstream oscillations are catalogued into three general groups. Figure 2.7*A* shows an example cell believed to be $PAC1R^+$ and directly-activated by PACAP because it showed strong PACAP response regardless of antagonists. Figure 2.7*B* shows an indirectly activated cell in which PACAP-induced Ca^{2+} oscillations were present when GABAR-only antagonists were co-applied with PACAP, but the GluR-only antagonists completely blocked the PACAP-induced calcium activity. Figure 2.7*C* shows an example cell in which PACAP responses are blocked by both groups of antagonists and displays only indirect post-PACAP activation after the antagonists and PACAP are washed out

(black arrows). The example cells showed that any of these cells may have different post-PACAP $[Ca^{2+}]_i$ oscillations compared to PACAP-control when GluRs and/or GABARs were blocked in PACAP treatment (Fig. 2.7, *A*, *B*, and *C*). Figure 2.6 showed that when antagonists block Glu/GABA input, the PACAP-induced Ca^{2+} responses are significantly reduced in terms of amplitude, time to peak, and total Ca^{2+} flux.

The vehicle controls of the antagonist cocktails showed no $[Ca^{2+}]_i$ activity in the presence of the Glu/GABA/Na cocktail. However, in the case of either GluR-only cocktail or GABAR-only cocktail antagonist controls, the cells often displayed brief $[Ca^{2+}]_i$ transients (~50 second bursts of Ca^{2+} activity; blue arrows, Fig. 2.7) before the typically delayed start of the PACAP long-term $[Ca^{2+}]_i$ activity. The antagonist-induced activity is likely due to a block of the essential feedforward and feedback signaling between the GABAergic and glutamatergic OB cells. When blocking only the GABARs (Fig. 2.7*B*), a temporary lack of inhibition in mature cells with GluRs may account for the increased $[Ca^{2+}]_i$ activity throughout the OB network. The lower effectiveness of GABAR antagonists in reducing indirect PACAP responses suggested that the majority of PAC1R negative cells are either mature GCs or immature GCs with GluRs.

GABA as an Excitatory Marker of Immature GCs

The neurotransmitter GABA has been was shown to either inhibit or excite the GCs depending on the $[Cl^-]_i$. GABA excitation occurs in immature cells with high $[Cl^-]_i$ and can be monitored as increased $[Ca^{2+}]_i$ in response to GABA-induced depolarization and activation of voltage-gated Ca^{2+} channels. Excitatory

GABA is believed to aid in the precise, orchestrated development of the OB interneurons (Mejia-Gervacio et al., 2011; Takayama and Inoue, 2004; Gascon et al., 2006). The GABA as an excitatory transmitter concept was challenged and proposed to be an artifact due to traumatic changes in conditions when making and recording from slices (Bregestovski and Bernard, 2012; Khakhalin, 2011). Ben-Ari (2012) counterchallenged the suggestion that GABA excitation was an artifact in slices. A few of the many points presented were 1) adult slices are more susceptible to energy deprivation, but they do not generate the GABA excitatory action thought to occur in injured neurons. 2) The MCs, which were matured by P0, were inhibited by GABA. GCs on the other hand are a mixture of immature and mature cells, especially during the first postnatal week and can be depolarized and/or excited by GABA. Both of these types of cells are at similar depths. 3) In many studies in which both surface and deep neurons were recorded, the cells showed similar profiles with no signs of swelling (Ben-Ari et al., 2012; Wang et al., 2005; Wang et al., 2008).

The GABA-induced simple Ca^{2+} transients, however, do not always show up, as in a couple of traces marked with a "?" in Fig. 2.7. Chub and O'Donovan (2001, 2005, and 2006) used data from chick embryos to suggest that the occasional absence of GABA-induced Ca^{2+} activity is because the intracellular Cl^- concentration has temporarily decreased to the point of being less excitatory when the $GABA_A$ receptors open. The Cl^- transporters are shown to be relatively slow in accumulating Cl^- back into the cell (Chub and O'Donovan, 2001; Chub et al., 2006; Marchetti et al., 2005).

Astrocytes Are Not a Factor in Data Analysis

Astrocytes are PACAP and GABA excitable (Hansson et al., 2009; Jozwiak-Bebenista et al., 2007). The EC_{50} of PACAP in cultured glial cells (astrocytes) is almost exactly the same as for cultured neuronal cells. However, when we used SR-101 (a red dye labeling astrocytes) on slices, we find astrocytes to be star-like shaped cells appearing as "background" and having little to no $[Ca^{2+}]_i$ response to 40 nM PACAP, suggesting that the astrocytes in OB slices have a different physiology than in cultures and/or higher EC_{50} than the surrounding OB interneurons. The concentration of GABA used in our experiments was 50 μM. Doengi et al. (2009) used $[Ca^{2+}]_i$ signaling to determine the GABA EC_{50} of 35 μM in neurons and 100 μM in astrocytes with a few astrocytes responding to 20 μM GABA (Doengi et al., 2009). Accordingly, our 50 μM GABA may excite a small number of astrocytes. However, the unique star-like shape of astrocytes with typically weak $[Ca^{2+}]_i$ intensity is discernible from the smaller, rounder, stronger $[Ca^{2+}]_i$ intensity GCs.

Cell Types and Development in GCL

For the age range (P2 to P5) studied, about 97–98% of the OB GCL is composed of GCs and the other 2–3% is made of primarily large, rotund, GABAergic Blanes cells. [The percentage of the Blanes cells to other types of OB cells diminishes down to 1–2% when the OB reaches adult size (Batista-Brito et al., 2008).] Thus, approximately all of the Dlx-2 labeled cells in the GCL are

GCs.[3]

The majority of Fig. 2.13*A* Dlx2-labeled GCs shifted from immature cells that only responded to GABA at P2 to mature GCs that only respond to PACAP by P5. The relatively rapid changes in maturation over the 3-day period may be affected by the migration of SVZ progenitors covering the distance to the OB in a matter of 3 days [in rats; this may happen in less time for mice, which are smaller and faster developing (Yang, 2008)]. The survivorship of newly generated cells in the GCL may change with age, but the data in the work done by Lemasson et al. (2005) suggested that the density of surviving cells was unchanged between P3 to P7 (Lemasson et al., 2005). This may mean the survival of cells in the age range studied may have little to no factor in the shift. Dlx2 labels both GAD65 and GAD67, so GAD65 was evaluated as a subtype of GCs. Interestingly, GAD65-labeled GCs showed no significant shift from GABA-only to PACAP-only (Fig. 2.13*B*). The significant shift from GABA-only to PACAP-only for $Dlx2^+$ GCs may be the GAD67 cells, the results for which (Fig. 2.13*C*) are similar to the results for $Dlx2^+$ GCs (Fig. 2.13*A*). The $PAC1R^+$ GAD67 cells in general may need to mature within the first week as they are multiglomerular neurons connecting to a broader complex network within the GCL, while GAD65s neurons have uniglomerular dendritic projections (Kiyokage et al., 2010; Parrish-Aungst et al., 2007). In the GAD65 cells, the ratio of GABA to PACAP responding cells

[3] In the Batista-Brito 2008 reference, the Blane cells are said to be derived from the Dlx1/2 expressing precursor domain, but in the Dlx2 dt-Tomato transgenic mice used for both the ICC and calcium imagings, the Blane cells do not appear to be labeled as Dlx2.

may change outside the age range studied. The hypothesis for any future evaluation is that the change among GAD65 cells may occur somewhere between about P7 and P14. Supporting this hypothesis are the other studies suggesting that the OB reaches 80% of the average adulthood number of cells at P7 (98% for P14) (Lemasson et al., 2005; Mirich et al., 2002). Furthermore, norepinephrine modifies the OB response in neonatal pups and the supply of this neurotransmitter from the locus coeruleus is reduced at P10 (Raineki et al., 2010). In addition, Lopez-Bendito et al. (2004) showed an increase in GABA production in $GAD65^+$ cells [indicating mature interneurons acting as inhibitors between E18 (48%) and P21 (70%) (Lopez-Bendito et al., 2004)]. Since we see no $GAD65^+$ cells shift from immature excitatory GABA responsive cells to mature GCs that only show excitatory responses to PACAP between P2 and P5, the significant maturation of $GAD65^+$ cells is expected to occur in the second to third postnatal week.

Conclusion

Cells that migrate into the OB during the first postnatal week initially have high excitatory responses to GABA and low responses to PACAP. However, even by P2 there are cells that are in all stages of functional maturation in terms of responding to both PACAP and GABA or only responding to PACAP. Our studies indirectly show that the cells mediating the shift in maturation profiles are the $GAD65^-$ cells, which we assume are $GAD67^+$ since that is the only other GAD expressing interneuron in the OB. PACAP seems to initiate long lasting $[Ca^{2+}]_i$ activity in the developing OB that is mainly amplified by glutamatergic pathways,

but there is also a significant contribution from GABA. While it is still unclear as to the developmental role of PACAP in postnatal development, these studies clearly show that PAC1 receptors become functional while the cells are still in the maturation process and remain functional after cells mature. The GCL network of GluRs and/or GABARs has an important role in modulating the $[Ca^{2+}]_i$ activity in both immature and mature GCs. The suggestions for future works are to better understand why GAD67 and GAD65 appear to have a majority shift from immature to mature cells at seemingly different time windows even through both subtypes develop and function during a similar time window. It is not as clear when most GAD65 cells will mature as it is as for GAD67 cells, but the GAD65 window appears to not be during the first neonatal week.

Reference List

1. Allen Brain Altas. 2013.
2. **Ago Y, Yoneyama M, Ishihama T, Kataoka S, Kawada K, Tanaka T, Ogita K, Shintani N, Hashimoto H, Baba A, Takuma K, Matsuda T**. Role of endogenous pituitary adenylate cyclase-activating polypeptide in adult hippocampal neurogenesis. *Neuroscience* 172: 554–561, 2011.
3. **Allais A, Burel D, Isaac ER, Gray SL, Basille M, Ravni A, Sherwood NM, Vaudry H, Gonzalez BJ**. Altered cerebellar development in mice lacking pituitary adenylate cyclase-activating polypeptide. *Eur J Neurosci* 25: 2604–2618, 2007.
4. **Arimura A**. Perspectives on pituitary adenylate cyclase activating polypeptide (PACAP) in the neuroendocrine, endocrine, and nervous systems. *Jpn J Physiol* 48: 301–331, 1998.
5. **Atlasz T, Szabadfi K, Kiss P, Tamas A, Toth G, Reglodi D, Gabriel R**. Evaluation of the protective effects of PACAP with cell-specific markers in ischemia-induced retinal degeneration. *Brain Res Bull* 81: 497–504, 2010.
6. **Basille-Dugay M, Vaudry H, Fournier A, Gonzalez B, Vaudry D**. Activation of PAC1 receptors in rat cerebellar granule cells stimulates both

calcium mobilization from intracellular stores and calcium influx through N-type calcium channels. *Front Endocrinol (Lausanne)* 4: 56, 2013.

7. **Batista-Brito R, Close J, Machold R, Fishell G**. The distinct temporal origins of olfactory bulb interneuron subtypes. *J Neurosci* 28: 3966–3975, 2008.

8. **Baxter PS, Martel MA, McMahon A, Kind PC, Hardingham GE**. Pituitary adenylate cyclase-activating peptide induces long-lasting neuroprotection through the induction of activity-dependent signaling via the cyclic AMP response element-binding protein-regulated transcription co-activator 1. *J Neurochem* 118: 365–378, 2011.

9. **Ben-Ari Y, Woodin MA, Sernagor E, Cancedda L, Vinay L, Rivera C, Legendre P, Luhmann HJ, Bordey A, Wenner P, Fukuda A, van den Pol AN, Gaiarsa JL, Cherubini E**. Refuting the challenges of the developmental shift of polarity of GABA actions: GABA more exciting than ever! *Front Cell Neurosci* 6: 35, 2012.

10. **Blechman J, Levkowitz G**. Alternative splicing of the pituitary adenylate cyclase-activating polypeptide receptor PAC1: mechanisms of fine tuning of brain activity. *Front Endocrinol (Lausanne)* 4: 55, 2013.

11. **Botia B, Basille M, Allais A, Raoult E, Falluel-Morel A, Galas L, Jolivel V, Wurtz O, Komuro H, Fournier A, Vaudry H, Burel D, Gonzalez BJ, Vaudry D**. Neurotrophic effects of PACAP in the cerebellar cortex. *Peptides* 28: 1746–1752, 2007.

12. **Bourgault S, Vaudry D, Dejda A, Doan ND, Vaudry H, Fournier A**. Pituitary adenylate cyclase-activating polypeptide: focus on structure-activity relationships of a neuroprotective Peptide. *Curr Med Chem* 16: 4462–4480, 2009.

13. **Bregestovski P, Bernard C**. Excitatory GABA: how a correct observation may turn out to be an experimental artifact. *Front Pharmacol* 3: 65, 2012.

14. **Breton-Provencher V, Lemasson M, Peralta MR, III, Saghatelyan A**. Interneurons produced in adulthood are required for the normal functioning of the olfactory bulb network and for the execution of selected olfactory behaviors. *J Neurosci* 29: 15245–15257, 2009.

15. **Chen Y, Samal B, Hamelink CR, Xiang CC, Chen Y, Chen M, Vaudry D, Brownstein MJ, Hallenbeck JM, Eiden LE**. Neuroprotection by endogenous and exogenous PACAP following stroke. *Regul Pept* 137: 4–19, 2006.

16. **Chub N, Mentis GZ, O'Donovan MJ**. Chloride-sensitive MEQ fluorescence in chick embryo motoneurons following manipulations of

chloride and during spontaneous network activity. *J Neurophysiol* 95: 323–330, 2006.

17. **Chub N, O'Donovan MJ**. Post-episode depression of GABAergic transmission in spinal neurons of the chick embryo. *J Neurophysiol* 85: 2166–2176, 2001.

18. **Costa L, Santangelo F, Li VG, Ciranna L**. Modulation of AMPA receptor-mediated ion current by pituitary adenylate cyclase-activating polypeptide (PACAP) in CA1 pyramidal neurons from rat hippocampus. *Hippocampus* 19: 99–109, 2009.

19. **Cowan CM, Roskams AJ**. Apoptosis in the mature and developing olfactory neuroepithelium. *Microsc Res Tech* 58: 204–215, 2002.

20. **Darcy DP, Isaacson JS**. L-type calcium channels govern calcium signaling in migrating newborn neurons in the postnatal olfactory bulb. *J Neurosci* 29: 2510–2518, 2009.

21. **De MS, Bovetti S, Carletti B, Hsieh YC, Garzotto D, Peretto P, Fasolo A, Puche AC, Rossi F**. Generation of distinct types of periglomerular olfactory bulb interneurons during development and in adult mice: implication for intrinsic properties of the subventricular zone progenitor population. *J Neurosci* 27: 657–664, 2007.

22. **Dejda A, Jolivel V, Bourgault S, Seaborn T, Fournier A, Vaudry H, Vaudry D**. Inhibitory effect of PACAP on caspase activity in neuronal apoptosis: a better understanding towards therapeutic applications in neurodegenerative diseases. *J Mol Neurosci* 36: 26–37, 2008.

23. **Dejda A, Sokolowska P, Nowak JZ**. Neuroprotective potential of three neuropeptides PACAP, VIP and PHI. *Pharmacol Rep* 57: 307–320, 2005.

24. **Delgado M, Abad C, Martinez C, Juarranz MG, Leceta J, Ganea D, Gomariz RP**. PACAP in immunity and inflammation. *Ann NY Acad Sci* 992: 141–157, 2003.

25. **Delwig A, Majumdar S, Ahern K, Lavail MM, Edwards R, Hnasko TS, Copenhagen DR**. Glutamatergic neurotransmission from melanopsin retinal ganglion cells is required for neonatal photoaversion but not adult pupillary light reflex. *PLoS One* 8: e83974, 2013.

26. **Di MM, Cavallaro S, Ciranna L**. Pituitary adenylate cyclase-activating polypeptide modifies the electrical activity of CA1 hippocampal neurons in the rat. *Neurosci Lett* 337: 97–100, 2003.

27. **Di MM, Peeters K, Loyen S, Thys C, Waelkens E, Overbergh L, Hoylaerts M, Van GC, Freson K**. Pituitary adenylate cyclase-activating

polypeptide (PACAP) impairs the regulation of apoptosis in megakaryocytes by activating NF-kappaB: a proteomic study. *Mol Cell Proteomics* 11: M111, 2012.

28. **Dickson L, Aramori I, Sharkey J, Finlayson K**. VIP and PACAP receptor pharmacology: a comparison of intracellular signaling pathways. *Ann NY Acad Sci* 1070: 239–242, 2006.

29. **Doan ND, Chatenet D, Letourneau M, Vaudry H, Vaudry D, Fournier A**. Receptor-independent cellular uptake of pituitary adenylate cyclase-activating polypeptide. *Biochim Biophys Acta* 1823: 940–949, 2012a.

30. **Doan ND, Letourneau M, Vaudry D, Doucet N, Folch B, Vaudry H, Fournier A, Chatenet D**. Design and characterization of novel cell-penetrating peptides from pituitary adenylate cyclase-activating polypeptide. *J Control Release* 163: 256–265, 2012b.

31. **Doengi M, Deitmer JW, Lohr C**. New evidence for purinergic signaling in the olfactory bulb: A2A and P2Y1 receptors mediate intracellular calcium release in astrocytes. *FASEB J* 22: 2368–2378, 2008.

32. **Doengi M, Hirnet D, Coulon P, Pape HC, Deitmer JW, Lohr C**. GABA uptake-dependent Ca(2+) signaling in developing olfactory bulb astrocytes. *Proc Natl Acad Sci USA* 106: 17570–17575, 2009.

33. **Doursout MF, Schurdell MS, Young LM, Osuagwu U, Hook DM, Poindexter BJ, Schiess MC, Bick DL, Bick RJ**. Inflammatory cells and cytokines in the olfactory bulb of a rat model of neuroinflammation; insights into neurodegeneration? *J Interferon Cytokine Res* 33: 376–383, 2013.

34. **Dzhala VI, Kuchibhotla KV, Glykys JC, Kahle KT, Swiercz WB, Feng G, Kuner T, Augustine GJ, Bacskai BJ, Staley KJ**. Progressive NKCC1-dependent neuronal chloride accumulation during neonatal seizures. *J Neurosci* 30: 11745–11761, 2010.

35. **Dziema H, Obrietan K**. PACAP potentiates L-type calcium channel conductance in suprachiasmatic nucleus neurons by activating the MAPK pathway. *J Neurophysiol* 88: 1374–1386, 2002.

36. **Falluel-Morel A, Aubert N, Vaudry D, Desfeux A, Allais A, Burel D, Basille M, Vaudry H, Laudenbach V, Gonzalez BJ**. Interactions of PACAP and ceramides in the control of granule cell apoptosis during cerebellar development. *J Mol Neurosci* 36: 8–15, 2008.

37. **Falluel-Morel A, Chafai M, Vaudry D, Basille M, Cazillis M, Aubert N, Louiset E, de JS, Le Bigot JF, Fournier A, Gressens P, Rostene W, Vaudry H, Gonzalez BJ**. The neuropeptide pituitary adenylate cyclase-

activating polypeptide exerts anti-apoptotic and differentiating effects during neurogenesis: focus on cerebellar granule neurones and embryonic stem cells. *J Neuroendocrinol* 19: 321–327, 2007.

38. **Gascon E, Dayer AG, Sauvain MO, Potter G, Jenny B, De RM, Zgraggen E, Demaurex N, Muller D, Kiss JZ**. GABA regulates dendritic growth by stabilizing lamellipodia in newly generated interneurons of the olfactory bulb. *J Neurosci* 26: 12956–12966, 2006.

39. **Glykys J, Dzhala VI, Kuchibhotla KV, Feng G, Kuner T, Augustine G, Bacskai BJ, Staley KJ**. Differences in cortical versus subcortical GABAergic signaling: a candidate mechanism of electroclinical uncoupling of neonatal seizures. *Neuron* 63: 657–672, 2009.

40. **Granados-Fuentes D, Tseng A, Herzog ED**. A circadian clock in the olfactory bulb controls olfactory responsivity. *J Neurosci* 26: 12219–12225, 2006.

41. **Han P, Lucero MT**. Pituitary adenylate cyclase activating polypeptide reduces A-type K+ currents and caspase activity in cultured adult mouse olfactory neurons. *Neuroscience* 134: 745–756, 2005.

42. **Han P, Lucero MT**. Pituitary adenylate cyclase activating polypeptide reduces expression of Kv1.4 and Kv4.2 subunits underlying A-type K(+) current in adult mouse olfactory neuroepithelia. *Neuroscience* 138: 411–419, 2006.

43. **Hansel DE, May V, Eipper BA, Ronnett GV**. Pituitary adenylyl cyclase-activating peptides and alpha-amidation in olfactory neurogenesis and neuronal survival in vitro. *J Neurosci* 21: 4625–4636, 2001.

44. **Hansson E, Westerlund A, Bjorklund U, Ronnback L**. PACAP attenuates 5-HT, histamine, and ATP-evoked Ca2+ transients in astrocytes. *Neuroreport* 20: 957–962, 2009.

45. **Hegg CC, Au E, Roskams AJ, Lucero MT**. PACAP is present in the olfactory system and evokes calcium transients in olfactory receptor neurons. *J Neurophysiol* 90: 2711–2719, 2003a.

46. **Hegg CC, Greenwood D, Huang W, Han P, Lucero MT**. Activation of purinergic receptor subtypes modulates odor sensitivity. *J Neurosci* 23: 8291–8301, 2003b.

47. **Hegg CC, Greenwood D, Huang W, Han P, Lucero MT**. Activation of purinergic receptor subtypes modulates odor sensitivity. *J Neurosci* 23: 8291–8301, 2003c.

48. **Inglott MA, Lerner EA, Pilowsky PM, Farnham MM**. Activation of PAC(1) and VPAC receptor subtypes elicits differential physiological responses from sympathetic preganglionic neurons in the anaesthetized rat. *Br J Pharmacol* 167: 1089–1098, 2012.

49. **Irwin RP, Allen CN**. Neuropeptide-mediated calcium signaling in the suprachiasmatic nucleus network. *Eur J Neurosci* 32: 1497–1506, 2010.

50. **Jaworski DM, Proctor MD**. Developmental regulation of pituitary adenylate cyclase-activating polypeptide and PAC(1) receptor mRNA expression in the rat central nervous system. *Brain Res Dev Brain Res* 120: 27–39, 2000.

51. **Jozwiak-Bebenista M, Dejda A, Nowak JZ**. Effects of PACAP, VIP and related peptides on cyclic AMP formation in rat neuronal and astrocyte cultures and cerebral cortical slices. *Pharmacol Rep* 59: 414–420, 2007.

52. **Kambe Y, Miyata A**. Role of mitochondrial activation in PACAP dependent neurite outgrowth. *J Mol Neurosci* 48: 550–557, 2012.

53. **Kanekar S, Gandham M, Lucero MT**. PACAP protects against TNFalpha-induced cell death in olfactory epithelium and olfactory placodal cell lines. *Mol Cell Neurosci* 45: 345–354, 2010.

54. **Kelsch W, Mosley CP, Lin CW, Lois C**. Distinct mammalian precursors are committed to generate neurons with defined dendritic projection patterns. *PLoS Biol* 5: e300, 2007.

55. **Khakhalin AS**. Questioning the depolarizing effects of GABA during early brain development. *J Neurophysiol* 106: 1065–1067, 2011.

56. **Kiss P, Tamas A, Lubics A, Lengvari I, Szalai M, Hauser D, Horvath ZS, Racz B, Gabriel R, Babai N, Toth G, Reglodi D**. Effects of systemic PACAP treatment in monosodium glutamate-induced behavioral changes and retinal degeneration. *Ann NY Acad Sci* 1070: 365–370, 2006.

57. **Kiyokage E, Pan YZ, Shao Z, Kobayashi K, Szabo G, Yanagawa Y, Obata K, Okano H, Toida K, Puche AC, Shipley MT**. Molecular identity of periglomerular and short axon cells. *J Neurosci* 30: 1185–1196, 2010.

58. **Kopp MD, Meissl H, Dehghani F, Korf HW**. The pituitary adenylate cyclase-activating polypeptide modulates glutamatergic calcium signalling: investigations on rat suprachiasmatic nucleus neurons. *J Neurochem* 79: 161–171, 2001.

59. **Kopp MD, Schomerus C, Dehghani F, Korf HW, Meissl H**. Pituitary adenylate cyclase-activating polypeptide and melatonin in the

suprachiasmatic nucleus: effects on the calcium signal transduction cascade. *J Neurosci* 19: 206–219, 1999.

60. **Lemasson M, Saghatelyan A, Olivo-Marin JC, Lledo PM**. Neonatal and adult neurogenesis provide two distinct populations of newborn neurons to the mouse olfactory bulb. *J Neurosci* 25: 6816–6825, 2005.

61. **Liu Z, Geng L, Li R, He X, Zheng JQ, Xie Z**. Frequency modulation of synchronized Ca2+ spikes in cultured hippocampal networks through G-protein-coupled receptors. *J Neurosci* 23: 4156–4163, 2003.

62. **Lopez-Bendito G, Sturgess K, Erdelyi F, Szabo G, Molnar Z, Paulsen O**. Preferential origin and layer destination of GAD65-GFP cortical interneurons. *Cereb Cortex* 14: 1122–1133, 2004.

63. **Macdonald DS, Weerapura M, Beazely MA, Martin L, Czerwinski W, Roder JC, Orser BA, Macdonald JF**. Modulation of NMDA receptors by pituitary adenylate cyclase activating peptide in CA1 neurons requires G alpha q, protein kinase C, and activation of Src. *J Neurosci* 25: 11374–11384, 2005.

64. **Makela J, Koivuniemi R, Korhonen L, Lindholm D**. Interferon-gamma produced by microglia and the neuropeptide PACAP have opposite effects on the viability of neural progenitor cells. *PLoS One* 5: e11091, 2010.

65. **Marchetti C, Tabak J, Chub N, O'Donovan MJ, Rinzel J**. Modeling spontaneous activity in the developing spinal cord using activity-dependent variations of intracellular chloride. *J Neurosci* 25: 3601–3612, 2005.

66. **Markhotina N, Liu GJ, Martin DK**. Contractility of retinal pericytes grown on silicone elastomer substrates is through a protein kinase A-mediated intracellular pathway in response to vasoactive peptides. *IET Nanobiotechnol* 1: 44–51, 2007.

67. **Masmoudi O, Gandolfo P, Leprince J, Vaudry D, Fournier A, Patte-Mensah C, Vaudry H, Tonon MC**. Pituitary adenylate cyclase-activating polypeptide (PACAP) stimulates endozepine release from cultured rat astrocytes via a PKA-dependent mechanism. *FASEB J* 17: 17–27, 2003.

68. **Matsuno R, Ohtaki H, Nakamachi T, Watanabe J, Yofu S, Hayashi D, Takeda T, Nonaka N, Seki M, Nakamura M, Itabashi K, Shioda S**. Distribution and localization of pituitary adenylate cyclase-activating polypeptide-specific receptor (PAC1R) in the rostral migratory stream of the infant mouse brain. *Regul Pept* 145: 80–87, 2008.

69. **Mei YA, Vaudry D, Basille M, Castel H, Fournier A, Vaudry H, Gonzalez BJ**. PACAP inhibits delayed rectifier potassium current via a

cAMP/PKA transduction pathway: evidence for the involvement of I k in the anti-apoptotic action of PACAP. *Eur J Neurosci* 19: 1446–1458, 2004.

70. **Mejia-Gervacio S, Murray K, Lledo PM**. NKCC1 controls GABAergic signaling and neuroblast migration in the postnatal forebrain. *Neural Dev* 6: 4, 2011.

71. **Merkle FT, Mirzadeh Z, Alvarez-Buylla A**. Mosaic organization of neural stem cells in the adult brain. *Science* 317: 381–384, 2007.

72. **Michel S, Itri J, Han JH, Gniotczynski K, Colwell CS**. Regulation of glutamatergic signalling by PACAP in the mammalian suprachiasmatic nucleus. *BMC Neurosci* 7: 15, 2006.

73. **Mirich JM, Williams NC, Berlau DJ, Brunjes PC**. Comparative study of aging in the mouse olfactory bulb. *J Comp Neurol* 454: 361–372, 2002.

74. **Miyata A, Arimura A, Dahl RR, Minamino N, Uehara A, Jiang L, Culler MD, Coy DH**. Isolation of a novel 38 residue-hypothalamic polypeptide which stimulates adenylate cyclase in pituitary cells. *Biochem Biophys Res Commun* 164: 567–574, 1989.

75. **Mulder H, Jongsma H, Zhang Y, Gebre-Medhin S, Sundler F, Danielsen N**. Pituitary adenylate cyclase-activating polypeptide and islet amyloid polypeptide in primary sensory neurons: functional implications from plasticity in expression on nerve injury and inflammation. *Mol Neurobiol* 19: 229–253, 1999.

76. **Nagai Y, Sano H, Yokoi M**. Transgenic expression of Cre recombinase in mitral/tufted cells of the olfactory bulb. *Genesis* 43: 12–16, 2005.

77. **Nakamachi T, Ohtaki H, Yofu S, Dohi K, Watanabe J, Hayashi D, Matsuno R, Nonaka N, Itabashi K, Shioda S**. Pituitary adenylate cyclase-activating polypeptide (PACAP) type 1 receptor (PAC1R) co-localizes with activity-dependent neuroprotective protein (ADNP) in the mouse brains. *Regul Pept* 145: 88–95, 2008.

78. **Nicot A, Dicicco-Bloom E**. Regulation of neuroblast mitosis is determined by PACAP receptor isoform expression. *Proc Natl Acad Sci USA* 98: 4758–4763, 2001.

79. **Ohtaki H, Nakamachi T, Dohi K, Aizawa Y, Takaki A, Hodoyama K, Yofu S, Hashimoto H, Shintani N, Baba A, Kopf M, Iwakura Y, Matsuda K, Arimura A, Shioda S**. Pituitary adenylate cyclase-activating polypeptide (PACAP) decreases ischemic neuronal cell death in association with IL-6. *Proc Natl Acad Sci USA* 103: 7488–7493, 2006.

80. **Ohtaki H, Nakamachi T, Dohi K, Shioda S**. Role of PACAP in ischemic neural death. *J Mol Neurosci* 36: 16–25, 2008.

81. **Olianas MC, Onali P**. GABA(B) receptor-mediated stimulation of adenylyl cyclase activity in membranes of rat olfactory bulb. *Br J Pharmacol* 126: 657–664, 1999.

82. **Parrish-Aungst S, Shipley MT, Erdelyi F, Szabo G, Puche AC**. Quantitative analysis of neuronal diversity in the mouse olfactory bulb. *J Comp Neurol* 501: 825–836, 2007.

83. **Plachez C, Puche AC**. Early specification of GAD67 subventricular derived olfactory interneurons. *J Mol Histol* 43: 215–221, 2012.

84. **Potter GB, Petryniak MA, Shevchenko E, McKinsey GL, Ekker M, Rubenstein JL**. Generation of Cre-transgenic mice using Dlx1/Dlx2 enhancers and their characterization in GABAergic interneurons. *Mol Cell Neurosci* 40: 167–186, 2009.

85. **Pressler RT, Strowbridge BW**. Blanes cells mediate persistent feedforward inhibition onto granule cells in the olfactory bulb. *Neuron* 49: 889–904, 2006.

86. **Pugh PC, Jayakar SS, Margiotta JF**. PACAP/PAC1R signaling modulates acetylcholine release at neuronal nicotinic synapses. *Mol Cell Neurosci* 43: 244–257, 2010.

87. **Raineki C, Pickenhagen A, Roth TL, Babstock DM, McLean JH, Harley CW, Lucion AB, Sullivan RM**. The neurobiology of infant maternal odor learning. *Braz J Med Biol Res* 43: 914–919, 2010.

88. **Ravni A, Bourgault S, Lebon A, Chan P, Galas L, Fournier A, Vaudry H, Gonzalez B, Eiden LE, Vaudry D**. The neurotrophic effects of PACAP in PC12 cells: control by multiple transduction pathways. *J Neurochem* 98: 321–329, 2006.

89. **Rieger A, Deitmer JW, Lohr C**. Axon-glia communication evokes calcium signaling in olfactory ensheathing cells of the developing olfactory bulb. *Glia* 55: 352–359, 2007.

90. **Robberecht P, Gourlet P, De NP, Woussen-Colle MC, Vandermeers-Piret MC, Vandermeers A, Christophe J**. Structural requirements for the occupancy of pituitary adenylate-cyclase-activating-peptide (PACAP) receptors and adenylate cyclase activation in human neuroblastoma NB-OK-1 cell membranes. Discovery of PACAP(6-38) as a potent antagonist. *Eur J Biochem* 207: 239–246, 1992.

91. **Ruan Y, Zheng XY, Zhang HL, Zhu W, Zhu J**. Olfactory dysfunctions in neurodegenerative disorders. *J Neurosci Res* 90: 1693–1700, 2012.

92. **Scharf E, May V, Braas KM, Shutz KC, Mao-Draayer Y**. Pituitary adenylate cyclase-activating polypeptide (PACAP) and vasoactive intestinal peptide (VIP) regulate murine neural progenitor cell survival, proliferation, and differentiation. *J Mol Neurosci* 36: 79–88, 2008.

93. **Sherwood NM, Adams BA, Isaac ER, Wu S, Fradinger EA**. Knocked down and out: PACAP in development, reproduction and feeding. *Peptides* 28: 1680–1687, 2007.

94. **Shioda S, Ohtaki H, Nakamachi T, Dohi K, Watanabe J, Nakajo S, Arata S, Kitamura S, Okuda H, Takenoya F, Kitamura Y**. Pleiotropic functions of PACAP in the CNS: neuroprotection and neurodevelopment. *Ann NY Acad Sci* 1070: 550–560, 2006.

95. **Shioda S, Shuto Y, Somogyvari-Vigh A, Legradi G, Onda H, Coy DH, Nakajo S, Arimura A**. Localization and gene expression of the receptor for pituitary adenylate cyclase-activating polypeptide in the rat brain. *Neurosci Res* 28: 345–354, 1997.

96. **Silveira MS, Costa MR, Bozza M, Linden R**. Pituitary adenylyl cyclase-activating polypeptide prevents induced cell death in retinal tissue through activation of cyclic AMP-dependent protein kinase. *J Biol Chem* 277: 16075–16080, 2002.

97. **Sun QQ, Prince DA, Huguenard JR**. Vasoactive intestinal polypeptide and pituitary adenylate cyclase-activating polypeptide activate hyperpolarization-activated cationic current and depolarize thalamocortical neurons in vitro. *J Neurosci* 23: 2751–2758, 2003.

98. **Szabadfi K, Atlasz T, Kiss P, Danyadi B, Tamas A, Helyes Z, Hashimoto H, Shintani N, Baba A, Toth G, Gabriel R, Reglodi D**. Mice deficient in pituitary adenylate cyclase activating polypeptide (PACAP) are more susceptible to retinal ischemic injury in vivo. *Neurotox Res* 21: 41–48, 2012.

99. **Szabadfi K, Szabo A, Kiss P, Reglodi D, Setalo G, Jr., Kovacs K, Tamas A, Toth G, Gabriel R**. PACAP promotes neuron survival in early experimental diabetic retinopathy. *Neurochem Int* 64: 84–91, 2014.

100. **Takayama C, Inoue Y**. GABAergic signaling in the developing cerebellum. *Anat Sci Int* 79: 124–136, 2004.

101. **Tanaka M, Kawahara K, Kosugi T, Yamada T, Mioka T**. Changes in the spontaneous calcium oscillations for the development of the

preconditioning-induced ischemic tolerance in neuron/astrocyte co-culture. *Neurochem Res* 32: 988–1001, 2007.

102. **Taniguchi H, He M, Wu P, Kim S, Paik R, Sugino K, Kvitsiani D, Fu Y, Lu J, Lin Y, Miyoshi G, Shima Y, Fishell G, Nelson SB, Huang ZJ**. A resource of Cre driver lines for genetic targeting of GABAergic neurons in cerebral cortex. *Neuron* 71: 995–1013, 2011.

103. **Taylor RD, Madsen MG, Krause M, Sampedro-Castaneda M, Stocker M, Pedarzani P**. Pituitary adenylate cyclase-activating polypeptide (PACAP) inhibits the slow afterhyperpolarizing current sIAHP in CA1 pyramidal neurons by activating multiple signaling pathways. *Hippocampus* 24: 32–43, 2014.

104. **Thyssen A, Stavermann M, Buddrus K, Doengi M, Ekberg JA, St John JA, Deitmer JW, Lohr C**. Spatial and developmental heterogeneity of calcium signaling in olfactory ensheathing cells. *Glia* 61: 327–337, 2013.

105. **Tong XP, Li XY, Zhou B, Shen W, Zhang ZJ, Xu TL, Duan S**. Ca(2+) signaling evoked by activation of Na(+) channels and Na(+)/Ca(2+) exchangers is required for GABA-induced NG2 cell migration. *J Cell Biol* 186: 113–128, 2009.

106. **Vaudry D, Falluel-Morel A, Basille M, Pamantung TF, Fontaine M, Fournier A, Vaudry H, Gonzalez BJ**. Pituitary adenylate cyclase-activating polypeptide prevents C2-ceramide-induced apoptosis of cerebellar granule cells. *J Neurosci Res* 72: 303–316, 2003.

107. **Vaudry D, Falluel-Morel A, Bourgault S, Basille M, Burel D, Wurtz O, Fournier A, Chow BK, Hashimoto H, Galas L, Vaudry H**. Pituitary adenylate cyclase-activating polypeptide and its receptors: 20 years after the discovery. *Pharmacol Rev* 61: 283–357, 2009.

108. **Vaudry D, Gonzalez BJ, Basille M, Anouar Y, Fournier A, Vaudry H**. Pituitary adenylate cyclase-activating polypeptide stimulates both c-fos gene expression and cell survival in rat cerebellar granule neurons through activation of the protein kinase A pathway. *Neuroscience* 84: 801–812, 1998.

109. **Vaudry D, Gonzalez BJ, Basille M, Fournier A, Vaudry H**. Neurotrophic activity of pituitary adenylate cyclase-activating polypeptide on rat cerebellar cortex during development. *Proc Natl Acad Sci USA* 96: 9415–9420, 1999.

110. **Vaudry D, Gonzalez BJ, Basille M, Pamantung TF, Fontaine M, Fournier A, Vaudry H**. The neuroprotective effect of pituitary adenylate cyclase-activating polypeptide on cerebellar granule cells is mediated

through inhibition of the CED3-related cysteine protease caspase-3/CPP32. *Proc Natl Acad Sci USA* 97: 13390–13395, 2000a.

111. **Vaudry D, Gonzalez BJ, Basille M, Pamantung TF, Fournier A, Vaudry H**. PACAP acts as a neurotrophic factor during histogenesis of the rat cerebellar cortex. *Ann NY Acad Sci* 921: 293–299, 2000b.

112. **Vaudry D, Gonzalez BJ, Basille M, Yon L, Fournier A, Vaudry H**. Pituitary adenylate cyclase-activating polypeptide and its receptors: from structure to functions. *Pharmacol Rev* 52: 269–324, 2000c.

113. **Vaudry D, Pamantung TF, Basille M, Rousselle C, Fournier A, Vaudry H, Beauvillain JC, Gonzalez BJ**. PACAP protects cerebellar granule neurons against oxidative stress-induced apoptosis. *Eur J Neurosci* 15: 1451–1460, 2002.

114. **Wang C, Ohno K, Furukawa T, Ueki T, Ikeda M, Fukuda A, Sato K**. Differential expression of KCC2 accounts for the differential GABA responses between relay and intrinsic neurons in the early postnatal rat olfactory bulb. *Eur J Neurosci* 21: 1449–1455, 2005.

115. **Wang DD, Kriegstein AR**. GABA regulates excitatory synapse formation in the neocortex via NMDA receptor activation. *J Neurosci* 28: 5547–5558, 2008.

116. **Wang DD, Kriegstein AR, Ben-Ari Y**. GABA regulates stem cell proliferation before nervous system formation. *Epilepsy Curr* 8: 137–139, 2008.

117. **Webb IC, Coolen LM, Lehman MN**. NMDA and PACAP receptor signaling interact to mediate retinal-induced scn cellular rhythmicity in the absence of light. *PLoS One* 8: e76365, 2013.

118. **Yan Y, Zhou X, Pan Z, Ma J, Waschek JA, Dicicco-Bloom E**. Pro- and anti-mitogenic actions of pituitary adenylate cyclase-activating polypeptide in developing cerebral cortex: potential mediation by developmental switch of PAC1 receptor mRNA isoforms. *J Neurosci* 33: 3865–3878, 2013.

119. **Yang Z**. Postnatal subventricular zone progenitors give rise not only to granular and periglomerular interneurons but also to interneurons in the external plexiform layer of the rat olfactory bulb. *J Comp Neurol* 506: 347–358, 2008.

120. **Yu R, Yi T, Zhang L, Hong A, Dai Y, Zhou T**. Intein-mediated rapid purification of recombinant maxadilan and M65 and their acute effects on plasma glucose. *Acta Biochim Biophys Sin (Shanghai)* 40: 1015–1022, 2008.

121. **Zhokhov SS, Desfeux A, Aubert N, Falluel-Morel A, Fournier A, Laudenbach V, Vaudry H, Gonzalez BJ**. Bax siRNA promotes survival of cultured and allografted granule cell precursors through blockade of caspase-3 cleavage. *Cell Death Differ* 15: 1042–1053, 2008.

122. **Zhou CJ, Shioda S, Yada T, Inagaki N, Pleasure SJ, Kikuyama S**. PACAP and its receptors exert pleiotropic effects in the nervous system by activating multiple signaling pathways. *Curr Protein Pept Sci* 3: 423–439, 2002.

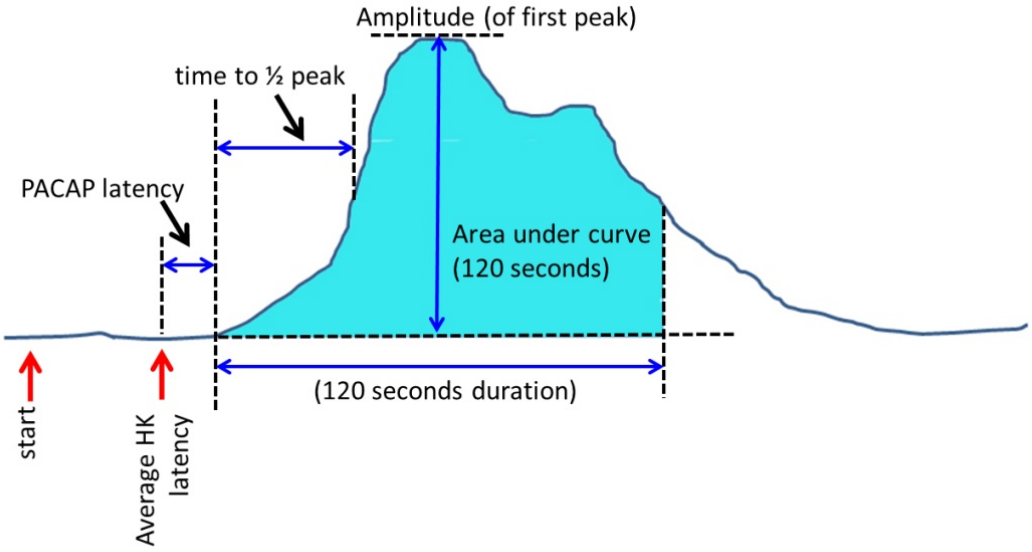

Fig. 2.1: The PACAP induced $[Ca^{2+}]_i$ transient was analyzed for latency, time to ½ peak, amplitude, and net Ca^{2+} flux (area under curve for the first 120 seconds of PACAP responses). All of the PACAP response latencies were measured relative to the average latency of elevated potassium (HK) responses.

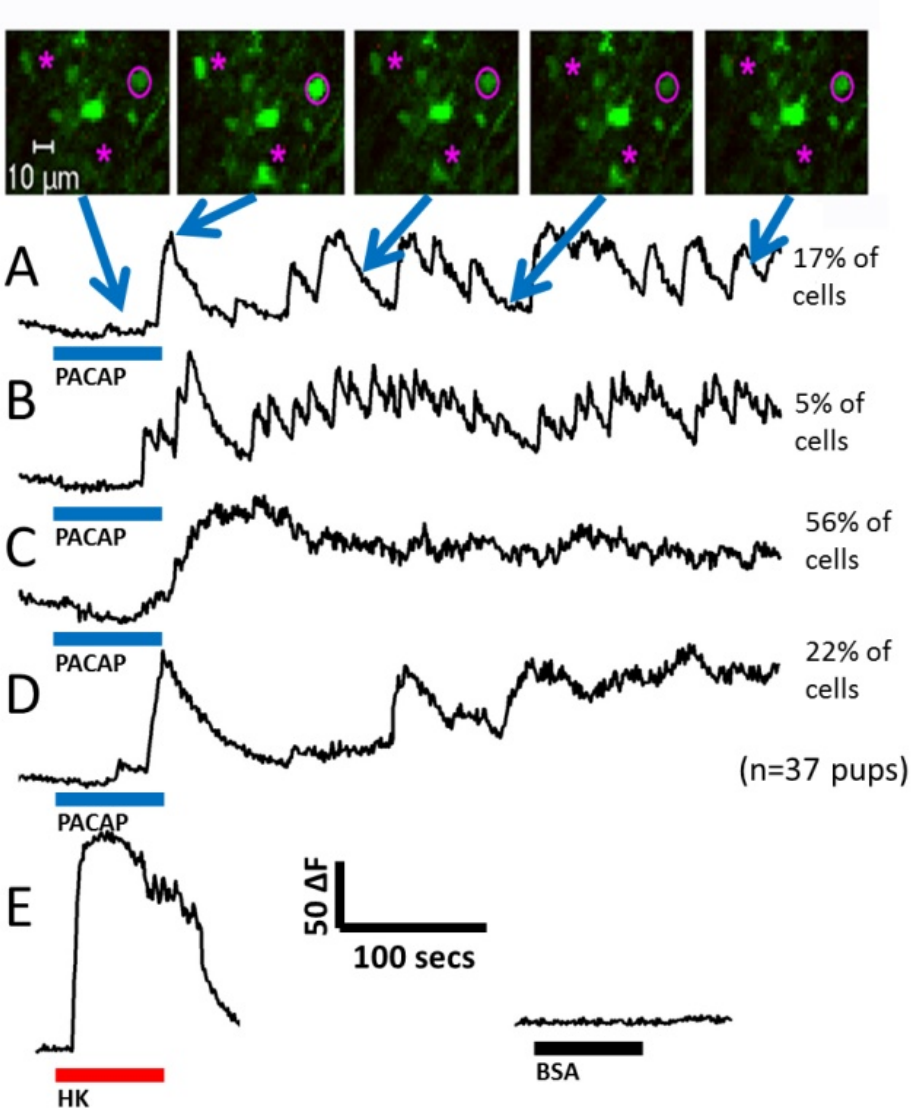

Fig. 2.2: PACAP induces a large initial transient increase in calcium followed by an increase in the number of oscillating neurons in OB slices. A time series of confocal images from a Fluo4-loaded slice of P4 mouse OB shows the changes in $[Ca^{2+}]_i$ in response to 40 nM PACAP. The trace in (*A*) reflects the ΔF changes over time for the region of interest (ROI) within the pink circle. The asterisks are near two additional cells that oscillated in response to 40 nM PACAP. The arrows match the images in A to the time points on the trace. The blue bar indicates the duration of 40 nM PACAP application (~100 secs). The PACAP-induced calcium oscillations of 1413 cells (from 37 pups) were categorized into four main groups: (*A*) Slow sawtooth oscillation, 17% of cells. (*B*) Fast sawtooth oscillation, 5% of cells (*C*) Sustained response, 56% of cells (*D*) Initial simple transient (returns to baseline within 100 seconds), 22% of cells. (*E*) The 50 mM HK is used to confirm the vitality of the cells and 0.1% BSA, which is mixed in with PACAP to keep the protein from sticking to the side of vials, is the negative control.

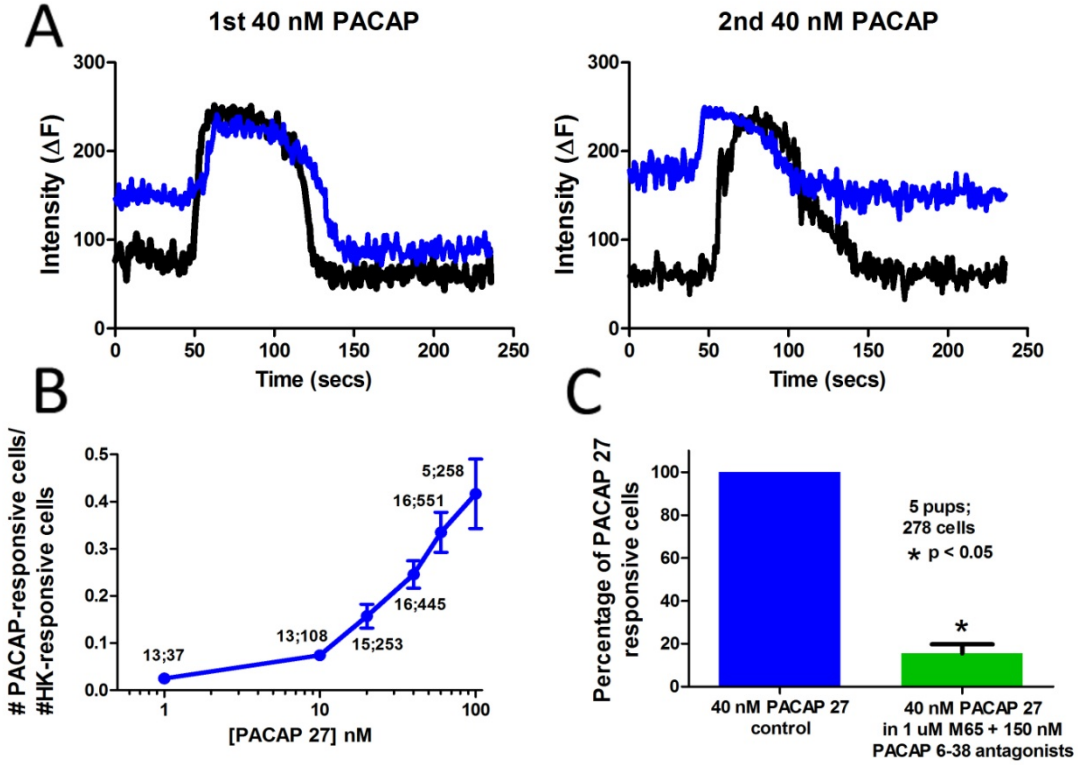

Fig. 2.3: PACAP elicits dose dependent increases in the numbers of activated cells. (*A*) Two sample examples of repeated 40 nM PACAP application on two different cells. (*B*) A log scale plot of the number of PACAP-responsive cells divided by the number of HK-responsive cells shows that the increases in cell numbers do not saturate with a relatively high PACAP concentration of 100 nM. (*C*) The percentage of cells responding to 40 nM PACAP is reduced by 84 ± 4% in the presence of PAC1R antagonists (1 μM M65 and 150 nM PACAP 6-38). Numbers near the dots indicate number of pups, then the number of PACAP-responsive cells analyzed.

Fig. 2.4: The kinetic and intensity responses to increasing PACAP concentrations are dose-dependent. (*A*) The response latency significantly decreased by 45% between 10 nM to 100 nM PACAP27. (*B*) The time to peak showed no significant change. (*C*) Amplitude did not follow a classic dose-response curve, with 40 nM PACAP significantly being the peak. (*D*) The Ca^{2+} flux measured during the first 120 secs increased significantly with increased concentration of PACAP. (*E*) The histogram of the response amplitudes fitted with a Gaussian distribution showed that a higher percentage of cells had lower amplitudes at 100 nM PACAP (75% of cell intensities are below 108) than at 40 nM PACAP (75% of cell intensities are below 122.) Numbers near the dots indicate number of pups, then number of cells analyzed.

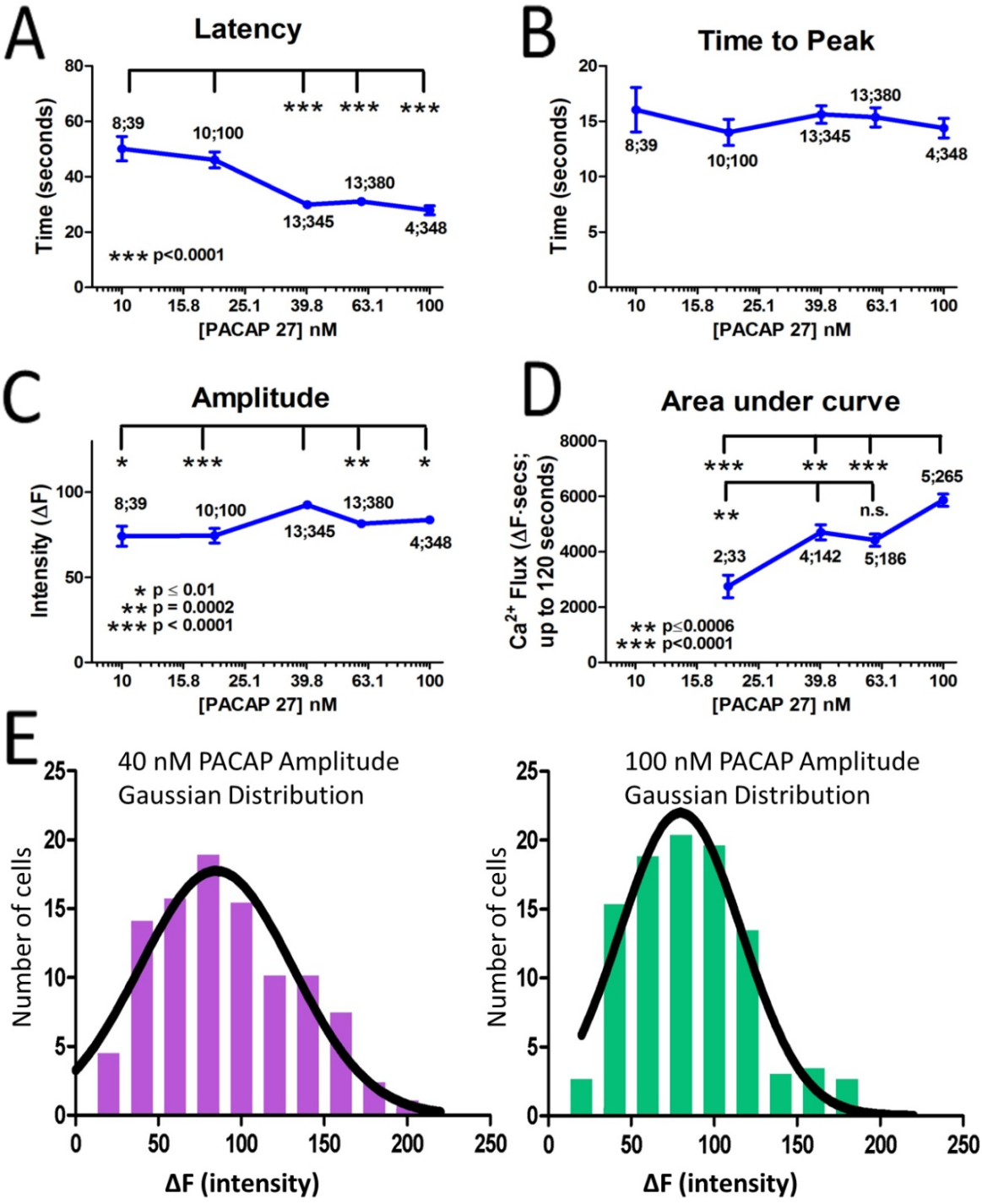
A
Latency
Time (seconds)
8;39
10;100
13;380
13;345
4;348
*** p<0.0001
[PACAP 27] nM
B
Time to Peak
Time (seconds)
8;39
10;100
13;345
13;380
4;348
[PACAP 27] nM
C
Amplitude
Intensity (ΔF)
8;39
10;100
13;345
13;380
4;348
* p ≤ 0.01
** p = 0.0002
*** p < 0.0001
[PACAP 27] nM
D
Area under curve
Ca2+ Flux (ΔF-secs; up to 120 seconds)
2;33
4;142
5;186
5;265
n.s.
** p≤0.0006
*** p<0.0001
[PACAP 27] nM
E
40 nM PACAP Amplitude
Gaussian Distribution
Number of cells
ΔF (intensity)
100 nM PACAP Amplitude
Gaussian Distribution
Number of cells
ΔF (intensity)

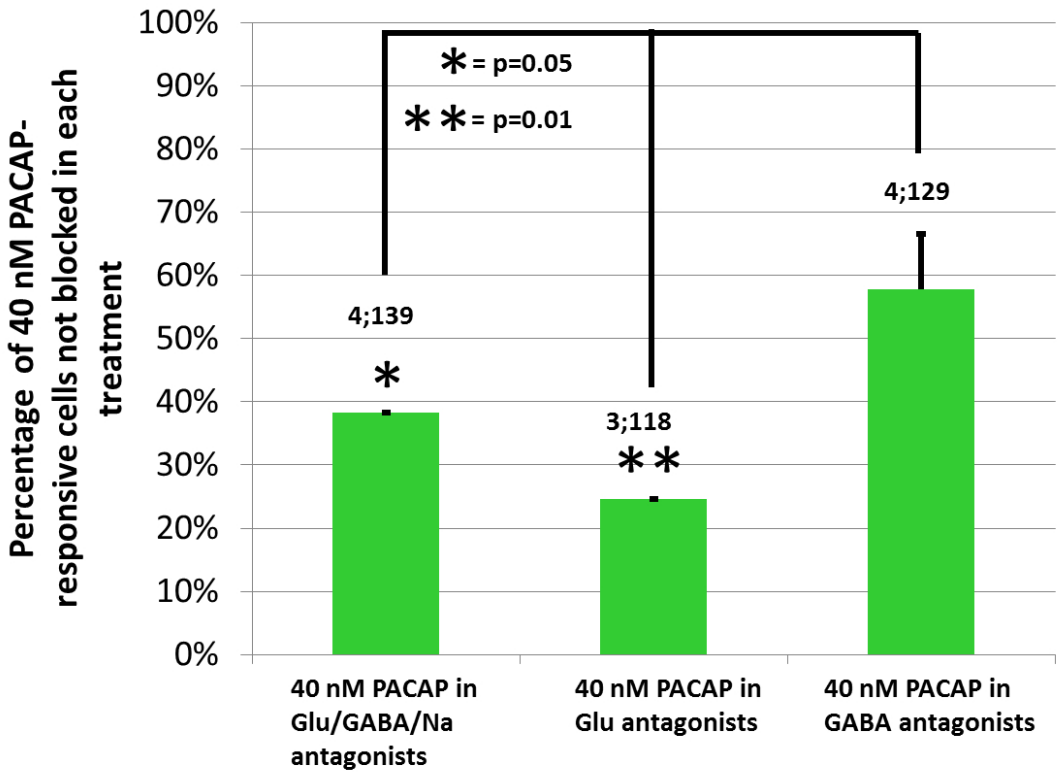

Fig. 2.5: PACAP directly and indirectly activates GC neurons. The bar graph shows the fraction of PACAP responding cells in each antagonist treatment relative to PACAP control (at 100%). Blocking neurotransmission and downstream receptors, especially glutamatergic receptors significantly reduces the percentages of PACAP responsive cells. The numbers above the graph indicate pups and number of cells responding in PACAP control.

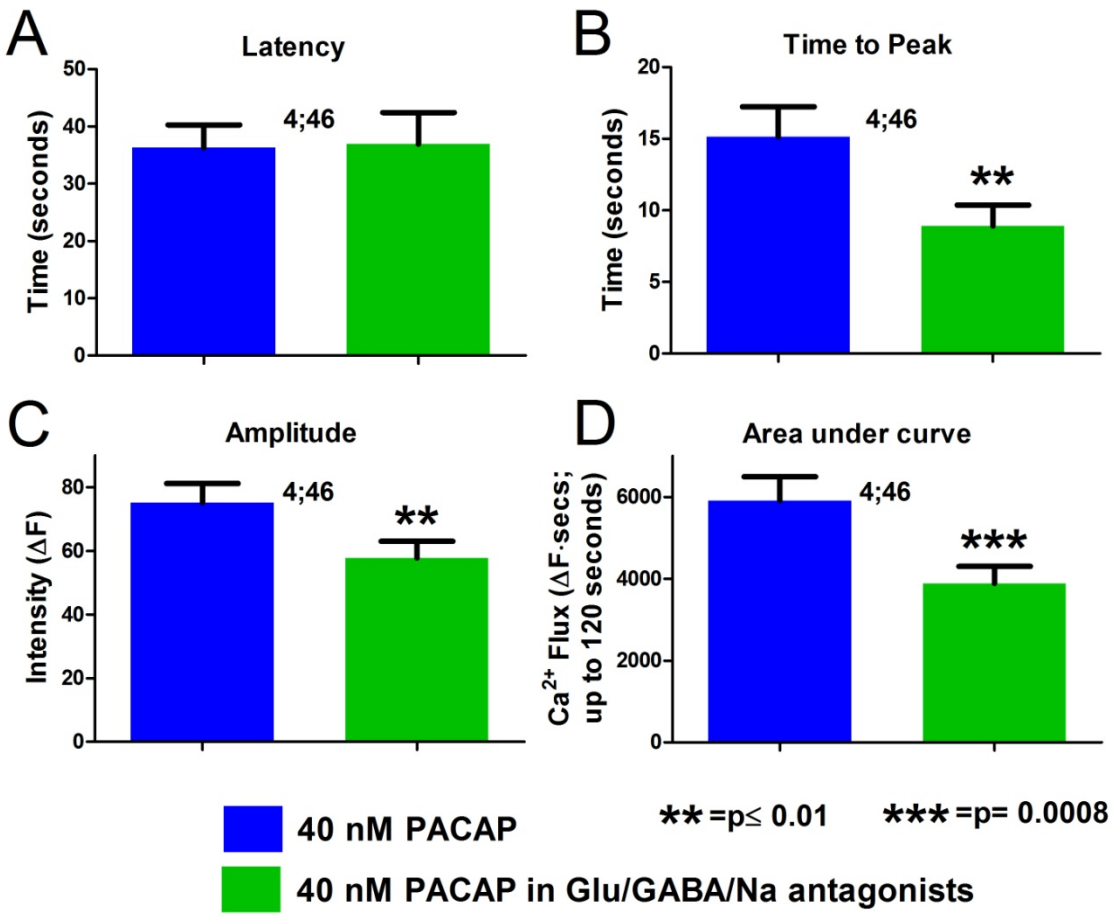

Fig. 2.6 The cells directly activated by PACAP have faster smaller responses compared to downstream cells. (*A*) Only the latency is unchanged between 40 nM PACAP-only controls and 40 nM PACAP in Glu/GABA/Na antagonists done on the same slice. The antagonists significantly reduced the (*B*) time to peak (63% of control), (*C*) amplitude (71% of control), and (*D*) area under curve (66% of control) (paired t-test). Numbers above the bar indicate number of pups, then number of cells analyzed.

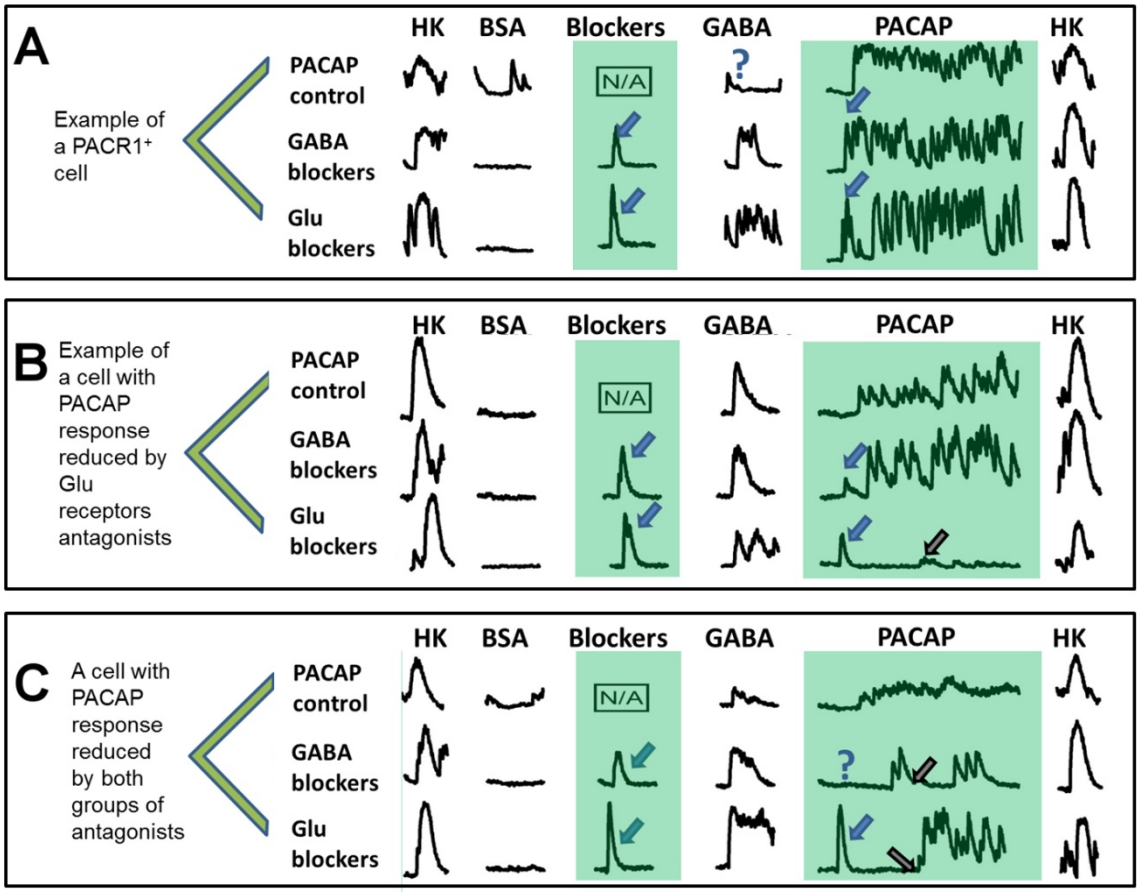

Fig. 2.7: Cells may be PACAP-activated by a combination of PAC1R$^+$ and Glu and/or GABA receptors. Sample traces of three different individual cells treated with GABA blockers, then GluR-blockers. The blockers-only controls showed initial, short bursts, which were not PACAP-induced responses (blue arrows). The short burst does not always occur in the GABA runs (blue "?" signs). The post-PACAP Ca^{2+} oscillations after the antagonists and PACAP are washed out is shown with black arrows. (*A*) The directly-activated PACR1$^+$ cell showed strong PACAP response regardless of antagonists. (*B*) The PACAP-induced Ca^{2+} responses in this cell were completely blocked by GluRs antagonists, suggesting PACAP indirectly activated the cell via glutamate release from an upstream cell. (*C*) PACAP responses were blocked by both groups of antagonists, suggesting the cell may have only indirect PACAP activation via both glutamate and GABA upstream release.

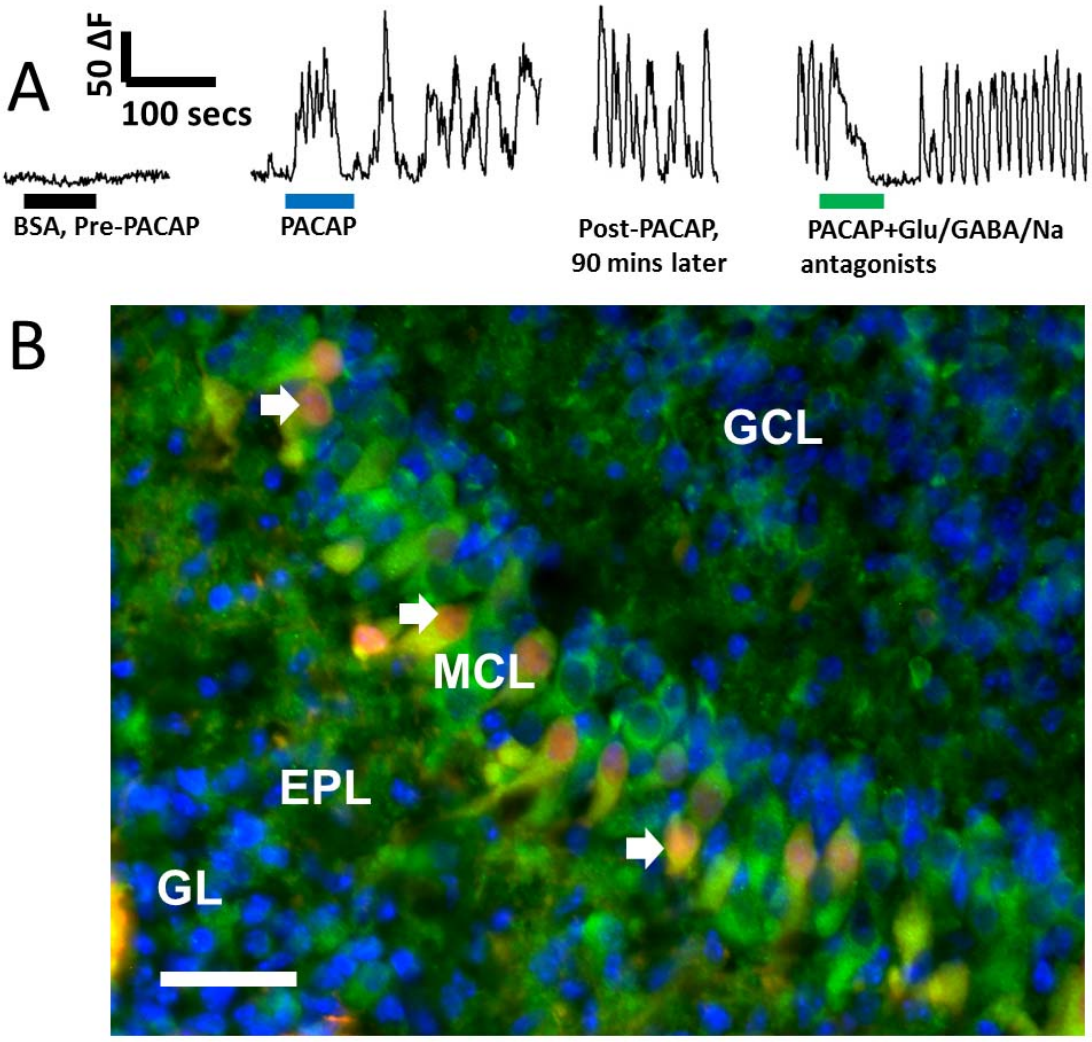

Fig. 2.8: Mitral Cells are PAC1R$^+$ and part of the PACAP-induced activity network. (*A*) Sample trace of a mitral cell starting with pre-PACAP BSA control. After 40 nM PACAP exposure, the mitral cell started to oscillate and the $[Ca^{2+}]_i$ oscillations lasted over 90 minutes post-PACAP. During application of PACAP + Glu/GABA/Na antagonists, the mitral cell responded to PACAP, but also responded to the antagonists by stopping oscillating for about 40 seconds. The scale bar indicates fluorescence intensity (ΔF) vs time (sec). (*B*) A P4 td-Tomato IRES-CRE-PCdh21 (red) OB tissue section was stained with anti-PAC1R antibodies (green). The arrows indicate PCdh21$^+$ mitral cells expressing PAC1 receptors. The blue nuclear stain is the DAPI. Scale bar is 50 μm. Abbreviations: glomerular layer (GL), external plexiform layer (EPL), mitral cell layer (MCL), granule cell layer (GCL).

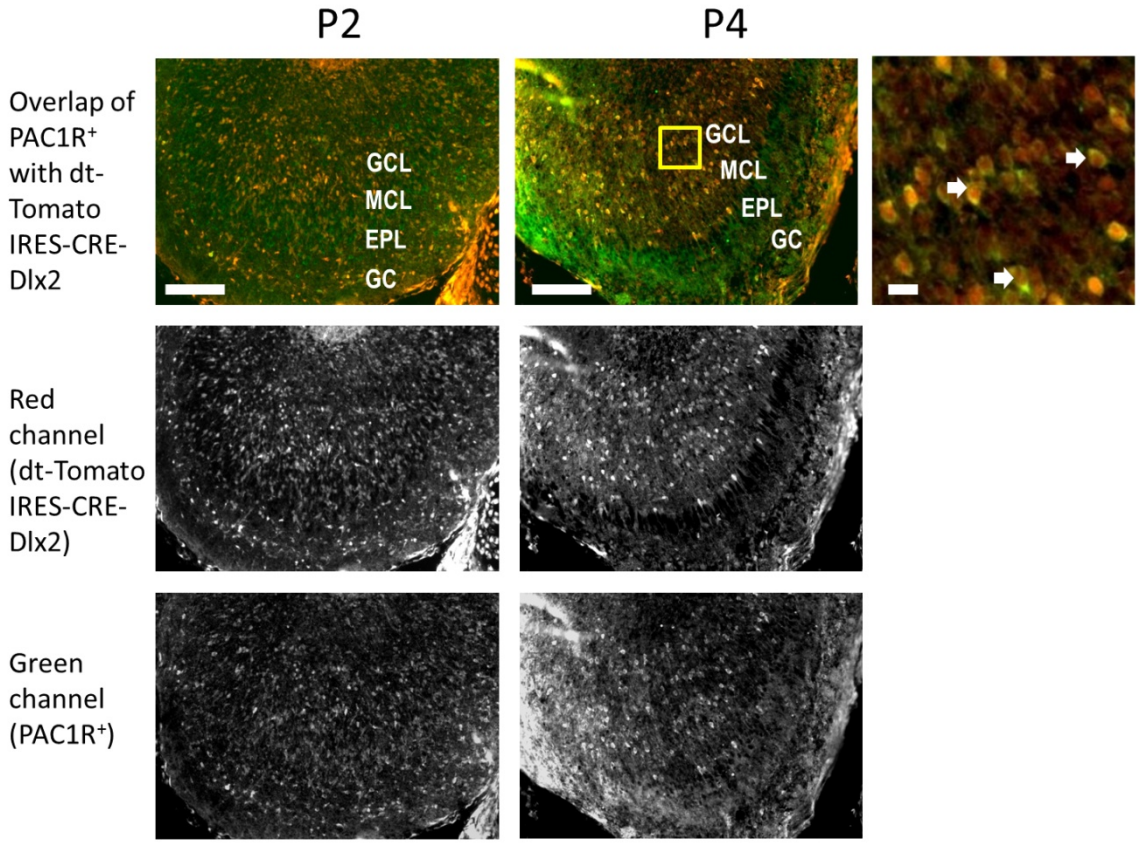

Fig. 2.9: PAC1R$^+$ expression is enriched throughout the GCL and MCL of the OB. OB from P2 and P4 Rosa tdTomato IRES-CRE-Dlx2 (red) was stained with anti-PAC1R antibodies (green). The black and white pictures are the red or green channels, showing the labeling separately. The region indicated by the yellow box in P4 is shown at higher magnification. Scale bars are 100 μm for P2 and P4. The scale bars in the zoom-ins of the magnified P4 are 20 μm. Abbreviations: glomerular layer (GL), external plexiform layer (EPL), mitral cell layer (MCL), granule cell layer (GCL).

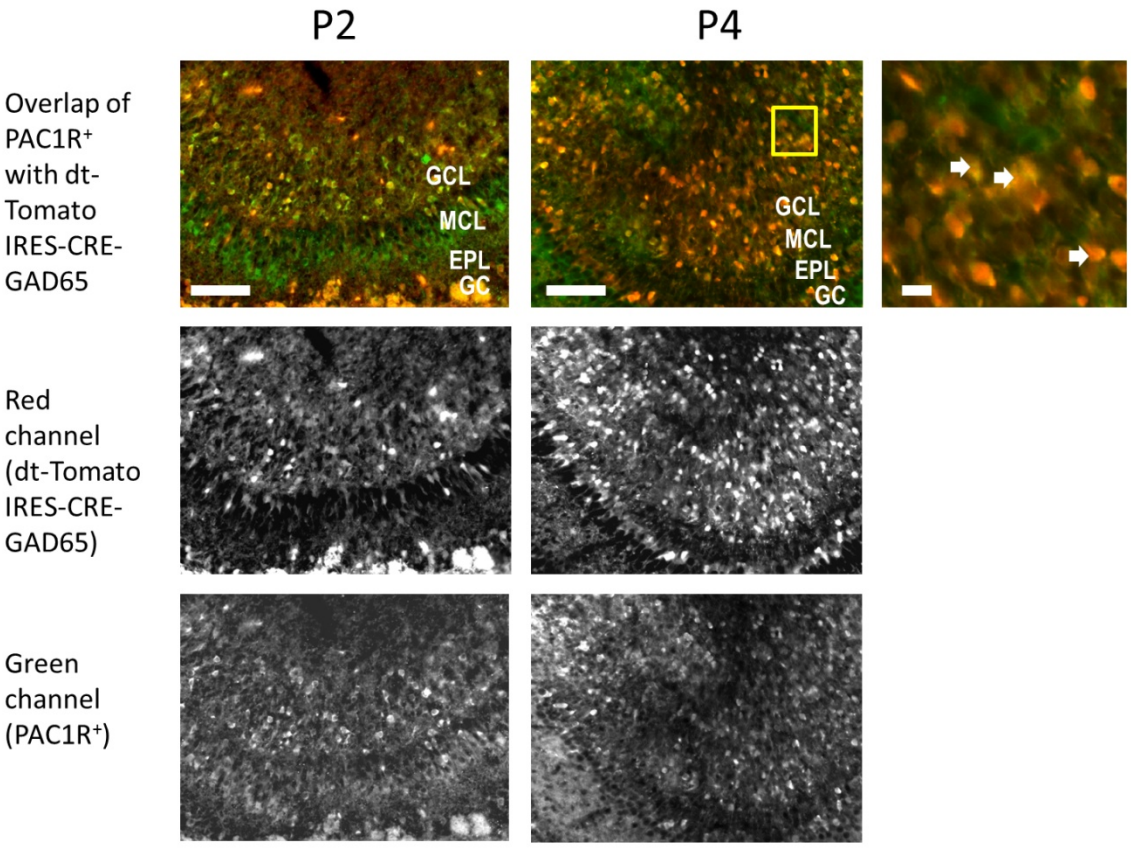

Fig. 2.10: PAC1R expression is enriched throughout the GCL of the OB. OB from P2 and P4 Rosa tdTomato IRES-CRE-Dlx2 (red) was stained with anti-PAC1R antibodies (green). The black and white pictures are the red or green channels, showing the labeling separately. The region indicated by the yellow box in P4 is shown at higher magnification. Scale bars are 100 μm for P2 and P4. The scale bars in the zoom-ins of the magnified P4 are 20 μm. Abbreviations: glomerular layer (GL), external plexiform layer (EPL), mitral cell layer (MCL), granule cell layer (GCL).

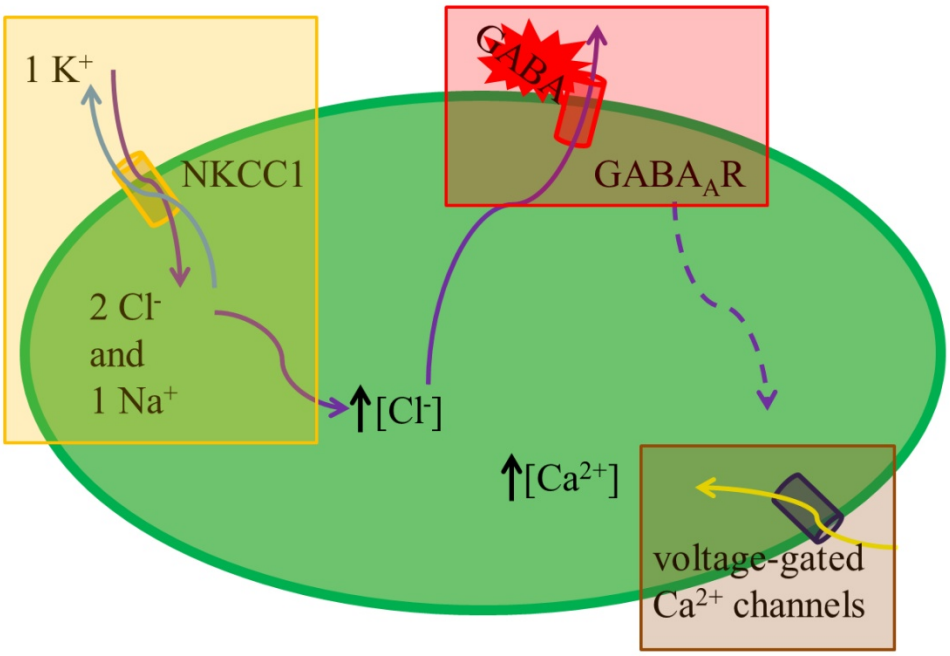

Fig. 2.11: Diagram of migrating or immature neurons, which have elevated $[Cl^-]_i$ due to high expression of the Na^+-K^+-Cl^- cotransporter 1 (NKCC1). When GABA opens the $GABA_AR$, the resulting Cl^- efflux depolarizes the cell and opens the voltage-gated Ca^{2+} channels.

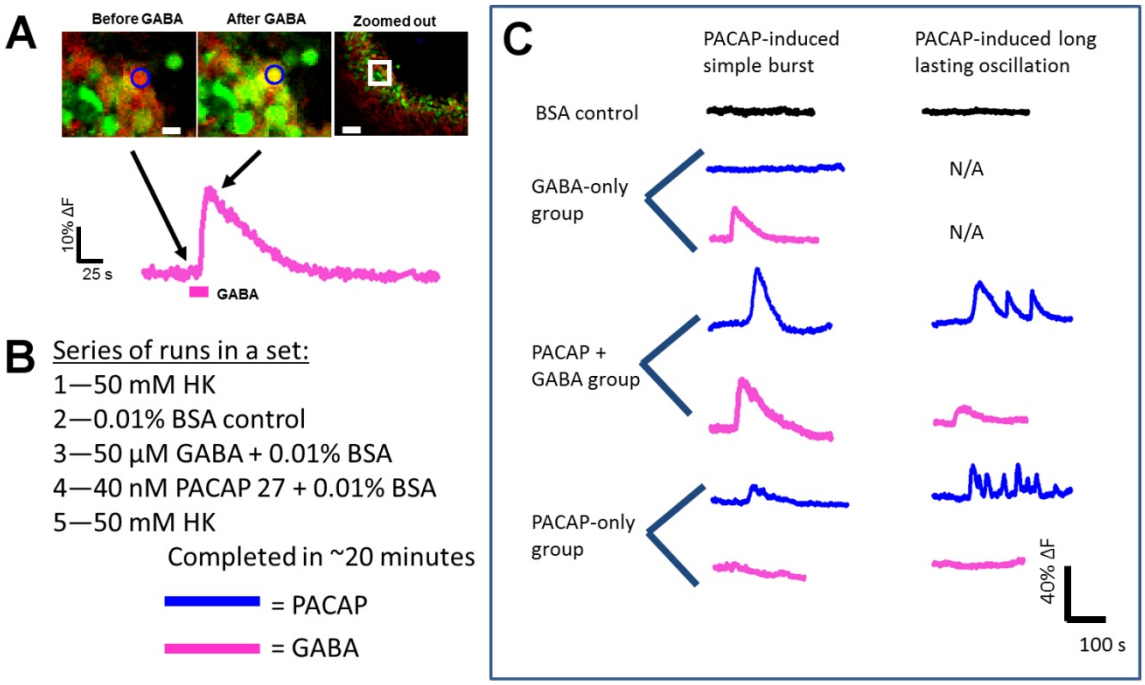

Fig. 2.12: Physiological identification of immature and mature GCs. (*A*) Image of the Fluo-4 loaded (green) Dlx2^{+} (red) cell responding to 50 µM GABA. Scale bars in images are 10 µm and 100 µm. (*B*) HK was tested at the start and end of each experiment to confirm the cells are healthy throughout. BSA and GABA were tested before PACAP to avoid false positives due to possible post-PACAP activity. Each set of runs takes about 20 minutes. (*C*) Sample recordings for each of three development stages with either PACAP-induced simple transients (left column) or $[Ca^{2+}]_i$ oscillations (right column). These data indicate heterogeneity among DLX2^{+} cells. Black is 0.1% BSA control, blue is 40 nM PACAP, and pink is 50 µM GABA.

Fig. 2.13: A subtype of GCs, GAD65$^-$, has a developmental switch from immature to mature between P2 to P5 that parallels increases in PACAP responses. (*A*) The percentage of total Dlx2-labeled GCs significantly switch from predominately migrating neuroblasts at P2 and P3 to predominately mature GCs at P5 ($p < 0.03$). The percentage of PACAP responsive cells also increases. (*B*) The percentage of total GAD65-labeled GCs remains fairly constant between P2 to P5 (*C*) The percentage of total unlabeled GCs in GAD65 data significantly switch from predominately migrating neuroblasts at P2 to predominately mature GCs at P5 ($p < 0.05$ to 0.01). Stimuli were 40 nM PACAP and 50 μM GABA.

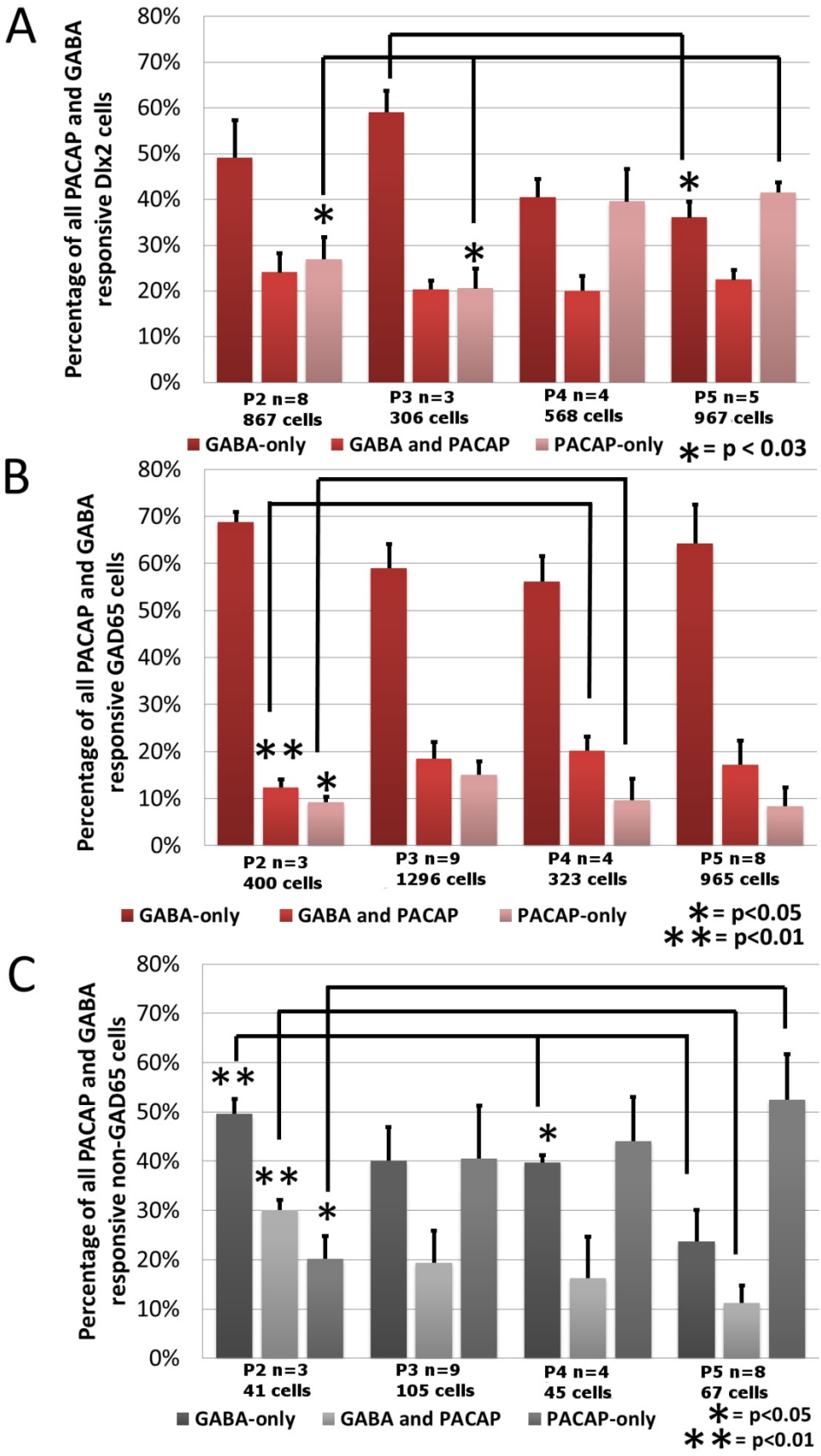
A
Percentage of all PACAP and GABA responsive Dlx2 cells
80%
70%
60%
50%
40%
30%
20%
10%
0%
P2 n=8
867 cells
P3 n=3
306 cells
P4 n=4
568 cells
P5 n=5
967 cells
GABA-only
GABA and PACAP
PACAP-only
* = p < 0.03
B
Percentage of all PACAP and GABA responsive GAD65 cells
P2 n=3
400 cells
P3 n=9
1296 cells
P4 n=4
323 cells
P5 n=8
965 cells
GABA-only
GABA and PACAP
PACAP-only
* = p<0.05
** = p<0.01
C
Percentage of all PACAP and GABA responsive non-GAD65 cells
P2 n=3
41 cells
P3 n=9
105 cells
P4 n=4
45 cells
P5 n=8
67 cells
GABA-only
GABA and PACAP
PACAP-only
* = p<0.05
** = p<0.01

CHAPTER 3

CALCIUM STORE-MEDIATED SIGNALING IN SUSTENTACULAR CELLS OF THE MOUSE OLFACTORY EPITHELIUM

Colleen Cosgrove Hegg[1], Mavis Irwin[2], Mary Lucero[2]

[1]Department of Pharmacology and Toxicology, Michigan State University, East Lansing, Michigan

[2] Department of Physiology, University of Utah, Salt Lake City, Utah

GLIA 57:634–644 (2009)

Calcium Store-Mediated Signaling in Sustentacular Cells of the Mouse Olfactory Epithelium

COLLEEN COSGROVE HEGG,[1]* MAVIS IRWIN,[2] AND MARY T. LUCERO[2]
[1]*Department of Pharmacology and Toxicology, Michigan State University, East Lansing, Michigan*
[2]*Department of Physiology, University of Utah, Salt Lake City, Utah*

KEY WORDS
glial cell; olfactory system; calcium oscillations; calcium waves; purinergic

ABSTRACT
Sustentacular cells have structural features that allude to functions of secretion, absorption, phagocytosis, maintenance of extracellular ionic gradients, metabolism of noxious chemicals, and regulation of cell turnover. We present data detailing their dynamic activity. We show, using a mouse olfactory epithelium slice model, that sustentacular cells are capable of generating two types of calcium signals: intercellular calcium waves where elevations in intracellular calcium propagate between neighboring cells, and intracellular calcium oscillations consisting of repetitive elevations in intracellular calcium confined to single cells. Sustentacular cells exhibited rapid, robust increases in intracellular calcium in response to G-protein coupled muscarinic and purinergic receptor stimulation. In a subpopulation of sustentacular cells, oscillatory calcium transients were evoked. We pharmacologically characterized the properties of purinergic-evoked increases in intracellular calcium. Calcium transients were elicited by release from intracellular stores and were not dependent on extracellular calcium. BAPTA-AM, a cytosolic calcium chelator, and cyclopiazonic acid, an endoplasmic reticulum Ca^{2+}-ATPase inhibitor irreversibly blocked the purinergic-induced calcium transient. Phospholipase C antagonist U73122 inhibited the purinergic-evoked calcium transient. 2-Aminoethoxydiphenyl borate, an inositol-1,4,5-trisphosphate (IP_3) receptor antagonist, and the ryanodine receptor (RyR) antagonists tetracaine and ryanodine, inhibited the UTP-induced calcium transients. Collectively, these data suggest that activation of the phospholipase C pathway, IP_3-mediated calcium release, and subsequent calcium-induced-calcium release is involved in ATP-elicited increases in intracellular calcium. Our findings indicate that sustentacular cells are not static support cells, and, like glia in the central nervous system, have complex calcium signaling.

INTRODUCTION

The olfactory epithelium (OE) of mammals consists of four primary cell types: basal progenitor cells, microvillar cells (the putative bipolar secondary chemosensory cells; Elsaesser et al., 2005; Elsaesser and Paysan, 2007), ciliated olfactory sensory neurons (the primary chemosensory cells), and sustentacular cells. Sustentacular cells function as both epithelial and glial support cells. As epithelial-like cells, sustentacular cells are involved in secretion (Menco and Morrison, 2003), endocytosis (Bannister and Dodson, 1992), and metabolism of toxicants (Dahl et al., 1982; Dahl, 1988). As glial-like cells (Okano and Takagi, 1974; Getchell, 1977), sustentacular cells physically and chemically insulate olfactory sensory neurons (Breipohl et al., 1974), actively phagocytose dead cells (Suzuki et al., 1996), and regulate the extracellular ionic environment (Breipohl et al., 1974; Rafols and Getchell, 1983; Getchell, 1986).

In the central nervous system, glial calcium regulates multiple cell functions including gene expression, cell proliferation, metabolism, ion transport systems, release of cell products, and cell death. Two types of glial calcium signals are intercellular Ca^{2+} waves where elevations in intracellular calcium propagate between neighboring cells, and intracellular calcium oscillations which consist of repetitive elevations in intracellular calcium that remain confined to single cells. Here, we demonstrate that sustentacular cells exhibit both types of glial calcium signals: intercellular calcium waves that may involve gap junctions or extracellular factors and intracellular calcium oscillations. We show that activation of G-protein coupled receptors including the P2Y purinergic receptor and the muscarinic acetylcholine receptor produce calcium oscillations in sustentacular cells. We pharmacologically determined that activation of the phospholipase C (PLC) pathway with subsequent production of inositol-1,4,5-trisphosphate (IP_3) is involved in G-protein coupled receptor evoked intracellular calcium increases. Our findings point to a key role for sustentacular cells in integrating communication between neurons, basal cells, and sustentacular cells (Masukawa et al., 1983; Hansel et al., 2001; Vogalis et al., 2005a; Vogalis et al., 2005b).

MATERIALS AND METHODS

Materials

All chemicals were obtained from Sigma Aldrich Chemicals (St. Louis, MO) except for ryanodine (Calbiochem,

Grant sponsor: NIH; Grant numbers: DC006897, DC002944.

*Correspondence to: Colleen C. Hegg, Department of Pharmacology and Toxicology, Michigan State University, B439 Life Sciences, East Lansing, MI 48824. E-mail: hegg@msu.edu

Received 21 June 2007; Accepted 9 September 2008

DOI 10.1002/glia.20792

Published online 22 October 2008 in Wiley InterScience (www.interscience.wiley.com).

San Diego, CA), cyclopiazonic acid (CPA, Alomone Labs, Jerusalem), and 2-aminoethoxydiphenyl borate (2-APB, Caymen Chemical, Ann Arbor, MI).

Solutions

Ringer's solution contained (mM): 140 NaCl, 5 KCl, 1 $MgCl_2$, 2 $CaCl_2$, 10 HEPES, and 10 glucose; pH 7.4, 290–320 mOsms. Probenecid (500 μM), an inhibitor of the organic anion transporter, was included to aid in the loading and retention of fluo-4 AM (Di et al., 1990; Manzini et al., 2008). Zero calcium Ringer's solution contained (mM) 130 NaCl, 5.5 KCl, 10 HEPES, and 10 glucose; 4 glycol-bis(2-aminoethylether)-N,N,N′,N′-tetra-acetic acid (EGTA), pH 7.4, 290–320 mOsms. In some experiments, NaCl was replaced with an equimolar amount of either KCl or caffeine. Concentrated stocks were made in water or Ringer's solution (ATP, UTP, ryanodine, Ni^{2+}, neomycin, mecamylamine, and acetylcholine), stored at −20°C and reconstituted on the day of the experiment. BAPTA-AM, U73122, U73343, and CPA stocks were made in DMSO (0.1–1% final concentration DMSO), and atropine was made in ethanol (0.03% final concentration ethanol). The odorants n-amyl acetate and R-carvone, (10 μM each) were added directly to Ringer's solution.

Preparation of Olfactory Epithelium Slices

All animal procedures were approved by the University of Utah or Michigan State University Institutional Animal Care and Use Committees, and all applicable guidelines from the National Institutes of Health Guide for Care and Use of Laboratory Animals were followed. To prepare olfactory epithelial (OE) slices, neonatal Swiss Webster or C57/BL6 mice (Charles River, Portage, MI or Simonsen, Gilroy, CA; postnatal day 0–6) were quickly decapitated, and the skin and lower jaw were removed. Tissue was embedded in a carrot, mounted on a vibratome-cutting block in ice cold Ringer's solution and 250–300 μm slices were made. For the chronic BAPTA-AM study, slices were exposed to 100 μM BAPTA-AM or vehicle (1% DMSO) at 37°C in 5% CO_2 in Neuroblast media (Invitrogen, Carlsbad, CA) and 2.5% antibiotic-antimycotic solution (Invitrogen, Carlsbad, CA). Slices were loaded with 18 μM fluo-4 AM (Molecular Probes, Eugene, OR) for 90 min at 25°C. A stock solution of fluo-4 AM was prepared weekly in DMSO containing 20% pluronic F-127 (Invitrogen, Carlsbad, CA). Ringer's solution was added to this stock solution for a final concentration of 18 μM fluo-4 AM, 0.04% pluronic F-127, and 0.4% DMSO.

Confocal Calcium Imaging

Slices were placed in a laminar flow chamber (Warner Instruments, Hamden, CT) and perfused continuously with Ringer's solution at a flow rate of 1.5–2.0 mL/min. Test solutions were applied using bath exchange and a small volume loop injector (200 μL). Our perfusion system exchanges the bath in ca. 7–10 s and traces were not corrected for this delay. Imaging occurred 50–100 μm below the surface of the slice to avoid damaged cells.

A Zeiss LSM 510 confocal laser scanning system (Zeiss, Thornwood, NY) was used for data collection and analysis. A krypton-argon ion laser was used for fluorescence excitation at 488 nm. Fluorescence emissions were filtered at 510 nm. Time series experiments were performed collecting 1400 × 700 pixel images at 0.2–1 Hz. Some experiments were performed using an Olympus Fluoview 100 laser scanning confocal microscope (Olympus, PA), an argon laser, and equivalent laser settings. The fluorometric signals obtained are expressed as relative fluorescence (F) change, $\Delta F/F = (F\text{-}F_0)/F_0$,where F_0 is the basal fluorescence level (mean F of first 10 frames). Increases in fluorescence greater than 10% above baseline were deemed responses.

Imaging Data Analysis

Experiments were performed by sequentially obtaining (1) initial control agonist-evoked calcium transients, (2) calcium transients evoked by coapplication of agonist in the presence of antagonists, and (3) recovery agonist-evoked calcium transients. To be included in our data set, the peak amplitude of the recovery Ca^{2+} transient had to be at least 75% of the initial transient amplitude. All data were normalized to the initial Ca^{2+} transient. Linear rundown occurred during multiple applications of test compounds. Thus, to determine if there were treatment effects, we performed a linear regression on the peak amplitude of the control and recovery purinergic responses for every sustentacular cell. Using the linear regressions, predicted peak amplitudes for a second agonist response were calculated. Unless noted otherwise, paired Student's t-tests were used to determine significant differences ($P < 0.05$) between the predicted peak amplitude and the observed peak amplitude.

Odorants (10 μM n-amyl acetate and/or 10–100 μM R-carvone) and elevated potassium Ringer's solution (50–145 mM) were superfused onto slices at the end of an experiment to distinguish odorant- and voltage-insensitive sustentacular cells, and olfactory sensory neurons. In addition, the locations of sustentacular cell somas in apical OE, versus olfactory sensory neuron somas, in middle OE, were used to identify cell types.

RESULTS

Sustentacular Cells Rarely Generate Spontaneous Calcium Waves

We used a neonatal mouse olfactory epithelium slice preparation loaded with fluo-4 AM to study sustentacular cell physiology. We occasionally observed intercellular calcium waves in sustentacular cells that propagated

to neighboring cells (Fig. 1A; see also supplementary movie). On average, a calcium wave traveled 107 ± 11 μm (n = 4) before extinguishing. Either an extracellular factor or chemical coupling between sustentacular cells may be involved in the propagation of these waves. There is ample evidence of gap junctions present in sustentacular cells (Menco, 1988; Miragall et al., 1992; Zhang and Restrepo, 2002; Rash et al., 2005), and we have shown that sustentacular cells are electrically coupled to each other (Vogalis et al., 2005a). Spontaneous intracellular calcium waves could be observed in a few slices that acquired fluo-4 AM loading in the thin cytoplasmic extensions and endfeet of sustentacular cells. The intracellular calcium increased in the cell soma first and slowly traveled to the basal region (Fig. 1B,C). In Fig. 1B, the wave traveled from the cell soma to the basal cell layer in 9.5 s (0.4 Hz sampling rate). The frequency of imaging a spontaneous intercellular or intracellular calcium wave was low (0.7%; 4/524 slices), although calcium waves may occur when the slices were not actively imaged. Thus, we did not investigate the mechanisms of initiation and propagation of the intercellular calcium waves.

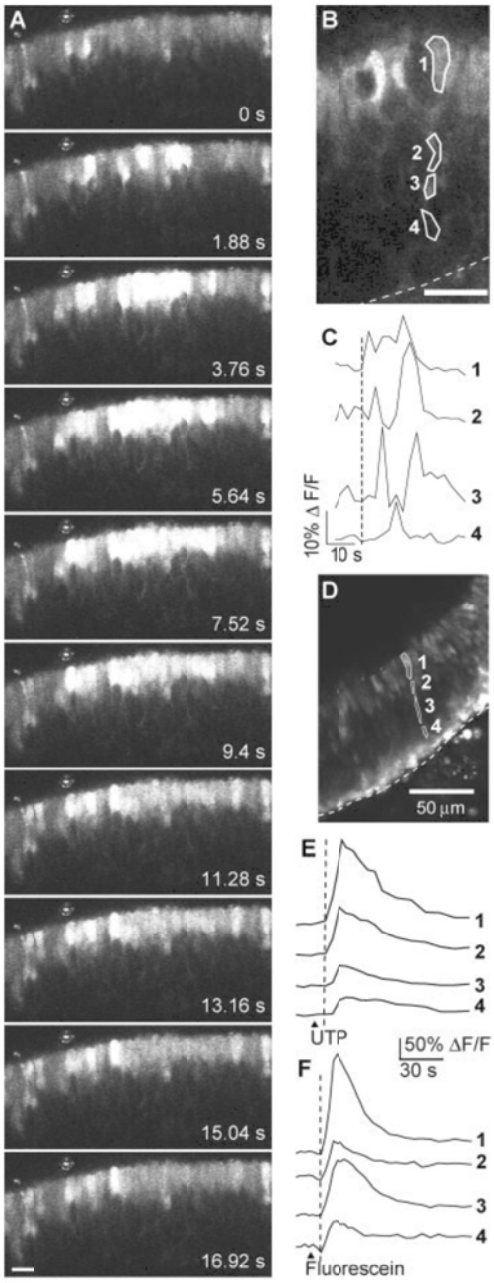

Fig. 1. Intercellular and intracellular calcium waves in sustentacular cells. **(A)** Shown are a series of images acquired during a spontaneous intercellular calcium wave in a Fluo-4AM loaded slice. See supplemental data for movie. Scale bar, 20 μm. **(B)** Example of a spontaneous intracellular calcium wave traveling from the apical to the basal cell layer. Numbered regions correspond to the traces shown in **(C)**. Dashed line, basement membrane. Scale bar, 20 μm. **(C)** Time course of the transient Ca^{2+} increase recorded from the sustentacular cell shown in **(B)**. Numbered traces correspond to the regions shown in **(B)**. **(D-F)** Confocal image **(D)**, and time course of the UTP evoked Ca^{2+} transients **(E)**, and fluorescein **(F)** fluorescence recorded from the sustentacular cell shown in **(D)**. Numbered traces correspond to the regions shown in **(D)**. ▲, time of loop injection of UTP or fluorescein.

Evoked Oscillatory Calcium Transients in Sustentacular Cells

We previously showed that sustentacular cells express G-protein coupled $P2Y_2$-type purinergic receptors (Hegg et al., 2003; Hegg and Lucero, 2006). Purinergics evoked intracellular calcium waves in sustentacular cells (Fig. 1D,E). Like the spontaneous intracellular calcium wave, the ATP-evoked calcium wave initiated in the cell soma and traveled to the basal layer at an average speed of 35 ± 20 μm/s (n = 4, range 6–77 μm/s). At the end of an experiment, fluorescein, an inert fluorescent compound, was used to monitor perfusion rates. The fluorescein fluorescence simultaneously reached the entire breadth of the OE (Fig. 1F), from apical surface to basal cell layer, suggesting that the intracellular wave was not due to a perfusion artifact.

The majority of increased intracellular calcium was measured in the cell soma, likely due to its size, and the low loading of fluo-4 AM in the thin cytoplasmic extensions of the sustentacular cells. Thus, we examined the increases in intracellular calcium from the soma. The selective P2Y receptor agonist UTP reproducibly evoked calcium transients in sustentacular cells (Fig. 2A). The average normalized peak calcium amplitudes from three successive applications of UTP superfused 5 min apart were 1.00 ± 0.00, 0.95 ± 0.05, and 1.02 ± 0.03 (Fig. 2B; n = 24 cells/3 slices, $P = 0.37$). Interestingly, in 61% of

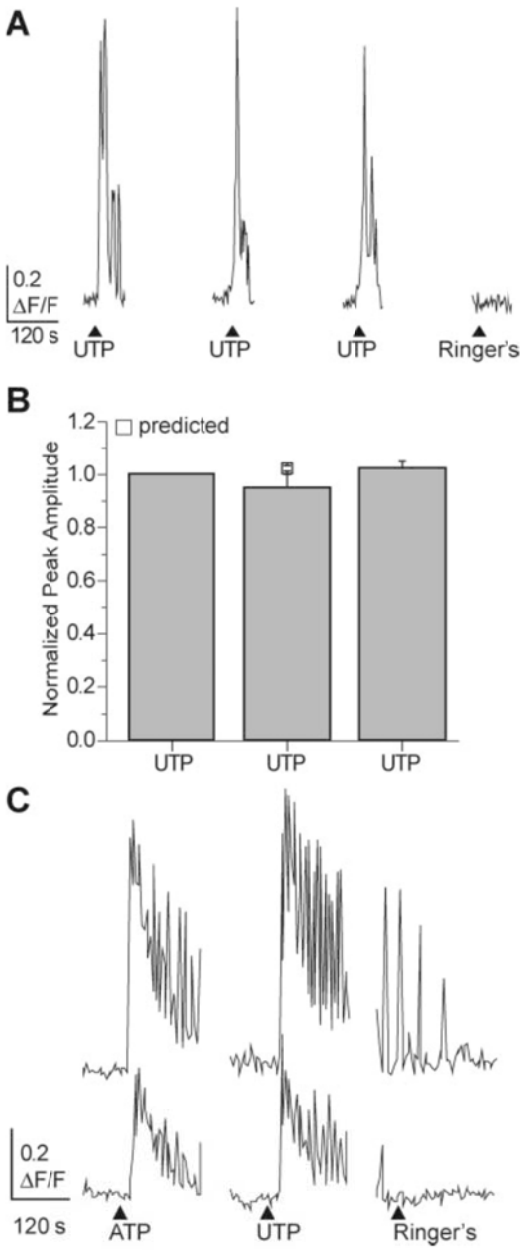

Fig. 2. Purinergic-evoked oscillatory calcium transients in sustentacular cells. **(A)** Multiple applications of 10 μM UTP produce similar changes in intracellular calcium. ▲ indicates time of UTP superfusion. In this figure and all subsequent figures, breaks in traces correspond to time when images were not collected. **(B)** Average normalized peak calcium transient amplitudes are not different from the predicted peak amplitude for the second application (□, mean ± SEM). **(C)** Representative traces showing oscillatory calcium transients evoked by the superfusion of 10 μM purinergic agonists ATP and UTP.

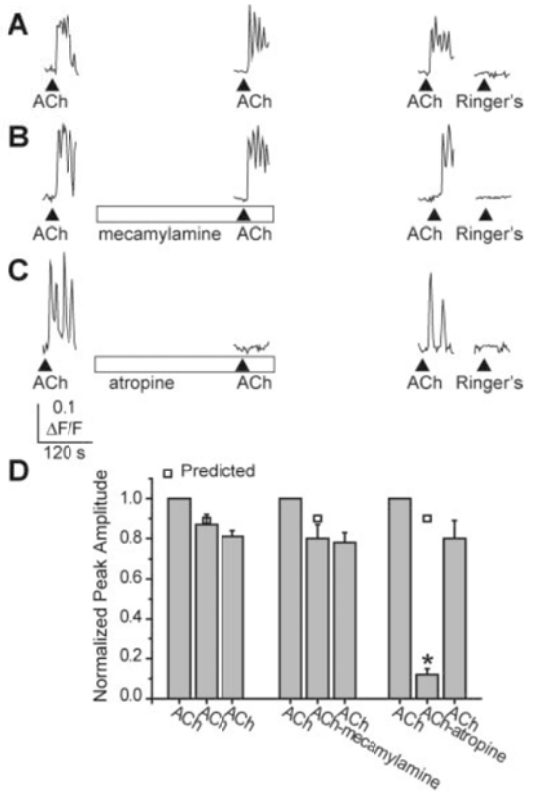

Fig. 3. Acetylcholine-evoked oscillatory calcium transients in sustentacular cells. **(A–C)** Oscillatory calcium transients evoked by the superfusion of 500 μM acetylcholine (ACh). (▲ indicates time of ACh superfusion, □ indicates time of antagonist superfusion). **(B,C)** ACh-evoked calcium transients were inhibited by 10 μM atropine, a muscarinic antagonist, but not 30 μM mecamylamine, a competitive nicotinic antagonist. **(D)** Average normalized peak amplitudes are shown, as are the predicted peak amplitudes for the second application (□). *, $P < 0.001$.

cells examined (106/175 cells), the UTP-stimulated response was complex with an initial calcium transient followed by calcium oscillations that could be fused and led to a sustained increase in calcium (Fig. 2A,C). Similar results were observed when the nonselective P2X and P2Y receptor agonist ATP was used (Fig. 2C). In 3% of the cells exhibiting oscillatory calcium responses (6/175 cells), the cyclical oscillations persisted long after UTP had been washed away (Fig. 2C, Ringer's). A total of 36% of sustentacular cells (63/175 cells) exhibited a single monophasic increase in intracellular calcium (see Fig. 1E) and 3% (6/175) exhibited unfused oscillations in intracellular calcium (similar to top trace in Fig. 2C Ringer's). Thus, sustentacular cells exhibit complex temporal patterns of calcium signaling upon purinergic stimulation.

Multiple calcium transients and oscillations could also be evoked in sustentacular cells by 500 μM acetylcholine (ACh), an agonist to both muscarinic and nicotinic ACh receptors (see Fig. 3). In 55% of the cholinergically-stimulated sustentacular cells (21/38 cells), the calcium

oscillations became fused leading to a sustained increase in calcium that eventually recovered to baseline (Fig. 3A–C). The average normalized peak calcium amplitudes from three successive applications of ACh superfused 5 min apart were 1.00 ± 0.00, 0.87 ± 0.05, and 0.81 ± 0.03 (Fig. 3A,D; n = 7 cells/3 slices, $P = 0.39$). The nicotinic acetylcholine receptor antagonist mecamylamine (30 μM) had no significant effect on the amplitude of evoked calcium transients (80 ± 7% of control; Fig. 3B,D; $P = 0.17$, n = 5 cells/3 slices) but atropine (10 μM), a competitive antagonist to G-protein coupled muscarinic ACh receptors, significantly inhibited the calcium transients by 89% (11 ± 3% of control; Fig. 3C,D; $P < 0.001$; n = 6 cells/3 slices). Thus, activation of G-protein coupled purinergic and muscarinic receptors evoked oscillatory calcium transients in sustentacular cells.

Purinergics Evoke Transient Calcium Increases via Release From Intracellular Stores

Increases in intracellular calcium can occur either by influx from the extracellular space or by release from intracellular calcium stores located within the endoplasmic reticulum (ER) (Berridge et al., 2000). We investigated the source of the intracellular calcium increase by comparing purinergic responses evoked in the presence and absence of extracellular calcium (Fig. 4A). When the slice was superfused with calcium-free Ringer's solution, the UTP-evoked calcium transients in sustentacular cells were not significantly different than in the presence of extracellular calcium (112 ± 9% of control, $P = 0.09$, n = 6 cells/3 slices), suggesting that increases in calcium were mainly mediated via activation of G-protein coupled P2Y receptors with subsequent release from intracellular stores. To further distinguish between release from calcium stores and calcium influx, we used the nonspecific voltage-dependent calcium channel blocker nickel (Fig. 4B). Nickel (100 μM) had no effect on the UTP-evoked calcium transients (103 ± 19% of control, $P = 0.71$, n = 5 cells/3 slices).

To test whether intracellular calcium is required, we used the cell-permeable cytosolic calcium chelator BAPTA-AM to buffer the intracellular level of calcium. BAPTA-AM (100 μM) or vehicle (1% DMSO) was applied to slices for 1 h before fluo-4 AM loading and calcium imaging to allow time for de-esterification of the AM component. Compared with the vehicle-treated slices, where two UTP applications evoked calcium transients that were on average 43 ± 8 and 39 ± 6% ΔF/F (n = 14 cells/4 slices), BAPTA-AM significantly reduced the UTP-induced calcium transients by 84 and 81% to 7 ± 2 and 7 ± 2% ΔF/F (n = 16 cells/5 slices, $P < 0.0001$, independent t-test, Fig. 4C). Interestingly, exposure to BAPTA-AM reduced the main monophasic calcium transient, but did not entirely eliminate the oscillatory calcium increases. To ensure that the BAPTA-AM treatment was not damaging the OE, we also applied odorant (100 μM R-carvone) and elevated potassium Ringer's solution (145 mM; high K^+) to the same slices. Odorants

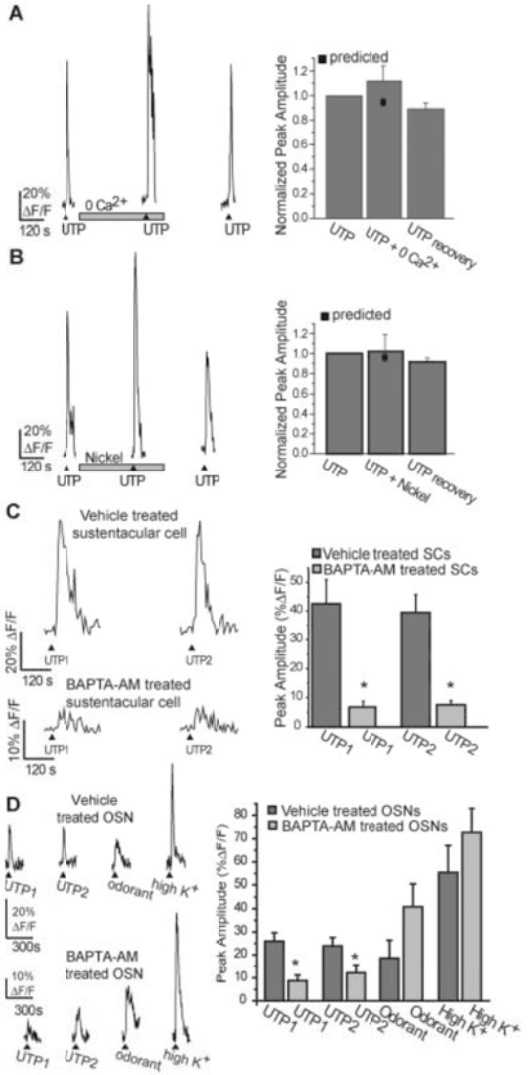

Fig. 4. Purinergic-evoked calcium transients are mediated via intracellular calcium. **(A,B)** Slices were superfused with multiple applications of 10 μM UTP in **(A)** the absence of extracellular calcium (+4 mM EGTA) or **(B)** the presence of 100 μM nickel. (▲ indicates time of UTP superfusion, □ indicates time of drug superfusion). Y-axis is normalized peak amplitude. Right panels: Average normalized peak amplitudes are shown as are the predicted peak amplitudes for the second application (■). **(C,D)** Representative calcium transients from slices pre-treated with BAPTA-AM (100 μM) or vehicle (1% DMSO) in **(C)** sustentacular cells (SCs) or in **(D)** olfactory sensory neurons (OSNs). Right panels: average peak amplitudes + SEM *, $P < 0.05$.

bind to G-protein coupled odorant receptors on olfactory sensory neurons (OSNs), elevating cAMP levels, and opening cyclic nucleotide-gated channels, allowing calcium influx from the extracellular space. Likewise, elevated potassium depolarizes the OSNs opening voltage-gated calcium channels with subsequent calcium

influx. We found that BAPTA-AM treatment had no effect on odorant ($P = 0.13$, Independent t-Test) or depolarization-evoked ($P = 0.30$) calcium responses in OSNs (n = 10 OSNs/4 vehicle slices and 17 OSNs/5 BAPTA-AM treated slices; Fig. 4D). As with the sustentacular cells, BAPTA treatment significantly reduced the UTP-evoked calcium transient in OSNs from 26 ± 4 and 24 ± 4% ΔF/F (n = 14 cells/4 slices) to 11 ± 3 and 13 ± 3% ΔF/F (n = 17 OSNs/5 slices, Independent t-tests, $P = 0.002$ and 0.05).

To further test whether intracellular calcium is required, we prevented the refilling of intracellular calcium stores with cyclopiazonic acid (CPA, 10 μM), a highly specific inhibitor of the endoplasmic reticulum Ca^{2+}-ATPase. After a 5 min application of CPA, the peak calcium response elicited by UTP was not significantly different than the initial control calcium transient (29.1 vs. 28.1% ΔF/F, $P = 0.51$, n = 51 cells/3 slices, Fig. 5A). However, none of the 51 cells had a recovery peak calcium transient that was greater than the 75% criteria to be included in the data set (7.4% F/F, 25 ± 2% of initial control response, $P < 0.001$). The slices were still viable after 5 min CPA exposure as odorant responses from OSNs were still observed (27.2 ± 2.5% ΔF/F, n = 20 OSNs/3 slices, data not shown). This suggested that CPA needed a longer exposure time to be more effective. Thus, we stopped the bath perfusion to prolong CPA application. The intracellular calcium concentrations were monitored every minute over a 15–30 min period. As previously reported in glia (Simpson and Russell, 1997), CPA caused a delayed and prolonged increase in intracellular calcium levels that returned to baseline levels over a 30 min period, presumably due to elevated intracellular calcium as the inhibited Ca^{2+}-ATPase is unable to resequester calcium into stores, followed by a return to baseline calcium levels as the cell's calcium buffering activity increases (Fig. 5B). After the intracellular calcium levels had returned to baseline, the bath perfusion was started and UTP was applied in the maintained presence of CPA. CPA depletion of intracellular stores significantly reduced the UTP-elicited calcium transient by 96% from 76.1 ± 5.4% ΔF/F to 2.3 ± 0.2% ΔF/F ($P < 0.001$, n = 59 cells/3 slices). Although CPA inhibition of the Ca^{2+}-ATPase is reversible in other systems, CPA inhibition of the UTP-evoked calcium increase was irreversible in the OE slices, even after up to 75 min wash, with a peak UTP calcium transient of 2.4 ± 0.2% ΔF/F ($P < 0.001$, n = 59 cells/3 slices, Fig. 5B). Odorants were able to evoke an increase in calcium from OSNs 10 min after washout of CPA (data not shown), suggesting that the slices were still viable following chronic CPA exposure. In comparison, when slices were treated with vehicle (0.1% DMSO) under a similar protocol, 52% of the cells that responded to the initial UTP application (14/27) also responded to the third recovery UTP application 10–30 min postwash with a peak calcium transient of 75% or greater. The vehicle-treated peak UTP-induced calcium transients were not significantly different with values of 7.0 ± 0.7, 6.1 ± 0.7, and 6.5 ± 0.5% ΔF/F, respectively ($P > 0.3$, n = 14 cells/3 slices, Fig. 5C). Collectively, with our previous report (Hegg et al., 2003), these data suggest that purinergics activate a P2Y receptor on sustentacular cells that evokes an increase in intracellular calcium via release from intracellular stores. Thus, for the rest of the study the selective G-protein coupled P2Y receptor agonist UTP was utilized.

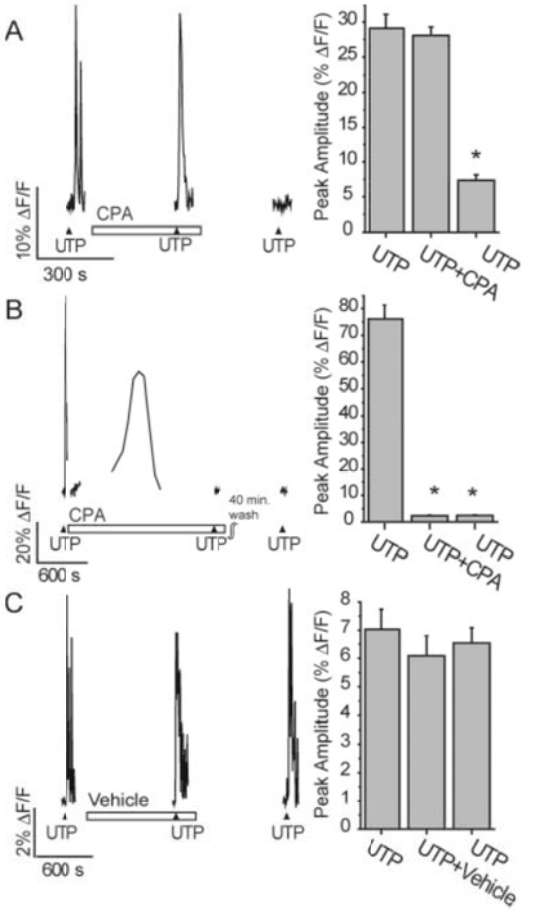

Fig. 5. Purinergic-evoked calcium transients are mediated via intracellular calcium release. Slices were superfused with multiple applications of 10 μM UTP in 5 min acute **(A)**, or 15–30 min chronic **(B,C)**, presence of 10 μM cyclopiazonic acid (CPA) or vehicle (0.1% DMSO). (▲ indicates time of UTP superfusion, □ indicates time of drug superfusion). Right panels: Average peak calcium transient amplitudes are shown *, $P < 0.001$.

The Phospholipase C Pathway Contributes to Purinergic-Evoked Increases in Intracellular Calcium

G-protein coupled receptor activation can trigger intracellular calcium increases via activation of PLC and subsequent production of IP_3 and diacylglycerol (DAG).

G-protein coupled receptor production of IP_3 could evoke cyclical release of calcium from IP_3-sensitive stores. We investigated the role of the PLC pathway by using the nonspecific PLC antagonist neomycin and the specific antagonist U73122. In the presence of neomycin, the UTP-induced calcium transient was significantly reduced by 68 ± 6% (Fig. 6A, n = 34 cells/3 slices, $P < 0.001$). Likewise, 5 min preincubation of U73312 (100 μM) inhibited the UTP-evoked calcium transient by 31 ± 9% (Fig. 6B, n = 20 cells/3 slices, $P = 0.01$) whereas the inactive structural analog, U73343 (100 μM), did not have any effect on the UTP-evoked calcium transients (99 ± 4% of recovery, n = 52 cells/3 slices; $P = 0.80$, Fig. 6C). Furthermore, slices incubated 20 min in U73312 (200 μM) were no longer responsive to UTP (Fig. 6D). The mean number of UTP-responsive cells following U73312 treatment was 0.8 ± 0.5/slice and following vehicle treatment (0.1% DMSO) was 23.8 ± 8.5 (n = 10 and 4 slices, $P = 0.0008$). Both the U73312- and vehicle-treated slices showed normal odorant responses indicating that the slices were healthy. Coapplication of UTP and 2-aminoethoxydiphenyl borate (2-APB; 100 μM), a membrane permeable antagonist of IP_3-sensitive Ca^{2+} channels and store-operated Ca^{2+} entry, significantly inhibited UTP-evoked calcium transients by 30% (n = 25 cells/3 slices, $P < 0.001$, Fig. 6E). Collectively, this suggests that the PLC pathway mediates the purinergic-evoked calcium increases.

Involvement of Calcium Release Channels

There are two families of calcium release channels located on the endoplasmic reticulum of most cells, the IP_3 receptors and the ryanodine receptors (RyR) (Berridge et al., 2000), which could contribute to the UTP-induced increases in intracellular calcium. To examine the role of ryanodine receptors, caffeine, a RyR agonist at millimolar concentrations, was acutely superfused onto our OE slices (Fig. 7A,B). Caffeine- (10, 50 mM) induced transient increases in intracellular calcium in both OSNs and sustentacular cells (Table 1, n = 5 slices). In sustentacular cells, the caffeine-induced calcium transients were significantly smaller than UTP-induced calcium increases (Table 1, $P < 0.001$, Fig. 7A,B). In contrast, in OSNs, only the 10 mM caffeine-induced calcium increase was significantly smaller than UTP-, 50 mM caffeine-, or odorant-induced calcium transients (Table 1, $P < 0.05$, Fig. 7A,B). These data suggest that sustentacular cells have smaller caffeine-sensitive stores than OSNs.

To examine the role of RyRs in purinergic-mediated sustentacular cell calcium oscillations, we used tetracaine, a nonspecific antagonist of RyRs. Tetracaine (500 μM) significantly reduced the UTP-induced calcium transient to 66 ± 7% of the initial UTP calcium transient peak (Fig. 7C, n = 19 cells/3 slices, $P < 0.001$). As expected, tetracaine had an even greater effect on the oscillatory portion of the calcium response. We examined all cells in which UTP-evoked an oscillatory calcium

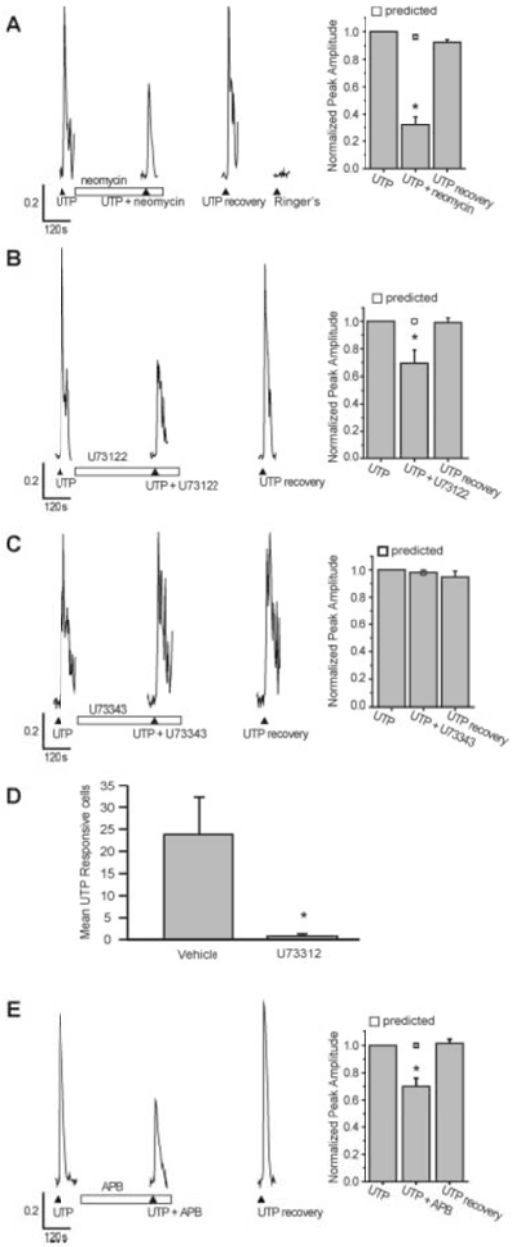

Fig. 6. The PLC pathway has a role in purinergic-evoked calcium increases. **(A-C, E)** Slices were superfused with multiple applications of 10 μM UTP in the presence of **(A)** 150 μM neomycin, **(B)** 100 μM U73122, **(C)** 100 μM U73343, **(E)** 100 μM 2-APE. (▲ indicates time of UTP superfusion, □ indicates time of drug superfusion). Y-axis is normalized peak amplitude. Right panels: Average normalized peak amplitudes and the predicted peak amplitudes for the second application (□) are shown. *, $P < 0.01$. **(D)** UTP responsive cells (mean ± SEM) from slices incubated 20 min in 0.1% DMSO vehicle (n = 4) or 200 μM U73122 (n = 10, $P = 0.0008$).

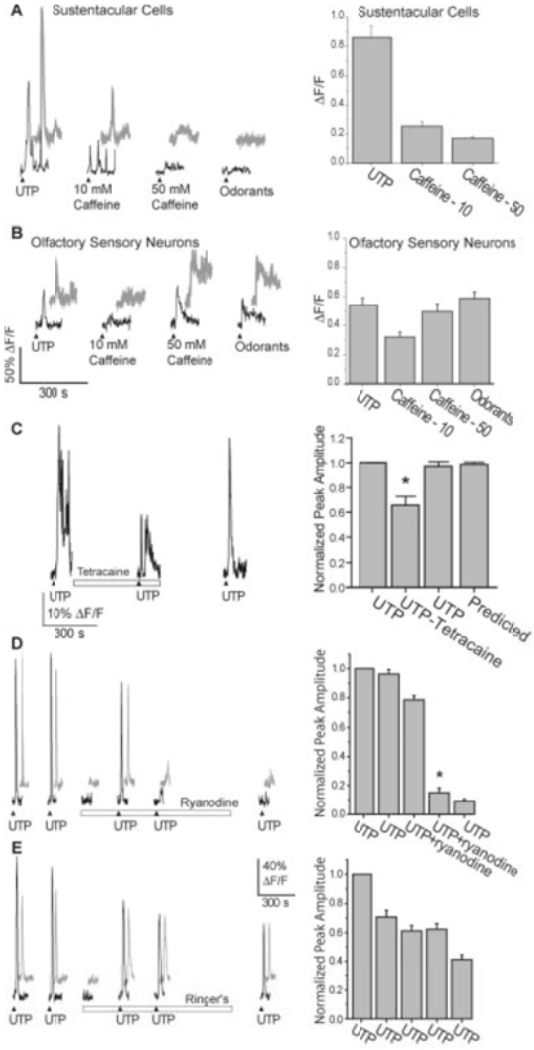

Fig. 7. Involvement of the ryanodine receptor in sustentacular cell calcium signaling. **(A-B)** Representative traces from two sustentacular **(A)** and two OSNs **(B)** during acute superfusion of caffeine (10–50 mM). (▲ indicates time of UTP, caffeine, or odorant superfusion). Right panels: Average peak amplitudes are shown *, $P < 0.01$. **(C)** Representative trace from a sustentacular cell superfused with UTP in the absence and presence of tetracaine (500 μM). (▲ indicates time of UTP superfusion, □ indicates time of drug superfusion). Right panel: Average normalized peak amplitudes are shown as is the predicted peak amplitude for the second application. *, $P < 0.001$. **(D-E)** Two representative traces from sustentacular cells repetitively superfused with UTP in the presence **(D)** or absence **(E)** of ryanodine (50 μM). (▲ indicates time of UTP superfusion, □ indicates time of drug superfusion). Right panels: Average normalized peak amplitudes are shown.*, $P < 0.001$.

transient, and compared the areas under the curves from the peak of the second calcium oscillation across repeated UTP applications. In control studies, the second UTP application actually increased the area under curve to 204 ± 25% of the initial UTP response (n = 17 cells from two slices; data not shown). In the presence of tetracaine, the area under the curve was significantly reduced to 51 ± 4% of the initial UTP transient's area under the curve (n = 19 cells from three slices, $P < 0.0001$).

Ryanodine was used to further ascertain the role of RyRs in purinergic-mediated calcium signaling (Fig. 7D). In these experiments, two control UTP-induced calcium transients were elicited with normalized peak heights of 1.0 ± 0.0 and 0.96 ± 0.03. Multiple UTP responses were elicited in the presence of 50 μM ryanodine. Ryanodine had no effect on the first UTP-evoked calcium transient with a peak height of 0.79 ± 0.03. However, the second UTP response was reduced to 0.15 ± 0.03 (n = 19 cells/2 slices, $P < 0.001$) and subsequent UTP responses remained reduced, even following washout (peak height = 0.09 ± 0.01). In comparison, in Ringer's control solution, UTP application elicited five similar calcium transients with normalized peak heights of 1.0 ± 0, 0.71 ± 0.05, 0.61 ± 0.04, 0.62 ± 0.04, and 0.41 ± 0.03 (Fig. 7E, n = 26 cells/2 slices). The difference in peak heights between the UTP-induced calcium transients elicited in the presence of ryanodine was significantly greater than the difference in peak heights elicited in Ringer's control ($P < 0.001$). These data suggest that ryanodine may bind to ryanodine receptors only after they have been activated. In this case, the first UTP application in the presence of ryanodine evokes calcium-induced calcium release (CICR), activating RyRs, and allows ryanodine to inhibit RyRs. Alternatively, ryanodine may partially activate RyRs and deplete calcium stores. With either mechanism, subsequent UTP-evoked calcium transients are reduced, suggesting that RyRs contribute to the UTP-evoked calcium signaling. Collectively, these data suggest that both IP_3 receptors and ryanodine receptors are involved in G-protein coupled receptor evoked intracellular calcium increases.

DISCUSSION

Historically, sustentacular cells have been thought of as epithelial support cells, but evidence is mounting to suggest that they are also glial-like. Using confocal calcium imaging of neonatal mouse olfactory epithelium slices, we observed spontaneous intercellular calcium waves and intracellular calcium oscillations in sustentacular cells that are characteristic of glial calcium signaling.

Intercellular and Intracellular Calcium Waves in Sustentacular Cells

Sustentacular cells may be chemically coupled and may propagate increases in intracellular calcium between cells via gap junctions. Both ultrastructural (Breipohl et al., 1974; Menco, 1988) and immunocytochemical (Miragall et al., 1992; Zhang and Restrepo, 2002; Rash et al., 2005) evidence supports that sustentacular cells form gap junctions with each other in the

TABLE 1. Characteristics of Caffeine-Elicited Calcium Increases

	Sustentacular cells		OSNs	
	Number of responding cells	Peak amplitude (% ΔF/F)	Number of responding cells	Peak amplitude (% ΔF/F)
UTP	117/117	86 ± 8	33/68	54 ± 5
10 mM caffeine	46/117	25 ± 3[b]	33/68	32 ± 3[a]
50 mM caffeine	41/117	17 ± 1[b]	39/68	50 ± 5
Odorants	na	na	64/68	59 ± 5

[a,b]Significantly different from UTP.
[a]$P < 0.05$;
[b]$P < 0.001$; na, not applicable.

apical zone at all stages of development. Our recent electrophysiological study (Vogalis et al., 2005a) explored the presence of gap junctions in mouse sustentacular cells. We found evidence for unopposed gap junction channels, or hemichannels, and electrical coupling between sustentacular cells. There are several possible intracellular messengers that could participate in the generation and propagation of intercellular calcium waves, including IP_3 and calcium itself. These factors may diffuse through gap junctions to neighboring cells and potentially trigger calcium release therein. It is also possible that a released factor, such as ATP, diffuses extracellularly to neighboring cells and stimulates cell-surface G-protein coupled receptors. In this way, the propagation of the intercellular calcium wave may depend on both intracellular and extracellular signals. Detailed characterization of intercellular wave propagation in sustentacular cells will be addressed in future studies.

Spontaneous and purinergic-evoked intracellular calcium waves were measured on occasions when the dye loaded from apex to base of the OE. The UTP-induced calcium transient initiated in the apical portion of the sustentacular cell and traveled to the basal cell layer at a speed ranging from 6–77 μm/s, similarly to that reported in sustentacular cells of *Xenopus laevis* tadpoles (Hassenklover et al., 2008).

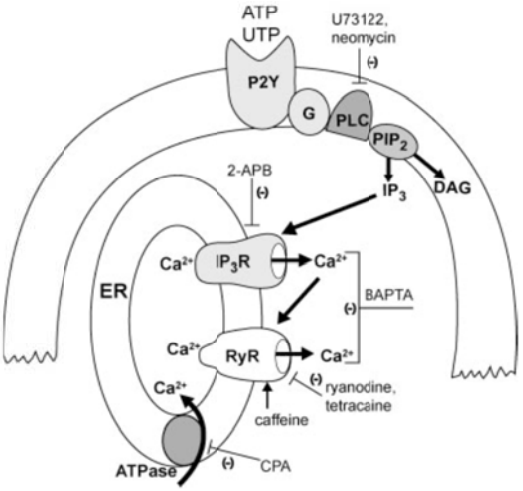

Fig. 8. Mechanism of G-protein coupled receptor calcium mobilization. Activation of GPCRs activates phospholipase C and production of DAG and IP_3. IP_3 activates the IP_3 receptor with subsequent release of calcium from stores. The increase in cytosolic calcium induces calcium-dependent calcium release via the ryanodine receptor. Large arrows depict pathway of GPCR activation and thin lines depict pharmacological targets. Abbreviations: 2-APB, 2-aminoethoxydiphenyl borate; ATPase, Ca^{2+}-ATPase; CPA, cyclopiazonic acid; DAG, diacylglycerol; ER, endoplasmic reticulum; GPCR, G-protein coupled receptor; G, G-protein; IP_3R, IP_3 receptor; PLC, phospholipase C; PIP_2, phosphoinositols; RyR, ryanodine receptor.

G-Protein Coupled Receptors Evoke Intracellular Calcium Oscillations

We routinely observed the second main form of glial calcium signaling, intracellular calcium oscillations, in sustentacular cells. We only observed calcium responses to agonists of purinergic and cholinergic metabotropic receptors on sustentacular cells, although we have screened a number of bioactive compounds, including norepinephrine, serotonin, GABA, glutamate, and histamine. It is possible that a faster stimulus delivery system would reveal other rapidly desensitizing receptor-mediated responses. We observed a variety of temporal patterns of sustentacular cell intracellular calcium increases. As in glia (Verkhratsky and Kettenmann, 1996), the time course of the increase was either a single spike, a transient followed by fused oscillations, or oscillations. Previous reports have shown that stimulation of metabotropic receptors evokes oscillatory increases in intracellular calcium in glia (Charles et al., 1991; Cornell-Bell and Finkbeiner, 1991; Kim et al., 1994).

We pharmacologically investigated the mechanism involved in UTP-mediated increases in intracellular calcium (see Fig. 8). We saw no change in calcium responses in the absence of calcium from the extracellular solution, whereas when intracellular calcium stores were depleted with cyclopiazonic acid, the UTP-induced calcium transient was completely abolished, suggesting an intracellular calcium source. G-protein coupled receptor (GPCR) activation can trigger intracellular calcium increases via activation of PLC and subsequent production of IP_3 and DAG. Inhibitors of the PLC pathway (neomycin, U73122) attenuated the UTP-elicited increase in calcium. Inhibitors of the IP_3 receptor reduced the UTP-elicited calcium increase, suggesting that IP_3 activation of the IP_3 receptor releases calcium from stores. Chronic

exposure to the membrane-permeant calcium chelator BAPTA-AM, which rapidly buffers cytosolic calcium, reduced both the main monophasic calcium transient and the oscillatory calcium increases induced by UTP. This suggests that under normal conditions, there is tight coupling between IP_3-induced calcium release from stores and activation of CICR from ryanodine receptors located on the endoplasmic reticulum. Indeed, inhibition of ryanodine receptors reduced the UTP-mediated peak calcium transient and decreased the amount of calcium released following the initial peak. Our data points to a role for both ryanodine and IP_3 receptors in producing the main monophasic increase in intracellular calcium, as well as the oscillatory increases in calcium.

Physiological Significance of Oscillatory Calcium Transients

The increases in intracellular calcium that occur in individual cells or as intercellular waves propagating through many cells are very similar to that which occurs in glia in the CNS. Glial calcium signaling has been implicated in a variety of physiological and pathological processes (Kurosinski and Gotz, 2002), including modulation of neuronal synaptic signaling (Hansson and Ronnback, 2003), modulation of the response of the retina to light (Newman, 2004), slowly propagated pathological phenomena, such as spreading depression (Lian and Stringer, 2004), and the multicellular response to localized injury (Kelley and Steward, 1997).

Dynamic intracellular calcium fluxes in sustentacular cells can serve as many different signals in the olfactory epithelium. Intracellular calcium fluxes may govern secretion, proliferation, and development in sustentacular cells, and, via calcium-dependent exocytosis, may release chemical signals to basal cells, neuronal precursors, or neurons. Transient increases in intracellular calcium have been reported in sustentacular cells of *Xenopus laevis* tadpoles and are proposed to mediate vesicle release which could modify mucus composition and modulate odorant sensitivity (Czesnik et al., 2006). It has been proposed that released ATP modulates the odorant sensitivity of both OSNs (Hegg et al., 2003) and trigeminal afferents (Spehr et al., 2004). Thus, calcium signals in sustentacular cells could play a role in setting the general excitability of the OE.

Calcium oscillations can serve as a developmental signal. All recordings in this study were performed in neonates, and it could be that, as with glia in CNS, the oscillations occur preferentially during neonatal development. The calcium fluxes could be a signal for cell turnover as calcium oscillations and waves in glia are important in regulating cell turnover, or neurogenesis (Weissman et al., 2004). In the olfactory system, the signals for injury-evoked regeneration are unknown; however, both positive and negative feedback signals have been proposed to play a role. In negative regulation of neurogenesis, a signal expressed in OSNs, such as GDF11 (Wu et al., 2003), inhibits proliferation and generation of new neurons in the OE. Thus, destruction of OSNs removes the source of the inhibitory antiproliferative signal, and promotes neuronal regeneration. Additionally, in positive regulation of neurogenesis, dead and dying OSNs or their neighboring sustentacular cells can release growth-promoting factors that initiate proliferation (Bauer et al., 2003). Secreted neurotrophic factors or stress factors, such as ATP, could activate receptors on sustentacular cells thereby inducing calcium oscillations. The oscillating calcium transients could act as a chemical signal to induce calcium-dependent exocytosis of growth factors onto progenitor or immature neurons.

Recent discoveries of voltage-gated channels, receptors, and transmitter release in both peripheral and central glial cells suggest direct communication between neurons and glia. The identification of similar components in sustentacular cells suggests that, like their glial counterparts, they are capable of rapid communication between themselves and the neural elements of the olfactory epithelium. Cell-attached patch recording revealed that murine sustentacular cells have calcium-dependent K^+ channels that oscillate in activity, presumably following the intracellular calcium oscillations (Vogalis et al., 2005b). Voltage-gated Na^+ channels in sustentacular cells generate action potentials following sufficient hyperpolarization (Vogalis et al., 2005b). Thus, the oscillatory intracellular calcium signal may be translated to an electrical membrane signal through K^+ and Na^+ channels. Electrical signaling along sustentacular cells provides a rapid way to send information from the apical to basal reaches of the olfactory epithelium. It was previously suggested that sustentacular cells form a network for intercellular communication within the sensory epithelium (Masukawa et al., 1983). The sustentacular cell syncytium may utilize specific calcium oscillations to decode the position and strength of various stimuli and, thus, integrate and coordinate multicellular functions. Our findings point to a key role for sustentacular cells in integrating communication between neurons, basal cells, and sustentacular cells themselves.

REFERENCES

Bannister LH, Dodson HC. 1992. Endocytic pathways in the olfactory and vomeronasal epithelia of the mouse: Ultrastructure and uptake of tracers. Microsc Res Tech 23:128–141.

Bauer S, Rasika S, Han J, Mauduit C, Raccurt M, Morel G, Jourdan F, Benahmed M, Moyse E, Patterson PH. 2003. Leukemia inhibitory factor is a key signal for injury-induced neurogenesis in the adult mouse olfactory epithelium. J Neurosci 23:1792–1803.

Berridge MJ, Lipp P, Bootman MD. 2000. The versatility and universality of calcium signaling. Nat Rev Mol Cell Biol 1:11–21.

Breipohl W, Laugwitz HJ, Bornfeld N. 1974. Topological relations between the dendrites of olfactory sensory cells and sustentacular cells in different vertebrates. An ultrastructural study. J Anat 117:89–94.

Charles AC, Merrill JE, Dirksen ER, Sanderson MJ. 1991. Intercellular signaling in glial cells: Calcium waves and oscillations in response to mechanical stimulation and glutamate. Neuron 6:983–992.

Cornell-Bell AH, Finkbeiner SM. 1991. Ca^{2+} waves in astrocytes. Cell Calcium 12:185–204.

Czesnik D, Kuduz J, Schild D, Manzini I. 2006. ATP activates both receptor and sustentacular supporting cells in the olfactory epithelium of Xenopus laevis tadpoles. Eur J Neurosci 23:119–128.

Dahl AR. 1988. The effect of cytochrome P-450-dependent metabolism and other enzyme activities on olfaction. In: Margolis FL, Getchell TV, editors. Molecular neurobiology of the olfactory system. New York: Plenum Press. p 51–70.

Dahl AR, Hadley WM, Hahn FF, Benson JM, McClellan RO. 1982. Cytochrome P-450-dependent monooxygenases in olfactory epithelium of dogs: Possible role in tumorigenicity. Science 216:57–59.

Di VF, Steinberg TH, Silverstein SC. 1990. Inhibition of Fura-2 sequestration and secretion with organic anion transport blockers. Cell Calcium 11:57–62.

Elsaesser R, Montani G, Tirindelli R, Paysan J. 2005. Phosphatidyl-inositide signalling proteins in a novel class of sensory cells in the mammalian olfactory epithelium. Eur J Neurosci 21:2692–2700.

Elsaesser R, Paysan J. 2007. The sense of smell, its signaling pathways, and the dichotomy of cilia and microvilli in olfactory sensory cells. BMC Neurosci 8:S1.

Getchell TV. 1977. Analysis of intracellular recordings from salamander olfactory epithelium. Brain Res 123:275–286.

Getchell TV. 1986. Functional properties of vertebrate olfactory receptor neurons. Physiol Rev 66:772–818.

Hansel DE, Eipper BA, Ronnett GV. 2001. Neuropeptide Y functions as a neuroproliferative factor. Nature 410:940–944.

Hansson E, Ronnback L. 2003. Glial neuronal signaling in the central nervous system. FASEB J 17:341–348.

Hassenklover T, Kurtanska S, Bartoszek I, Junek S, Schild D, Manzini I. 2008. Nucleotide-induced Ca(2+) signaling in sustentacular supporting cells of the olfactory epithelium. Glia (in press)

Hegg CC, Greenwood D, Huang W, Han P, Lucero MT. 2003. Activation of purinergic receptor subtypes modulates odor sensitivity. J Neurosci 23:8291–8301.

Hegg CC, Lucero MT. 2006. Purinergic receptor antagonists inhibit odorant-induced heat shock protein 25 induction in mouse olfactory epithelium. Glia 53:182–190.

Kelley MS, Steward O. 1997. Injury-induced physiological events that may modulate gene expression in neurons and glia. Rev Neurosci 8:147–177.

Kim WT, Rioult MG, Cornell-Bell AH. 1994. Glutamate-induced calcium signaling in astrocytes. Glia 11:173–184.

Kurosinski P, Gotz J. 2002. Glial cells under physiologic and pathologic conditions. Arch Neurol 59:1524–1528.

Lian XY, Stringer JL. 2004. Astrocytes contribute to regulation of extracellular calcium and potassium in the rat cerebral cortex during spreading depression. Brain Res 1012:177–184.

Manzini I, Schweer TS, Schild D. 2008. Improved fluorescent (calcium indicator) dye uptake in brain slices by blocking multidrug resistance transporters. J Neurosci Methods 167:140–147.

Masukawa LM, Kauer JS, Shepherd GM. 1983. Intracellular recordings from two cell types in an in vitro preparation of the salamander olfactory epithelium. Neurosci Lett 35:59–64.

Menco BP. 1988. Tight-junctional strands first appear in regions where three cells meet in differentiating olfactory epithelium: A freeze-fracture study. J Cell Sci 89:495–505.

Menco BP, Morrison EE. 2003. Morphology of the mammalian olfactory epithelium: Form, fine structure and pathology. In: Doty R, editor. Handbook of olfaction and gustation. New York: Marcel Dekker. p 17–49.

Miragall F, Hwang TK, Traub O, Hertzberg EL, Dermietzel R. 1992. Expression of connexins in the developing olfactory system of the mouse. J Comp Neurol 325:359–378.

Newman EA. 2004. Glial modulation of synaptic transmission in the retina. Glia 47:268–274.

Okano M, Takagi SF. 1974. Secretion and electrogenesis of the supporting cell in the olfactory epithelium. J Physiol Lond 242:353–370.

Rafols JA, Getchell TV. 1983. Morphological relations between the receptor neurons, sustentacular cells and Schwann cells in the olfactory mucosa of the salamander. Anat Rec 206:87–101.

Rash JE, Davidson KG, Kamasawa N, Yasumura T, Kamasawa M, Zhang C, Michaels R, Restrepo D, Ottersen OP, Olson CO, Nagy JI. 2005. Ultrastructural localization of connexins (Cx36, Cx43, Cx45), glutamate receptors, and aquaporin-4 in rodent olfactory mucosa, olfactory nerve and olfactory bulb. J Neurocytol 34:307–341.

Simpson PB, Russell JT. 1997. Role of sarcoplasmic/endoplasmic-reticulum Ca^{2+}-ATPases in mediating Ca^{2+} waves and local Ca^{2+}-release microdomains in cultured glia. Biochem J 325:239–247.

Spehr J, Spehr M, Hatt H, Wetzel CH. 2004. Subunit-specific P2X-receptor expression defines chemosensory properties of trigeminal neurons. Eur J Neurosci 19:2497–2510.

Suzuki Y, Takeda M, Farbman AI. 1996. Supporting cells as phagocytes in the olfactory epithelium after bulbectomy. J Comp Neurol 376: 509–517.

Verkhratsky A, Kettenmann H. 1996. Calcium signaling in glial cells. Trends Neurosci 19:346–352.

Vogalis F, Hegg CC, Lucero MT. 2005a. Electrical coupling in sustentacular cells of the mouse olfactory epithelium. J Neurophysiol 94:1001–1012.

Vogalis F, Hegg CC, Lucero MT. 2005b. Ionic conductances in sustentacular cells of the mouse olfactory epithelium. J Physiol 562:785–799.

Weissman TA, Riquelme PA, Ivic L, Flint AC, Kriegstein AR. 2004. Calcium waves propagate through radial glial cells and modulate proliferation in the developing neocortex. Neuron 43:647–661.

Wu HH, Ivkovic S, Murray RC, Jaramillo S, Lyons KM, Johnson JE, Calof AL. 2003. Autoregulation of neurogenesis by GDF11. Neuron 37:197–207.

Zhang C, Restrepo D. 2002. Expression of connexin 45 in the olfactory system. Brain Res 929:37–47.

CHAPTER 4

MOUSE CENTRIN 2 IS REQUIRED FOR OLFACTORY CILIARY TRAFFICKING AND EPENDYMAL CILIA PLANAR POLARITY

Guoxin Ying[1], Prachee Avasthi[1,*], Mavis Irwin[2], Cecilia Gerstner[1], Jeanne M. Frederick[1], Mary T. Lucero[2,3], Wolfgang Baehr[1,3,4,5]

[1]Department of Ophthalmology, University of Utah Health Science Center, Salt Lake City, UT 84132, USA

[2]Department of Physiology, University of Utah, 420 Chipeta Way Ste 1700, Salt Lake City, UT, 84108, USA

[3]The Brain Institute, University of Utah, 383 Colorow Drive, Salt Lake City, UT 84108, USA

[4]Department of Biology, University of Utah, 257 South 1400 East, Salt Lake City, Utah 84112, USA

[5]Department of Neurobiology and Anatomy, University of Utah Health Science Center, Salt Lake City UT 84132, USA

*Current address: Departments of Biochemistry & Biophysics, University of California, San Francisco, CA 94158, USA

Introduction

Cilia play important roles in cellular sensory, motility, and signaling functions. In mammals, olfaction and vision both rely on the sensory cilia located at the nasal olfactory epithelium (OE) and retina. Olfactory cilia emanate from the dendritic knob of the olfactory sensory neuron (OSN) and harbor the signaling proteins needed to convert odor stimuli into electrical signals. Photoreceptor outer segments are specialized light-sensing cilium housing phototransduction cascade proteins. Meanwhile, mammalian motile cilia of multiciliated cells, mainly ependymal cilia lining the brain ventricle wall, respiratory cilia covering the surface of airway epithelium, and cilia of fallopian tubes, are responsible for moving cerebrospinal fluid (CSF), mucus/dirt, and eggs along the luminal surface, respectively. Cilia dysfunction can cause a wide range of human diseases collectively called ciliopathies. Disruption of olfactory cilia causes anosmia (inability to perceive odors) or dysosmia (reduced sensitivity to odors) (McEwen et al., 2008), while ependymal cilia dysfunction leads to CSF flow failure and hydrocephalus (Del Bigio, 2010).

Sensory receptors and other transmembrane proteins enter cilia through a highly conserved mechanism “intraflagellar transport (IFT),” mediated by a large multiprotein complex-based machinery that transports ciliary proteins bidirectionally (Rosenbaum and Witman, 2002; Scholey, 2003). Motile cilia additionally require planar cell polarity (PCP) for proper function, e.g., the cilia need to be oriented uniformly so that their coordinated beating can generate a directional fluid flow. In both cases of signaling protein ciliary entry and

establishment of motile cilia planar polarity, the function of basal body, the transformed centriole that templates cilia axoneme, appears to be critical. Basal body distal appendage “transitional fiber” is believed to be critical for cilia entry regulation (Nachury et al., 2010), while subdistal appendage “basal foot” is a dictator of cilia polarity, and its absence causes uncoordinated cilia beating in mice (Kunimoto et al., 2012).

Centrins, small ~20 kD Ca^{2+}-binding proteins, are core basal body/centriole proteins that are among several hundred so-called “signature proteins” of eukaryotes. It is well established that centrins are required for basal body genesis and positioning in lower eukaryotes such as algae, ciliates, and yeast (spindle pole body) (Salisbury, 2007). Mammals have four centrin genes: *Chlamydomonas* centrin (*vfl2)-related CETN1, 2 and 4, and y*east centrin (CDC31)-related *CETN3* (Bornens and Azimzadeh, 2007), and their exact functions *in vivo* are largely undefined. To date, available *in vitro* studies showed controversial results regarding the function of vertebrate centrin in basal body replication (Dantas et al., 2011; Kleylein-Sohn et al., 2007; Middendorp et al., 2000; Salisbury et al., 2002; Yang et al., 2010). Germline knockout of *Cetn1* in mouse leads to male infertility due to centriole rearrangement defect that causes spermiogenesis failure (Avasthi et al., 2013). Interestingly, CETN2 was recently found to be required for primary ciliogenesis in mammalian cell lines (Graser et al., 2007) and in zebrafish embryos (Delaval et al., 2011).

Here, we show that *Cetn2*$^{\Delta Ex2,3}$ mice develop syndromic ciliopathies including dysosmia, hydrocephalus, sinusitis, and *situs inversus*. The dysosmia

phenotype is caused by impaired transport of olfactory signaling proteins to cilia with subsequent cilia loss, attributed to compromised basal body anchoring of IFT components, while the hydrocephalus is caused by impaired CSF directional flow attributed to disrupted ependymal cilia PCP without cilia loss. These phenotypes can be rescued by transgenic expression of a GFP-CETN2 fusion protein. Our findings indicate that CETN2 is required for olfactory cilia trafficking, survival, and ependymal cilia planar polarity establishment in mice.

Materials and Methods

Generation of *Cetn2*$^{\Delta Ex2,3}$ Mice

Cetn2$^{\Delta Ex2,3}$ mice were generated using standard gene targeting protocol. C57Bl/6 mice were purchased from Charles River, EIIa-Cre, and GFP-*Cetn2* transgenic mouse (Higginbotham et al., 2004) were obtained from The Jackson Laboratory. All experiments were approved by the University of Utah Institutional Animal Care and Use Committee (IACUC). BAC clone RP23-307G22 (205.2KB) containing the *Cetn2* gene was purchased from Children's Hospital Oakland Research Institute. An 8.5 Kb XhoI/ClaI fragment was subcloned into plasmid vector pBS-SK+. We inserted a loxP site into the first intron by NheI cloning and a neomycin selection cassette flanked by 2 loxP sites into intron 3 by XbaI cloning. The target vector sequence was confirmed by complete sequencing of the insertion. Plasmid electroporation of 129SV-derived embryonic stem cells, blastocyst injection, and generation of agouti and F1 heterozygous mice were performed by Ingenious Targeting (Stony Brook, NY). PCR was used to screen correctly-recombined ES cell clones and F1 animals. PCR primers included 1)

random integration: *Cetn2*VecScr.F: TGGCGTAATCATGGTCATAGC and *Cetn2*VecScr.R: CACGACAGGTTTCCCGAC; 2) 5' primer recombination arm: *Cetn2*SAS.F: AGGAACAGAGTGTGAAGTTAGAC and *Cetn2*SAS.R: AGACAGAATAAAACGCACGGG ; 3) 5' loxP: SpeLinkerChk.F: AAACCAATGGGAAGCGGGC and SpeLinker Chk.R: CTGAAGGTGACTTGGGCGAG; 4) 3' recombination arm: *Cetn2*LAS.F: GAAGTAGCCGTTATTAGTGG and *Cetn2*LAS.R: TCTCTGGTACAGTCATGC. Animals with targeted allele are designated *Cetn2* 3 loxP mice and were crossed with an EIIa-Cre driver to generate progeny with the exon 2 and 3-deleted allele (*Cetn2*$^{\Delta Ex2,3}$). PCR genotyping primers were 1ST loxP F: GAGTACGCCGTTGCCTTAAC; 1ST loxP R: GTTTGACTGAGGCGGAAGTC and 3rd loxP R: GGCCCTGAGTCCTTGTAATG, which amplify fragments at 357 bp (WT) and 593 bp (mutant).

RT-PCR

OE tissue was dissected from WT and *Cetn2* mutant animals and total RNA was extracted using TRIzol reagent (Invitrogen). Reverse transcription was done using SuperScript® II reverse transcriptase (with random primers). PCR primer for centrin isoforms and cycle numbers are: *Cetn1* (32cycels, 390 bp), forward: GTCCACCTTCAGGAAGTCAAAC and reverse: TCATTGGCCACACGCTTGAG; *Cetn2* (27 cycles, 601bp for WT,313 bp for mutant,),forward: GAGTACGCCGTTGCCTTAAC and reverse: GTCACATGTGCTTGCAGTAG; *Cetn3* (24 cycles,403 bp), forward: GCTCTGAGAGGTGAGCTTGTAG and reverse:

CCTCATCGCTCATGTTCTCAC;*Cetn4* (26 cycles, 216 pb), forward: CCAGCCAGCGCATAACTTTAG and reverse: CCTTGTCGATTTCAGCGATCAG. We used *GAPDH* as an internal control (18cycles, 703bp), forward: GCCATCAACGACCCCTTCAT and reverse: ATGCCTGCTTCACCACCTTC. RT-PCR was repeated once.

Electro-olfactogram and Electroretinogram

Electro-olfactograms were performed on 4–6 week *Cetn2* mutant (n = 9) and WT littermates (n = 7). Dose-response curves were generated for amyl acetate and 2-heptanone (0%, 0.1%, 1%, and 10% in mineral oil as vehicle). Additional odorants were tested at 10% dilution and included s-butanol, acetophenone, cineole, R-carvone, and citral. Mineral oil was used as baseline control. Animals were sacrificed by cervical dislocation, hemisectioned, and olfactory turbinates were exposed. Mounted onto a stereomicroscope stage, the olfactory turbinates were maintained under humidified, filtered air stream at 35^{o}C. Odorants (10 µl of diluted stock solutions) were applied to a sterile pipette filter and introduced into the humidified air stream using a picospritzer. Recordings were made at three locations (turbinates II, II', and III) with a glass electrode filled with Ringer's solution (140 mMNaCl, 5 mMKCl, 1 mM $MgCl_2$, 2 mM $CaCl_2$, 10 mM HEPES, 10 mM glucose). The preparation was grounded by a silver chloride wire inserted into a 3 M KCl agar bridge placed near the skull bone. EOG responses were acquired at a sampling rate of 400 Hz and filtered at 200 HZ using an Axoclamp 200B and Digidata 1340 interface running Axoscope 7.2

software. Averaged peak amplitudes from all 3 recording locations were used for data analysis using two-way ANOVA with Bonferroni posttests.

Scotopic electroretinograms were performed on 1 month-old *Cetn2* mutant and WT littermates (n = 3 each). After dark-adaption overnight, mice were anesthetized by intraperitoneal injection of a mixture of ketamine (100 mg/Kg body weight) and xylazine (10 mg/Kg bodyweight). Following pupil dilation with 1% tropicamide, animals were loaded for ERG recording using UTAS E-3000 universal electrophysiological system (LKC Technologies). We placed the recording electrode immediately adjacent to the cornea and the ground electrode at the skull midline. Gradually increasing light intensities, ranging from –20 to 20 db, were used for scotopic ERG recordings. Peak amplitudes for both a- and b-waves were used for analysis using one-way ANOVA test.

Confocal Immunolocalization of Olfactory Epithelia/retina Proteins

Animals were sacrificed by cervical dislocation. To harvest nasal epithelia, animals were decapitated and lower jaws were removed from the head; for retinas, eyes were enucleated and anterior segments removed. Specimens were fixed by immersion in ice-cold 4% paraformaldehyde for 3 to 8 hrs for olfactory tissue and 2 hrs for retina. P10 to adult olfactory tissues were decalcified in 10% EDTA, pH 7.3, before cryoprotection in 30% sucrose; embryonic and neonatal olfactory tissues/retinas were directly transferred to sucrose after fixation. Specimens were embedded in OCT compound and frozen. Sections (12 μm-thick) were cut using a Micron cryostat and mounted on charged

Superfrost® Plus slides (Fisher). Sections were washed in 0.1M PBS, blocked using 10% normal goat serum or 2% BSA with 0.1–0.3% Triton X-100 in PBS and incubated with primary antibodies at 4°C overnight. After washes in PBS, the signals were detected with Cy3 conjugated- or Alexa 488-conjuated goat anti-rabbit/mouse, or donkey anti-goat/rabbit secondary antibodies, and counterstained with DAPI. Primary antibodies and dilutions were rabbit anti-CETN2 (1:200, Santa Cruz), ACIII (1:1000, Santa Cruz), CNGA2 (1:300, Alomone Labs), $G\alpha_{olf}$ (1:200, Santa Cruz), KIF3A(1:500 Sigma), and rod PDE6, ML- and S-opsin, rod transducin-α, rod arrestin (all 1:1000, Cell Signaling), DYNC2H1 (1:500, Dr. Vallee, Columbia University), OR257-17 (1:500, Dr. Breer, University of Hohenheim), mouse anti-acetylated α- tubulin (1:1000, Sigma), γ-tubulin (1:500, Sigma), α-tubulin (1:1000, Sigma), CNGA1/A3 (1:2000, NeuroMab, UC Davis), GC1 (1:2000, IS4), and Rhodoposin (1D4), Rom1, Peripherin 2 (1:1000, Dr. Robert Molday, University of British Columbia); goat anti-CETN2 (1:400, Dr. Wolfrum, Johannes Gutenberg University), IFT88 (1:200, Dr. Besharse, Medical College of Wisconsin).

For wholemount OR256-17 immunolabeling, essentially the same procedure was used with antibody incubation occurring overnight. Sections and whole mounts were imaged using an Olympus Fluoview 1000 confocal microscope. Some images were adjusted for brightness and contrast using Adobe Photoshop CS3.

Electron Microscopy

For scanning electron microscopy, P16 *Cetn2* mutant and WT control animals were sacrificed, hemisectioned, and turbinates were exposed (n=3 each). Tissues were fixed in 2.5% glutaraldehyde, 1% paraformaldehyde in 0.1 M sodium cacodylate buffer, pH7.4, at 4^{o}C overnight. After several washes, samples were dehydrated in an ascending ethanol solution series and dried in hexamethyldisilazane. Dried samples were coated with gold particles and examined using the University of Utah EM core facility scanning microscope (Hitachi S-2460N) at 20 KV.

For transmission electron microscopy, P14 *Cetn2* mutant and WT control samples (n = 3 each) were fixed in the same fixative used for SEM at 4^{o}C for 2 hrs, washed and fixed further in 2% osmium tetroxide in 0.1 M sodium cacodylate buffer, pH 7.4 at 4^{o}C for 2 hrs. Washed samples were dehydrated through ascending series of ethanol, dried in propylene oxide, and infiltrated with Epon resin mix/propylene oxide (1:1) mixture overnight, followed by 100% Epon resin for 2 days. Samples were embedded and the plastic cured by incubation in a 60^{o}C oven for 2 days. Samples were trimmed and 1 μm sections were cut and examined until the desired area was reached. Ultrathin sections were cut, stained with uranyl acetate and lead citrate, and examined with an electron transmission microscope (FEI Tecnai 12) at the University of Utah EM core facility.

Co-IP and Western Blot

Olfactory epithelia from transgenic GFP-Cetn2 and WT mice were dissected while immersed under ice-cold PBS. Pooled tissues were homogenized in lysis buffer (50 mMTris-Cl pH 7.6, 120 mM NaCl, 0.5% IGEPAL CA-630, 1 mM PMSF, 1x protease inhibitor mixture, 2 mM NaF, 2 mM Na_3VO_4, supplemented with 100 µM $CaCl_2$, 100 µM $MgCl_2$ for Ca^{2+}-containing buffer or 1mM EDTA and 1mM EGTA for Ca^{2+}-free buffer), centrifuged at 13,000g, 4^{o}C, for 20 min, and supernatants were collected. Supernatants were precleared by incubating with 50% protein G-sepharose beads and normal rabbit IgG for 30 min. Precleared lysates were mixed with GFP primary antibody for 2 hrs (Rockland 011-0102), followed by protein G-sepharose beads for 45 min. Beads were collected by centrifugation at 3000g for 1 min, and washed 8 times in lysis buffer without protease inhibitors. After a final wash, 2X SDS buffer was added, and the samples were boiled for 3 minutes, centrifuged briefly, and supernatant were collected. Precipitated proteins were separated by SDS-PAGE and transferred to PVDF membrane. For immunoblot, we followed a standard protocol using an ECL-plus kit (Pierce) to detect the signal. Antibodies used for Western blot were rabbit anti-GFP (Rockland, 1:1000), KIF3A (1:500 Sigma), DYNC2H1, and DYNC1H1 (both 1:500, Dr. Vallee, Columbia University).

Ependymal Cilia Beating Assay

P13 Wt and *Cetn2* mutant brain lateral ventricle walls were isolated as described in L15 medium (Mirzadeh et al., 2010). Red fluorescent microbeads (Sigma, 2µm diameter) were added into the medium, and the beads movement

was recorded using a Nikon Ti-E Widefield CCD microscope. NIH Image J with manual tracking plugin was used to track individual particle movement and to calculate the speed.

Statistical Analysis

Data are presented as mean ± sd. *n* represents the number of mice or OSNs analyzed. Statistical comparisons were done using two-way ANOVA with Bonferroni posttest for EOG results, and one-way ANOVA for all other experimental data. Differences were considered to be statistically significant for $p < 0.05$.

Results

Generation of *Cetn2*$^{\Delta Ex2,3}$ Mice

In mice, the X chromosome-located *Cetn2* gene contains 5 exons. To generate a CETN2 knockout mouse, we inserted a loxP site into intron 1 and a neomycin selection cassette flanked by two loxP sites into intron 3 to create the conditional allele (Fig. 4.1). By mating the floxed mouse with an EIIa-Cre driver, we generated an allele in which exons 2 and 3 were deleted in frame (*Cetn2*$^{\Delta Ex2,3}$) (Fig. 4.1, *A*–*C*). Truncated *Cetn2* mRNA (encompassing exons 1, 4, and 5) was detectable by RT/PCR but at very low levels (5–10% of WT) (Fig. 4.1, arrow). In the absence of *Cetn2*, *Cetn1* and *3* mRNA levels were normal with *Cetn4* being slightly upregulated in RT-PCR examination (Fig. 4.1*D*). Endogenous CETN2 protein localizes to the basal body/centriole of OSN denditric knob layer in wildtype (WT) mouse, while in *Cetn2*$^{\Delta Ex2,3}$, the protein

encoded by truncated mRNA was undetectable (Fig. 4.1*E*, left panels). In a GFP-Cetn2 transgenic mouse (Higginbotham et al., 2004), GFP-CETN2 protein is similarly concentrated in basal bodes of OSN, brain ependymal cells, or retina photoreceptor cells (also in connecting cilium) (Fig. 4.1*E*, right panels).

Cetn2 Mutant Mice Display Dysosmia, Hydrocephalus, Sinusitis, and *Situs Inversus*

Cetn2 mutants (*Cetn2*$^{\Delta Ex2,3/\Delta Ex2,3}$ females or *Cetn2*$^{\Delta Ex2,3/Y}$ males) were born in a Mendelian ratio as expected for an X-linked gene. The mutant mouse appears normal at birth, but its body size becomes smaller with age compared to WT or heterozygous littermates (~30% lower than WT at weaning, Fig. 4.2*A*). Weight loss is frequently associated with olfaction-deficiency (Weiss et al., 2011). We confirmed that in electro-olfactograms (EOG), amplitudes of *Cetn2* mutants were reduced by 48–69% with all tested odorants: 58% reduction for citral, 48% for S-butanol, 61% for acetophenone, 69% for cineole and 67% for R-carvone (Fig. 4.2, *C* and *E*). Dose-dependent EOG recordings with amyl acetate showed amplitude reduction at every tested concentration (Fig. 4.2, *D* and *F*). Consistent with EOG results, a behavioral test revealed that overnight-fasted *Cetn2* mutants took over seven times longer to locate food than WT controls (45 sec vs. 350 sec) (Fig. 4.2*B*). These results indicated that Cetn2 mutants are dysosmic.

Cetn2 mutants also presented with hydrocephalus with variable severity. About 30% of mutants develop dome-shaped heads and huge dilated brain ventricles (Fig. 4.2*G*), and die within 1.5 months. About 70% of animals have normal skull shape, but their brain ventricles are also dilated in histology

examination (Fig. 4.2*H*, ages checked from 1 month to 1 year), suggesting later onset of hydrocephaly after the sealing of cranial sutures. Interestingly, in animals with mild hydrocephalus, the dilation of the lateral ventricle is more obvious than that of midbrain aqueduct or fourth ventricle (Fig. 2*H*).

Finally, *Cetn2* mutants also show sinusitis and *situs inversus* in ~30% animals (10 of 32 animals examined; Fig. 4.3, *A* and *B*). We did not observe other primary cilia-related disease phenotypes, such as polycystic kidney disease, polydactyly or other hedgehog signaling-related developmental defects.

Loss of Olfactory Cilia, but Maintenance
of Ependymal Cilia in *Cetn2* Mutant Mice

Based on ciliopathy phenoytpes, we investigated whether there is disruption of olfactory cilia or ependymal cilia in mutants. In OE, cilia marker Ac-a-tubulin immunostaining showed that there is a substantial decrease of ciliary layer thickness and Ac-a-tubulin-negative spots in mutant compared to WT at P14 and other ages (p21, P60, P180) (Fig. 4.4*A*). In scanning electron microscopy (SEM) of P16 OE tissues (turbinates II and II'), cilia form a fine, dense meshwork in WT (Fig. 4.4*B*), but *Cetn2* mutant cilia are reduced in density, appearing short and stubby with slightly enlarged tips (Fig. 4.4*B*, arrows). Many dendritic knobs (arrow head) are enlarged. In transmission electron microscopy (TEM), many mutant dendritic knobs were devoid of cilia and many remaining cilia were shorter with swelling tips (Fig. 4.5, *A*–*D*). To better demarcate the cilia morphology, we labeled a subset of olfactory cilia with anti-OR256-17 (Olfactory Receptor 15) antibody (Schwarzenbacher et al., 2005).

Compared to WT, OR256-17-postive cilia are dramatically reduced in either coronal sections (Fig. 4.6, *A* and *B*, arrows) or in whole mount staining, and morphologically the remaining cilia are short and varicose (Fig. 4.6, *C*–*F*, arrows). Quantification results confirmed significant decrease of knobs density (170.5 vs. 93, knobs per 0.1 mm^2), cilia density (17 vs. 6 cilia number per knob), and average cilia length (22 μm vs. 7 μm) in mutants (Fig. 4.6, *G*–*I*).

Surprisingly, the density of ependymal cilia of lateral ventricle in *Cetn2* mutants (animals with early onset of hydrocephalus) is comparable to WT in whole mount Ac-a-tubulin staining (Fig. 4.6, *J* and *K*). However, the uniform anterior-pointing cilia orientation appears to be disrupted in *Cetn2* mutants (Fig. 4.2*K*, arrows). Consistently, in SEM, WT ependymal cilia tufts showed regular spacing and the cilia within the same tufts or between different tufts show largely uniform orientation (Fig. 4.6*L*). Frequently, however, mutant ependymal cilia within a single tuft or among adjacent tufts pointed in variable directions (Fig. 4.6*M*, arrows). Mutant respiratory cilia also do not show cilia loss either in TEM examination (Fig. 4.7, *A* and *B*) or Ac-a-tubulin staining (Fig. 4.8), and the axoneme ultrastructure appears normal (Fig. 4.7, *C* and *D*). Further, IFT motor cytoplasmic dynein 2 and KIF3A are normally concentrated at respiratory cilia bases (Fig. 4.8, *A*–*D*), which is in contrast to olfactory epithelium (see below).

<u>Olfactory Cilia Trafficking Failure Occurs Prior</u>

<u>to Cilia Loss</u>

In investigating the onset of cilia loss phenotype, we found that at early stages (E14.5, P0, P5 examined), WT and mutant olfactory cilia density and

morphology is comparable, as judged by Ac-a-tubulin and OR256-17 labeling (Fig. 4.9, *A* and *B*). Quantification of P5 whole mount OR256-17 staining verified that there is no difference of dendritic knob density (170 WT vs. 175 mutant, knobs per 0.1mm^2), cilium density (19.2 WT vs 18.5 mutant, cilia number per knob), or average cilium length (8.2 μm WT vs 8.5 μm mutant) (Fig. 4.9, *C*–*E*). These observations indicate that olfactory ciliogenesis progresses normally in the absence of CETN2. However, from as early as P5, many turbinate I OSNs showed dendrite and soma mislocalization of olfactory signaling protein ACIII in mutants (compare Fig. 4.9, *F* and *G*, green). At this time point the olfactory cilia axoneme was present and intact as determined by a-tubulin staining (Fig. 4.9, *F* and *G*, red), suggesting CETN2 deficiency results in early membrane protein transport defects following normal cilia development and before ciliary loss.

Mistrafficking in cilia spreads from turbinate I and II to other turbinates and septum. By P14 (or later) ACIII and CNGA2, two major transmembrane signaling proteins, mislocalized to mutant OSN dendrites and cell bodies (Fig. 4.9, *I* and *L*), in contrast to exclusive cilia layer localization in WT (Fig. 4.9, *H* and *K*). Localization of the olfactory G protein, $G\alpha_{olf}$, a peripheral membrane-associated protein, appeared normal (Fig. 4.9, *N* and *O*).

Transgenic GFP-Cetn2 Rescues Olfactory Mistrafficking and Other Phenotypes

Since overexpression of GFP-CETN2 rescues the centriole assembly defect in CETN2-depleted mammalian cells (Yang et al., 2010), we crossed *Cetn2*$^{\Delta Ex2,3/Y}$ and GFP-Cetn2 mice in an attempt to 'rescue' the OSN ciliary

trafficking defect. As expected, ciliary localizations of ACIII, CNGA2 and $G\alpha_{olf}$ were normal in *Cetn2*$^{\Delta Ex2,3/Y}$; GFP-Cetn2 mice (Fig. 4.9, *J*, *M,* and *P*). Further, the body weights of *Cetn2*$^{\Delta Ex2,3/Y}$; GFP-Cetn2 mice were indistinguishable from those of WT mice, and hydrocephalus, sinusitis, or *situs inversus* were not detected (among >10 mutants).

Photoreceptor Ciliary Trafficking Proceeds
Normally in *Cetn2* Mutants

All four centrin genes are expressed in murine photoreceptors (Giessl et al., 2004). Deletion of CETN2 did not affect the subcellular localizations of photoreceptor outer segment proteins, including rod and cone visual pigments (rhodopsin, ML-opsin and S-opsin), cGMP-gated channel subunits (CNGA1/CNGA3), guanylate cyclase 1 (GC1), rod arrestin, and the structural proteins ROM1 and peripherin-2 (Fig. 4.10). Electroretinograms of 1 month old WT and *Cetn2* mutant mice were indistinguishable (Fig. 4.11). It has been proposed that photoreceptor centrins may regulate visual G-protein translocation (Trojan et al., 2008). However, neither the light-driven translocation nor the dark-driven return of both rod transducin-α and arrestin are impaired in *Cetn2* mutants (Fig. 4.12).

Mislocalization of IFT Components IFT88, KIF3A
and DYNC2H1 in *Cetn2* Mutant OSNs

Ciliary membrane proteins are presumably transported into cilia compartments by anterograde IFT (Rosenbaum and Witman, 2002; Scholey,

2003). To test whether the mislocalization of ACIII and CNGA2 could be a result of altered IFT in *Cetn2* mutant OSN, we examined the distributions of IFT components IFT88, KIF3A (the obligatory subunit of the anterograde motor kinesin-II), and DYNC2H1 (IFT retrograde motor cytoplasmic dynein 2 heavy chain 1). As reported (Miyoshi et al., 2009), IFT-88 and KIF3A concentrate at the dendritic knob layer, beneath the Ac-α-tubulin-positive ciliary layer (Fig. 4.13, *A* and *C*), and overlap with y-tubulin (Fig. 4.13*E*). In mutants, IFT88-and KIF3A-positive layers are uneven, and portions of each are colocalized with Ac-α-tubulin (Fig. 4.13, *B* and *D*, arrows), suggesting that IFT88 and KIF3A are trapped in olfactory cilia. KIF3A and y-tubulin double-labeling confirmed the KIF3A trapping in the ciliary layer (Fig. 4.13*F*). Interestingly, homodimeric KIF17, another member of the kinesin-II family required for sensory ciliogenesis in *C. elegans* and olfactory CNG channel cilium transport in mammalian cells (Jenkins et al., 2006; Snow et al., 2004), localized correctly in the olfactory cilium layer of mutant *Cetn2* mice (Fig. 4.14, *A*–*F*). Trapping of IFT88 and KIF3A in the *Cetn2* mutant cilia layer suggests abnormal retrograde IFT, mediated cytoplasmic dynein 2 (Collet et al., 1998; Pazour et al., 1999). Indeed, we found that DYNC2H1 cilia base localization is dramatically decreased in *Cetn2* mutants compared to WT, while DYNC2H1soma layer labeling appeared unaltered (Fig. 4.15, *G* and *H*, arrows). However, using GFP CETN2 transgenic OE lysate and GFP antibody as a bait, we did not detect a direct interaction between CETN2 and DYNC2H1 or KIF3A in co-immunoprecipitation assays (Fig. 4.16).

Uncoordinated Fluid Flow Generated by

Cetn2 Mutant Ependymal Cilia

The altered orientation of ependymal cilia (Fig. 4.6, *J*–*M*) predicts there is a CSF flow phenotype in Cetn2 mutant. To test this possibility, we isolated lateral ventricle walls from P13 animals, kept them in a culture dish, and recorded the movement of fluorescent latex microbeads (2 μm diameter) that were directly added into the culture medium. As reported (Tissir et al., 2010), the beads move from posterior to anterior in WT (Fig. 4.17*A*), but in mutants, the directional beads movement is disrupted, with observed movement in multiple directions (Fig. 4.17*B*). In addition, the beads moved much more slowly than in WT (mutant 8 μm/sec vs WT 45 μm/sec) (Fig. 4.17*C*). These data suggest that the CSF flow in the Cetn2 mutant is decreased and less directional, which could be causative of hydrocephalus.

Disrupted Rotational Planar Polarity of

Ependymal Cilia in Cetn2 Mutants

The ependymal cilia morphology and impaired directional CSF flow suggest improper development of planar polarity of ependymal tissue in *Cetn2* mutants. Indeed, in longitudinal TEM sections, we frequently observed misaligned ependymal cilia in mutant but not in WT (Fig. 4.17, *D* and *E*). Since the basal foot direction of basal bodies determines ependymal cilia planar polarity and cilia beating direction (Kishimoto and Sawamoto, 2012; Wallingford, 2010), we therefore investigated the basal foot direction using TEM in P13 mutants. As expected, most basal feet point to anterior in WT; in contrast, basal

feet pointing appears less directional, with many pointing in random directions (Fig. 4.17, *F* and *G*, arrows). We also frequently observed basal bodies with two or more basal feet in both longitudinal (Fig. 18*B*, allows) and cross views (Fig. 4.17*D*, dashed arrows). Finally, ependymal cilia 9+2 axoneme organization and 9 blade-like transitional fibers appear normal in *Cetn2* mutants (Fig. 4.18), which rules out the possibility that the fluid flow phenotype results from ciliary structure deficiencies. Taken together, these data suggest that CETN2 deficiency impairs ependymal planar polarity development.

Discussion

Here we show that CETN2 is not essential for centrosome replication, mitotic cell division, or ciliogenesis in mice as *Cetn2*$^{\Delta Ex2,3}$ pups are born normally and are fertile. Rather, *Cetn2* mutants showed selective ciliopathies, e.g., dysosmia, hydrocephalus, sinusitis, and *situs inversus*. The differential etiology of dysosmia and hydrocephalus in postnatal *Cetn2* mutants indicate that mammalian CETN2 is a versatile basal body protein that has adopted cell- and tissue-specific functions.

Centrins are required for the centriole/basal body duplication in various lower eukaryotes such as *Chlamydomonas*, yeast (spindle pole body) and *Tetrahymena* (Salisbury, 2007). CETN2 knockdown in zebrafish (Delaval et al., 2011) and in mammalian cell lines (Graser et al., 2007; Mikule et al., 2007) lead to the hypothesis that vertebrate centrin may be important for ciliogenesis (Dantas et al., 2012). Our results suggest that mouse CETN2 is dispensable for ciliogenesis since the formation of both primary cilium (renal tubule epithelia and

photoreceptors) and motile cilia of multiciliated cells (olfactory, respiratory, and ependymal cilia) progress normally in mutant animals. Despite the normal early ciliogenesis in olfactory epithelium, continued olfactory cilia growth and maintenance appeared to be disrupted *in Cetn2* mutants, which lead to massive cilia loss in young postnatal animals (Figs. 4.6 and 4.9). In general, ciliogenesis requires coordinated microtubule axoneme assembly and ciliary membrane expansion, during which cilia grow relatively fast (Westlake et al., 2011). However, during ciliary maintenance, the turnover of ciliary axoneme tubulin is slow (Thazhath et al., 2004); thus, the membrane protein turnover is likely not coupled to the axoneme renewal. In mouse OE, ciliary trafficking of olfactory signaling proteins ACIII, CNG and Golf occurs later than ciliogenesis (McEwen et al., 2008). As ciliary mistrafficking occurs prior to ciliary loss in *Cetn2* mutants, we speculate that CETN2 is required for transmembrane protein ciliary transport and that the olfactory cilia loss is a secondary effect of ciliary signaling protein trafficking failure.

OSN-specific mechanisms controlling the cilium entry of olfactory signaling proteins have been proposed (McEwen et al., 2008). Identified regulators include centrosomal protein CEP290/NPHP6, which controls $G\alpha_{olf}$ and Gγ13 ciliary entry (McEwen et al., 2007) and PACS-1 (phosphofurin acidic cluster-sorting protein 1) regulating CNG channel trafficking (Jenkins et al., 2009). Here we show that CETN2 is required for the ciliary transport of ACIII and CNGA2, but not cytoplasmic $G\alpha_{olf}$, in agreement with a previous conclusion that olfactory G protein targeting is uncoupled to ACIII or CNG channels (McEwen et al., 2007).

The abnormal basal body recruitment of IFT components (IFT88, KIF3A, and DYNC2H1) suggests that compromised IFT may be a cause of ciliary mistrafficking in *Cetn2* mutants. It is also possible that the mistrafficking phenotype may reflect the apically polarized intracellular transport from soma to knob basal bodies along a dendritic microtubule track since most of centrin could be cytoplasmic and not centrosome-associated (Paoletti et al., 1996). Interestingly, we noticed that *Cetn2* mutants share significant phenotypic similarity with a hypomorphic pericentrin mutant ($Pctn^{ocd/ocd}$) in olfactory cilia loss, ACIII mistrafficking, and defective basal body-anchoring of IFT components (Miyoshi et al., 2009). Deletion of BBSome proteins and MKS proteins also disrupt olfactory ciliary transport including ACIII and CNGA2 and lead to cilium structural abnormalities attributed to compromised IFT (Kulaga et al., 2004; Nishimura et al., 2004; Pluznick et al., 2011).

In mouse ependymal cells (and other multiciliated cells), the establishment of ciliary polarity requires hydrodynamic forces and its coordination with PCP protein VangL2 (Guirao et al., 2010; Mitchell et al., 2007). Deletion of the core PCP protein CELSR 3 (Drosophila flamingo ortholog) also results in ependymal PCP deficiency and ciliogenesis defects (Tissir et al., 2010). How exactly flow and PCP signals instruct cilia orientation is poorly understood. The elucidation of mechanisms is complicated by the finding that some PCP proteins can also locate to cilia and rootlet (Guirao et al., 2010; Park et al., 2008). Inevitably, all ciliary orientation instructional cues ultimately impinge on the basal body, the dictator of cilia polarity. We show for the first time that a core basal body protein,

CETN2, is required for PCP development in multiciliated cells. The nature of CETN2 function in ependymal polarity development is currently unknown. In mouse airway epithelium, the initial PCP signal can induce the polarization of basal body-associated microtubules that is subsequently required for orienting the basal body (Vladar et al., 2012). In frog embryo epidermal cilia, it appears that the rootlet-associated subapical actin network and basal foot-associated microtubule network regulate establishment of global and local ciliary polarity, respectively (Werner and Mitchell, 2012). We hypothesize that CETN2 functions downstream of core PCP proteins and is involved in PCP signal-mediated cytoskeleton rearrangement.

Acknowledgments

We thank R. Vallee (Columbia University, NYC) for DYNC2H1 and DTYNC1H1 antibodies, J. Besharse (Medical College of Wisconsin, Milwaukee) for IFT88 antibody, U. Wolfrum (Johannes Gutenberg University, Germany) for CETN2 antibody, H. Breer (Universität Hohenheim, Germany) for OR256-17 antibody, and R Molday (University of British Columbia, Canada) for Rhodopsin, ROM1 and Peripherin2 antibodies. This work was supported by NIH grants EY08123, EY019298 (WB), EY014800-039003 (NEI core grant), DC011686 (MI), DC 002994 (ML), Blackman Trust Fund (MI) University of Utah Graduate Research Fellowship (MI), and unrestricted grants to the Departments of Ophthalmology at the University of Utah from Research to Prevent Blindness (RPB; New York). WB is a recipient of a Research to Prevent Blindness Senior Investigator Award.

Reference List

1. **Avasthi P, Scheel JF, Ying G, Frederick JM, Baehr W, Wolfrum U**. Germline deletion of Cetn1 causes infertility in male mice. *J Cell Sci* 126: 3204–3213, 2013.

2. **Bornens M, Azimzadeh J**. Origin and evolution of the centrosome. *Adv Exp Med Biol* 607: 119–129, 2007.

3. **Collet J, Spike CA, Lundquist EA, Shaw JE, Herman RK**. Analysis of osm-6, a gene that affects sensory cilium structure and sensory neuron function in Caenorhabditis elegans. *Genetics* 148: 187–200, 1998.

4. **Dantas TJ, Daly OM, Morrison CG**. Such small hands: the roles of centrins/caltractins in the centriole and in genome maintenance. *Cell Mol Life Sci* 69: 2979–2997, 2012.

5. **Dantas TJ, Wang Y, Lalor P, Dockery P, Morrison CG**. Defective nucleotide excision repair with normal centrosome structures and functions in the absence of all vertebrate centrins. *J Cell Biol* 193: 307–318, 2011.

6. **Del Bigio MR**. Ependymal cells: biology and pathology. *Acta Neuropathol* 119: 55–73, 2010.

7. **Delaval B, Covassin L, Lawson ND, Doxsey S**. Centrin depletion causes cyst formation and other ciliopathy-related phenotypes in zebrafish. *Cell Cycle* 10: 3964–3972, 2011.

8. **Giessl A, Pulvermuller A, Trojan P, Park JH, Choe HW, Ernst OP, Hofmann KP, Wolfrum U**. Differential expression and interaction with the visual G-protein transducin of centrin isoforms in mammalian photoreceptor cells. *J Biol Chem* 279: 51472–51481, 2004.

9. **Graser S, Stierhof YD, Lavoie SB, Gassner OS, Lamla S, Le CM, Nigg EA**. Cep164, a novel centriole appendage protein required for primary cilium formation. *J Cell Biol* 179: 321–330, 2007.

10. **Guirao B, Meunier A, Mortaud S, Aguilar A, Corsi JM, Strehl L, Hirota Y, Desoeuvre A, Boutin C, Han YG, Mirzadeh Z, Cremer H, Montcouquiol M, Sawamoto K, Spassky N**. Coupling between hydrodynamic forces and planar cell polarity orients mammalian motile cilia. *Nat Cell Biol* 12: 341–350, 2010.

11. **Higginbotham H, Bielas S, Tanaka T, Gleeson JG**. Transgenic mouse line with green-fluorescent protein-labeled Centrin 2 allows visualization of the centrosome in living cells. *Transgenic Res* 13: 155–164, 2004.

12. **Jenkins PM, Hurd TW, Zhang L, McEwen DP, Brown RL, Margolis B, Verhey KJ, Martens JR**. Ciliary targeting of olfactory CNG channels requires the CNGB1b subunit and the kinesin-2 motor protein, KIF17. *Curr Biol* 16: 1211–1216, 2006.

13. **Jenkins PM, Zhang L, Thomas G, Martens JR**. PACS-1 mediates phosphorylation-dependent ciliary trafficking of the cyclic-nucleotide-gated channel in olfactory sensory neurons. *J Neurosci* 29: 10541–10551, 2009.

14. **Kishimoto N, Sawamoto K**. Planar polarity of ependymal cilia. *Differentiation* 83: S86–S90, 2012.

15. **Kleylein-Sohn J, Westendorf J, Le CM, Habedanck R, Stierhof YD, Nigg EA**. Plk4-induced centriole biogenesis in human cells. *Dev Cell* 13: 190–202, 2007.

16. **Kulaga HM, Leitch CC, Eichers ER, Badano JL, Lesemann A, Hoskins BE, Lupski JR, Beales PL, Reed RR, Katsanis N**. Loss of BBS proteins causes anosmia in humans and defects in olfactory cilia structure and function in the mouse. *Nat Genet* 36: 994–998, 2004.

17. **Kunimoto K, Yamazaki Y, Nishida T, Shinohara K, Ishikawa H, Hasegawa T, Okanoue T, Hamada H, Noda T, Tamura A, Tsukita S, Tsukita S**. Coordinated ciliary beating requires Odf2-mediated polarization of basal bodies via basal feet. *Cell* 148: 189–200, 2012.

18. **McEwen DP, Jenkins PM, Martens JR**. Olfactory cilia: our direct neuronal connection to the external world. *Curr Top Dev Biol* 85: 333–370, 2008.

19. **McEwen DP, Koenekoop RK, Khanna H, Jenkins PM, Lopez I, Swaroop A, Martens JR**. Hypomorphic CEP290/NPHP6 mutations result in anosmia caused by the selective loss of G proteins in cilia of olfactory sensory neurons. *Proc Natl Acad Sci USA* 104: 15917–15922, 2007.

20. **Middendorp S, Kuntziger T, Abraham Y, Holmes S, Bordes N, Paintrand M, Paoletti A, Bornens M**. A role for centrin 3 in centrosome reproduction. *J Cell Biol* 148: 405–416, 2000.

21. **Mikule K, Delaval B, Kaldis P, Jurcyzk A, Hergert P, Doxsey S**. Loss of centrosome integrity induces p38-p53-p21-dependent G1-S arrest. *Nat Cell Biol* 9: 160–170, 2007.

22. **Mirzadeh Z, Han YG, Soriano-Navarro M, Garcia-Verdugo JM, Alvarez-Buylla A**. Cilia organize ependymal planar polarity. *J Neurosci* 30: 2600–2610, 2010.

23. **Mitchell B, Jacobs R, Li J, Chien S, Kintner C**. A positive feedback mechanism governs the polarity and motion of motile cilia. *Nature* 447: 97–101, 2007.

24. **Miyoshi K, Kasahara K, Miyazaki I, Shimizu S, Taniguchi M, Matsuzaki S, Tohyama M, Asanuma M**. Pericentrin, a centrosomal protein related to microcephalic primordial dwarfism, is required for olfactory cilia assembly in mice. *FASEB J* 23: 3289–3297, 2009.

25. **Nachury MV, Seeley ES, Jin H**. Trafficking to the ciliary membrane: how to get across the periciliary diffusion barrier? *Annu Rev Cell Dev Biol* 26: 59–87, 2010.

26. **Nishimura DY, Fath M, Mullins RF, Searby C, Andrews M, Davis R, Andorf JL, Mykytyn K, Swiderski RE, Yang B, Carmi R, Stone EM, Sheffield VC**. Bbs2-null mice have neurosensory deficits, a defect in social dominance, and retinopathy associated with mislocalization of rhodopsin. *Proc Natl Acad Sci USA* 101: 16588–16593, 2004.

27. **Paoletti A, Moudjou M, Paintrand M, Salisbury JL, Bornens M**. Most of centrin in animal cells is not centrosome-associated and centrosomal centrin is confined to the distal lumen of centrioles. *J Cell Sci* 109 (Pt 13): 3089–3102, 1996.

28. **Park TJ, Mitchell BJ, Abitua PB, Kintner C, Wallingford JB**. Dishevelled controls apical docking and planar polarization of basal bodies in ciliated epithelial cells. *Nat Genet* 40: 871–879, 2008.

29. **Pazour GJ, Dickert BL, Witman GB**. The DHC1b (DHC2) isoform of cytoplasmic dynein is required for flagellar assembly. *J Cell Biol* 144: 473–481, 1999.

30. **Pluznick JL, Rodriguez-Gil DJ, Hull M, Mistry K, Gattone V, Johnson CA, Weatherbee S, Greer CA, Caplan MJ**. Renal cystic disease proteins play critical roles in the organization of the olfactory epithelium. *PLoS ONE* 6: e19694, 2011.

31. **Rosenbaum JL, Witman GB**. Intraflagellar transport. *Nat Rev Mol Cell Biol* 3: 813–825, 2002.

32. **Salisbury JL**. A mechanistic view on the evolutionary origin for centrin-based control of centriole duplication. *J Cell Physiol* 213: 420–428, 2007.

33. **Salisbury JL, Suino KM, Busby R, Springett M**. Centrin-2 is required for centriole duplication in mammalian cells. *Curr Biol* 12: 1287–1292, 2002.

34. **Scholey JM**. Intraflagellar transport. *Annu Rev Cell Dev Biol* 19: 423–443, 2003.

35. **Schwarzenbacher K, Fleischer J, Breer H**. Formation and maturation of olfactory cilia monitored by odorant receptor-specific antibodies. *Histochem Cell Biol* 123: 419–428, 2005.

36. **Snow JJ, Ou G, Gunnarson AL, Walker MR, Zhou HM, Brust-Mascher I, Scholey JM**. Two anterograde intraflagellar transport motors cooperate to build sensory cilia on C. elegans neurons. *Nat Cell Biol* 6: 1109–1113, 2004.

37. **Thazhath R, Jerka-Dziadosz M, Duan J, Wloga D, Gorovsky MA, Frankel J, Gaertig J**. Cell context-specific effects of the beta-tubulin glycylation domain on assembly and size of microtubular organelles. *Mol Biol Cell* 15: 4136–4147, 2004.

38. **Tissir F, Qu Y, Montcouquiol M, Zhou L, Komatsu K, Shi D, Fujimori T, Labeau J, Tyteca D, Courtoy P, Poumay Y, Uemura T, Goffinet AM**. Lack of cadherins Celsr2 and Celsr3 impairs ependymal ciliogenesis, leading to fatal hydrocephalus. *Nat Neurosci* 13: 700–707, 2010.

39. **Trojan P, Krauss N, Choe HW, Giessl A, Pulvermuller A, Wolfrum U**. Centrins in retinal photoreceptor cells: regulators in the connecting cilium. *Prog Retin Eye Res* 27: 237–259, 2008.

40. **Vladar EK, Bayly RD, Sangoram AM, Scott MP, Axelrod JD**. Microtubules enable the planar cell polarity of airway cilia. *Curr Biol* 22: 2203–2212, 2012.

41. **Wallingford JB**. Planar cell polarity signaling, cilia and polarized ciliary beating. *Curr Opin Cell Biol* 22: 597–604, 2010.

42. **Weiss J, Pyrski M, Jacobi E, Bufe B, Willnecker V, Schick B, Zizzari P, Gossage SJ, Greer CA, Leinders-Zufall T, Woods CG, Wood JN, Zufall F**. Loss-of-function mutations in sodium channel Nav1.7 cause anosmia. *Nature* 472: 186–190, 2011.

43. **Werner ME, Mitchell BJ**. Planar cell polarity: microtubules make the connection with cilia. *Curr Biol* 22: R1001–R1004, 2012.

44. **Westlake CJ, Baye LM, Nachury MV, Wright KJ, Ervin KE, Phu L, Chalouni C, Beck JS, Kirkpatrick DS, Slusarski DC, Sheffield VC, Scheller RH, Jackson PK**. Primary cilia membrane assembly is initiated by Rab11 and transport protein particle II (TRAPPII) complex-dependent trafficking of Rabin8 to the centrosome. *Proc Natl Acad Sci USA* 108: 2759–2764, 2011.

45. **Yang CH, Kasbek C, Majumder S, Yusof AM, Fisk HA**. Mps1 phosphorylation sites regulate the function of centrin 2 in centriole assembly. *Mol Biol Cell* 21: 4361–4372, 2010.

Fig. 4.1: Generation of *Cetn2*$^{\Delta Ex2,3}$ mice. (*A*) Schematic of gene targeting strategy. (*B*) Screen of *Cetn2*$^{\Delta Ex2,3}$ ES cells and mice. We used PCR to screen 1st LoxP [shown are 4 positive mice out of total 16 mice (top row left)], 2nd LoxP site (top row, right), the 5' and 3 recombination arm (lower row, left and middle) and 3rd LoxP site (lower row, right). (*C*) Representative PCR genotyping result of one litter germline deletion pups, showing amplification of WT band at 357 bp and mutant band at 593 bp. (D) RT-PCR examination of Cetn1-4 mRNA expression in *Cetn2*$^{\Delta Ex2,3}$ mice. GAPDH mRNA was used as an internal control. Red arrow marks the faint band of truncated *Cetn2* mRNA in mutant. (*E*) Anti-CETN2 antibody labels basal bodies of dendrite knob layer of WT OE, but is negative for *Cetn2*$^{\Delta Ex2,3}$ OE (left two panels), while transgenic GFP-CETN2 similarly concentrates at basal bodies at OE, ependyma, and retina photoreceptors (right three panels). Scale bar: 5 μm.

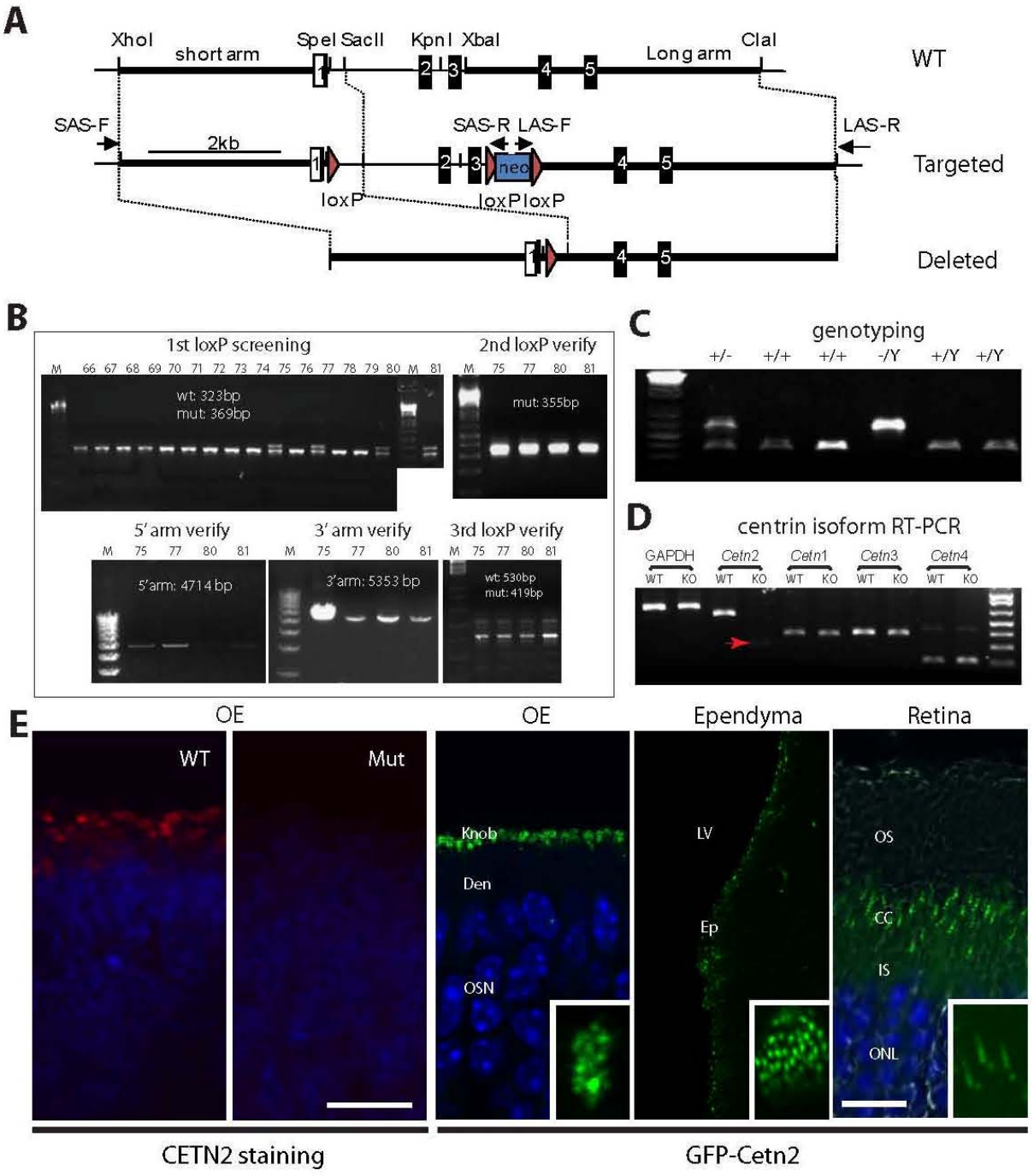
A
XhoI
short arm
SpeI SacII
KpnI XbaI
Long arm
ClaI
WT
SAS-F
2kb
SAS-R LAS-F
LAS-R
neo
Targeted
loxP
loxP loxP
Deleted
B
1st loxP screening
2nd loxP verify
wt: 323bp
mut: 369bp
mut: 355bp
5' arm verify
3' arm verify
3rd loxP verify
5'arm: 4714 bp
3'arm: 5353 bp
wt: 530bp
mut: 419bp
C
genotyping
+/- +/+ +/+ -/Y +/Y +/Y
D
centrin isoform RT-PCR
GAPDH Cetn2 Cetn1 Cetn3 Cetn4
WT KO
E
OE
OE
Ependyma
Retina
WT
Mut
Knob
Den
OSN
LV
Ep
OS
CC
IS
ONL
CETN2 staining
GFP-Cetn2

Fig. 4.2: Phenotypes of *Cetn2*$^{\Delta Ex2,3}$ animals. (*A*) *Cetn2*$^{\Delta Ex2,3}$ and WT animals body size. At P21, the average *Cetn2*$^{\Delta Ex2,3}$ body weight is ~35% less than that of WT (n = 10 for each group, one-way ANOVA, ** $p < 0.01$). (*B*) In a behavioral test, *Cetn2* mutants require a significantly longer time to locate hidden food than WT after overnight fasting (n = 13 WT, n = 12 mutants, one-way ANOVA, *** $p < 0.001$). Dysosmia and hydrocephalus in *Cetn2* mutant mice. (*C, E*) Representative electroolfactogram (EOG) traces for various odors (*C*) and dose-dependent test of amyl acetate (*D*). (*E, F*) Evaluation of EOG results, showing reduced voltage responses to tested odors (*E*), and at three different amyl acetate concentrations (*F*). Bars indicate mean ± sd. (n = 8 WT, n = 10 mutants, two-way ANOVA, *$p < 0.05$, **$p < 0.01$, *** $p < 0.001$). (*G*) Severe hydrocephalus of *Cetn2* mutants, showing dome-shaped head and huge dilated brain lateral ventricle. (*H*) *Cetn2* mutants with mild hydrocephalus, showing dilation of lateral ventricle but not of aqueduct or of 4th ventricle.

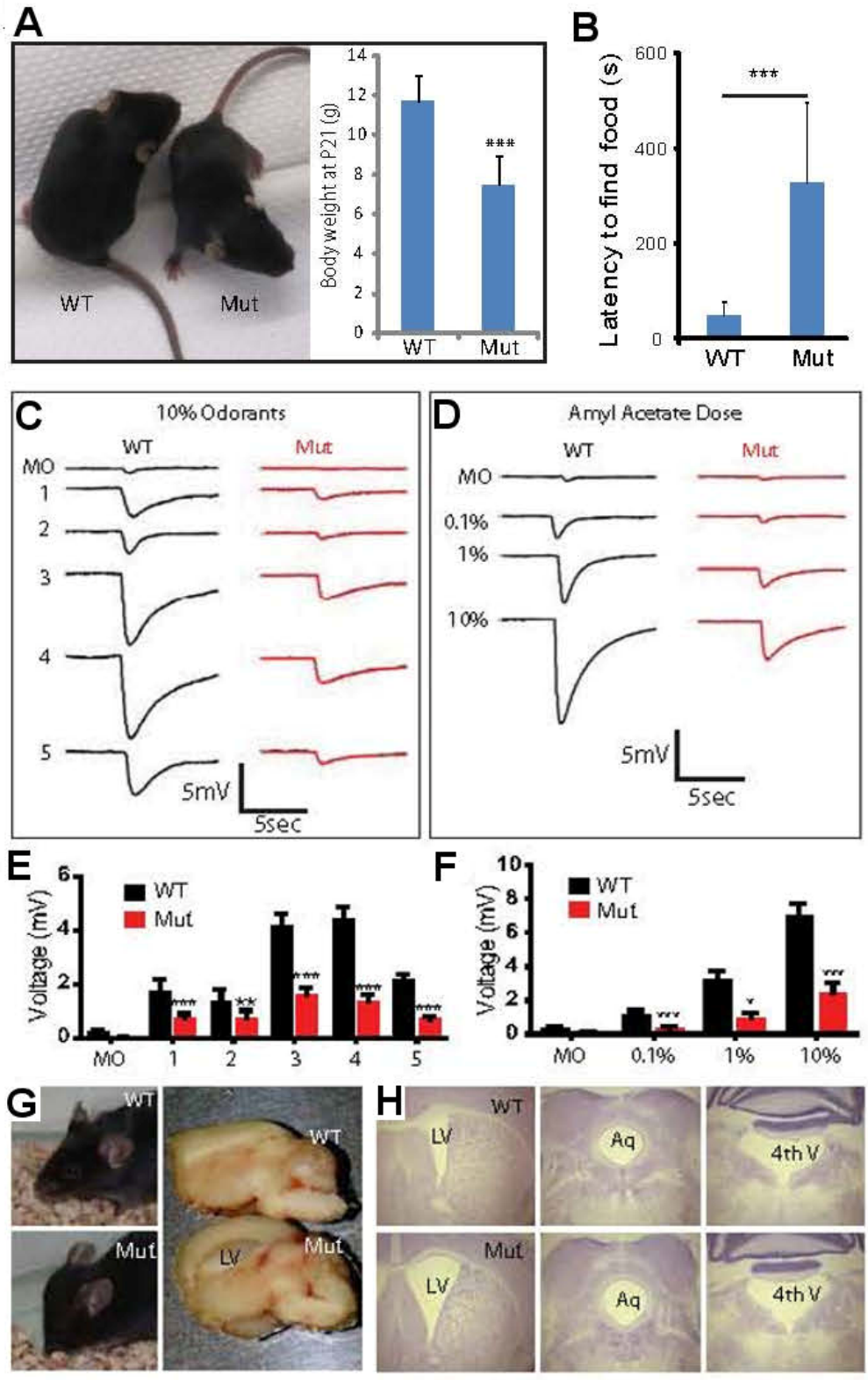
A
WT
Mut
Body weight at P21 (g)
14
12
10
8
6
4
2
0
***
WT
Mut
B
Latency to find food (s)
600
400
200
0
***
WT
Mut
C
10% Odorants
WT
Mut
MO
1
2
3
4
5
5mV
5sec
D
Amyl Acetate Dose
WT
Mut
MO
0.1%
1%
10%
5mV
5sec
E
Voltage (mV)
WT
Mut
MO
1
2
3
4
5
F
Voltage (mV)
WT
Mut
MO
0.1%
1%
10%
G
WT
Mut
WT
LV
Mut
H
WT
LV
Aq
4th V
Mut
LV
Aq
4th V

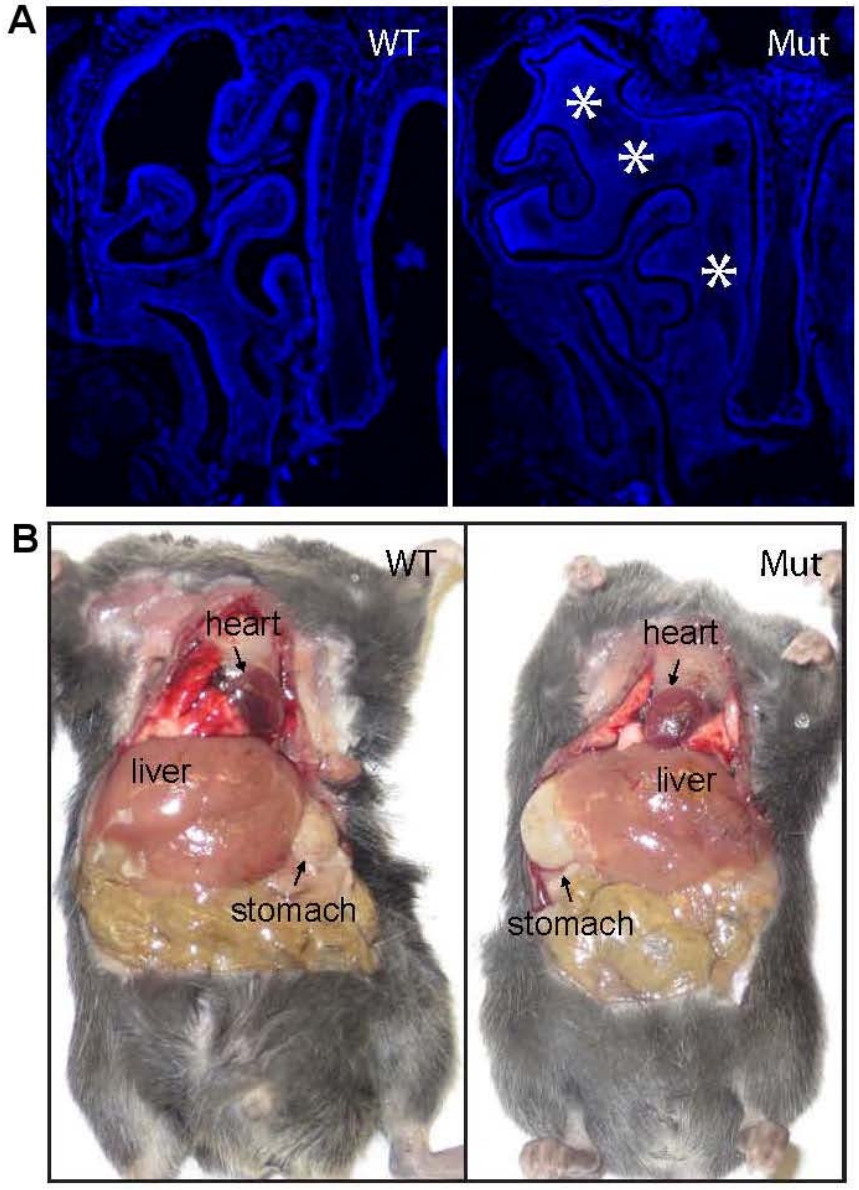

Fig. 4.3: Overall anatomy of *Cetn2*$^{\Delta Ex2,3}$ animals. (*A*) Sinusitis of *Cetn2*$^{\Delta Ex2,3}$ animals shown in DAPI staining. Stars mark the dead cells and accumulated mucus. (*B*) *Situs inversus* of *Cetn2*$^{\Delta Ex2,3}$ animals.

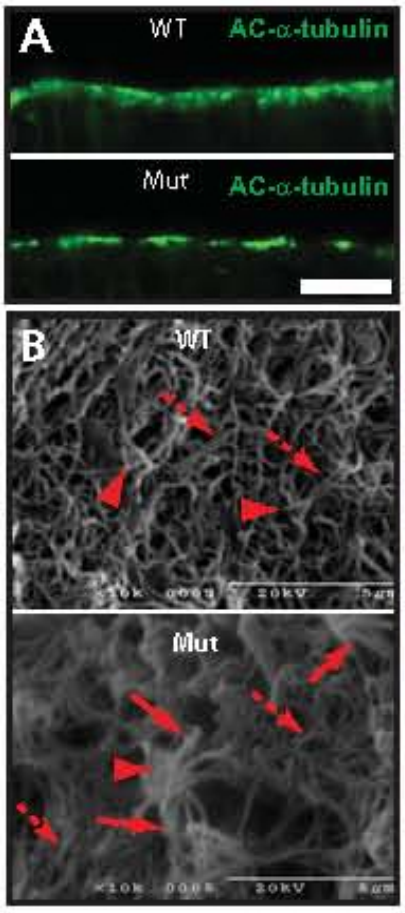

Fig. 4.4: Loss of olfactory cilia but not ependymal cilia in *Cetn2* mutants. (*A*) Decrease of cilia marker Actubulin in mutant OE at P14. (*B*) SEM images of P16 OE revealed reduced cilia density, short and stubby cilia, and enlarged knobs in mutants. Arrowheads point to individual knobs, dashed arrows identify cilia, and arrows in lower panel indicate abnormal cilia in mutant. Scale bars: *A*, 10 μm.

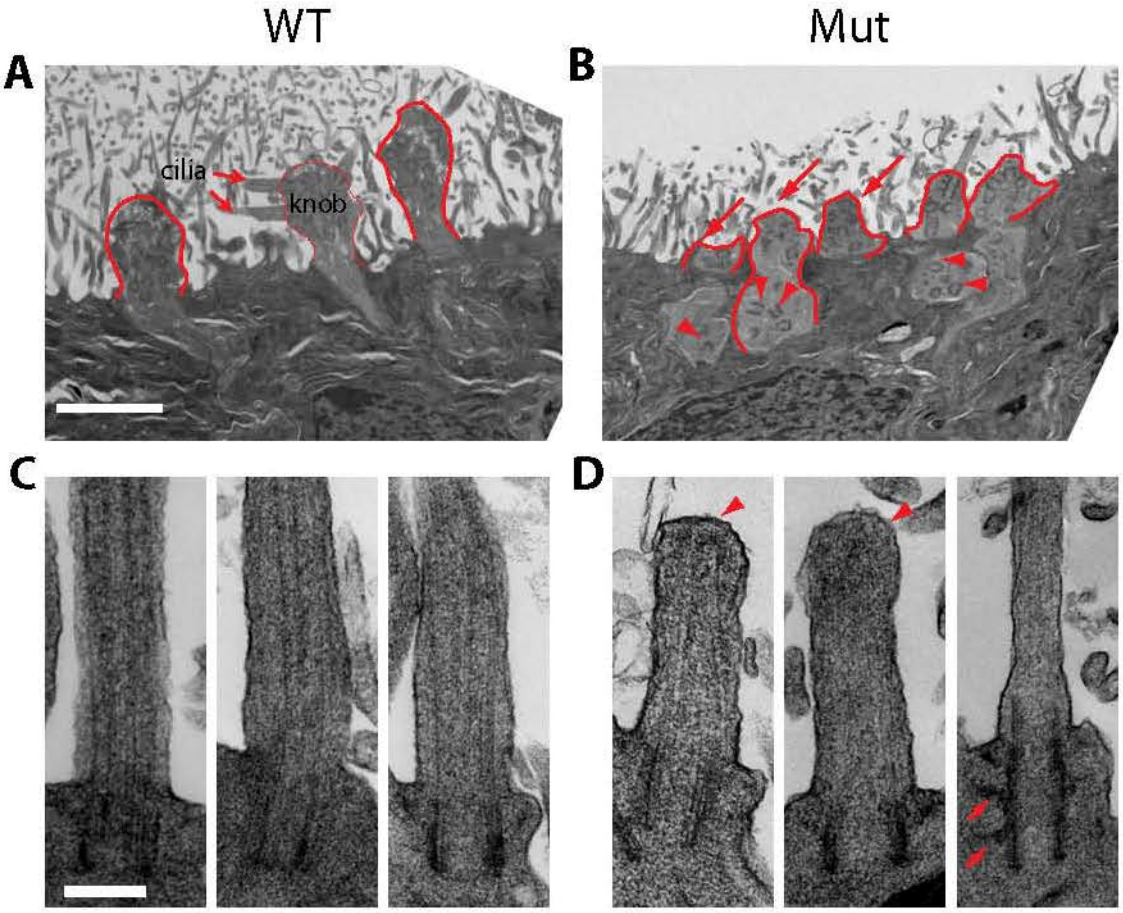

Fig. 4.5: TEM of WT and *Cetn2* mutant olfactory cilia. (*A, B*) In P14 OE, olfactory cilia emanate from dendritic knobs in WT (*A*), but are absent from many knobs in mutants (*B*). Dashed lines outline knobs, arrows indicate cilia, and arrowhead labels mislocalized basal bodies in mutants. (*C, D*) High power TEM image indentified shorter olfactory cilia with swelling tip in mutant (*C*, arrows) but not in WT (*D*) OE. Arrowheads indicate extra decoration of basal body wall in mutants.

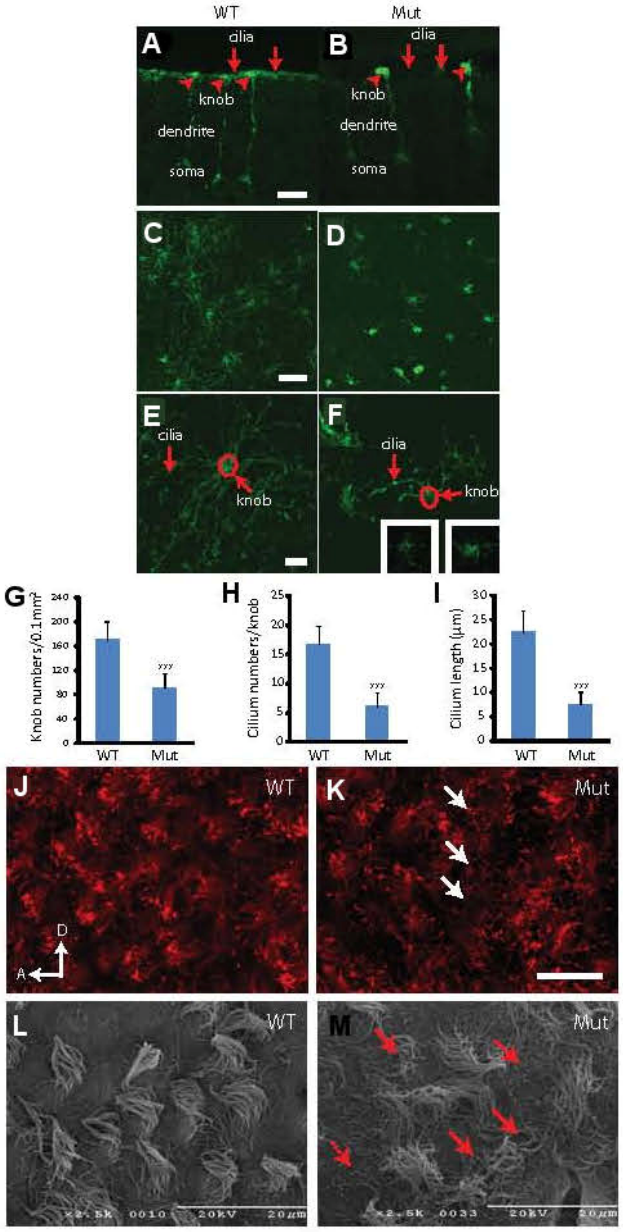

Fig. 4.6: WT and *Cetn2* mutant olfactory cilia. (*A–F*) Identification of cilia with anti-OR256-17 antibody in frozen sections (*A, B*) and wholemount tissues (*C–F*), showing greatly reduced cilia density and abnormal cilia morphology in mutants. Arrows point to cilia and arrow heads (*A, B*) or dashed circles (*D, F*) label dendritic knobs. (*G–I*) Knob density (*G*), cilia density (*H*) and average cilia length (*I*) are all decreased significantly in mutants. Data shown as mean ± sd. (n=45 OSNs from 3 animals for each group, one-way ANOVA, *** $p<0.001$). (*J, K*) WT, and mutant wholemount Ac-a-tubulin immunostaining of P13 brain lateral ventricle. Mutant ependymal cilia density is comparable to WT, but the cilia orientation is disrupted. D, dorsal; A, anterior. (*L, M*) SEM of P13 ependymal cilia confirmed disorganized cilia orientation in mutants. Arrows in *M* and *O* label disorganized cilia tufts. Scale bars: *A–D, J, K,* 10 μm; *E, F,* 5 μm; *L, M*, 20 μm.

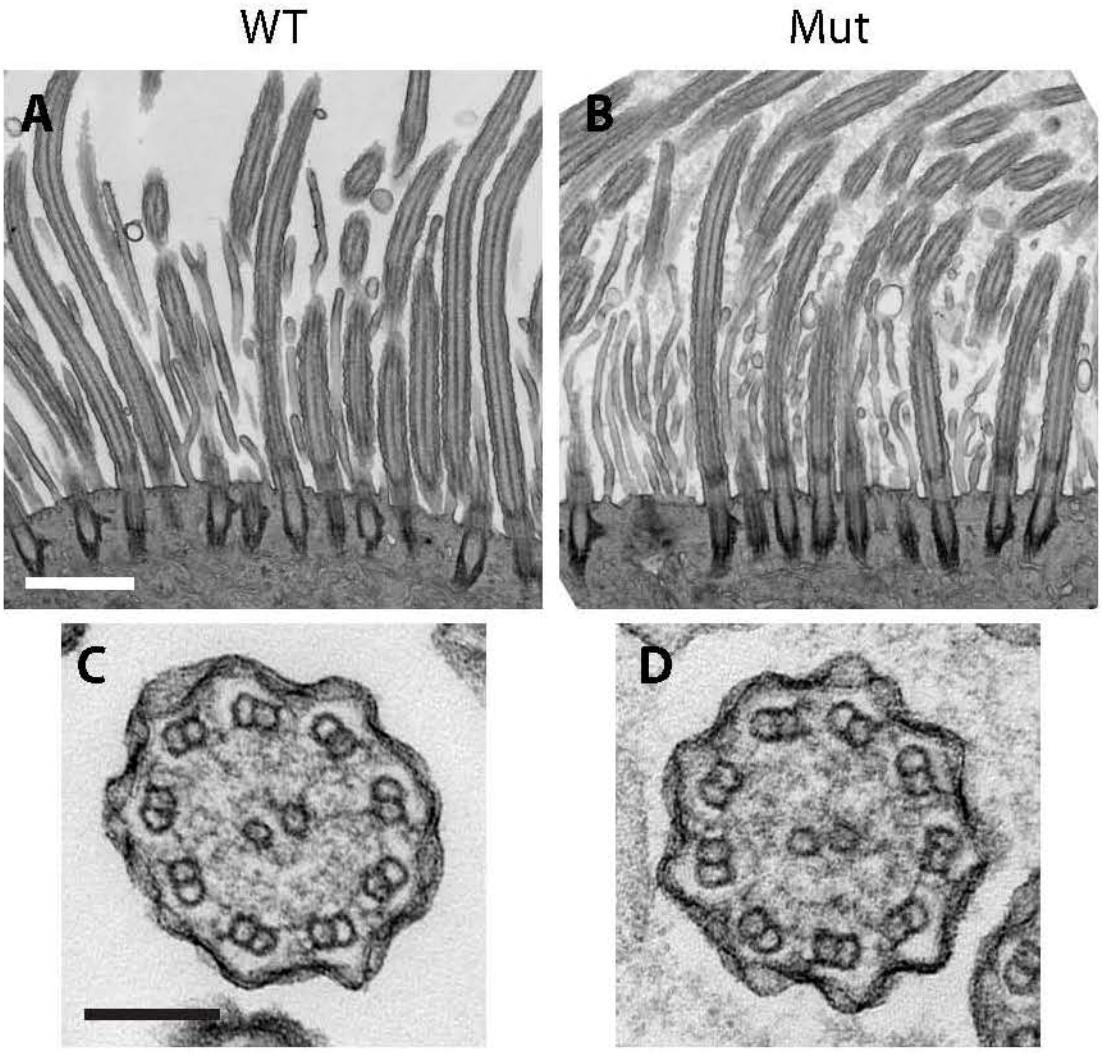

Fig. 4.7: Respiratory cilia density and morphology in WT and *Cetn2* mutants. (*A, B*) In longitudinal section TEM, both the cilium density and morphology are comparable between P14 WT (*A*) and mutant (*B*). (*C, D*) Cross sections TEM showed both WT (*C*) and mutant (*D*) have typical motile cilium 9+2 axoneme microtubule structures. Scale bar, *A, B*, 1 μm; *C, D*, 100 nm.

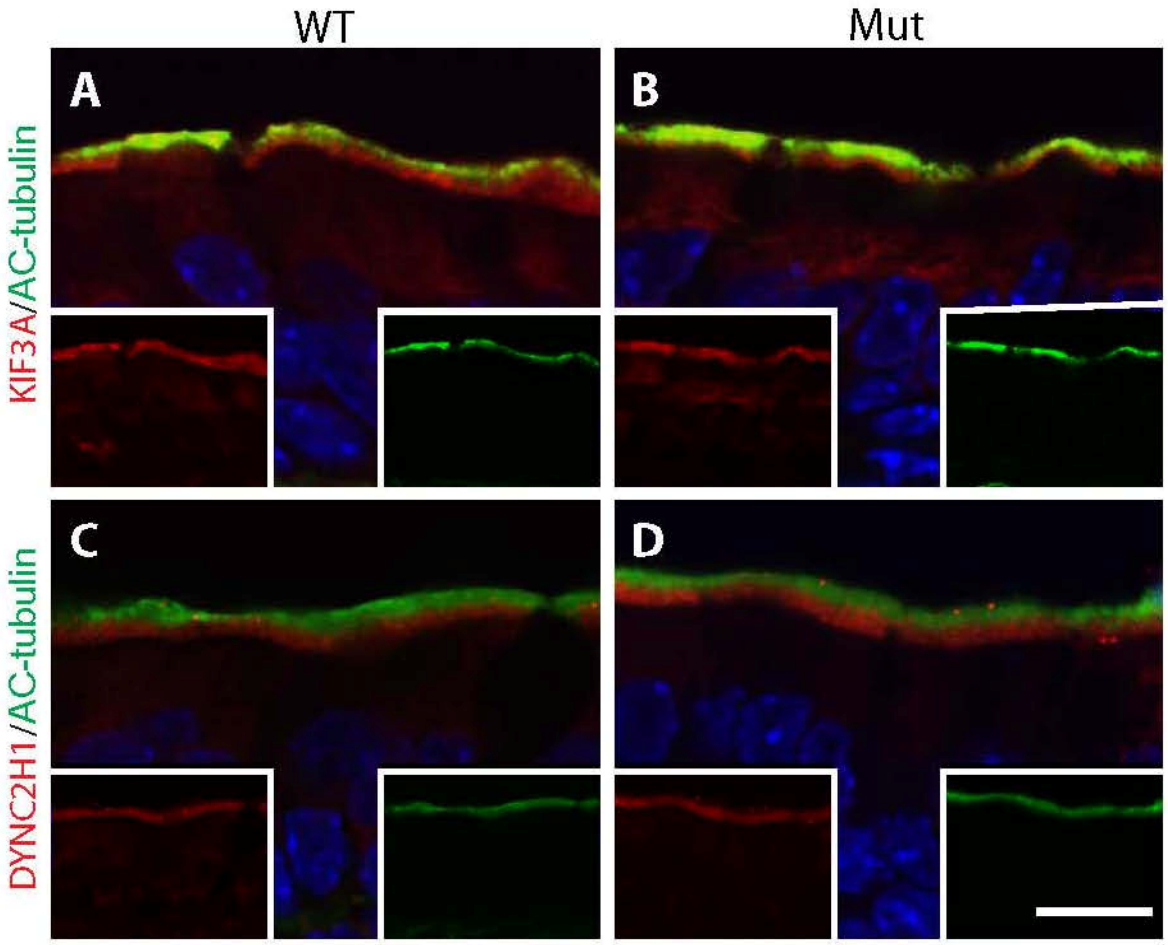

Fig. 4.8: IFT motor localization in *Cetn2* respiratory epithelium. (*A, B*) Double staining KIF3A (red) and Ac-α-tubulin (green) showed KIF3A concentration at cilia base in both P14 WT (*A*) and mutant (*B*). (*C, D*) Double staining of DYNC2H1 (red) and Ac-α-tubulin (green) showed cytoplasmic dynein 2 concentration at cilia base in both P14 WT (*C*) and mutant (*D*). Scale bar, 50 μm.

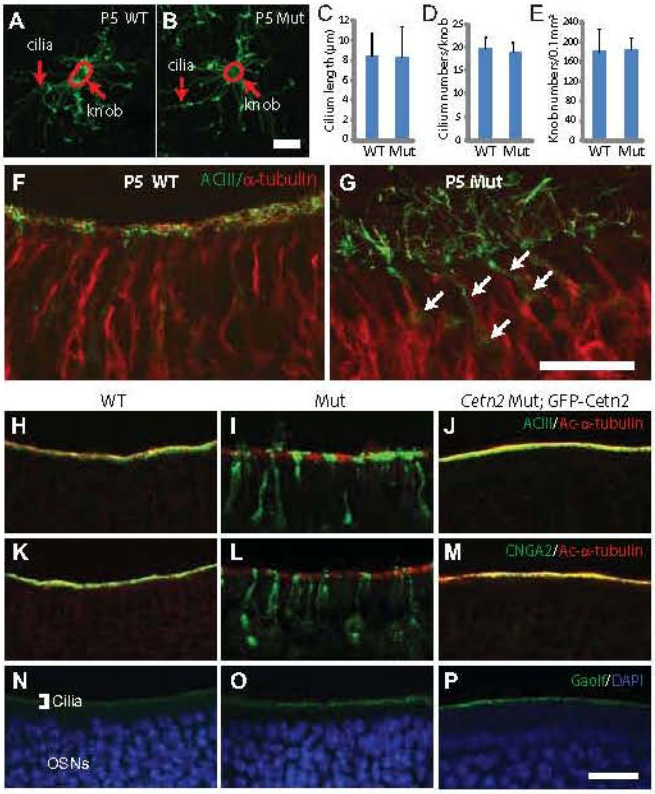

Fig. 4.9: Mislocalization of ACIII and CNGA2 in *Cetn2* mutant and rescue by transgenic GFP-CETN2 expression. (*A, B*) Wholemount identification of cilia with anti-OR256-17 in P5 WT (*A*) and mutant (*B*) OE. (*C–E*) Quantification of knob density (*C*), cilia per knob (*D*) and average cilia length (*E*). Data are mean ± sd (one-way ANOVA, $p > 0.8$, n45 OSNs from 3 animals for each group). (*F, G*) Immunolocalization of ACIII and a-tubulin at turbinate I of P5 OE. ACIII (green) colocalizes with atubulin (red) at cilium layer in WT (*F*), but is mislocalized to the dendrite and cell body (arrows) in mutant (see arrows in *G*). Note that mutant olfactory cilia appear intact at this stage. (*H–P*) Immunolocalization of ACIII (green; *H–J*); CNGA2 (green; *K–M*), $G_{\alpha olf}$ (green; *N–P*) and Ac-a-tubulin (red) in P14 WT (*H, K, N*), *Cetn2* mutant (*I, L, O*) and *Cetn*2 Mut;GFP-Cetn2 (*J, M, P*) OE. Note the mislocalization of ACIII and CNGA2, but not $G_{\alpha olf}$ in mutants and the rescue in *Cetn2* Mut; GFP-CETN2. Scale bars: *A, B*, 5 μm; *F, G* 10 μm; *H–P* 30 μm.

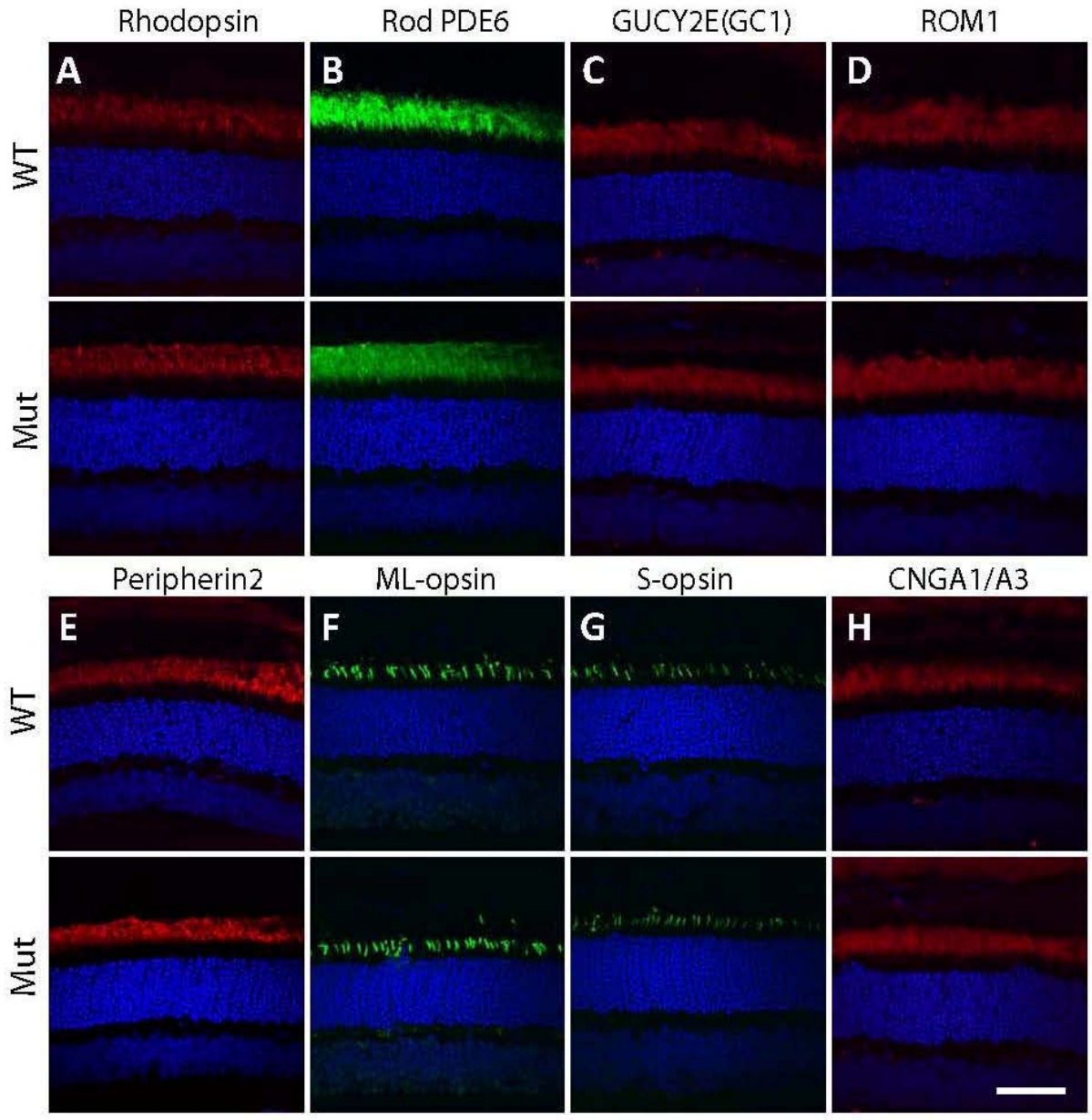

Fig. 4.10: Immmunolocalization of phototransduction components in WT and *Cetn2* mutant photoreceptor cells. The photoreceptor outer segment proteins include rhodopsin (*A*), PDE6 (*B*), GC1 (*C*), Rom-1 (*D*), Peripherin2 (*E*), ML-opsin (*F*), S-Opsin (*G*), and CNGA1/A3 (*H*). All outer segment proteins are correctly targeted in 1 month Cetn2 mutant (lower row) and in WT photoreceptors (upper row), Scale bar, 50 μm.

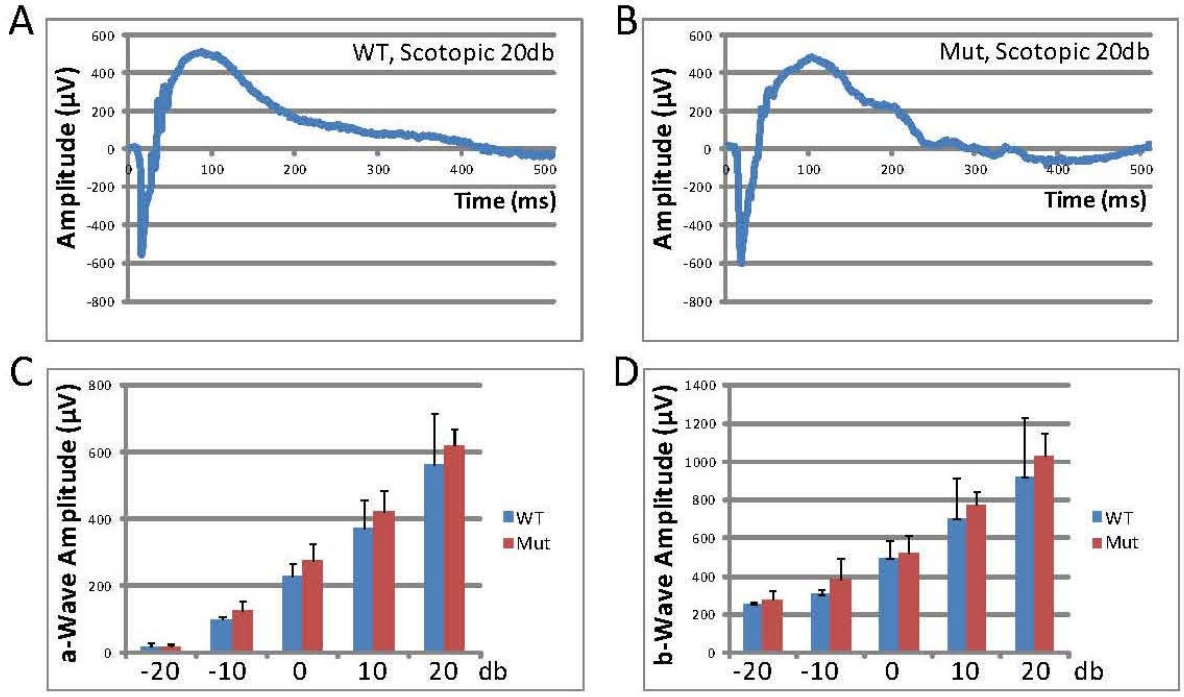

Fig. 4.11: Electroretinograms of WT and *Cetn2* mutant mice. (*A, B*) Typical Scotopic ERG trace of WT (*A*) and Cetn2 mutant (*B*) at 20 db. (*C, D*) No significant difference was detected for a-wave or b-wave amplitudes at multiple light intensities tested. Data are shown as mean ± sd (n = 3, one-way ANOVA, $p > 0.7$).

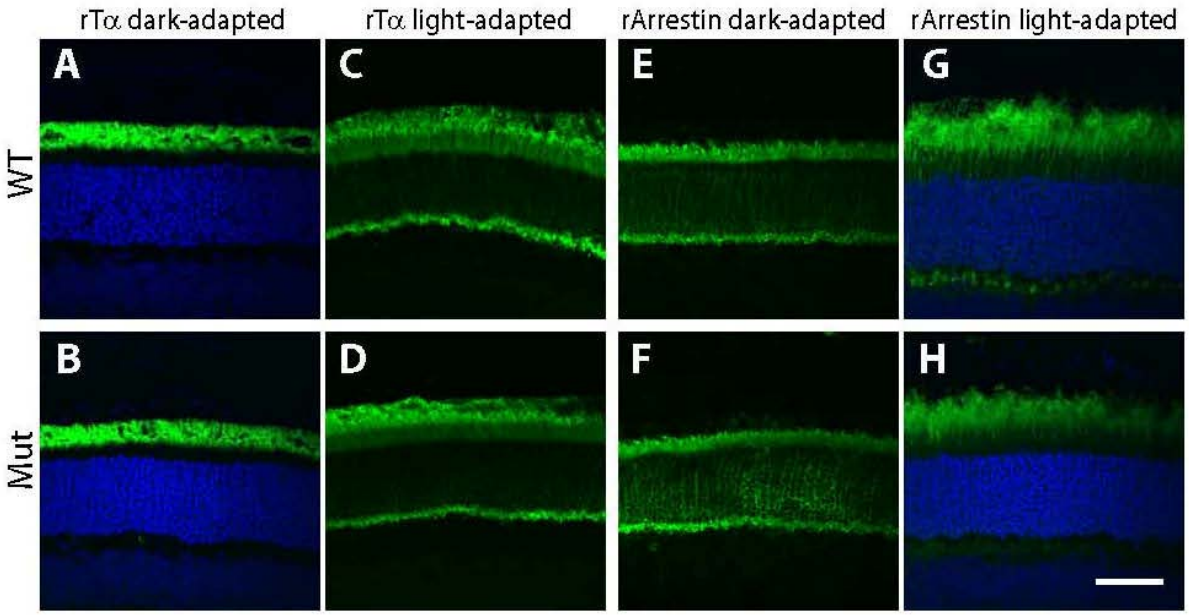

Fig. 4.12: Transducin and arrestin translocation in *Cetn2* mutant mice. (*A–D*) Rod transducin-α is concentrated at the outer segment after overnight dark-adapted animals of both genotypes (*A, B*) and translocated into the inner segment, outer nuclei layer and synaptic layer for 1 hr light-adaptation in both WT (*C*) and mutant (*D*) animals. (*E–H*) Rod arrestin is concentrated in the inner segment, outer nuclei layer and synaptic layer in overnight dark-adapted animals of both genoytypes (*E, F*) and is translocated into the outer segment after 1 hr light adaption in both WT (*G*) and mutant (*H*) animals. Scale bar, 50 μm.

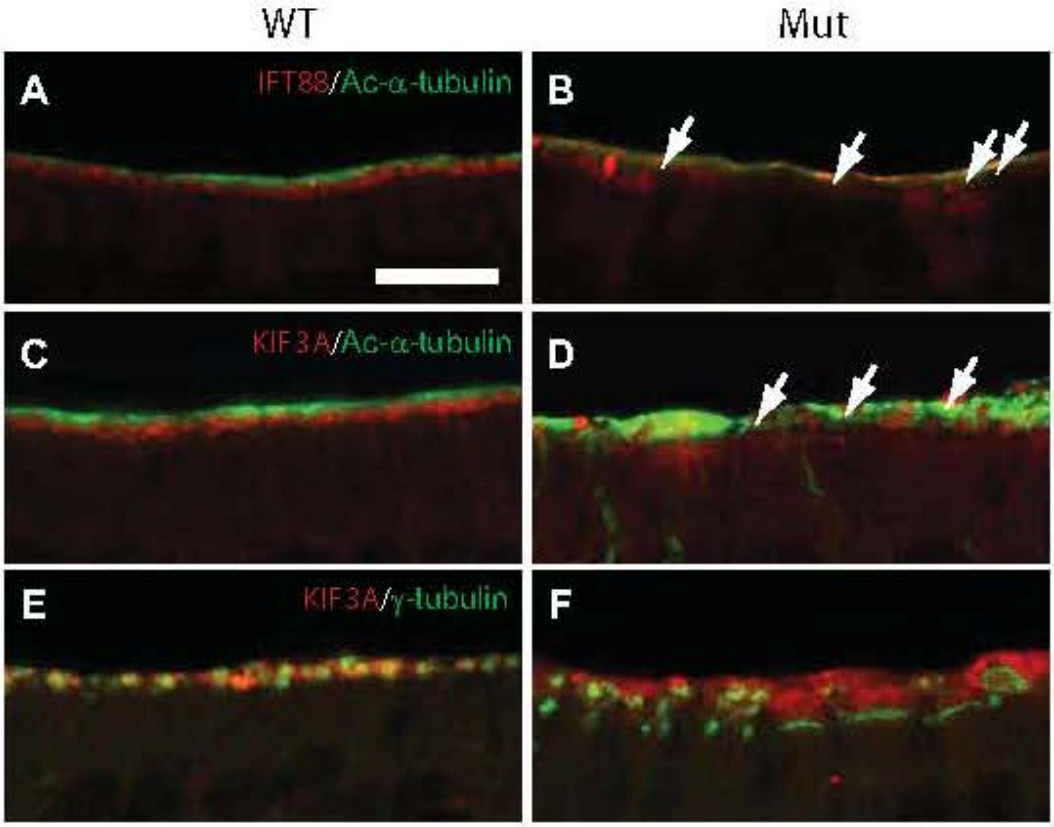

Fig. 4.13: Mislocalization IFT components in P14 *Cetn2* mutant OE. (*A*, *B*) Colabeling of IFT88 (red) and Ac-a-tubulin (green), showing overlap in the cilia layer in mutant (*B*, arrows), but not in WT (*A*). (*C, D*) Colabeling of KIF3A (red) and Ac-a-tubulin (green) in the cilia layer in mutant (*D*) in comparison to WT (*C*). (*E, F*) Colocalization of KIF3A (red) with y-tubulin (green) in WT (*E*), but separation of KIF3A and y-tubulin in mutant OE (*F*). Scale bar: 20 μm.

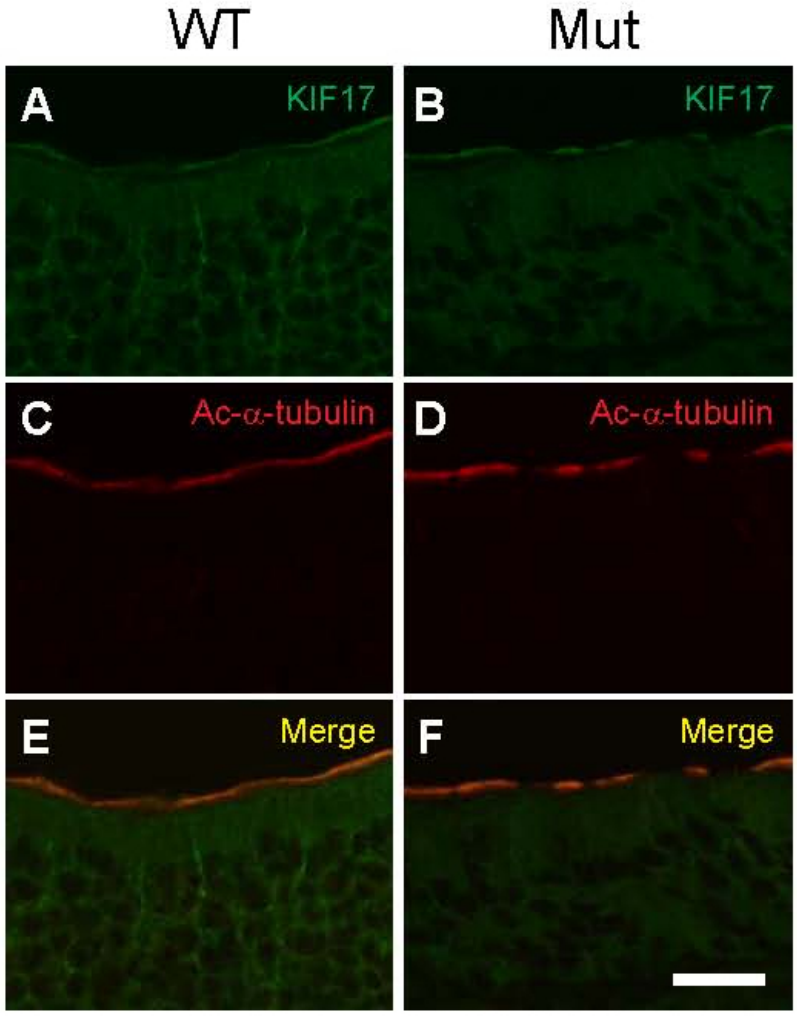

Fig. 4.14: KIF17 localization in WT and mutant olfactory cilia and GFP-Cetn2 co-immunoprecipitation. (*A*–*F*) Double immunofluorescence showed that KIF17 (green) colocalizes with cilia layer marker Ac-tubulin (red) in both WT (*A, C,* and *E*) and *Cetn2* mutant (*B, D,* and *F*) OE. Scale bar, 20 μm.

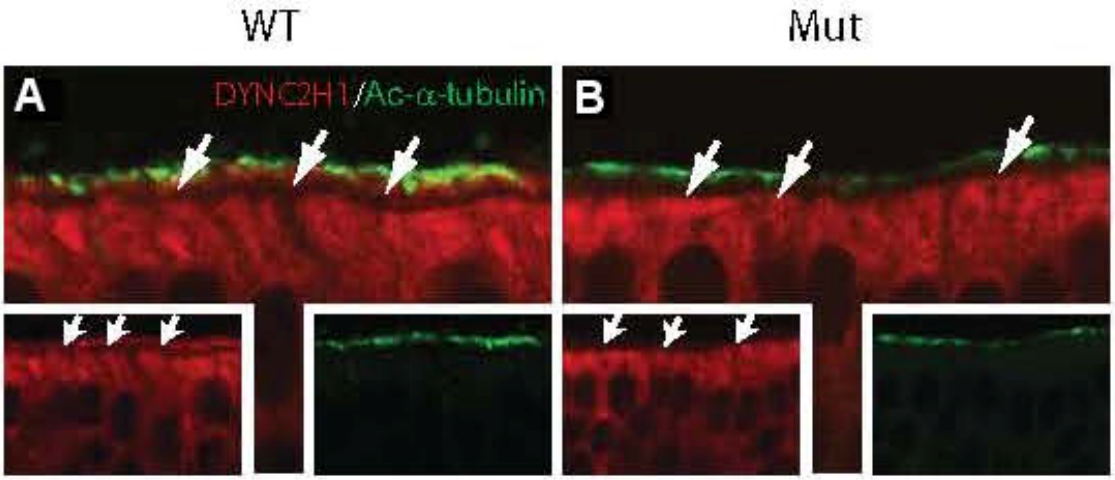

Fig. 4.15: Mislocalization IFT components in P14 *Cetn2* mutant OE. (*A*, *B*) Colabeling of DYNC2H1 (red) and Ac-a-tubulin in the knob layer (arrows). Scale bar: 20 µm.

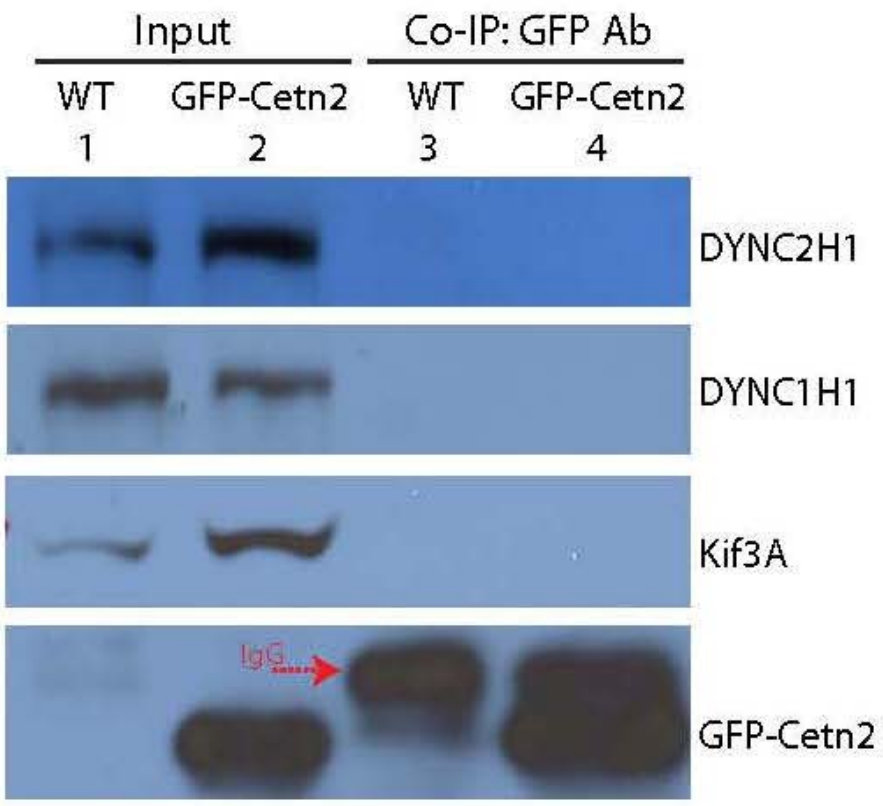

Fig. 4.16: Co-IP of GFP-CETN2 and DYNC2H1 or KIF3A. Antibody directed against GFP was used to immunoprecipitate CETN2-binding proteins from transgenic GFP-*Cetn2* olfactory epithelia lysate. WT type OE lysate was used as control. All input bands appeared as expected (lanes 1 and 2), yet we were unable to detect immunoblot bands for DYNC2H1, KIF3A, and DYNC1H1 among co-IP products (lanes 3 and 4).

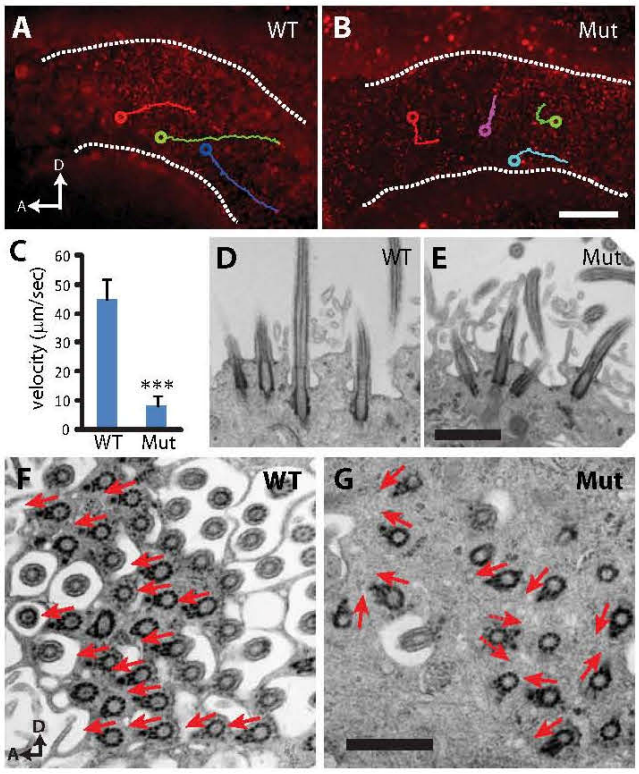

Fig. 4.17: Impaired CSF flow and disrupted ependymal planar polarity in *Cetn2* mutants. (*A, B*) Tracking of latex bead movements along the lateral ventricle surface. Dashed lines outline the edge of lateral ventricle. Colored lines indicate the trajectory of several tracked particles, and circles mark the end of tracking. Fluorescent beads largely moved in one direction from posterior to anterior in WT (*A*), but moved in multiple directions in mutant (*B*). D, dorsal, A, anterior. (*C*). Microbeads moved significantly slower in mutant than in WT. Data shown as mean ± sd (> 20 beads from 2 animals in each group, one-way ANOVA, ***p < 0.001). (*D, E*) Sagittal TEM of P13 lateral ventricle ependymal tissue, showing well-aligned WT cilia (*D*) but disoriented mutant cilia (*E*). (*F, G*) TEM image of ependymal tissue at basal foot level. In WT, the basal feet uniformly point to the anterior (*F*), but in mutant, they point to random directions (*G*). Red arrows mark the basal foot direction. Scale bar: *A, B,* 20 µm; *D–G*, 10 µm.

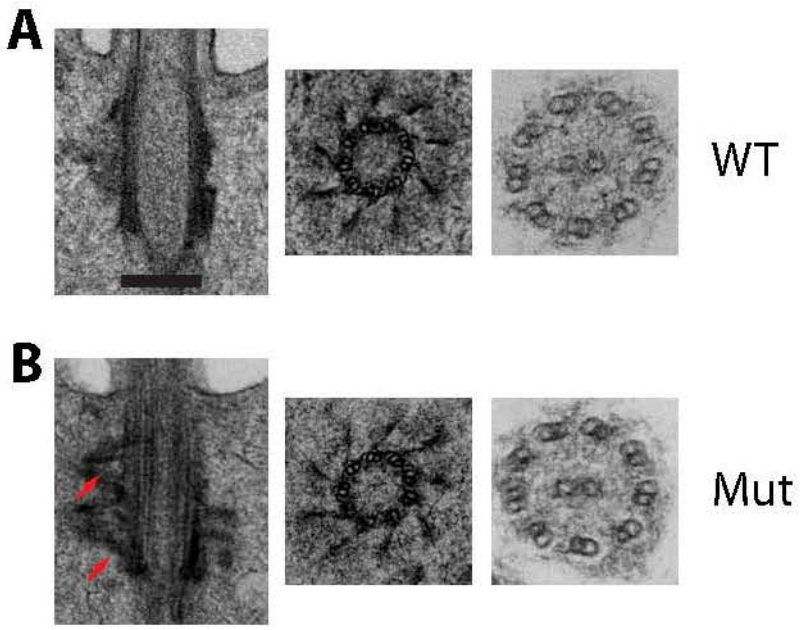

Fig. 4.18: TEM examination of WT and mutant ependymal cilia. P13 ependymal basal body showed additional basal feet in mutant (*B*) but not WT (*A*) in longitudinal sections (first panel, arrows). In cross sections, basal body triplet microtubule structure and distal transitional fibers (middle panel), as well as 9+2 cilia axoneme organization (right panel) appeared normal in mutants compared to WT. Scale bar. 100 nm.

CHAPTER 5

DISCUSSION

The olfactory system is sometimes used as a model to better understand neuronal mechanisms and functions in the central nervous system (CNS) (Doursout et al., 2013; Riggio et al., 2013; Ruan et al., 2012; Shepherd and Charpak, 2008). Unlike most of the CNS, mammalian (including human) olfactory systems are capable of replacing some types of neuronal cells throughout life (Kelsch et al., 2007; Breton-Provencher and Saghatelyan, 2012). This unique CNS feature is made possible by a steady supply of migrating precursor cells from the subventricular zone (SVZ), where stem cells are being produced (Bath and Lee, 2010; Bovetti et al., 2011; Lemasson et al., 2005). The ability to replace olfactory cells is essential for the sense of smell to be effective (Breton-Provencher et al., 2009; Cowan and Roskams, 2002). Research has been done on the regenerating CNS neurons in hopes of finding effective ways to treat neurodegenerative diseases and possibly ischemic injuries to the more permanent CNS neurons (Kuwabara and Asashima, 2012; Ubeda-Banon et al., 2013; Christie and Turnley, 2012; Cowan and Roskams, 2002; Ohtaki et al., 2008).

G-protein coupled receptors (GPCRs) have a wide variety of binding sites, types of G-protein specific to receptor, G-protein combinations, and dependencies of GPCR-induced mechanisms on strength of receptor activation (Oldham and Hamm, 2008; Zhou et al., 2002). Supplying neuropeptides and transmitters to GPCRs is one of the most popular methods for medical/clinical treatments and therapies (Pierce et al., 2002; Oldham and Hamm, 2008). The functions of GPCRs include the modulation of $[Ca^{2+}]_i$, and all three of the projects in this dissertation involve some aspect of GPCRs. In Chapter 2 we studied neonatal olfactory bulb $[Ca^{2+}]_i$ activity in response to activation of the PAC1 receptor (PAC1R), which is a GPCR specific to a pleiotropic neuropeptide called PACAP (Blechman and Levkowitz, 2013; Zhou et al., 2002). We also studied the modulation of intracellular $[Ca^{2+}]_i$ through two other GPCRs (P2Y purinergic receptors and muscarinic acetylcholine receptors) in sustentacular cells of the olfactory epithelium. The sustentacular cells act like glial cells to the olfactory neurons and basal cells, and may be important for integrating communications within the OE (Chapter 3). Lastly, we identified the roles of a centrin, Cetn2, in transporting GPCR-associated proteins to the cilia of OSNs. Studies of the readily accessible cilia in the OE can provide clues relating to the reasons various GPCRs are dysfunctional in various organs (Chapter 4).

Experiments Using PACAP in Neonatal Mouse OB

Chapter 2 is about PACAP, which is a neuropeptide that has the potential to clinically treat neurodegenerative diseases. This peptide has a strong effect on reducing cell mortality (Atlasz et al., 2010; Bourgault et al., 2009; Chen et al.,

2006; Dejda et al., 2008; Kanekar et al., 2010; Ohtaki et al., 2006; Vaudry et al., 2002; Yang et al., 2006). Furthermore, PACAP aids cells that develop during adulthood to mature and proliferate throughout the body, especially in the nervous system (Makela et al., 2010; Scharf et al., 2008; Sherwood et al., 2007; Shioda et al., 2006; Ravni et al., 2006). The anti-apoptotic and developmental effects of PACAP are often times studied in cultured neurons from various parts of the nervous system, including but not limited to the retina (Atlasz et al., 2010; Delwig et al., 2013; Kiss et al., 2006; Markhotina et al., 2007; Silveira et al., 2002; Szabadfi et al., 2012; Szabadfi et al., 2014), cerebellum (Botia et al., 2007; Jozwiak-Bebenista et al., 2007; Allais et al., 2007; Falluel-Morel et al., 2007; Falluel-Morel et al., 2008; Mei et al., 2004; Vaudry et al., 1998b; Vaudry et al., 1999; Vaudry et al., 2000b; Vaudry et al., 2000a; Vaudry et al., 2002; Vaudry et al., 2003; Zhokhov et al., 2008), hippocampus (Kambe and Miyata, 2012; Ago et al., 2011; Costa et al., 2009; Di et al., 2003; Liu et al., 2003; Macdonald et al., 2005; Taylor et al., 2014), and suprachiasmatic nucleus (SCN) (Dziema and Obrietan, 2002; Irwin and Allen, 2010; Kopp et al., 1999; Kopp et al., 2001; Michel et al., 2006; Webb et al., 2013). A few studies were done in the OE region, but there are no physiological studies of PACAP in the PAC1R-rich OB (Han and Lucero, 2005; Han and Lucero, 2006; Hegg et al., 2003). However, it is the readily accessible CNS OB that has a straightforward entrance route from the rostral migratory stream (RMS) for the newly generated precursor cells, which actively replace interneurons, especially granule cells and periglomerular cells, throughout life. One significant aspect of my work is that it provides the first

physiological studies of PACAP in the mammalian olfactory bulb and lays the foundation for future studies on the role of PACAP in neuronal maturation and survival in the CNS. I chose to look at the rapid actions of PACAP on the Ca^{2+} activity in the granule cell layer of the neonatal mouse olfactory bulb. This is mainly because in other developing brain regions, the experience-independent (before the onset of any external sensory input) $[Ca^{2+}]_i$ signal is suggested to be an essential part of neuronal development during the migrating neuroblast and immature neuron stages (Delwig et al., 2013; Hanganu-Opatz, 2010; Momose-Sato and Sato, 2013; Cameron et al., 2009). First week neonatal mice pups were used both for their adaptability to a relatively simple acute live slicing method and for study of PACAP effects during early maturation. Rodents in general are valuable tools for studying neuronal development because they are born at the development stage corresponding to the end of the second gestational trimester in humans. Thus, the majority of rodent brain network development occurs postnatally (Hanganu-Opatz, 2010).

One of the biggest problems in the usage of PACAP for experiments or therapy is its rapid degradation. Bourgault et al. (2008) evaluated the kinetics of two sizes of PACAP, the 38-amino acid version and the 27-amino acid version, using a calcium mobilization assay. Both PACAP 38 and PACAP 27 are produced throughout the body and have similar EC_{50} and efficacy maximums. PACAP 38 was, however, more unstable in plasma, having a half-life of only 5 minutes. PACAP 27 has a half-life of more than 120 minutes (Bourgault et al., 2008) and the degradation process should be slowed down by keeping the

solutions on ice for the day. For the initial PACAP experiments, we used PACAP 38 and found considerable variability in eliciting Ca^{2+} responses. For the experiments in Chapter 2, a new vial of dry PACAP 27 powder was freshly dissolved every experiment day and kept on ice until use.

The interesting question about PACAP in the granule cell layer (GCL) of the OB is where the peptides are naturally made. We had some difficulty discerning endogenous PACAP protein expression in both OE and OB of neonatal mice because control studies revealed that the antibody staining was not specific.

The available published data for PACAP expression in the mouse OB pertains to the pattern of expression of messenger RNA for PACAP, which is seen mostly in the mitral cell layer (MCL) of OB, RMS, hippocampus, and cerebellum, whereas mRNA for PAC1 receptors is expressed in the granule cell layer (GCL) of OB and other regions of mouse brain (Allen Brain Altas, 2013; Jaworski and Proctor, 2000; Shioda et al., 1997; Matsuno et al., 2008). Whether the patterns of mRNA expression give a practical answer as to where proteins are actually made is open to question. For example, neuroblast cells do not express their GAD65 or 67 proteins until they enter the OB, but the cell characters are predetermined in the SVZ as shown by mRNA expression (Lopez-Bendito et al., 2004; Plachez and Puche, 2012). All we reliably know at this point is that most of the mRNA expression for PACAP peptide is in the MCL and RMS, while the highest mRNA expression for PAC1R within the OB is in the GCL. Either way, the mRNA expression suggests that PACAP is endogenously made

in neonatal OB. Until we have a better idea of which regions and types of cell release PACAP, we may assume that PACAP is released into the GCL from the MCL and perhaps the RMS.

Effects of PACAP on Granule Cells of the Neonatal Mouse OB

Briefly, the application of PACAP in acute OB slices shows that the activation of $PAC1R^{+}$ granule cells (GCs) leads to activation of $PAC1R^{-}$ GCs, and provides a wide variety of $[Ca^{2+}]_i$ activity responses ranging from simple transients (22%), slow to fast sawtooth oscillations (22% total), and sustained oscillations (56%) (Fig. 2.2). Kopp et al. (1999) found somewhat similar percentages in cultured SCNs: simple transients (20%), $[Ca^{2+}]_i$ oscillations (15%) and "sustained oscillations" (called biphasic response with initial $[Ca^{2+}]_i$ followed by plateau phase; 65%) (Kopp et al., 1999). Possible factors contributing to the variety of responses are the dose of PACAP (Figs. 2.3 and 2.4) and the amount of downstream PACAP-induced activation of glutamate and/or GABA receptors (Figs. 2.5, 2.6, and 2.7). The noted variable responses and mechanisms of PACAP-induced $[Ca^{2+}]_i$ signaling in the CNS (Ago et al., 2011; Bath and Lee, 2010; Costa et al., 2009; Dziema and Obrietan, 2002; Irwin and Allen, 2010; Kopp et al., 1999; Kopp et al., 2001; Vaudry et al., 1998a; Vaudry et al., 1999; Vaudry et al., 2000a) were also suggested to depend on the majority expression of PAC1R splice variants (Ago et al., 2011; Blechman and Levkowitz, 2013; Yan et al., 2013; Nicot and Dicicco-Bloom, 2001; Zhou et al., 2002). The similar results between OB slices and Kopp et al. (1999) cultured SCNs suggest that

both regions may have similar heterogeneous expression of PAC1R splice variants. It is, however, not clear whether the cultured SCNs have a similar amount of downstream PACAP-induced activation. According to my work and that of Hanganu et al. (2009), glutamate and/or GABA do not need synaptic connections to activate multiple cells (Hanganu et al., 2009). Further support that synaptic connections are not required for post-PACAP-induced types of $[Ca^{2+}]_i$ responses is the observation that many aspects of the responses are not age-dependent. OB slices from mice from the P2, P3, P4, and P5 age groups show similar PACAP-induced kinetics, intensity, and types of $[Ca^{2+}]_i$ responses (data not shown). The lack of age dependence occurs despite day-to-day changes in the percentage of immature versus mature PACAP-responding cells during the first neonatal week (Fig. 2.13). The data suggest a decrease in the population of immature, non-PACAP-responding GCs (excitatory response to GABA) and an increase in the population of mature PACAP-responding GCs between P2 and P5. Thus PACAP appears to be increasingly active in modulating $[Ca^{2+}]_i$ within days after birth, especially with the increasing number of $PAC1R^+$ GCs and their increasingly complicated connections with the $PAC1R^+$ MCs in particular (Fig 2.8). Despite the age-related increase in the population of mature PACAP-responding GCs, the average kinetics and intensities of PACAP-induced $[Ca^{2+}]_i$ are not age-dependent.

Eight PAC1 splice variants have been officially identified and seven of these activate the phosphoinositide-phospholipase C (PLC) or/and acetylate cyclase (AC) second messenger pathways. The eighth splice variant of PAC1

has no effect on PLC or AC pathways, but has been suggested to activate the L-type voltage-gated $[Ca^{2+}]_i$ channels (Zhou et al., 2002). Recently, Basille-Dugay et al. (2013) showed that the immature cerebellar granule neurons have a partial decrease in PACAP-induced $[Ca^{2+}]_i$ activity in N-type Ca^{2+} channel blocker, and the L, P, and Q blockers have no effect (Basille-Dugay et al., 2013). It is not known why these neurons have what may be a unique PACAP-induced $[Ca^{2+}]_i$ activity, but the actions of PACAP are apparently complex. Variations in the mechanisms and intensities of PACAP-induced $[Ca^{2+}]_i$ activity responses can arise from the type of PAC1R splice variant expressed (Ago et al., 2011; Blechman and Levkowitz, 2013; Nicot and Dicicco-Bloom, 2001; Yan et al., 2013; Zhou et al., 2002). Adding to the complicated $[Ca^{2+}]_i$ activity is the relationship between PACAP-induced indirect release of glutamate and GABA transmitters. Figures 2.5, 2.6, and 2.7 show evidence that PACAP indirectly releases transmitters, which was also observed in SCN (Dziema and Obrietan, 2002; Kopp et al., 1999; Kopp et al., 2001) and the hippocampus (Roberto and Brunelli, 2000; Roberto et al., 2001). However, several labs suggested that PACAP mainly acts as an excitatory or inhibitory modulator of glutamatergic activity and has no significant effect on GABA activity in SCNs (Dziema and Obrietan, 2002; Kopp et al., 2001; Michel et al., 2006), hippocampus (53), and retina (Webb et al., 2013). On the other hand, the scientists who accept the concept of excitatory GABA responses believe that coordinated $[Ca^{2+}]_i$ activity through the release and modulation of glutamate and GABA is critical to the development of the CNS, especially during the stage when the animal has no experience-dependent

activity for shaping sensory perception (Hanganu-Opatz, 2010). Hanganu et al. (2009) showed that the depolarizing GABA is released within the developing neonatal cortex from both synaptic and nonsynaptic sources (Hanganu et al., 2009), which may be what happened to the OB GCs in my findings. My work is the first to show the significant involvement of PACAP-induced GABA release as an excitatory factor in developing CNS neurons. Furthermore, I have shown that PACAP by itself induced an overall strong increase in $[Ca^{2+}]$ activity, and that this increase of $[Ca^{2+}]$ activity is often further boosted by the cell-supplied glutamate and GABA.

Dose-dependent Effects of PACAP

My interpretation of the dose-dependent effects is based on the changes of $[Ca^{2+}]_i$. There is not a good way for me to know whether PACAP actually depolarized or hyperpolarized the membrane potential because PACAP could in many cases be simply modulating/enhancing the activity of other neurotransmitters, which we know usually leads to depolarization (Costa et al., 2009; Michel et al., 2006; Pugh et al., 2010). PACAP is capable of hyperpolarizing mature cells via the release of GABA. Although the overwhelming percentage of migrating and immature neurons have a GABA-induced excitatory response, I did rarely find cells (out of 90 slices I used for the paper) displaying a clear PACAP-induced rapid decrease in $[Ca^{2+}]_i$ activity with a recovery of less than 120 seconds. Two possible factors for having so few decreased Ca^{2+} responses are that GABA usually only reduces (not blocks)

glutatmatergic responses and there are not as many mature GCL cells during the first neonatal week as in adult.

Based on PACAP dose-response studies and use of PAC1R antagonists, I believe that the dose of PACAP used in experiments should be carefully determined for future investigations. The main reason is that there are possible artifactual effects in using excessive PACAP, which is suggested to be toxic (Di et al., 2012; Freson et al., 2004; Lang et al., 2006). Some researchers that did *in vitro* experiments used extremely high [PACAP] doses of 100–200 nM to obtain maximal neuroprotective effects and to avoid the variability in kinetics and intensities of responses observed at the lower concentrations (Masmoudi et al., 2003; Pugh et al., 2010; Scharf et al., 2008; Vaudry et al., 2002; Basille-Dugay et al., 2013; Dziema and Obrietan, 2002; Kopp et al., 1999; Kopp et al., 2001). At least one lab also used extremely high [PACAP] of 100 nM in slices (Sun et al., 2003). The concern of using lower doses closer to EC_{50} is warranted because my data had an overall larger standard error at lower PACAP concentrations for latency, time to peak, amplitude, and area under curve (Fig. 2.4). There, however, may be drawbacks with using high doses because 100 nM PACAP had lower average amplitudes than 40 nM PACAP (Fig. 2.4*C*). Our frequency histogram analysis suggests that 100 nM PACAP activates more cells that either have excessively low $PAC1R^+$ expression or weaker GluR and/or GABAR connections (Fig. 2.4*E*).

My studies focused on the GCL region of the OB, where PAC1R mRNA expression is very high (Allen Brain Altas, 2013; Jaworski and Proctor, 2000).

Michel et al. (2006), who tested PACAP on hippocampal slices using Ca^{2+} imaging, used 10 nM as an experimental working concentration. This lab, however, did test 100 nM PACAP and recorded that the slices have a small $[Ca^{2+}]_i$ increase (only 6% ± 1%) (Michel et al., 2006). In comparison, I observed a small $[Ca^{2+}]_i$ average increase at concentrations below 10 nM, but significantly larger average PACAP-induced $[Ca^{2+}]_i$ for concentrations above 10 nM PACAP (Fig. 2.4*C*) than what Michel et al. (2006) found for 100 nM. Part of the reason for the difference between my OB slices and those in the hippocampus may be the expression of PAC1Rs and the dominant PAC1R splice variety (Ago et al., 2011; Blechman and Levkowitz, 2013; Nicot and Dicicco-Bloom, 2001; Yan et al., 2013; Zhou et al., 2002). Thus, although 40 nM PACAP was optimal for the OB slices, it may not be the most fitting for other regions. In the case of the first week neonatal mouse OB, a concentration of 10 nM PACAP yields fewer cells with more variability (high standard error as seen in Fig. 2.4) and 100 nM may be excessive.

Another reason to carefully determine the dose of PACAP is the difference in the ability to block PACAP between cultured cells and slices. Despite using PACAP concentrations as much as 10–30 fold higher (10–100 nM) than the known EC_{50} (0.25–3 nM for cultured cells) (Jozwiak-Bebenista et al., 2007; Kambe and Miyata, 2012; Nicot and Dicicco-Bloom, 2001; Dickson et al., 2006), the researchers using *in vitro* assays successfully proved that they could block their chosen PACAP doses with 600–1000 nM PACAP6-38 (PACAP 38 with first 6 peptides deleted) (Masmoudi et al., 2003; Shioda et al., 2006; Vaudry et al.,

2002; Ohno et al., 2005). Unfortunately, we never had the same success in our *in situ* work without adding 1 µM M65 [a PAC1R-specific antagonist (Uchida et al., 1998)] to the 150 nM PACAP6-38 (Fig. 2.3*C*). Costa et al. (2009) had a similar PACAP 6-38 blockage problem in their hippocampus slices. They were able to block 0.5 nM PACAP with 500 nM PACAP 6-38. However, at 10 nM, PACAP was not blockable at 500 nM PACAP 6-38 (Costa et al., 2009). Furthermore, the recent findings by Doan et al. (2012) suggested that the prolonged, post-PACAP $[Ca^{2+}]_i$ activity perseveres, especially *in situ,* and requires higher antagonist concentrations compared to *in vitro* (Doan et al., 2012a; Doan et al., 2012b). This is possibly because of intact cell connections in acute slices that are rarely present in culture.

Future Directions for Evaluating PACAP-induced $[Ca^{2+}]_i$ Activity in OB

The following paragraphs discuss the experimental projects I did not foresee we would like to do until the data was analyzed.

I would have liked to directly confirm that $GAD67^+$ GCs are responsible for the observed shift in PACAP responsiveness between P2 and P5 by using GAD 67 tdTomato mice. Unfortunately, I did not have access to this mouse line and did not realize they would be important until after all of the experiments using $Dlx2^+$ and $GAD65^+$ labeled cells were completed and analyzed. On the other hand, given that there are so many studies showing that almost all $GAD65^-$ GCL cells are $GAD67^+$, I am convinced it is safe to call the unlabeled GCL cells in GAD65 dt Tomato mice “GAD67 cells” (Parrish-Aungst et al., 2007).

A second experiment I would have liked to do was to follow the time course of glutamate responses in P2–P5 OB. Since glutamate amplifies the PACAP response, I hypothesized that the increase in PACAP responsive cells at P5 is a combination of increased glutamatergic connectivity in addition to the increased PAC1R expression that I found using ICC.

The third experiment of interest would be to address the possibility of action potentials having an influence on the pattern of PACAP-induced $[Ca^{2+}]_i$ activity. The role of PACAP-induced action potentials is thoroughly dismissed in Baxter et al. (2011) (Baxter et al., 2011). TTX was shown to block PACAP-induced $[Ca^{2+}]_i$ activity in cultured brain (cortical) neurons. Curiously, I found no significant reduction in the number of PACAP $[Ca^{2+}]_i$ activity responding cells in the presence of TTX (data not shown). The main reason I used TTX in the cocktail containing both glutamate and GABA antagonists was to reduce possible spontaneous $[Ca^{2+}]_i$ activity not induced by PACAP (Baxter et al., 2011; Costa et al., 2009). Baxter et al. (2011), however, used cultures and I used slices. On the other hand, other investigators acquired data indicating that TTX did not block PACAP-induced changes in $[Ca^{2+}]_i$ activity in cultured cells (Kopp et al., 2001) and brain slices (Sun et al., 2003; Michel et al., 2006; Costa et al., 2009). This leads me to the question of whether the PACAP responses obtained in the presence of the glutamate and GABA antagonists were a direct effect of PACAP binding to PAC1Rs and increasing $[Ca^{2+}]_i$, or some of the $PAC1R^-$ cells are mediated through gap junctional-couplings (Hanganu et al., 2009). The more straightforward mechanism would be the PAC1R-direct increase of $[Ca^{2+}]_i$ activity

through mainly the PLC and/or AC pathways in the neurons [data not shown (Azuma et al., 2013; Kanekar et al., 2010; Pardi and Margiotta, 1999; Zhou et al., 2002)].

PACAP-induced Activation of PLC and/or AC Pathways

There is still some controversy over the type of pathways activated by PACAP in CNS. The factors for the controversy include types of experiments done, the kind of cells used, and especially the stage of development. According to the majority of references, usually using H89 or cAMPS-Rp as a PKA inhibitor for the AC pathway, the PKA-dependent pathway activates multiple neuroprotection mechanisms, which reduce the cleavage of pro-apoptotic caspace (Botia et al., 2007; Inoue et al., 2000; Masmoudi et al., 2003; McIlvain et al., 2006; Mei et al., 2004; Onoue et al., 2002; Payet et al., 2003; Shoge et al., 1999; Vaudry et al., 1998a; Vaudry et al., 2003; Wang et al., 2005; Costa et al., 2009; Dziema and Obrietan, 2002; Vaudry et al., 2000a; Bhave and Hoffman, 2004; Nakamachi et al., 2006). Evidence of the neuroprotective roles of the PLC pathway, which include PKC, is sparse (Bhave and Hoffman, 2004; Han and Lucero, 2006; Kanekar et al., 2010; Nakamachi et al., 2006; Vaudry et al., 2000a). This is because some references directly addressing the PKA pathway in neuroprotection do not provide data concerning the PKC pathway (McIlvain et al., 2006; Onoue et al., 2002; Shoge et al., 1999; Costa et al., 2009). The study of the PKC pathway used various approaches. For some work, PMA was used as an agonist to support the involvement of the PKC pathway in neuroprotection (Kanekar et al., 2010; Masmoudi et al., 2003; Vaudry et al., 2000a; Watanabe et

al., 2006). Other labs indirectly block downstream PKC by blocking the upstream PLC pathway. U-73122, is commonly used as an indirect inhibitor of PKC in this way (Han and Lucero, 2006; Masmoudi et al., 2003; Payet et al., 2003; Bhave and Hoffman, 2004; Nakamachi et al., 2006; Watanabe et al., 2006). However, the inhibition of PKC can be done with bisindolylmaleimide I or chelerythrine (Kopp et al., 1999; Vaudry et al., 2003; Vaudry et al., 1998a; Dziema and Obrietan, 2002; Masmoudi et al., 2003; Vaudry et al., 2000a). Additionally, there are PACAP-induced neuroprotective pathways that are suggested to be independent of PKA or/and PKC. For example, the AC pathway can bypass PKA, activating the mechanisms that inhibit apoptosis (Baxter et al., 2011; Vaudry et al., 2003). Although not included, my preliminary studies showed that in mouse OB slices, both the AC and PLC pathways are activated by PACAP; however, further work is needed to verify the results.

Ca^{2+} Activity in Sustentacular Cells of Mouse OE

Chapter 3 evaluated the recently evolving understanding of the role of sustentacular cells in the OE. Sustentacular cells are one of the four primary cell types found in the OE. These cells were thought to be simply epithelial support cells before evidence produced in the 1970s and 1980s suggested that they also have glial-like functions (Breipohl et al., 1974; Getchell, 1986; Okano and Takagi, 1974; Rafols and Getchell, 1983). What we did was to use the modern calcium imaging technique to evaluate the regulation of $[Ca^{2+}]_i$, observing the effect of sustentacular cells on neighboring cells. The ATP/UTP or ACh-induced $[Ca^{2+}]_i$ oscillation among the sustentacular cells shows that the GPCRs responding to

ATP/UTP or ACh have a key role in initiating $[Ca^{2+}]_i$ oscillations through the PLC pathway (Figs. 3.2, 3.3, 3.5, 3.6, and 3.7). Given that the PLC pathway is involved and there was no significant evidence for electrically signaled extracellular Ca^{2+} entry (Fig. 3.4), the coordination of the $[Ca^{2+}]_i$ oscillation between cells is suggested to be primarily through gap junctions (Vogalis et al., 2005a; Vogalis et al., 2005b). The Ca^{2+} and IP_3 ions and molecules are believed to diffuse through gap junctions and provide a communication method between adjacent sustentacular cells, basal cells, and neurons.

I did the Ca^{2+} imaging data for Fig. 3.1 (calcium waves, UTP-induced Ca^{2+} transient starting at apical surface and reaching the basal cell layer), 3.2 (multiple applications of UTP), 3.4*C* and *D* (BAPTA-AM treated and odorant treated), and 3.6*B, C*, and *D* (PLC antagonist) for the project covered in Chapter 3. This project was one of my first successful experimental projects, and the paper was published in 2005. Back then, I used Ringer's solution for running experiments on OE slices. After my later work, using the extremely vulnerable OB slices (Chapter 2), I wonder what kind of intracellular $[Ca^{2+}]$ oscillation I would see in the OE if I were able to have more intact neurons to work with, that is, if I sliced and tested the OE using the solutions (low Na^+/high Mg^{2+} bicarbonate buffer for cutting and low Ca^{2+} artificial cerebral spinal fluid for imaging) I used for the OB in Chapter 2. According to the data using Ringer's solution, we saw spontaneous intracellular calcium waves in 4 out of 524 slices tested (Fig. 3.1) and fast sawtooth $[Ca^{2+}]_i$ oscillations among the sustentacular cells (Fig. 3.2). If we had used the solution used in Chapter 2, would we have seen more slices with

spontaneous intracellular calcium waves? Larger intensity sustained $[Ca^{2+}]_i$ activity, since more of the sensitive neurons possibly would be intact? Since only a few of the possible OSNs responded to odorants (Fig. 3.4*D*), would we see more OSNs responding to the odorant cocktail mixture (containing a wide variety of odorants)? Would the odorant-induced $[Ca^{2+}]_i$ activity of the OSNs have a larger intensity?

Figure 3.1*C* shows the Ca^{2+} transients starting at the apical surface and reaching the basal layer. This was one of the things I noticed and pointed out. Unfortunately, the drawback of using slices was the high flexibility of severed connections and not having all of the cells from the apical to basal layer present in the same imaging range. Since we suggested that the gap junctions between sustentacular cells (Vogalis et al., 2005a) may be a potential unopposed route factor in the ongoing post-UTP $[Ca^{2+}]_i$ oscillation, it would be a good project to study the mechanisms of initiation and propagation of the intercellular calcium waves. If one could improve the opportunities to Ca^{2+} image the connections between sustentacular cells as well as OE connections between the apical to basal layer, we could get data showing whether the spread of elevated $[Ca^{2+}]_i$ between sustentacular cells was done mostly through gap junctions or not.

Role of Cetn2 in Development and Maintenance of Olfactory Cilia

Chapter 4 is the evaluation of an evolutionarily well-preserved calmodulin-related Ca^{2+}-binding protein in the mouse OE. The Cetn2 gene was one of the four identified centrins, and it was chosen for its ubiquitous expression across

eukaryotes from protists and yeast to humans (Dantas et al., 2011; Kleylein-Sohn et al., 2007; Koblenz et al., 2003; Selvapandiyan et al., 2004).

So far, the known germline centrin study done was on Cetn1, which is expressed mainly in male germ cells (Avasthi et al., 2013). We looked at the *Cetn2* knockout, which showed multiple signs of mutation deficiencies (Fig. 4.1). Previously, a *Cetn2* study was done in zebrafish (Delaval et al., 2011), but since the role of centrins appears to vary among species and cell types, the fish results may not be similar to those in mammal models such as mice. As an association with basal bodies of OEs, the *Cetn2* deletion mutant has shown its effect on mouse cilia development (e.g., loss of cilia) (Figs. 4.2, *A, G*, and *H*, 4.3, 4.4, 4.5, and 4.17) and function (impaired transport of transmembrane signaling) (Figs. 4.2, *B–F*, 4.8, 4.9, 4.13, 4.14, 4.15, 4.16, and 4.17). The project was a collaboration with the Baehr lab, which developed the knockout mice lines for both the *Cetn2* and *Pde6δ* gene (Appendix B) projects. The target genes in both projects were believed to have roles in the transportation of proteins for transmission mechanisms, which models some of the defects in ciliagenesis seen in human patients. The study of ciliagenesis is currently a popular field of research because better understanding of defects in cilia (and flagella) may aid in the treatment of ciliated cells in multiple organs from sensory systems to lungs (Benadiba et al., 2012; Bontems et al., 2014; Dammermann et al., 2009; Gate et al., 2012; Liu et al., 2011; Mata et al., 2012; Rachel et al., 2012; Wu and Tang, 2012). For the *Cetn2* case, we summarized that the CETN2 proteins may recruit nonmuscle myosin II to the OSN dendritic knob, a question for further

investigation. That is because the nonmuscle myosin II may have a role in regulating ACIII and CNGA2 vesicle trafficking at the cilia base (Figs. 4.9, 4.13, and 4.17), given that ACIII and CNGA2 are absent from the region in *Cetn2* knockouts. As a result, the *Cetn2* knockouts have dysosmia. The knockouts may also have *situs inversus* and hydrocephalus (in ~30% of animals examined). Since the *Cetn2* gene is expressed across a wide range of living organisms, there must be more systems being affected in animals with *Cetn2* defection. The retinal system, which has ciliary cells, was examined and no defects were noted (Figs. 4.10, 4.11, and 4.12). No defects were noted in the respiratory system either (Figs. 4.7 and 4.8). However, defects were noted in ependymal cells (Figs. 4.17 and 4.18). Further studies in collaboration with urinary/excretory and/or auditory system labs could lead to discovering other less obvious phenotypical effects.

My part in this work was testing the OE tissue of *Cetn2* mutants and their wild type littermates using an electro-olfactogram (EOG), which revealed that the *Cetn2* mutants have dysomia. The most important observation was that when doing EOG testing, using heterozygous mice as wildtypes has not worked out well. In theory, the heterozygous mice are supposed to develop and function like wildtypes because they displayed normal wildtype-like phenotypes in physical appearance (weight, size), behavior (food locating), and physiology (no hydrocephalus or *situs inversus*). However, odorant responses as measured by the EOG were always 10 to 30% lower in OE tissue from heterozygous mice than responses in wildtype OE. This was true for each of the five different lines I

tested; I never had even one heterozygote display the expected wildtype level of responses.

All of these three projects have advanced the basic understanding of Ca^{2+}-dependent processes through the GPCRs in OE and OB. In summary, PACAP activates multiple pathways, mainly PLC and/or AC pathways, through PAC1 GPCRs, elevating intracellular Ca^{2+}. The PACAP-induced Ca^{2+} activity is further modulated through the cell-supplied glutamate and GABA. In sustentacular cells, intracellular Ca^{2+} is elevated through the activation of purinergic (UTP) and muscarinic (acetylcholine) GPCRs. Cetn2 mutants are dysosmic due to the lack of cilia surface for their odorant GPCRs, which activate the AC pathway, in part due to the delocalization of the AC protein.

Reference List

1. Allen Brain Altas. 2013.
2. **Ago Y, Yoneyama M, Ishihama T, Kataoka S, Kawada K, Tanaka T, Ogita K, Shintani N, Hashimoto H, Baba A, Takuma K, Matsuda T**. Role of endogenous pituitary adenylate cyclase-activating polypeptide in adult hippocampal neurogenesis. *Neuroscience* 172: 554–561, 2011.
3. **Allais A, Burel D, Isaac ER, Gray SL, Basille M, Ravni A, Sherwood NM, Vaudry H, Gonzalez BJ**. Altered cerebellar development in mice lacking pituitary adenylate cyclase-activating polypeptide. *Eur J Neurosci* 25: 2604–2618, 2007.
4. **Atlasz T, Szabadfi K, Kiss P, Tamas A, Toth G, Reglodi D, Gabriel R**. Evaluation of the protective effects of PACAP with cell-specific markers in ischemia-induced retinal degeneration. *Brain Res Bull* 81: 497–504, 2010.
5. **Avasthi P, Scheel JF, Ying G, Frederick JM, Baehr W, Wolfrum U**. Germline deletion of Cetn1 causes infertility in male mice. *J Cell Sci* 126: 3204–3213, 2013.
6. **Azuma M, Wada K, Leprince J, Tonon MC, Uchiyama M, Takahashi A, Vaudry H, Matsuda K**. The octadecaneuropeptide stimulates

somatolactin release from cultured goldfish pituitary cells. *J Neuroendocrinol* 25: 312–321, 2013.

7. **Basille-Dugay M, Vaudry H, Fournier A, Gonzalez B, Vaudry D**. Activation of PAC1 receptors in rat cerebellar granule cells stimulates both calcium mobilization from intracellular stores and calcium influx through N-type calcium channels. *Front Endocrinol (Lausanne)* 4: 56, 2013.

8. **Bath KG, Lee FS**. Neurotrophic factor control of adult SVZ neurogenesis. *Dev Neurobiol* 70: 339–349, 2010.

9. **Baxter PS, Martel MA, McMahon A, Kind PC, Hardingham GE**. Pituitary adenylate cyclase-activating peptide induces long-lasting neuroprotection through the induction of activity-dependent signaling via the cyclic AMP response element-binding protein-regulated transcription co-activator 1. *J Neurochem* 118: 365–378, 2011.

10. **Benadiba C, Magnani D, Niquille M, Morle L, Valloton D, Nawabi H, Ait-Lounis A, Otsmane B, Reith W, Theil T, Hornung JP, Lebrand C, Durand B**. The ciliogenic transcription factor RFX3 regulates early midline distribution of guidepost neurons required for corpus callosum development. *PLoS Genet* 8: e1002606, 2012.

11. **Bhave SV, Hoffman PL**. Phosphatidylinositol 3'-OH kinase and protein kinase A pathways mediate the anti-apoptotic effect of pituitary adenylyl cyclase-activating polypeptide in cultured cerebellar granule neurons: modulation by ethanol. *J Neurochem* 88: 359–369, 2004.

12. **Blechman J, Levkowitz G**. Alternative splicing of the pituitary adenylate cyclase-activating polypeptide receptor PAC1: mechanisms of fine tuning of brain activity. *Front Endocrinol (Lausanne)* 4: 55, 2013.

13. **Bontems F, Fish RJ, Borlat I, Lembo F, Chocu S, Chalmel F, Borg JP, Pineau C, Neerman-Arbez M, Bairoch A, Lane L**. C2orf62 and TTC17 are involved in actin organization and ciliogenesis in zebrafish and human. *PLoS One* 9: e86476, 2014.

14. **Botia B, Basille M, Allais A, Raoult E, Falluel-Morel A, Galas L, Jolivel V, Wurtz O, Komuro H, Fournier A, Vaudry H, Burel D, Gonzalez BJ, Vaudry D**. Neurotrophic effects of PACAP in the cerebellar cortex. *Peptides* 28: 1746–1752, 2007.

15. **Bourgault S, Vaudry D, Botia B, Couvineau A, Laburthe M, Vaudry H, Fournier A**. Novel stable PACAP analogs with potent activity towards the PAC1 receptor. *Peptides* 29: 919–932, 2008.

16. **Bourgault S, Vaudry D, Dejda A, Doan ND, Vaudry H, Fournier A**. Pituitary adenylate cyclase-activating polypeptide: focus on structure-

activity relationships of a neuroprotective Peptide. *Curr Med Chem* 16: 4462–4480, 2009.

17. **Bovetti S, Gribaudo S, Puche AC, De MS, Fasolo A**. From progenitors to integrated neurons: role of neurotransmitters in adult olfactory neurogenesis. *J Chem Neuroanat* 42: 304–316, 2011.

18. **Breipohl W, Laugwitz HJ, Bornfeld N**. Topological relations between the dendrites of olfactory sensory cells and sustentacular cells in different vertebrates. An ultrastructural study. *J Anat* 117: 89–94, 1974.

19. **Breton-Provencher V, Lemasson M, Peralta MR, III, Saghatelyan A**. Interneurons produced in adulthood are required for the normal functioning of the olfactory bulb network and for the execution of selected olfactory behaviors. *J Neurosci* 29: 15245–15257, 2009.

20. **Breton-Provencher V, Saghatelyan A**. Newborn neurons in the adult olfactory bulb: unique properties for specific odor behavior. *Behav Brain Res* 227: 480–489, 2012.

21. **Cameron DB, Raoult E, Galas L, Jiang Y, Lee K, Hu T, Vaudry D, Komuro H**. Role of PACAP in controlling granule cell migration. *Cerebellum* 8: 433–440, 2009.

22. **Chen Y, Samal B, Hamelink CR, Xiang CC, Chen Y, Chen M, Vaudry D, Brownstein MJ, Hallenbeck JM, Eiden LE**. Neuroprotection by endogenous and exogenous PACAP following stroke. *Regul Pept* 137: 4–19, 2006.

23. **Christie KJ, Turnley AM**. Regulation of endogenous neural stem/progenitor cells for neural repair-factors that promote neurogenesis and gliogenesis in the normal and damaged brain. *Front Cell Neurosci* 6: 70, 2012.

24. **Costa L, Santangelo F, Li VG, Ciranna L**. Modulation of AMPA receptor-mediated ion current by pituitary adenylate cyclase-activating polypeptide (PACAP) in CA1 pyramidal neurons from rat hippocampus. *Hippocampus* 19: 99–109, 2009.

25. **Cowan CM, Roskams AJ**. Apoptosis in the mature and developing olfactory neuroepithelium. *Microsc Res Tech* 58: 204–215, 2002.

26. **Dammermann A, Pemble H, Mitchell BJ, McLeod I, Yates JR, III, Kintner C, Desai AB, Oegema K**. The hydrolethalus syndrome protein HYLS-1 links core centriole structure to cilia formation. *Genes Dev* 23: 2046–2059, 2009.

27. **Dantas TJ, Wang Y, Lalor P, Dockery P, Morrison CG**. Defective nucleotide excision repair with normal centrosome structures and functions in the absence of all vertebrate centrins. *J Cell Biol* 193: 307–318, 2011.

28. **Dejda A, Jolivel V, Bourgault S, Seaborn T, Fournier A, Vaudry H, Vaudry D**. Inhibitory effect of PACAP on caspase activity in neuronal apoptosis: a better understanding towards therapeutic applications in neurodegenerative diseases. *J Mol Neurosci* 36: 26–37, 2008.

29. **Delaval B, Covassin L, Lawson ND, Doxsey S**. Centrin depletion causes cyst formation and other ciliopathy-related phenotypes in zebrafish. *Cell Cycle* 10: 3964–3972, 2011.

30. **Delwig A, Majumdar S, Ahern K, Lavail MM, Edwards R, Hnasko TS, Copenhagen DR**. Glutamatergic neurotransmission from melanopsin retinal ganglion cells is required for neonatal photoaversion but not adult pupillary light reflex. *PLoS One* 8: e83974, 2013.

31. **Di MM, Cavallaro S, Ciranna L**. Pituitary adenylate cyclase-activating polypeptide modifies the electrical activity of CA1 hippocampal neurons in the rat. *Neurosci Lett* 337: 97–100, 2003.

32. **Di MM, Peeters K, Loyen S, Thys C, Waelkens E, Overbergh L, Hoylaerts M, Van GC, Freson K**. Pituitary adenylate cyclase-activating polypeptide (PACAP) impairs the regulation of apoptosis in megakaryocytes by activating NF-kappaB: a proteomic study. *Mol Cell Proteomics* 11: M111, 2012.

33. **Dickson L, Aramori I, Sharkey J, Finlayson K**. VIP and PACAP receptor pharmacology: a comparison of intracellular signaling pathways. *Ann NY Acad Sci* 1070: 239–242, 2006.

34. **Doan ND, Chatenet D, Letourneau M, Vaudry H, Vaudry D, Fournier A**. Receptor-independent cellular uptake of pituitary adenylate cyclase-activating polypeptide. *Biochim Biophys Acta* 1823: 940–949, 2012a.

35. **Doan ND, Letourneau M, Vaudry D, Doucet N, Folch B, Vaudry H, Fournier A, Chatenet D**. Design and characterization of novel cell-penetrating peptides from pituitary adenylate cyclase-activating polypeptide. *J Control Release* 163: 256–265, 2012b.

36. **Doursout MF, Schurdell MS, Young LM, Osuagwu U, Hook DM, Poindexter BJ, Schiess MC, Bick DL, Bick RJ**. Inflammatory cells and cytokines in the olfactory bulb of a rat model of neuroinflammation; insights into neurodegeneration? *J Interferon Cytokine Res* 33: 376–383, 2013.

37. **Dziema H, Obrietan K**. PACAP potentiates L-type calcium channel conductance in suprachiasmatic nucleus neurons by activating the MAPK pathway. *J Neurophysiol* 88: 1374–1386, 2002.

38. **Falluel-Morel A, Aubert N, Vaudry D, Desfeux A, Allais A, Burel D, Basille M, Vaudry H, Laudenbach V, Gonzalez BJ**. Interactions of PACAP and ceramides in the control of granule cell apoptosis during cerebellar development. *J Mol Neurosci* 36: 8–15, 2008.

39. **Falluel-Morel A, Chafai M, Vaudry D, Basille M, Cazillis M, Aubert N, Louiset E, de JS, Le Bigot JF, Fournier A, Gressens P, Rostene W, Vaudry H, Gonzalez BJ**. The neuropeptide pituitary adenylate cyclase-activating polypeptide exerts anti-apoptotic and differentiating effects during neurogenesis: focus on cerebellar granule neurones and embryonic stem cells. *J Neuroendocrinol* 19: 321–327, 2007.

40. **Freson K, Hashimoto H, Thys C, Wittevrongel C, Danloy S, Morita Y, Shintani N, Tomiyama Y, Vermylen J, Hoylaerts MF, Baba A, Van GC**. The pituitary adenylate cyclase-activating polypeptide is a physiological inhibitor of platelet activation. *J Clin Invest* 113: 905–912, 2004.

41. **Gate D, Danielpour M, Levy R, Breunig JJ, Town T**. Basic biology and mechanisms of neural ciliogenesis and the B9 family. *Mol Neurobiol* 45: 564–570, 2012.

42. **Getchell TV**. Functional properties of vertebrate olfactory receptor neurons. *Physiol Rev* 66: 772–818, 1986.

43. **Han P, Lucero MT**. Pituitary adenylate cyclase activating polypeptide reduces A-type K+ currents and caspase activity in cultured adult mouse olfactory neurons. *Neuroscience* 134: 745–756, 2005.

44. **Han P, Lucero MT**. Pituitary adenylate cyclase activating polypeptide reduces expression of Kv1.4 and Kv4.2 subunits underlying A-type K(+) current in adult mouse olfactory neuroepithelia. *Neuroscience* 138: 411–419, 2006.

45. **Hanganu IL, Okabe A, Lessmann V, Luhmann HJ**. Cellular mechanisms of subplate-driven and cholinergic input-dependent network activity in the neonatal rat somatosensory cortex. *Cereb Cortex* 19: 89–105, 2009.

46. **Hanganu-Opatz IL**. Between molecules and experience: role of early patterns of coordinated activity for the development of cortical maps and sensory abilities. *Brain Res Rev* 64: 160–176, 2010.

47. **Hegg CC, Au E, Roskams AJ, Lucero MT**. PACAP is present in the olfactory system and evokes calcium transients in olfactory receptor neurons. *J Neurophysiol* 90: 2711–2719, 2003.

48. **Inoue M, Fujishiro N, Ogawa K, Muroi M, Sakamoto Y, Imanaga I, Shioda S**. Pituitary adenylate cyclase-activating polypeptide may function as a neuromodulator in guinea-pig adrenal medulla. *J Physiol* 528: 473–487, 2000.

49. **Irwin RP, Allen CN**. Neuropeptide-mediated calcium signaling in the suprachiasmatic nucleus network. *Eur J Neurosci* 32: 1497–1506, 2010.

50. **Jaworski DM, Proctor MD**. Developmental regulation of pituitary adenylate cyclase-activating polypeptide and PAC(1) receptor mRNA expression in the rat central nervous system. *Brain Res Dev Brain Res* 120: 27–39, 2000.

51. **Jozwiak-Bebenista M, Dejda A, Nowak JZ**. Effects of PACAP, VIP and related peptides on cyclic AMP formation in rat neuronal and astrocyte cultures and cerebral cortical slices. *Pharmacol Rep* 59: 414–420, 2007.

52. **Kambe Y, Miyata A**. Role of mitochondrial activation in PACAP dependent neurite outgrowth. *J Mol Neurosci* 48: 550–557, 2012.

53. **Kanekar S, Gandham M, Lucero MT**. PACAP protects against TNFalpha-induced cell death in olfactory epithelium and olfactory placodal cell lines. *Mol Cell Neurosci* 45: 345–354, 2010.

54. **Kelsch W, Mosley CP, Lin CW, Lois C**. Distinct mammalian precursors are committed to generate neurons with defined dendritic projection patterns. *PLoS Biol* 5: e300, 2007.

55. **Kiss P, Tamas A, Lubics A, Lengvari I, Szalai M, Hauser D, Horvath ZS, Racz B, Gabriel R, Babai N, Toth G, Reglodi D**. Effects of systemic PACAP treatment in monosodium glutamate-induced behavioral changes and retinal degeneration. *Ann NY Acad Sci* 1070: 365–370, 2006.

56. **Kleylein-Sohn J, Westendorf J, Le CM, Habedanck R, Stierhof YD, Nigg EA**. Plk4-induced centriole biogenesis in human cells. *Dev Cell* 13: 190–202, 2007.

57. **Koblenz B, Schoppmeier J, Grunow A, Lechtreck KF**. Centrin deficiency in Chlamydomonas causes defects in basal body replication, segregation and maturation. *J Cell Sci* 116: 2635–2646, 2003.

58. **Kopp MD, Meissl H, Dehghani F, Korf HW**. The pituitary adenylate cyclase-activating polypeptide modulates glutamatergic calcium signalling: investigations on rat suprachiasmatic nucleus neurons. *J Neurochem* 79: 161–171, 2001.

59. **Kopp MD, Schomerus C, Dehghani F, Korf HW, Meissl H**. Pituitary adenylate cyclase-activating polypeptide and melatonin in the

suprachiasmatic nucleus: effects on the calcium signal transduction cascade. *J Neurosci* 19: 206–219, 1999.

60. **Kuwabara T, Asashima M**. Regenerative medicine using adult neural stem cells: the potential for diabetes therapy and other pharmaceutical applications. *J Mol Cell Biol* 4: 133–139, 2012.

61. **Lang B, Song B, Davidson W, MacKenzie A, Smith N, McCaig CD, Harmar AJ, Shen S**. Expression of the human PAC1 receptor leads to dose-dependent hydrocephalus-related abnormalities in mice. *J Clin Invest* 116: 1924–1934, 2006.

62. **Lemasson M, Saghatelyan A, Olivo-Marin JC, Lledo PM**. Neonatal and adult neurogenesis provide two distinct populations of newborn neurons to the mouse olfactory bulb. *J Neurosci* 25: 6816–6825, 2005.

63. **Liu L, Zhang M, Xia Z, Xu P, Chen L, Xu T**. Caenorhabditis elegans ciliary protein NPHP-8, the homologue of human RPGRIP1L, is required for ciliogenesis and chemosensation. *Biochem Biophys Res Commun* 410: 626–631, 2011.

64. **Liu Z, Geng L, Li R, He X, Zheng JQ, Xie Z**. Frequency modulation of synchronized Ca2+ spikes in cultured hippocampal networks through G-protein-coupled receptors. *J Neurosci* 23: 4156–4163, 2003.

65. **Lopez-Bendito G, Sturgess K, Erdelyi F, Szabo G, Molnar Z, Paulsen O**. Preferential origin and layer destination of GAD65-GFP cortical interneurons. *Cereb Cortex* 14: 1122–1133, 2004.

66. **Macdonald DS, Weerapura M, Beazely MA, Martin L, Czerwinski W, Roder JC, Orser BA, Macdonald JF**. Modulation of NMDA receptors by pituitary adenylate cyclase activating peptide in CA1 neurons requires G alpha q, protein kinase C, and activation of Src. *J Neurosci* 25: 11374–11384, 2005.

67. **Makela J, Koivuniemi R, Korhonen L, Lindholm D**. Interferon-gamma produced by microglia and the neuropeptide PACAP have opposite effects on the viability of neural progenitor cells. *PLoS One* 5: e11091, 2010.

68. **Markhotina N, Liu GJ, Martin DK**. Contractility of retinal pericytes grown on silicone elastomer substrates is through a protein kinase A-mediated intracellular pathway in response to vasoactive peptides. *IET Nanobiotechnol* 1: 44–51, 2007.

69. **Masmoudi O, Gandolfo P, Leprince J, Vaudry D, Fournier A, Patte-Mensah C, Vaudry H, Tonon MC**. Pituitary adenylate cyclase-activating polypeptide (PACAP) stimulates endozepine release from cultured rat astrocytes via a PKA-dependent mechanism. *FASEB J* 17: 17–27, 2003.

70. **Mata M, Sarrion I, Armengot M, Carda C, Martinez I, Melero JA, Cortijo J**. Respiratory syncytial virus inhibits ciliagenesis in differentiated normal human bronchial epithelial cells: effectiveness of N-acetylcysteine. *PLoS One* 7: e48037, 2012.

71. **Matsuno R, Ohtaki H, Nakamachi T, Watanabe J, Yofu S, Hayashi D, Takeda T, Nonaka N, Seki M, Nakamura M, Itabashi K, Shioda S**. Distribution and localization of pituitary adenylate cyclase-activating polypeptide-specific receptor (PAC1R) in the rostral migratory stream of the infant mouse brain. *Regul Pept* 145: 80–87, 2008.

72. **McIlvain HB, Baudy A, Sullivan K, Liu D, Pong K, Fennell M, Dunlop J**. Pituitary adenylate cyclase-activating peptide (PACAP) induces differentiation in the neuronal F11 cell line through a PKA-dependent pathway. *Brain Res* 1077: 16–23, 2006.

73. **Mei YA, Vaudry D, Basille M, Castel H, Fournier A, Vaudry H, Gonzalez BJ**. PACAP inhibits delayed rectifier potassium current via a cAMP/PKA transduction pathway: evidence for the involvement of I k in the anti-apoptotic action of PACAP. *Eur J Neurosci* 19: 1446–1458, 2004.

74. **Michel S, Itri J, Han JH, Gniotczynski K, Colwell CS**. Regulation of glutamatergic signalling by PACAP in the mammalian suprachiasmatic nucleus. *BMC Neurosci* 7: 15, 2006.

75. **Momose-Sato Y, Sato K**. Large-scale synchronized activity in the embryonic brainstem and spinal cord. *Front Cell Neurosci* 7: 36, 2013.

76. **Nakamachi T, Li M, Shioda S, Arimura A**. Signaling involved in pituitary adenylate cyclase-activating polypeptide-stimulated ADNP expression. *Peptides* 27: 1859–1864, 2006.

77. **Nicot A, Dicicco-Bloom E**. Regulation of neuroblast mitosis is determined by PACAP receptor isoform expression. *Proc Natl Acad Sci USA* 98: 4758–4763, 2001.

78. **Ohno F, Watanabe J, Sekihara H, Hirabayashi T, Arata S, Kikuyama S, Shioda S, Nakaya K, Nakajo S**. Pituitary adenylate cyclase-activating polypeptide promotes differentiation of mouse neural stem cells into astrocytes. *Regul Pept* 126: 115–122, 2005.

79. **Ohtaki H, Nakamachi T, Dohi K, Aizawa Y, Takaki A, Hodoyama K, Yofu S, Hashimoto H, Shintani N, Baba A, Kopf M, Iwakura Y, Matsuda K, Arimura A, Shioda S**. Pituitary adenylate cyclase-activating polypeptide (PACAP) decreases ischemic neuronal cell death in association with IL-6. *Proc Natl Acad Sci USA* 103: 7488–7493, 2006.

80. **Ohtaki H, Nakamachi T, Dohi K, Shioda S**. Role of PACAP in ischemic neural death. *J Mol Neurosci* 36: 16–25, 2008.

81. **Okano M, Takagi SF**. Secretion and electrogenesis of the supporting cell in the olfactory epithelium. *J Physiol* 242: 353–370, 1974.

82. **Oldham WM, Hamm HE**. Heterotrimeric G protein activation by G-protein-coupled receptors. *Nat Rev Mol Cell Biol* 9: 60–71, 2008.

83. **Onoue S, Ohshima K, Endo K, Yajima T, Kashimoto K**. PACAP protects neuronal PC12 cells from the cytotoxicity of human prion protein fragment 106–126. *FEBS Lett* 522: 65–70, 2002.

84. **Pardi D, Margiotta JF**. Pituitary adenylate cyclase-activating polypeptide activates a phospholipase C-dependent signal pathway in chick ciliary ganglion neurons that selectively inhibits alpha7-containing nicotinic receptors. *J Neurosci* 19: 6327–6337, 1999.

85. **Parrish-Aungst S, Shipley MT, Erdelyi F, Szabo G, Puche AC**. Quantitative analysis of neuronal diversity in the mouse olfactory bulb. *J Comp Neurol* 501: 825–836, 2007.

86. **Payet MD, Bilodeau L, Breault L, Fournier A, Yon L, Vaudry H, Gallo-Payet N**. PAC1 receptor activation by PACAP-38 mediates Ca2+ release from a cAMP-dependent pool in human fetal adrenal gland chromaffin cells. *J Biol Chem* 278: 1663–1670, 2003.

87. **Pierce KL, Premont RT, Lefkowitz RJ**. Seven-transmembrane receptors. *Nat Rev Mol Cell Biol* 3: 639–650, 2002.

88. **Plachez C, Puche AC**. Early specification of GAD67 subventricular derived olfactory interneurons. *J Mol Histol* 43: 215–221, 2012.

89. **Pugh PC, Jayakar SS, Margiotta JF**. PACAP/PAC1R signaling modulates acetylcholine release at neuronal nicotinic synapses. *Mol Cell Neurosci* 43: 244–257, 2010.

90. **Rachel RA, May-Simera HL, Veleri S, Gotoh N, Choi BY, Murga-Zamalloa C, McIntyre JC, Marek J, Lopez I, Hackett AN, Zhang J, Brooks M, den Hollander AI, Beales PL, Li T, Jacobson SG, Sood R, Martens JR, Liu P, Friedman TB, Khanna H, Koenekoop RK, Kelley MW, Swaroop A**. Combining Cep290 and Mkks ciliopathy alleles in mice rescues sensory defects and restores ciliogenesis. *J Clin Invest* 122: 1233–1245, 2012.

91. **Rafols JA, Getchell TV**. Morphological relations between the receptor neurons, sustentacular cells and Schwann cells in the olfactory mucosa of the salamander. *Anat Rec* 206: 87–101, 1983.

92. **Ravni A, Bourgault S, Lebon A, Chan P, Galas L, Fournier A, Vaudry H, Gonzalez B, Eiden LE, Vaudry D**. The neurotrophic effects of PACAP in PC12 cells: control by multiple transduction pathways. *J Neurochem* 98: 321–329, 2006.

93. **Riggio C, Nocentini S, Catalayud MP, Goya GF, Cuschieri A, Raffa V, Del Rio JA**. Generation of magnetized olfactory ensheathing cells for regenerative studies in the central and peripheral nervous tissue. *Int J Mol Sci* 14: 10852–10868, 2013.

94. **Roberto M, Brunelli M**. PACAP-38 enhances excitatory synaptic transmission in the rat hippocampal CA1 region. *Learn Mem* 7: 303–311, 2000.

95. **Roberto M, Scuri R, Brunelli M**. Differential effects of PACAP-38 on synaptic responses in rat hippocampal CA1 region. *Learn Mem* 8: 265–271, 2001.

96. **Ruan Y, Zheng XY, Zhang HL, Zhu W, Zhu J**. Olfactory dysfunctions in neurodegenerative disorders. *J Neurosci Res* 90: 1693–1700, 2012.

97. **Scharf E, May V, Braas KM, Shutz KC, Mao-Draayer Y**. Pituitary adenylate cyclase-activating polypeptide (PACAP) and vasoactive intestinal peptide (VIP) regulate murine neural progenitor cell survival, proliferation, and differentiation. *J Mol Neurosci* 36: 79–88, 2008.

98. **Selvapandiyan A, Debrabant A, Duncan R, Muller J, Salotra P, Sreenivas G, Salisbury JL, Nakhasi HL**. Centrin gene disruption impairs stage-specific basal body duplication and cell cycle progression in Leishmania. *J Biol Chem* 279: 25703–25710, 2004.

99. **Shepherd GM, Charpak S**. The olfactory glomerulus: a model for neuro-glio-vascular biology. *Neuron* 58: 827–829, 2008.

100. **Sherwood NM, Adams BA, Isaac ER, Wu S, Fradinger EA**. Knocked down and out: PACAP in development, reproduction and feeding. *Peptides* 28: 1680–1687, 2007.

101. **Shioda S, Ohtaki H, Nakamachi T, Dohi K, Watanabe J, Nakajo S, Arata S, Kitamura S, Okuda H, Takenoya F, Kitamura Y**. Pleiotropic functions of PACAP in the CNS: neuroprotection and neurodevelopment. *Ann NY Acad Sci* 1070: 550–560, 2006.

102. **Shioda S, Shuto Y, Somogyvari-Vigh A, Legradi G, Onda H, Coy DH, Nakajo S, Arimura A**. Localization and gene expression of the receptor for pituitary adenylate cyclase-activating polypeptide in the rat brain. *Neurosci Res* 28: 345–354, 1997.

103. **Shoge K, Mishima HK, Saitoh T, Ishihara K, Tamura Y, Shiomi H, Sasa M**. Attenuation by PACAP of glutamate-induced neurotoxicity in cultured retinal neurons. *Brain Res* 839: 66–73, 1999.

104. **Silveira MS, Costa MR, Bozza M, Linden R**. Pituitary adenylyl cyclase-activating polypeptide prevents induced cell death in retinal tissue through activation of cyclic AMP-dependent protein kinase. *J Biol Chem* 277: 16075–16080, 2002.

105. **Sun QQ, Prince DA, Huguenard JR**. Vasoactive intestinal polypeptide and pituitary adenylate cyclase-activating polypeptide activate hyperpolarization-activated cationic current and depolarize thalamocortical neurons in vitro. *J Neurosci* 23: 2751–2758, 2003.

106. **Szabadfi K, Atlasz T, Kiss P, Danyadi B, Tamas A, Helyes Z, Hashimoto H, Shintani N, Baba A, Toth G, Gabriel R, Reglodi D**. Mice deficient in pituitary adenylate cyclase activating polypeptide (PACAP) are more susceptible to retinal ischemic injury in vivo. *Neurotox Res* 21: 41–48, 2012.

107. **Szabadfi K, Szabo A, Kiss P, Reglodi D, Setalo G, Jr., Kovacs K, Tamas A, Toth G, Gabriel R**. PACAP promotes neuron survival in early experimental diabetic retinopathy. *Neurochem Int* 64: 84–91, 2014.

108. **Taylor RD, Madsen MG, Krause M, Sampedro-Castaneda M, Stocker M, Pedarzani P**. Pituitary adenylate cyclase-activating polypeptide (PACAP) inhibits the slow afterhyperpolarizing current sIAHP in CA1 pyramidal neurons by activating multiple signaling pathways. *Hippocampus* 24: 32–43, 2014.

109. **Ubeda-Banon I, Saiz-Sanchez D, Rosa-Prieto C, Martinez-Marcos A**. alpha-Synuclein in the olfactory system in Parkinson's disease: role of neural connections on spreading pathology. *Brain Struct Funct* 2013.

110. **Uchida D, Tatsuno I, Tanaka T, Hirai A, Saito Y, Moro O, Tajima M**. Maxadilan is a specific agonist and its deleted peptide (M65) is a specific antagonist for PACAP type 1 receptor. *Ann NY Acad Sci* 865: 253–258, 1998.

111. **Vaudry D, Basille M, Anouar Y, Fournier A, Vaudry H, Gonzalez BJ**. The neurotrophic activity of PACAP on rat cerebellar granule cells is associated with activation of the protein kinase A pathway and c-fos gene expression. *Ann NY Acad Sci* 865: 92–99, 1998a.

112. **Vaudry D, Falluel-Morel A, Basille M, Pamantung TF, Fontaine M, Fournier A, Vaudry H, Gonzalez BJ**. Pituitary adenylate cyclase-activating polypeptide prevents C2-ceramide-induced apoptosis of cerebellar granule cells. *J Neurosci Res* 72: 303–316, 2003.

113. **Vaudry D, Gonzalez BJ, Basille M, Anouar Y, Fournier A, Vaudry H**. Pituitary adenylate cyclase-activating polypeptide stimulates both c-fos gene expression and cell survival in rat cerebellar granule neurons through activation of the protein kinase A pathway. *Neuroscience* 84: 801–812, 1998b.

114. **Vaudry D, Gonzalez BJ, Basille M, Fournier A, Vaudry H**. Neurotrophic activity of pituitary adenylate cyclase-activating polypeptide on rat cerebellar cortex during development. *Proc Natl Acad Sci USA* 96: 9415–9420, 1999.

115. **Vaudry D, Gonzalez BJ, Basille M, Pamantung TF, Fontaine M, Fournier A, Vaudry H**. The neuroprotective effect of pituitary adenylate cyclase-activating polypeptide on cerebellar granule cells is mediated through inhibition of the CED3-related cysteine protease caspase-3/CPP32. *Proc Natl Acad Sci USA* 97: 13390–13395, 2000a.

116. **Vaudry D, Gonzalez BJ, Basille M, Pamantung TF, Fournier A, Vaudry H**. PACAP acts as a neurotrophic factor during histogenesis of the rat cerebellar cortex. *Ann NY Acad Sci* 921: 293–299, 2000b.

117. **Vaudry D, Pamantung TF, Basille M, Rousselle C, Fournier A, Vaudry H, Beauvillain JC, Gonzalez BJ**. PACAP protects cerebellar granule neurons against oxidative stress-induced apoptosis. *Eur J Neurosci* 15: 1451–1460, 2002.

118. **Vogalis F, Hegg CC, Lucero MT**. Electrical coupling in sustentacular cells of the mouse olfactory epithelium. *J Neurophysiol* 94: 1001–1012, 2005a.

119. **Vogalis F, Hegg CC, Lucero MT**. Ionic conductances in sustentacular cells of the mouse olfactory epithelium. *J Physiol* 562: 785–799, 2005b.

120. **Wang C, Ohno K, Furukawa T, Ueki T, Ikeda M, Fukuda A, Sato K**. Differential expression of KCC2 accounts for the differential GABA responses between relay and intrinsic neurons in the early postnatal rat olfactory bulb. *Eur J Neurosci* 21: 1449–1455, 2005.

121. **Watanabe J, Ohba M, Ohno F, Kikuyama S, Nakamura M, Nakaya K, Arimura A, Shioda S, Nakajo S**. Pituitary adenylate cyclase-activating polypeptide-induced differentiation of embryonic neural stem cells into astrocytes is mediated via the beta isoform of protein kinase C. *J Neurosci Res* 84: 1645–1655, 2006.

122. **Webb IC, Coolen LM, Lehman MN**. NMDA and PACAP receptor signaling interact to mediate retinal-induced scn cellular rhythmicity in the absence of light. *PLoS One* 8: e76365, 2013.

123. **Wu KS, Tang TK**. CPAP is required for cilia formation in neuronal cells. *Biol Open* 1: 559–565, 2012.

124. **Yan Y, Zhou X, Pan Z, Ma J, Waschek JA, Dicicco-Bloom E**. Pro- and anti-mitogenic actions of pituitary adenylate cyclase-activating polypeptide in developing cerebral cortex: potential mediation by developmental switch of PAC1 receptor mRNA isoforms. *J Neurosci* 33: 3865–3878, 2013.

125. **Yang S, Yang J, Yang Z, Chen P, Fraser A, Zhang W, Pang H, Gao X, Wilson B, Hong JS, Block ML**. Pituitary adenylate cyclase-activating polypeptide (PACAP) 38 and PACAP4-6 are neuroprotective through inhibition of NADPH oxidase: potent regulators of microglia-mediated oxidative stress. *J Pharmacol Exp Ther* 319: 595–603, 2006.

126. **Zhokhov SS, Desfeux A, Aubert N, Falluel-Morel A, Fournier A, Laudenbach V, Vaudry H, Gonzalez BJ**. Bax siRNA promotes survival of cultured and allografted granule cell precursors through blockade of caspase-3 cleavage. *Cell Death Differ* 15: 1042–1053, 2008.

127. **Zhou CJ, Shioda S, Yada T, Inagaki N, Pleasure SJ, Kikuyama S**. PACAP and its receptors exert pleiotropic effects in the nervous system by activating multiple signaling pathways. *Curr Protein Pept Sci* 3: 423–439, 2002.

APPENDIX A

EXCESSIVE CONCENTRATIONS OF PACAP ARE PRO-APOPTOTIC

Introduction

The grant was originally written in 2007 as part of the grant writing class course at the University of Utah. Even though this proposal was not actively pursued, it is a project worth some consideration because of the observations that excessive PACAP concentrations can be toxic. As outlined in Chapter 2 and Chapter 5, the dose of PACAP should be carefully determined for each experimental preparation. The EC_{50} for PACAP activation of PAC1 receptors is typically in the range of 30–50 nM for slices. Some researchers that did *in vitro* experiments used extremely high doses of PACAP (100–200 µM) (Basille-Dugay et al., 2013; Dziema and Obrietan, 2002; Kopp et al., 1999; Kopp et al., 2001; Masmoudi et al., 2003; Pugh et al., 2010; Scharf et al., 2008; Vaudry et al., 2002a). At least one lab used 100 µM PACAP in slices (Sun et al., 2003). The rationale for not using doses closer to the PACAP EC_{50} is warranted because my data show an overall larger standard error at lower PACAP concentrations for latency, time to peak, amplitude, and area under curve (Fig. 2.4). However, a few studies reported that there are possible artifactual effects when using

excessive PACAP, which is suggested to be toxic (Di et al., 2012; Freson et al., 2004b; Lang et al., 2006a). The grant on the following pages is organized according to the guidelines for an NIH grant application.

A: Specific Aims

Pituitary Adenylate Cyclase-Activating Polypeptide (PACAP) is an essential peptide in development and throughout life and is studied as a candidate for preventing the oxidative stress associated with neurodegenerative diseases. With better understanding of PACAP's mechanisms, possible treatments including therapeutic use of PACAP may be in the making. There are however limits on how much PACAP is good or bad for the body. Normal PACAP levels are known to have effects on proliferation, maturation, and preventing apoptosis, but high PACAP levels can induce apoptosis and animals with elevated PACAP receptor or elevated PACAP protein mutations display mental retardation and delayed development. It is unknown whether the negative effects of elevated PACAP are due to increased proliferation, decreased apoptosis of cells that need to die, or increased apoptosis. Based on our observations of cultured cells dying in elevated PACAP media, the increase of apoptosis is the most congruent hypothesis.

I hypothesize that higher than normal PACAP concentrations lead to increased apoptosis and neuronal cell death. The pro-apoptotic effects of elevated PACAP may be due to a down regulation of the transcription processes associated with the anti-apoptotic pathway or due to stimulating pro-apoptotic pathways.

Specific Aim1: Determine whether PACAP-induced apoptosis is mediated by the PAC-1, VPAC1, VPAC2, or other G-protein receptors. Increasing concentrations of PACAP will be applied to OP6 and OP27 cell lines to determine the EC_{50} for inducing apoptosis. The apoptotic cells will be identified using live cell labeling of activated caspases and propidium iodide. Once the EC_{50} for PACAP-induced apoptosis is determined, the specific antagonists for PAC-1, VPAC1, or VPAC2 will be used to identify the receptor(s) involved in the apoptotic effects.

Specific Aim 2: Determine whether there is a dose-dependent shift in PACAP-induced expression of anti- and pro-apoptotic factors. Increasing concentrations of PACAP will be applied to OP6 and OP27 cell lines and the dose-dependent expression of PACAP-induced anti-apoptotic factors will be measured through the use of RT-PCR or/and Western blotting quantification of c-fos, Bcl-2, and ERK. In addition, the PACAP-treated cell lines will be assayed for a shift in the activation or expression levels of pro-apoptotic factors such as JNK, BAX, c-jun, and the caspases.

Specific Aim 3: Determine whether high PACAP concentrations could prevent or make the cells more vulnerable to external apoptotic stimulation.

The OP6 and OP27 cell lines will be treated with high PACAP concentrations in the presence and absence of the membrane permeant apoptosis activator C2-ceramide. The effects of adding C2-ceramide at various time points after the

initial PACAP treatment will be assayed using live cell labeling of activated caspases and propidium iodide.

The picture of PACAP's mechanisms at higher than normal PACAP concentrations, which are reducing the cell's ability to proliferate and mature, may give better ideas about how to get the best out of PACAP treatments in the studies using PACAP as a tool to preserve the neuronal cells.

B: Background and Significance

PACAP and olfactory system overview

PACAP was first discovered and characterized as a factor/neuropeptide that stimulates cAMP formation in the pituitary cells by Miyata et al. in 1989 (Miyata et al., 1989). Even though PACAP's official discovery came after the majority of hypophysiotropic neurohormones had been identified, PACAP is now considered to be one of the most important regulators of biological functions and affects proliferation, maturation, and apoptosis. Not surprisingly, PACAP is highly evolutionarily conserved from protochordates to mammals. PACAP is important in a wide spectrum of tissues including the pituitary gland, liver, respiratory system, immune system, and even bones (Vaudry et al., 2000). The functions of PACAP in the central nervous system are largely neurotrophic during development and neuroprotective or neuromodulatory during adulthood (Vaudry et al., 2002b; Delgado et al., 2003; Arimura, 1998). Within the central nervous system, PACAP expression is highest in the sensory systems such as the olfactory system (Mulder et al., 1999; Hansel et al., 2001a; Shioda et al., 1997).

Starting in the periphery of the olfactory system, PACAP and PACAP receptors are expressed in the olfactory epithelium and the ensheathing glia, which escorts the unmyelinated axons of olfactory neurons to the olfactory bulb (OB). The distinctive glomeruli of the olfactory bulb are the site of the first synapse of olfactory sensory neurons (OSNs) and the periglomerular cells surrounding each glomerulus have both PACAP and PACAP receptors. The mitral cells or output neurons that synapse with olfactory receptor neurons (ORNs) in the glomeruli also have high levels of PACAP and PACAP receptors. Importantly, some of the highest densities of PACAP receptors in the adult central neuron system (CNS) are on the adult-born granule neurons in the OB as well as olfactory epithelium (OE). These granule neurons originate in the subventricular zone (SVZ), a region also high in PACAP signaling throughout life (De Marchis et al., 2007). Despite the anatomical presence of PACAP and PACAP receptors in the olfactory system, only a few functional studies have been performed in the olfactory epithelium (Han and Lucero, 2005; Hegg et al., 2003; Hansel et al., 2001b) and no functional studies on PACAP have been done in olfactory bulb or SVZ.

Nature of PACAP's anti-apoptosis function

PACAP stimulates two groups of PACAP receptors: 1) Type I with a higher affinity for PACAP over VIP (PAC1 receptors) and 2) Type II with equal affinity for both PACAP and VIP, (VPAC1 and VPAC2 receptors). The PAC1 receptor has splice variants with slightly different binding affinities for PACAP and differential coupling to second messenger pathways. Depending on the type of

cell and receptor subtype involved, the second messenger pathways stimulated by these receptors generally govern the expression of transduction factors and channels, which determine cell fate. The known channels that are modulated by PACAP are the K^+, Ca^{2+}, Ca^{2+}-dependent K^+, Cl^-, nonselective cation, IP3-coupled, and/or TRP channels (May et al., 1998).

In normal circumstances, PACAP has been found to be neuroprotective in the central nervous system and sensory systems. The neuronal tissues expressing high levels of PACAP and PACAP receptors are thought to prevent apoptosis in conditions that normally induce apoptosis (Canonico et al., 1996). PACAP has been found to be of therapeutic use in recovery of function in PACAP deprived cultured cells and knockout mice (Przywara et al., 1998; Bhattacharya et al., 2004). Thus, PACAP may be promising as a novel therapeutic agent for regenerating lost neurons and for preventing apoptosis in neurodegenerative diseases such as Alzheimer's (Nonaka et al., 2002) and Parkinson's disease (Reglodi et al., 2004; Reglodi et al., 2006).

Nature of apoptosis and where PACAP comes in

In normal conditions, apoptosis is a delicate, balanced process found in all types of cells and occurs especially during development and immediately following injury to OB, nerve or epithelium. The characteristics include cell shrinkage, DNA fragmentation, increased activation of caspases in response to ongoing increase of pro-apoptotic factors, and then reversing of phosphatidylserine from cytoplasmic side to external surface of cell membrane. Cowan and Roskams (Cowan and Roskams, 2002) further discussed these

characteristics and the pro- and anti-apoptotic factors in the olfactory system. Figure 1.3 shows the known anti-apoptotic factors triggered by activation of PAC1 receptors and the pro-apoptotic factors that cross paths with these anti-apoptotic factors.

PACAP-induced factors activate kinases such as ERK, which lead to phosphorylation of c-fos, which binds to the c-jun from the pro-apoptosis route stimulated by JNK (Fig. 1.3). The c-fos/c-jun pair then binds to the activator protein-1 (AP-1) complexes. The c-fos/c-jun AP-1 complex builds up the expression of Bcl-2, which can inhibit the mitochondrial apoptotic pathway. However, without c-fos, the AP-1 complex is formed with the c-jun/c-jun pair for carrying out the Bax expression favoring apoptosis. When the expressions of genes are in favor of apoptosis, the mitochondrial cytochrome c is released to activate caspase-9 and so forth. (Be aware that other signals such as caspase-8 activated by the death receptors may be involved. These were reviewed by (Jin and El Deiry, 2005; Falluel-Morel et al., 2008).)

As one will see in Aim 3, Fig. 1.3 shows C2-ceramide, which will be used to test the high PACAP treated cell's susceptibility to cell death. The cell-permeable C2-ceramide mimics natural ceramides, which are involved in the control of the cell survival or death during central nervous system development and during stress. Natural ceramides are produced by sphingolipid catabolism or de novo synthesis as discussed in Falluel-Morel et al. (Falluel-Morel et al., 2008)

PACAP overexpression may be killing cells

As for many physiologically-beneficial proteins, too much of a good thing could be bad. Initial experiments on PACAP in our lab suggest that overexpression of the neuropeptide can be harmful to the organism because our cultured cells were dying [unpublished]. Freson et al. 2004 (Freson et al., 2004a) reported that a family with the genetic history of three copies of the PACAP gene yielding higher than normal PACAP concentrations in plasma, suffered from severe mental retardation. Lang et al. 2006 reported that overexpression of the human PAC1 receptor in the mouse nervous system reduced neuronal proliferation and massively increased neuronal apoptosis in the developing cortex. Furthermore, the ependymal cilia, which are important for directing the cerebrospinal fluid flow, are disrupted in these PAC1 overexpressing mice, leading to hydrocephalus.

In Studies of Bcl-2, a downstream factor for PACAP, reported that when a cell expresses more Bcl-2 than Bax, pro-apoptotic characters are reported. To have Bcl-2 act as an anti-apoptotic factor, the concentrations of both Bcl-2 and Bax need to be equal (Belizario et al., 2007; Hanson et al., 2008).

Olfactory bulbs as an ideal research model

Jaworski and Proctor (Jaworski and Proctor, 2000) examined the murine expression patterns of both PACAP and PAC1 expression from E12 to adult. By about P4, the mice started expressing a significantly higher level of PAC1 receptors in the olfactory bulb compared to the cerebral cortex. In the mice with overexpression of PAC1 receptors, which is parallel to prolonged elevation of

PACAP, the picture published showed what appears to be either a reduce or absence of olfactory bulb (Lang et al., 2006b) (Fig. A.1). This suggests a possible role of PACAP initiating necessary apoptotic effects on the PAC1 enriched region of olfactory bulb.

Even though neurodegenerative diseases are of prime importance in the cerebral cortex, the olfactory glomerulus may be considered as a viable research model for the cortex as a whole. In addition to being anatomically easy to discern from the remainder of the cortex, many of the olfactory bulb's principles are believed to be applicable to other parts of the brain (Shepherd and Charpak, 2008). Furthermore, PACAP is proven to be ubiquitous in the central nervous system (Arimura, 1998). Thus, the olfactory bulb with its enriching PAC1 receptor concentration is a favorable model to examine the role of PACAP in both pro-apoptotic and anti-apoptotic functions in the CNS.

Since our lab studied PACAP in the olfactory placode-derived cell lines OP6 and OP27 (Illing et al., 2002) for years, the parameters of timing and concentrations will be established on the cell lines first in part to avoid the unnecessary number of mice used for primary cultures. Furthermore, the cell lines are more stable and pure than the primary cultured cells, providing the confidence that the apoptosis not due to non-PACAP causes. Once the details have been worked out in cell lines, the experiments will be done on primary cultures of adult OE as well as the more PACAP receptor enriched OB cultures. It is possible that the parameters between the lines and the primary cultures will

be different, but they will be good comparisons and beneficial to previous works done on OP6 and OP27.

Specific antagonists for PACAP receptors

We will use a number of antagonists to determine the effects of elevated PACAP. M65, a relatively specific antagonist for PAC1 receptors, was made through the deleting portions of a specific PAC1 receptor agonist named maxadilian. The agonist maxadilian was isolated from sand fly salivary gland extracts in 1991. Maxadilian specifically binds to mammalian PAC1 even though maxadilian has no significant amino acid sequence in common with PACAP. Apparently, the deleted peptide of maxadilian, known as M65, is proven as a specific antagonist of PAC1 (Reed et al., 2002; Uchida et al., 1998).

PG 97-269 came into the scene as a new highly selective VIP1 (currently known as VPAC1) receptor antagonist in 1997 and was proven up to 300 nM concentration to not affect the functions of VIP2 (currently known as VPAC2) and PAC1 receptors (Gourlet et al., 1997). PG99-465 is an antagonist for VPAC2 receptors and it was a modified VIP peptide already used by various labs (Reed et al., 2002). GDP beta-S is a non-phosphorylatable analogue of GDP that blocks any of the G-protein receptors involving PAC1 and VPAC1/2's activation through the block of the G protein activation.

Significance

PACAP is a promising candidate as a therapeutic drug for clinical treatment against neurodegenerative diseases such as Alzheimer's (Nonaka et

al., 2002) and Parkinson's (Reglodi et al., 2004; Reglodi et al., 2006). Over expression of PACAP, however, is suspected to be potentially harmful. The potential use of PACAP as a therapeutic agent makes it extremely important to determine the effective therapeutic dose as well as any potential harmful effects of over-dosing. No one has looked at how PACAP over expression affects its function as an anti-apoptotic factor in the CNS. We propose to look at various aspects of the effects of PACAP over expression in the olfactory epithelia and olfactory bulbs, including the receptor subtypes and anti-apoptotic and pro-apoptotic factors employed at different doses of PACAP expression. A look at exactly how high doses of PACAP can kill or otherwise harm cells will be highly beneficial in fine-tuning the therapeutic use of PACAP in diseases of both the CNS and other tissues, such as elimination of unfavorable side effects.

D1: Research Design

Specific Aim 1: Determine whether PACAP-induced apoptosis is mediated by the PAC-1, VPAC1, and/or VPAC2 receptors.

PACAP activates PAC-1, VPAC1, and VPAC2 receptors, but the differences in affinity of PACAP for each type of receptor and the levels of other signaling proteins available lead to differences in potency for PACAP (Lutz et al., 2006). While it is known that PACAP's affinity for each type of receptor varies, it is not known whether PACAP's effects are different at higher doses. It is however known that in mice, PAC-1 over expression reduced their overall growth (Lang et al., 2006b). In the following Aim 1, the effects of elevated PACAP on PAC1 and other receptors will be investigated.

Aim1A: What concentration of PACAP is required to induce apoptosis?

We will apply PACAP to cultures of OP6/OP27 cell lines in increasing concentrations from 10^{-8}M to 10^{-3}M (10^{-7}M is the estimated normal concentration) for up to 120 minutes. This will give cells a long enough time to produce the anti-apoptotic mRNAs such as c-fos and Bcl-2 (Falluel-Morel et al., 2004; Aubert et al., 2006). The percentage of cells showing activated caspases in each of the PACAP concentration treatments will be sampled from the cultures and measured at 30, 60, 90, and 120 minutes using the live cell labeling of activated caspases assay (see detailed Methods). To support the confirmation of apoptosis onset leading to cell death, the propidium iodide (PI) dye assay, which measures dead cells, will be applied to a subset of samples at 30, 60, 90, and 120 minutes. The controls will be the cultures getting vehicle instead of PACAP treatments. The control levels will be compared to the treatments and any significant differences will be determined with ANOVA and post-hoc testing. After the parameters have been optimized using the OP6/27 cells, this experiment will be repeated in OE and OB primary cell cultures prepared from young adult mice.

Predicted outcomes: Elevated PACAP will induce apoptosis in the cell lines. The percentage of the cells showing activated caspases may start increasing starting at 10^{-6}M of PACAP and become significant at 10^{-5}M or 10^{-4}M. Higher concentrations of PACAP will show activated caspases at earlier time points than lower concentrations. The percentage of cells at the late apoptosis stage will increase after the increase in the activated caspase. The PACAP concentration

that induces apoptosis in 50% of the cells (EC_{50}) will be used as the minimum PACAP concentration in Aims 1B, 2 and 3.

Potential Problems: If little to no apoptosis is observed, the cells likely need longer than 120 minutes for apoptotic mechanisms to be triggered. In this case, the cells will be incubated in PACAP treatments and measured at four or five time intervals for up to 8 or 24 hours and compared with controls.

Aim1B: Which receptor(s) are involved in the apoptotic process?

After completing Aim 1A to find the PACAP EC_{50} concentration needed to trigger apoptosis in the OP6/OP27 cell lines, the receptor(s) involved will be identified by testing whether specific antagonists of PAC-1, VPAC1, VPAC2, or other G-protein receptors can block the apoptotic effects of high PACAP. We will use the EC_{50} point of the PACAP concentration found in Aim 1A as a minimum of PACAP concentration required to kill cells to see if the receptor antagonists make cell overall survival higher or lower. Various G-protein receptor antagonists will be added to OP6/OP27 cell cultures in the following tests:

Test 1: Block PAC-1 with 100 uM M65 (Cunha-Reis et al., 2005; Dickson et al., 2006; Girard et al., 2007; Girard et al., 2008; Uchida et al., 1998)

Test 2: Block VPAC1 with 100 uM PG97-269 (Cunha-Reis et al., 2005; Dickson et al., 2006; Fizanne et al., 2004; Gourlet et al., 1997; Grant et al., 2006)

Test 3: Block VPAC2 with 100 uM PG99-465 (Cunha-Reis et al., 2005; Cutler et al., 2003; Grant et al., 2006; Itri and Colwell, 2003; Reed et al., 2002)

Test 4: Block VPAC1 and VPAC2

Test 5: Block PAC-1 and VPAC1 and VPAC2

Test 6: Block all G-protein receptors with 300uM (in pipette) GDP-beta-S-block (Gerevich et al., 2007)

The level of apoptosis (% caspase activated cells/total cells) in all tests will be compared to cultures that received PACAP and vehicle. Higher or lower PACAP concentrations than Aim1A's EC_{50} amount required to trigger apoptosis may be required to confirm the improvement or worsening of the cells. After the parameters have been optimized using the OP6/27 cells, this experiment will be repeated in OE and OB primary cell cultures prepared from young adult mice.

Predicted outcome: PAC-1 will be the key receptor and the blockage of PAC-1 [24] as shown in Test 1 will significantly reduce the apoptotic effects of elevated PACAP. VPAC1/2 blockage in Test 2, 3, and 4 will likely yield a partial reduction of PACAP-induced apoptosis and is expected to be minor in comparison to PAC-1 receptor blockade. If PACAP peptides act only on the G-protein coupled receptors, then an observation of incomplete apoptotic blockage in Test 5 and complete apoptotic blockage in Test 6 will indirectly indicate that non-PACAP specific receptors are also stimulated by high PACAP concentrations.

Potential Problems: The potential problem will be there may be insufficient concentrations of the specific receptors types in OP6/27 cells for observable EC_{50} apoptotic results. Overexpression of one or another receptor types may be required to obtain significant levels of apoptosis and rescue.

Aim 2: Determine whether there is a dose-dependent shift in PACAP-induced expression of anti- and pro-apoptotic factors.

Under normal circumstances, PACAP stimulates the expression of what are determined as anti-apoptotic factors (Fig. 1.3). The question is whether there is a shift in these factors's expression in a high PACAP environment toward apoptosis instead of anti-apoptosis. There are no published data looking at the quantification of the key anti-apoptosis or pro-apoptosis factors induced by abnormally high PACAP concentrations over 10^{-6}M (Falluel-Morel et al., 2004). Aubert et al. (Aubert et al., 2006) however showed indirect data that at normal PACAP concentrations, anti-apoptosis factors increased then decreased over 120 minutes. The following experiments will hopefully give clues on how the mechanisms may be working

Aim2A: Do anti-apoptotic factors decrease or increase in abnormally high PACAP situations?

Using RT-PCR and Western blotting, the quantity of anti-apoptotic factors c-fos and Bcl-2 will be measured at 30, 60, 90, and 120 minutes (Falluel-Morel et al., 2004; Aubert et al., 2006) after application of the PACAP concentration found to induce apoptosis in Aim 1. We will also measure the ratio of c-fos to actin (using Western blotting) as an indirect measure of the transportation and usage of c-fos protein. The control levels will be compared to the treatments and their significant differences will be checked with ANOVA test. Caspase-3 will be measured as a positive control to ensure apoptosis is indeed occurring. Both OP6/OP27 and adult mouse OE and OB primary cultures will be used.

Predicted outcome: The high PACAP exposure will make the anti-apoptosis factors's mRNA expression increase then decrease due to the likelihood of

PACAP receptors desensitizing in response to high PACAP concentrations as shown in previous experiments (Niewiadomski et al., 2002; Taupenot et al., 1999).

Potential Problems: If it takes longer than 120 minutes to get the results in Aim 1A, the time required to complete Aim 1A will be applied here. If we instead find a continuous overexpression of any anti-apoptotic factors compared to controls, then we will have to consider whether the balance rather than the absolute amounts of the anti-apoptotic versus pro-apoptotic pathways has shifted.

Aim2B: Do the pro-apoptotic factors increase in abnormally high PACAP environment?

Using RT-PCR and Western blotting, the quantities of pro-apoptotic factors c-jun and Bax will be measured at 30, 60, 90, and 120 minutes (Falluel-Morel et al., 2004; Aubert et al., 2006) after application of the PACAP concentration found to induce apoptosis in Aim 1. We will also measure the ratio of phophorylated c-jun to normal c-jun (using Western blotting) as an indirect measure of the transportation and usage of c-jun protein. The control levels will be compared to the treatments and their significant differences will be checked with ANOVA test. Caspase-3 will be measured as a positive control to ensure apoptosis is indeed occurring. Both OP6/OP27 and adult mouse OE and OB primary cultures will be used.

Predicted outcome: After about 90 or so minutes in the presence of elevated PACAP, the pro-apoptosis factor expression will increase.

Potential Problems: If elevated PACAP is instead able to keep the pro-apoptotic factors's expression from increasing, this may mean the pro-apoptotic factors are interfering with the PACAP-induced anti-apoptotic factors. Thus, these PACAP-induced factors are not part of the apoptosis process. To ensure apoptosis is nonetheless still occurring in the elevated PACAP treated cells, the caspase expression will be monitored as a positive control.

Aim 3: Determine whether high PACAP concentrations could prevent or make the cells more vulnerable to external apoptotic stimulation.

So far, we were looking at high PACAP concentrations on healthy cells which are different from the cells in the neurodegenerative diseases people want to treat with PACAP. Here, we will look at whether the high PACAP concentrations could prevent or make the cells more vulnerable to external apoptotic stimulation. The experiments involve three different timings of high PACAP and C2-ceramide applications to include all of the possible systems we may find in the neurodegenerative diseases: 1) Both high PACAP and C2-ceramide added at same time; 2) High PACAP first then C2-ceramide; 3) C2-ceramide first then high PACAP.

C2-ceramide is an apoptotic stimulating factor that interferes with the PACAP pathway and was previously used to better understand PACAP's anti-apoptotic mechanisms (Falluel-Morel et al., 2008; Aubert et al., 2006).

Aim3A: In ceramide treated cells, do high concentrations of PACAP protect against or promote apoptosis?

The high PACAP concentration found in Aim 1A to trigger apoptosis and 30 µM C2-ceramide will be applied to the OP6/OP27 cells at the same time. The early apoptosis characteristics will be determined by taking samples from the cultures at 30, 60, 90, and 120 minutes (Falluel-Morel et al., 2004; Aubert et al., 2006) and measured using the live cell labeling of activated caspases assay (see Methods). To support the confirmation of apoptosis onset leading to cell's death, the propidium iodide (PI) dye assay, which measures dead cells, will be applied to a subset of samples at 30, 60, 90, and 120 minutes. The controls will be the cultures getting vehicle, only PACAP, or only C2-ceramide treatments instead of both PACAP and C2-ceramide treatments. The control levels will be compared to the treatments and their significant differences will be checked with Student's t-test (Fig. A.2.) After the parameters have been optimized using the OP6/27 cells, this experiment will be repeated in OE and OB primary cell cultures prepared from young adult mice.

Predicted outcome: We predict that in the presence of both elevated PACAP and C2-ceramide, the cells will show a delay in shifting toward apoptosis compared to cells treated with ceramide alone. A potential mechanism for this observation is that elevated PACAP's apoptotic-like effects will possibly be reduced with probably more pro-apoptotic factors to act upon.

Potential Problems: Once again, if the time required for results to occur is found to be longer in Aim 1, the time course outlined above will be adjusted appropriately. The other possible problem will be that 30 µM of C2-ceramide concentration may be insufficient in this experiment because it was the

concentration used by Aubert 2006 (Aubert et al., 2006) to shift the balance of c-fos and c-jun expression in the presence of normal PACAP concentrations in cerebellar granule neurons. More C2-ceramide may be needed to offset the abnormally high PACAP levels in our proposed experiments. However, it is possible that higher C2-ceramide concentrations may not increase pro-apoptosis factor expression and we will perform a dose-response for C2-ceramide alone if necessary.

Aim3B: Will the pre-incubated application of high PACAP fail to prevent the apoptotic influences of the C2-ceramide?

OP6/OP27 cells will be preincubated in the high PACAP concentration required to trigger apoptosis before the addition of apoptosis stimulating C2-ceramide at 20, 30, 40, 50, and 60 minutes after PACAP application. The anti-apoptosis resistance performance of high PACAP on the C2-ceramide at 30, 60, 90, and 120 minutes after the addition of C2-ceramide will be measured. The data of the samples will be collected using the live cell labeling of activated caspases assay. The results from Aim 3B will be compared to the results from Aim 3A. To support the confirmation of apoptosis onset leading to cell death, the propidium iodide (PI) dye assay, which measures dead cells, will be applied to a subset of samples at 30, 60, 90, and 120 minutes. The controls will be the cultures receiving only PACAP and C2-ceramide treatments. The control levels will be compared to the treatments and their significant differences will be checked with Student's t-test (Fig. A.2). After the parameters have been

optimized using the OP6/27 cells, this experiment will be repeated in OE and OB primary cell cultures prepared from young adult mice.

The entire experiment in the paragraph above will be repeated in the reverse order of PACAP and C2-ceramide. The apoptosis stimulating C2-ceramide will be preincubated in the cell cultures then high PACAP concentration required to trigger apoptosis will be added.

Predicted outcome: The high PACAP treated cells will be given the time required to start the apoptotic process. By the time C2-ceramide is added, the apoptotic process is already in full force and we predict that ceramide will accelerate the apoptotic process. Other potential outcomes are that ceramide has no effect on the rate of PACAP-induced apoptosis or that ceramide actually slows PACAP apoptosis by an unknown mechanism. In the case of C2-ceramide pre-incubation, the late addition of PACAP is predicted to slow down the apoptotic process, which may be useful information for future investigations on treating neurodegenerative diseases.

Potential Problems: The timing of PACAP preincubation and addition of C2-ceramide may need some adjusting such as addition of C2-ceramide at 120 minutes instead of 30 to 60 minutes. The incubation time may need to be even longer if the time required to complete Aim1 is longer. If the late addition of C2-ceramide is able to “save” the cells through the interfering of late pro-apoptotic factor to PACAP-induced factors, this can suggest that when overexpressing the PACAP, having the overexposure of pro-apoptotic factor expression will help block the PACAP’s apoptosis side effects.

D2: Methods

Cell Lines: OP6 and OP27 are the olfactory system's cell lines harvested by Dr. Roskams from E18 mice embryos. Both were characterized to have different responses to PACAP treatments. For start, both have different ratios of PAC1 receptors. These cell lines are necessary for some preliminary work because they are more stable than primary cell cultures. For the passaging, maintenance, and differentiation of these cells, we will follow the methods published by Illing et al. (Illing et al., 2002).

Animals: PAC-1 receptors are present on OB GABAergic interneurons. Either the GAD65-GFP mice from Dr. Dudek's lab, which have high quantity of greenish tagged GABAergic interneurons in the OBs (Lopez-Bendito et al., 2004) or the wild type C57/B16 strain mice injected with a live cell marker alamarBlue® (Invitrogen, Eugene, OR) in the SVZ will be used to make olfactory bulb primary cell cultures and/or olfactory bulb slices to confirm the results collected from OP6/OP27 cell lines. These cell markers will discern the primary culture mixture of olfactory and non-olfactory cells. An estimated minimum of twelve mice will be used at sets of two in each primary culture. The animals are housed in the 24˚C departmental animal facility on a 12 hr light/dark cycle and provided with unlimited food and water.

Tracer injection: If the wild type C57/B16 strain mice have to be used, the live cell marker will be stereotaxic injected into mice pups between one to two days old as described (De Marchis et al., 2001). Briefly, the pups were anesthetized

by hypothermia, heads immobilized on a chilled (4 ˚C) stereotaxic apparatus during surgery. The skin is peeled to expose the skull and small holes will be drilled for injection access. A total of 100 nl of alamarBlue® (Invitrogen, Eugene, OR) will be injected with a glass micropipette at stereotaxic coordinates of 0 mm bregma, 0.8 mm lateral to sagittal sinus, and 1.5 mm deep. After injection, the skin will be sutured and the pups quickly warmed under a heat lamp, then returned to their mothers. In about 30 days, the injected pups will have alamarBlue-labeled cells integrated into the OB (De Marchis et al., 2007).

Primary cultures: Young adult mice between 21 to 35 days old will be anesthetized (50:50 of ketamine and xyleme at 65 mg/kg) then decapitated. After quick removal of skin and lower jaw, the skull is immediately placed in cold Ringer's solution bath. The OEs and OBs are then are separately removed and kept in cold Ringer's solution bath until the next step. For the individual cell cultures to last over 8 hours, they are prepared using the published procedure (Cunningham et al., 1999). For the cultures to be used within six hours, the OEs and OBs will be chopped up with a sterile razor and incubated in treatments at 37˚C.

Quantitative RT-PCR: The cultured cells will be washed twice with PBS at 37˚C and resuspended in 0.1 M PBS at 4˚C. These cells are then pelleted by centrifugation (350 x g; 4˚C; 10 minutes). The total RNA will be isolated using Trizol (GIBCO BRL) followed by polyadenylation selection using a cellulose oligo(dT) matrix (QuickPrep® Mirco mRNA purification kit, Amersham Pharmacia

Biotech). An aliquot of each will be incubated in RNAse to use as a negative control. First-strand cDNA synthesis will be carried out with 40 ng of mRNA in a random hexamer-primed 20-ul reverse transcriptase (RT) reaction using SuperScriptTM II RNase H- RT and reagents (GIBCO BRL), incubated at 42˚C for 50 minutes. A second control reaction omitting the reverse transcriptase will be included to confirm absence of genomic contamination. A 2-ul sample of the first stand cDNA will be used as a template for each 50 µl PCR, and will be amplified using Platinum® Taq DNA polymerase (GIBCO BRL). Primers for detection of transcripts will be the following: Bcl-2 forward primer, 5'-CTGGCATCTTCTCCTTCCAGC-3'; Bcl-2 reverse primer, 5'-ACCTACCCAGCCTCCGTTATC-3'; Bax forward primer, 5'-TCGCTCTGTGGATGACTGAGTAC-3'; Bax reverse primer, 5'-GGGCCATATAGTTCCACAAAGG-3'; c-jun forward primer, 5'-TCCACGGCCAACATGCT-3'; c-jun reverse primer, 5'-GGTGACAATTGCACCAAGTACTG-3'; c-fos forward primer, 5'-GATGTTCTCGGGTTTCAACGCG-3'; c-fos reverse primer, 5'-ACGTCGGTAGAATAAGGAAAGGG-3'; beta-actin forward primer, 5'-TTCTTTGCAGCTCCT TCGTTGCCG-3'; beta-actin reverse primer, 5'-TGGATGGCTACGTACATGGCTGGG-3'

The initial PCR experiment will use primer pairs (100 µM) with a 35 cycle profile performed as follows: 95˚C denaturation (5 min), start 94˚C denaturation (30 sec), 55˚C annealing (1 min) and 72˚C extension (3 min) and 4 ˚C hold (Perkin-Elmer PCR thermal cycler). PCR products will be separated and

visualized using ethidium bromide-stained agarose gels (1%), and will be viewed under UV transillumination followed by densitometric scanning. Values are corrected for differences in fragment size because equal numbers of the larger cDNA products will stain more strongly in proportion to the size difference.

To verify PCR products, resulting cDNA will be excised from the gel and purified using the GlassMAX DNA Isolation Matrix System (GIBCO BRL) and then sequenced at the University Sequencing Center.

Quantitative Western blotting: The solubilized proteins will be prepared from cell cultures after treatment. First, they will be homogenized in ice-cold Buffer A (50mM Tris-HCL, 8 mM MgCl2, 5 mM EDTA, 10 µg/ml leupeptin, 5 µg/ml pepstatin, 5 µg/ml aprotinin, and 1 mM phenylmethyl sulfonylfluoride pH 7.4). This homogenate will be centrifuged at 49,000 x g for 20 minutes at 4˚C. The intermediate pellet will be resuspended in Buffer A and centrifuged again for 20 minutes. The final pellet will be resuspended in Buffer B (50 mM Tris-HCl, 120 mM NaCl, 5 mM KCl, 5 mM MgCl2, 1.5 mM CaCl2, 1 mM EDTA, 10 uM pargylin-HCl, 0.1% ascorbic acid, 0.001% bovine serum albumin pH 7.4) at a concentration of 2 mg/ml. They will be stored at –80˚C until use with trace amounts of bromphenyl blue loaded on 4–15% sodium dodecyl sulfate polyacrylamide gels along with molecular weight standards. The gels will be electrophoresed at 80–120V until the tracking dye reaches the bottom. The proteins in the gels then will be transferred to nitrocellulose. They then will undergo antibody procedures of first being blocked in block buffer (10mM Tris-HCl, 154 mM NaCl, 0.02% thimerosal, 5% (w/v) non-fat dry milk) for 30 minutes

at room temperature. The membrane is then incubated in the chosen primary antibody washing buffer (10mM Tris-HCl, 154 mM NaCl, 0.05% Tween-20) with 5% non-fat milk added for two hours at room temperature, then washed three times in washing buffer without non-fat dry milk. These primary antibodies will be against c-fos, actin, phosphor-c-jun, Bcl-2 (Santa Cruz Biotechnology, Santa Cruz, CA, USA), and c-jun (Oncogene, Fontenay-sous-Bois, France). Finally, the secondary antibody will be applied in washing buffer with 5% non-fat milk for an hour and washed three times in washing buffer without non-fat dry milk. The blot bands then are developed with 4-choloronapthol, exposed to film, then quantified with a densitometer. This data will be normalized to the amount of protein in the loaded samples.

Measurements of apoptosis onset: The cultured cells will be washed twice with PBS at 37˚C and resuspended in 0.1 M PBS at 4˚C. These cells are then harvested by centrifugation (350 x g; 4˚C; 10 minutes) and treated with the fluorometric caspase assay systems (Promega and R&D Systems). In brief, the pellet is resuspended in 10 ul hypotonic cell lysis buffer and then incubated with 10 ul of the appropriate caspase substrate at 30˚C for one hour. The substrates for the different caspases will be, respectively: Ac-YVADAMC for caspase 1, Ac-VDVAD-AFC for caspase 2, Ac-DEVD-AMC for caspase-3, Ac-VEID-AFC for caspase-6, AcIETD-pNA for caspase-8, and Ac-LEHD-AFC for caspase-9. Fluorescence intensity will be measured with a microplate reader. The specificity of the assay will be verified by adding 2.5 mM caspase 1 inhibitor Ac-YVAD-CHO or the caspase-3 inhibitor Ac-DEVD-CHO to the incubation mixture.

Reference List

1. **Arimura A**. Perspectives on pituitary adenylate cyclase activating polypeptide (PACAP) in the neuroendocrine, endocrine, and nervous systems. *Jpn J Physiol* 48: 301–331, 1998.

2. **Aubert N, Falluel-Morel A, Vaudry D, Xifro X, Rodriguez-Alvarez J, Fisch C, de Jouffrey S, Lebigot JF, Fournier A, Vaudry H, Gonzalez BJ**. PACAP and C2-ceramide generate different AP-1 complexes through a MAP-kinase-dependent pathway: involvement of c-Fos in PACAP-induced Bcl-2 expression. *J Neurochem* 99: 1237–1250, 2006.

3. **Basille-Dugay M, Vaudry H, Fournier A, Gonzalez B, Vaudry D**. Activation of PAC1 receptors in rat cerebellar granule cells stimulates both calcium mobilization from intracellular stores and calcium influx through N-type calcium channels. *Front Endocrinol (Lausanne)* 4: 56, 2013.

4. **Belizario JE, Alves J, Occhiucci JM, Garay-Malpartida M, Sesso A**. A mechanistic view of mitochondrial death decision pores. *Braz J Med Biol Res* 40: 1011–1024, 2007.

5. **Bhattacharya A, Lakhman SS, Singh S**. Modulation of L-type calcium channels in Drosophila via a pituitary adenylyl cyclase-activating polypeptide (PACAP)-mediated pathway. *J Biol Chem* 279: 37291–37297, 2004.

6. **Canonico PL, Copani A, D'Agata V, Musco S, Petralia S, Travali S, Stivala F, Cavallaro S**. Activation of pituitary adenylate cyclase-activating polypeptide receptors prevents apoptotic cell death in cultured cerebellar granule cells. *Ann NY Acad Sci* 805: 470–472, 1996.

7. **Cowan CM, Roskams AJ**. Apoptosis in the mature and developing olfactory neuroepithelium. *Microsc Res Tech* 58: 204–215, 2002.

8. **Cunha-Reis D, Ribeiro JA, Sebastiao AM**. VIP enhances synaptic transmission to hippocampal CA1 pyramidal cells through activation of both VPAC1 and VPAC2 receptors. *Brain Res* 1049: 52–60, 2005.

9. **Cunningham AM, Manis PB, Reed RR, Ronnett GV**. Olfactory receptor neurons exist as distinct subclasses of immature and mature cells in primary culture. *Neuroscience* 93: 1301–1312, 1999.

10. **Cutler DJ, Haraura M, Reed HE, Shen S, Sheward WJ, Morrison CF, Marston HM, Harmar AJ, Piggins HD**. The mouse VPAC2 receptor confers suprachiasmatic nuclei cellular rhythmicity and responsiveness to vasoactive intestinal polypeptide in vitro. *Eur J Neurosci* 17: 197–204, 2003.

11. **De Marchis S, Bovetti S, Carletti B, Hsieh YC, Garzotto D, Peretto P, Fasolo A, Puche AC, Rossi F**. Generation of distinct types of periglomerular olfactory bulb interneurons during development and in adult mice: implication for intrinsic properties of the subventricular zone progenitor population. *J Neurosci* 27: 657–664, 2007.

12. **De Marchis S, Fasolo A, Shipley M, Puche A**. Unique neuronal tracers show migration and differentiation of SVZ progenitors in organotypic slices. *J Neurobiol* 49: 326–338, 2001.

13. **Delgado M, Abad C, Martinez C, Juarranz MG, Leceta J, Ganea D, Gomariz RP**. PACAP in immunity and inflammation. *Ann NY Acad Sci* 992: 141–157, 2003.

14. **Di MM, Peeters K, Loyen S, Thys C, Waelkens E, Overbergh L, Hoylaerts M, Van GC, Freson K**. Pituitary adenylate cyclase-activating polypeptide (PACAP) impairs the regulation of apoptosis in megakaryocytes by activating NF-kappaB: a proteomic study. *Mol Cell Proteomics* 11: M111, 2012.

15. **Dickson L, Aramori I, McCulloch J, Sharkey J, Finlayson K**. A systematic comparison of intracellular cyclic AMP and calcium signalling highlights complexities in human VPAC/PAC receptor pharmacology. *Neuropharmacology* 51: 1086–1098, 2006.

16. **Dziema H, Obrietan K**. PACAP potentiates L-type calcium channel conductance in suprachiasmatic nucleus neurons by activating the MAPK pathway. *J Neurophysiol* 88: 1374–1386, 2002.

17. **Falluel-Morel A, Aubert N, Vaudry D, Basille M, Fontaine M, Fournier A, Vaudry H, Gonzalez BJ**. Opposite regulation of the mitochondrial apoptotic pathway by C2-ceramide and PACAP through a MAP-kinase-dependent mechanism in cerebellar granule cells. *J Neurochem* 91: 1231–1243, 2004.

18. **Falluel-Morel A, Aubert N, Vaudry D, Desfeux A, Allais A, Burel D, Basille M, Vaudry H, Laudenbach V, Gonzalez BJ**. Interactions of PACAP and ceramides in the control of granule cell apoptosis during cerebellar development. *J Mol Neurosci* 2008.

19. **Fizanne L, Sigaudo-Roussel D, Saumet JL, Fromy B**. Evidence for the involvement of VPAC1 and VPAC2 receptors in pressure-induced vasodilatation in rodents. *J Physiol* 554: 519–528, 2004.

20. **Freson K, Hashimoto H, Thys C, Wittevrongel C, Danloy S, Morita Y, Shintani N, Tomiyama Y, Vermylen J, Hoylaerts MF, Baba A, Van Geet C**. The pituitary adenylate cyclase-activating polypeptide is a physiological inhibitor of platelet activation. *J Clin Invest* 113: 905–912, 2004a.

21. **Freson K, Hashimoto H, Thys C, Wittevrongel C, Danloy S, Morita Y, Shintani N, Tomiyama Y, Vermylen J, Hoylaerts MF, Baba A, Van GC**. The pituitary adenylate cyclase-activating polypeptide is a physiological inhibitor of platelet activation. *J Clin Invest* 113: 905–912, 2004b.

22. **Gerevich Z, Zadori Z, Muller C, Wirkner K, Schroder W, Rubini P, Illes P**. Metabotropic P2Y receptors inhibit P2X3 receptor-channels via G protein-dependent facilitation of their desensitization. *Br J Pharmacol* 151: 226–236, 2007.

23. **Girard BM, Wolf-Johnston A, Braas KM, Birder LA, May V, Vizzard MA**. PACAP-mediated ATP release from rat urothelium and regulation of PACAP/VIP and receptor mRNA in micturition pathways after cyclophosphamide (CYP)-induced cystitis. *J Mol Neurosci* 36: 310–320, 2008.

24. **Girard BM, Young BA, Buttolph TR, White SL, Parsons RL**. Regulation of neuronal pituitary adenylate cyclase-activating polypeptide expression during culture of guinea-pig cardiac ganglia. *Neuroscience* 146: 584–593, 2007.

25. **Gourlet P, De Neef P, Cnudde J, Waelbroeck M, Robberecht P**. In vitro properties of a high affinity selective antagonist of the VIP1 receptor. *Peptides* 18: 1555–1560, 1997.

26. **Grant S, Lutz EM, McPhaden AR, Wadsworth RM**. Location and function of VPAC1, VPAC2 and NPR-C receptors in VIP-induced vasodilation of porcine basilar arteries. *J Cereb Blood Flow Metab* 26: 58–67, 2006.

27. **Han P, Lucero MT**. Pituitary adenylate cyclase activating polypeptide reduces A-type K+ currents and caspase activity in cultured adult mouse olfactory neurons. *Neuroscience* 134: 745–756, 2005.

28. **Hansel DE, May V, Eipper BA, Ronnett GV**. Pituitary adenylyl cyclase-activating peptides and alpha-amidation in olfactory neurogenesis and neuronal survival in vitro. *J Neurosci* 21: 4625–4636, 2001a.

29. **Hansel DE, May V, Eipper BA, Ronnett GV**. Pituitary adenylyl cyclase-activating peptides and alpha-amidation in olfactory neurogenesis and neuronal survival in vitro. *J Neurosci* 21: 4625–4636, 2001b.

30. **Hanson CJ, Bootman MD, Distelhorst CW, Maraldi T, Roderick HL**. The cellular concentration of Bcl-2 determines its pro- or anti-apoptotic effect. *Cell Calcium* 44: 243–258, 2008.

31. **Hegg CC, Au E, Roskams AJ, Lucero MT**. PACAP is present in the olfactory system and evokes calcium transients in olfactory receptor neurons. *J Neurophysiol* 90: 2711–2719, 2003.

32. **Illing N, Boolay S, Siwoski JS, Casper D, Lucero MT, Roskams AJ**. Conditionally immortalized clonal cell lines from the mouse olfactory placode differentiate into olfactory receptor neurons. *Mol Cell Neurosci* 20: 225–243, 2002.

33. **Itri J, Colwell CS**. Regulation of inhibitory synaptic transmission by vasoactive intestinal peptide (VIP) in the mouse suprachiasmatic nucleus. *J Neurophysiol* 90: 1589–1597, 2003.

34. **Jaworski DM, Proctor MD**. Developmental regulation of pituitary adenylate cyclase-activating polypeptide and PAC(1) receptor mRNA expression in the rat central nervous system. *Brain Res Dev Brain Res* 120: 27–39, 2000.

35. **Jin Z, El Deiry WS**. Overview of cell death signaling pathways. *Cancer Biol Ther* 4: 139–163, 2005.

36. **Kopp MD, Meissl H, Dehghani F, Korf HW**. The pituitary adenylate cyclase-activating polypeptide modulates glutamatergic calcium signalling: investigations on rat suprachiasmatic nucleus neurons. *J Neurochem* 79: 161–171, 2001.

37. **Kopp MD, Schomerus C, Dehghani F, Korf HW, Meissl H**. Pituitary adenylate cyclase-activating polypeptide and melatonin in the suprachiasmatic nucleus: effects on the calcium signal transduction cascade. *J Neurosci* 19: 206–219, 1999.

38. **Lang B, Song B, Davidson W, MacKenzie A, Smith N, McCaig CD, Harmar AJ, Shen S**. Expression of the human PAC1 receptor leads to dose-dependent hydrocephalus-related abnormalities in mice. *J Clin Invest* 116: 1924–1934, 2006a.

39. **Lang B, Song B, Davidson W, MacKenzie A, Smith N, McCaig CD, Harmar AJ, Shen S**. Expression of the human PAC1 receptor leads to dose-dependent hydrocephalus-related abnormalities in mice. *J Clin Invest* 116: 1924–1934, 2006b.

40. **Lopez-Bendito G, Sturgess K, Erdelyi F, Szabo G, Molnar Z, Paulsen O**. Preferential origin and layer destination of GAD65-GFP cortical interneurons. *Cereb Cortex* 14: 1122–1133, 2004.

41. **Lutz EM, Ronaldson E, Shaw P, Johnson MS, Holland PJ, Mitchell R**. Characterization of novel splice variants of the PAC1 receptor in human neuroblastoma cells: consequences for signaling by VIP and PACAP. *Mol Cell Neurosci* 31: 193–209, 2006.

42. **Masmoudi O, Gandolfo P, Leprince J, Vaudry D, Fournier A, Patte-Mensah C, Vaudry H, Tonon MC**. Pituitary adenylate cyclase-activating

polypeptide (PACAP) stimulates endozepine release from cultured rat astrocytes via a PKA-dependent mechanism. *FASEB J* 17: 17–27, 2003.

43. **May V, Beaudet MM, Parsons RL, Hardwick JC, Gauthier EA, Durda JP, Braas KM**. Mechanisms of pituitary adenylate cyclase activating polypeptide (PACAP)-induced depolarization of sympathetic superior cervical ganglion (SCG) neurons. *Ann NY Acad Sci* 865: 164–175, 1998.

44. **Miyata A, Arimura A, Dahl RR, Minamino N, Uehara A, Jiang L, Culler MD, Coy DH**. Isolation of a novel 38 residue-hypothalamic polypeptide which stimulates adenylate cyclase in pituitary cells. *Biochem Biophys Res Commun* 164: 567–574, 1989.

45. **Mulder H, Jongsma H, Zhang Y, Gebre-Medhin S, Sundler F, Danielsen N**. Pituitary adenylate cyclase-activating polypeptide and islet amyloid polypeptide in primary sensory neurons: functional implications from plasticity in expression on nerve injury and inflammation. *Mol Neurobiol* 19: 229–253, 1999.

46. **Niewiadomski P, Nowak JZ, Sedkowska P, Zawilska JB**. Rapid desensitization of receptors for pituitary adenylate cyclase-activating polypeptide (PACAP) in chick cerebral cortex. *Pol J Pharmacol* 54: 717–721, 2002.

47. **Nonaka N, Banks WA, Mizushima H, Shioda S, Morley JE**. Regional differences in PACAP transport across the blood-brain barrier in mice: a possible influence of strain, amyloid beta protein, and age. *Peptides* 23: 2197–2202, 2002.

48. **Przywara DA, Kulkarni JS, Wakade TD, Leontiev DV, Wakade AR**. Pituitary adenylyl cyclase-activating polypeptide and nerve growth factor use the proteasome to rescue nerve growth factor-deprived sympathetic neurons cultured from chick embryos. *J Neurochem* 71: 1889–1897, 1998.

49. **Pugh PC, Jayakar SS, Margiotta JF**. PACAP/PAC1R signaling modulates acetylcholine release at neuronal nicotinic synapses. *Mol Cell Neurosci* 43: 244–257, 2010.

50. **Reed HE, Cutler DJ, Brown TM, Brown J, Coen CW, Piggins HD**. Effects of vasoactive intestinal polypeptide on neurones of the rat suprachiasmatic nuclei in vitro. *J Neuroendocrinol* 14: 639–646, 2002.

51. **Reglodi D, Lubics A, Tamas A, Szalontay L, Lengvari I**. Pituitary adenylate cyclase activating polypeptide protects dopaminergic neurons and improves behavioral deficits in a rat model of Parkinson's disease. *Behav Brain Res* 151: 303–312, 2004.

52. **Reglodi D, Tamas A, Lengvari I, Toth G, Szalontay L, Lubics A**. Comparative study of the effects of PACAP in young, aging, and castrated males in a rat model of Parkinson's disease. *Ann NY Acad Sci* 1070: 518–524, 2006.

53. **Scharf E, May V, Braas KM, Shutz KC, Mao-Draayer Y**. Pituitary adenylate cyclase-activating polypeptide (PACAP) and vasoactive intestinal peptide (VIP) regulate murine neural progenitor cell survival, proliferation, and differentiation. *J Mol Neurosci* 36: 79–88, 2008.

54. **Shepherd GM, Charpak S**. The olfactory glomerulus: a model for neuro-glio-vascular biology. *Neuron* 58: 827–829, 2008.

55. **Shioda S, Shuto Y, Somogyvari-Vigh A, Legradi G, Onda H, Coy DH, Nakajo S, Arimura A**. Localization and gene expression of the receptor for pituitary adenylate cyclase-activating polypeptide in the rat brain. *Neurosci Res* 28: 345–354, 1997.

56. **Sun QQ, Prince DA, Huguenard JR**. Vasoactive intestinal polypeptide and pituitary adenylate cyclase-activating polypeptide activate hyperpolarization-activated cationic current and depolarize thalamocortical neurons in vitro. *J Neurosci* 23: 2751–2758, 2003.

57. **Taupenot L, Mahata M, Mahata SK, O'Connor DT**. Time-dependent effects of the neuropeptide PACAP on catecholamine secretion : stimulation and desensitization. *Hypertension* 34: 1152–1162, 1999.

58. **Uchida D, Tatsuno I, Tanaka T, Hirai A, Saito Y, Moro O, Tajima M**. Maxadilan is a specific agonist and its deleted peptide (M65) is a specific antagonist for PACAP type 1 receptor. *Ann NY Acad Sci* 865: 253–258, 1998.

59. **Vaudry D, Gonzalez BJ, Basille M, Yon L, Fournier A, Vaudry H**. Pituitary adenylate cyclase-activating polypeptide and its receptors: from structure to functions. *Pharmacol Rev* 52: 269–324, 2000.

60. **Vaudry D, Pamantung TF, Basille M, Rousselle C, Fournier A, Vaudry H, Beauvillain JC, Gonzalez BJ**. PACAP protects cerebellar granule neurons against oxidative stress-induced apoptosis. *Eur J Neurosci* 15: 1451–1460, 2002a.

61. **Vaudry D, Pamantung TF, Basille M, Rousselle C, Fournier A, Vaudry H, Beauvillain JC, Gonzalez BJ**. PACAP protects cerebellar granule neurons against oxidative stress-induced apoptosis. *Eur J Neurosci* 15: 1451–1460, 2002b.

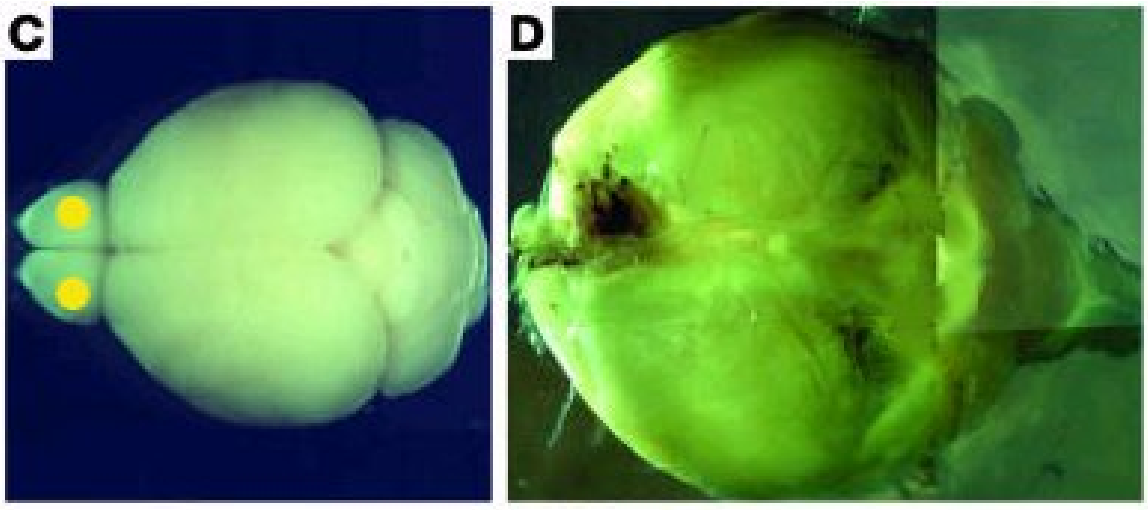

Fig. A.1: Appearance of olfactory bulbs in WT and PAC1-overexpressing mouse. The brain on left was from wild type mouse and has olfactory bulbs (yellow dots.) The brain on right was from PAC1-overexpressing mouse and the olfactory bulb appears either reduced or absence. (Modified from Lang et al., 2006b).

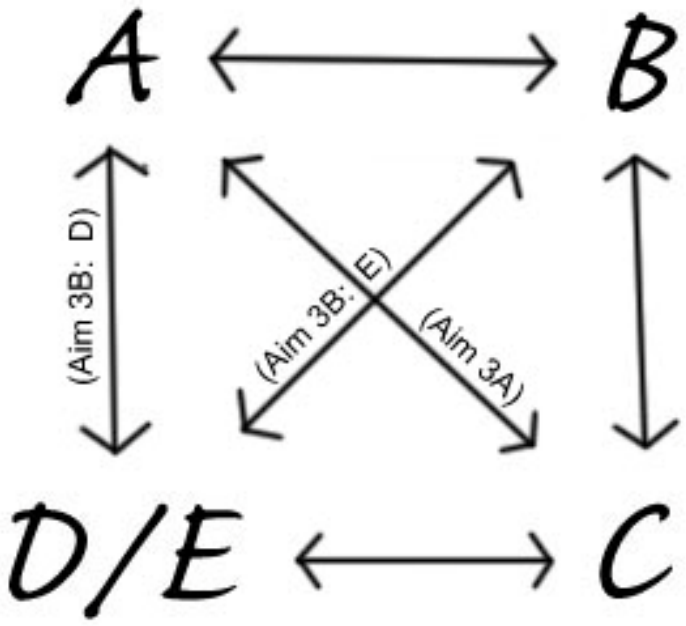

Fig. A.2: Approach for testing PACAP with and without C2-ceramide. (A) Only PACAP control; (B) Only C2-ceramide control; (C) PACAP and C2-ceramide at same time (Aim 3A); (D) PACAP then C2-ceramide (Aim 3B); (E) C2-ceramide then PACAP (Aim 3B.) All arrows are independent Student's t-test pairings and unless noted on arrows. The testing will be done in both Aim 3A and 3B.

APPENDIX B

THE PRENYL BINDING PROTEIN δ ENABLES TRAFFICKING OF GOLF TO OLFACTORY CILIA

Michelle Stamm[a,1], Houbin Zhang[b,1], Mavis Irwin[c], Guoxin Ying[b], Mary T. Lucero[ac,f,g,2] and Wolfgang Baehr[b,d,e,f,2]

[a] Interdepartmental Neuroscience Program, University of Utah, 20 North 1900 East, Salt Lake City, Utah 84132, USA

[b] Department of Ophthalmology, University of Utah Health Science Center, 65 Mario Capecchi Dr., Salt Lake City, UT, 84132, USA

[c] Department of Physiology, University of Utah, 420 Chipeta Way Ste 1700, Salt Lake City, UT, 84108, USA

[d]Department of Neurobiology and Anatomy, University of Utah Health Science Center, Salt Lake City UT 84132, USA

[e]Department of Biology, University of Utah, 257 South 1400 East, Salt Lake City, Utah 84112, USA

[f] The Brain Institute, University of Utah, 383 Colorow Drive, Salt Lake City, UT 84108, USA

[g] Utah Center on Aging, University of Utah, 10 South 2000 East, Salt Lake City, UT 84112, USA

[1] MS and HZ contributed equally to this work
[2] To whom correspondence should be addressed: E-mail: mary.lucero@utah.edu or wbaehr@hsc.utah.edu

Introduction

The olfactory system is composed of a number of distinct subsystems that can be distinguished by the location of their sensory neurons, their specific receptors, and their signaling pathways (Munger et al., 2009; Kaupp, 2010). In the canonical olfactory transduction pathway (Buck and Axel, 1991; Reed, 1992; Ache and Young, 2005), the binding of an odorant molecule to an odorant receptor (OR) activates the olfactory heterotrimeric G-protein comprised of $G_{olf}\alpha$ (Jones and Reed, 1989), $G\beta_1$, and $G\gamma_{13}$ (Kerr et al., 2008). In contrast to phototransduction, one odorant-bound OR activates just one G_{olf}, providing no amplification at the OR/G protein interface of the transduction cascade (Ben-Chaim et al., 2011). $G_{olf}\alpha$ activation of adenylate cyclase III (ACIII) (Bakalyar and Reed, 1990) increases levels of cAMP, thereby opening CNG channels consisting of two CNGA2, one CNGA4, and one CNGB1b subunit (Bonigk et al., 1999). The resulting Ca^{2+} influx depolarizes the membrane and activates additional Ca^{2+}- and voltage-gated channels (Ronnett and Moon, 2002).

While studying the retina phenotype of *Pde6d*$^{-/-}$ mice, we noted a reduced body weight in the first month of life. We suspected dysosmia (impaired sense of smell) to occur in these mutants as the *Pde6d*$^{-/-}$ mice recover their body weight after weaning. The *Pde6d* gene encodes a ubiquitous prenyl-binding proteins termed PrBP/δ that associates with prenylated proteins by inserting their prenyl anchors into a hydrophobic pocket formed by a immunoglobulin-like β-sandwich fold (Hanzal-Bayer et al., 2002). PrBP/δ interacts with multiple partners, such as small GTPases of the Ras superfamily, including Ras and Rap (Nancy et al.,

2002), Rho6 and Rheb (Hanzal-Bayer et al., 2002), Rab8 (Norton et al., 2005) and Rab13 (Marzesco et al., 2002; Marzesco et al., 1998), all of which are prenylated. In the retina, this interaction regulates stability and ciliary transport of several prenylated proteins, including G protein-coupled receptor kinase 1 (GRK1) and cGMP phosphodiesterase 6 (PDE6) subunits (Zhang et al., 2007). Deletion of the *Pde6d* gene resulted in disrupted trafficking of GRK1 and PDE to the outer segments and a recessive rod/cone degeneration phenotype.

A second lipid binding protein abundantly expressed in photoreceptors is Uncoordinated 119 (UNC119), which shares structural similarity with PrBP/δ (Zhang et al., 2011). It was recognized to be an acyl-binding protein with specificity for the acylated N-terminus of the transducin α-subunit (Tα). In photoreceptors, UNC119 plays a key role in regulating the return of Tα to the outer segments in the dark, after its light-induced translocation to the inner segment. UNC119, originally identified in C. elegans, was also shown to interact with G protein α-subunits ODR-3 and GPA-13 in *C. elegans* olfactory neurons (Zhang et al., 2011). UNC119 deletion leads to photoreceptor degeneration in mouse (Ishiba et al., 2007) and deficiencies in chemosensation in *C. elegans* (Maduro and Pilgrim, 1995).

In this communication, we investigated the consequences of PrBP/δ and UNC119 deletion on transport of G_{olf} in mouse olfactory neurons. We reasoned that these lipid binding proteins may regulate trafficking of G_{olf} as $G_{olf}\alpha$ and $G\gamma_{13}$ are myristoylated and prenylated, respectively. Mistrafficking of G_{olf} subunits and absence in cilia may lead to impaired or loss of ability to smell (Zufall and

Munger, 2001; Belluscio et al., 1998; Brunet et al., 1996; Jenkins et al., 2009; Kulaga et al., 2004). $G\alpha_{olf}$ is predicted to be N-acylated at its N-terminal Gly (G2) and S-palmitoylated at C3, whereas $G\gamma_{13}$, forming a tight complex with $G\beta_1$, is predicted to be geranylgeranylated at its C-terminal cysteine (Schwindinger and Robishaw, 2001; Linder and Deschenes, 2007; Marrari et al., 2007). These posttranslational processing steps are essential for membrane association, protein-protein interactions, and trafficking (Kizhatil et al., 2009; Magee and Seabra, 2005; Jenkins et al., 2009).

We show that in the *Unc119*$^{-/-}$ mice, $G_{olf}\alpha$ trafficked normally to the cilia and olfaction was largely normal. In *Pde6d*$^{-/-}$ OSNs, in contrast, $G_{olf}\alpha$ mislocalized and electrical responses to odorants were significantly reduced compared to age-matched control mice. EOG responses evoked by forskolin, bypassing olfactory receptors, were similar in WT and *Pde6d*$^{-/-}$ mice consistent with a defect upstream of ACIII at G_{olf}. Our studies suggest that PrBP/δ plays a role in trafficking of heterotrimeric G_{olf} to the cilia of mouse OSNs and is required for normal transduction of odorant information in OSNs.

Materials and Methods

Animals

Four *PDE6d*$^{-/-}$ (SV129/C57BL mixed background), four *Unc119*$^{-/-}$, and twelve WT mice (C57BL) between 7 weeks to 28 months old were used for behavioral experiments. All animal procedures were approved by the University of Utah Institutional Animal Care and Use Committee and were conducted under the guidelines of the NIH Guide for Care and Use of Laboratory Animals.

Odor Habituation

The ability of mice to discriminate a second novel odorant (odor 2) following habituation to a first repeated odorant (odor 1) was tested. A 10 mm diameter disk of filter paper was placed into a 1 ml pipette tip and 6 µl of pure odorant was applied to the filter paper. Mice were removed from the home cage and placed in a clean testing cage for 30 min. The odor was introduced by attaching the pipette tip to the top of the cage, and the time of active investigative sniffing was recorded. There were a total of 5 odor presentations or trials, each lasting 2 min with 1 min between presentations. R-carvone was used for the first three and last presentations, whereas the enantiomer S-carvone was the novel odor used for the fourth trial. Investigation time was compared between WT and *Pde6d*$^{-/-}$ or *Unc119*$^{-/-}$ mice for each odorant trial (unpaired) and within a genotype across trials (paired) using Student's *t*-test ($p < 0.05$).

Preparation for EOG

Mice were anesthetized with CO_2, followed by cervical dislocation and decapitation. The EOG recordings were performed on a subset of the behaviorally tested mice: 3 each of *Pde6d*$^{-/-}$ and *Unc119*$^{-/-}$ mice, as well as their respective age-matched WT control mice (n = 3 each, 6 total). The lower jaw and skin were removed, and the skull was hemisectioned along the midsagittal plane. The left half of each skull was immediately immersion fixed and used for immunocytochemistry. The other half with turbinates exposed was secured on a stereomicroscope stage and maintained in a constant low-pressure 34°C humidified stream of air.

EOG Recording

The glass recording electrode (~1 μm tip) was filled with Ringer's solution (140 mM NaCl, 5 mM KCl, 1 mM $MgCl_2$, 2 mM $CaCl_2$, 10 mM HEPES, 10 mM glucose) and recordings were made at three locations on the exposed turbinates using a stereomicroscope. The ground electrode was a silver chlorided wire inserted into a 3 M KCl agar bridge and placed just inside the skull. EOG responses were acquired at a sampling rate of 5 ms and filtered at 200 Hz using Axoscope 7.0 software, an Axoclamp 200B, and Digidata 1340 interface. Odorants (15 μl) were applied to a pipette filter and introduced into the humidified air stream using a picospritzer. The picospritzer durations were adjusted to generate approximately the same peak amplitudes for the three odorants: 2-heptanone (200 ms), n-amyl acetate (500 ms), and (-)-menthone (1 sec). Each odorant was applied twice at 2 min intervals except for the menthone application, which had a 4–5 min interval. Following odorant testing, a water control was applied through the same setup. Stock solutions of forskolin (10 mM), to directly stimulate ACIII, and IBMX (50 mM), to inhibit the breakdown of ACIII, were made up in EtOH and diluted to create a working concentration of 100 μM forskolin and 1 mM IBMX (F/I) in water. The F/I mixture and water controls were applied using a hand-held nebulizer.

EOG Data Analysis

Axoscope 7.0 software was used to determine the amplitude in mV of the EOG responses. Initial analysis indicated that the EOG amplitudes were not significantly different at the three different recording sites within the same animal.

Thus, the peak amplitudes of all three recording sites were recorded for each mouse and averaged across all mice according to odorant and genotype. The experimenter was blind to genotype when making the recordings and measurements. Statistical analyses included unpaired Student's *t*-tests ($p < 0.01$) of the EOG responses in WT versus *Pde6d*$^{-/-}$, WT versus *Unc119*$^{-/-}$, overall odorant responses versus water controls ($p < 0.01$), and WT and *Pde6d*$^{-/-}$ F/I versus water controls ($p < 0.05$).

Immunocytochemistry

The hemisection of the mouse head was immersion-fixed in 4% paraformaldehyde for 2 hr at 4°C followed by decalcifying (Rapid decalcifier, Apex Engineering Products Corp. Plainfield, IL) for 4 hr at room temperature. For cryoprotection, the tissue was incubated in 30% sucrose in PBS overnight at 4°C. The tissue was embedded in OCT and 12 μm thick sections were cut. For immunostaining, the sections were blocked in PBS buffer containing 10% goat serum,1% BSA, 0.1% Triton X-100 for 1 hr at room temperature in a humidified, rotating chamber. Primary antibodies were applied to the sections overnight at 4°C. FITC or TRIC-conjugated secondary antibodies (1:300; Jackson Immuno Research Laboratory) were incubated with the sections for 1 hr at room temperature. Zero primary and secondary controls were used to confirm specificity. The images of the sections were acquired by a Zeiss LSM510 confocal microscope. The dilutions for the primary antibodies were 1:100 for anti-$G\alpha_{olf}$ (Santa Cruz Biotechnology), 1:200 for anti-ACIII (Santa Cruz Biotechnology), 1:1:00 for anti-$G\gamma_{13}$ (gift from Dr. R. Margolskee, Mount Sinai

School of Medicine of New York University), 1:100 for anti-CNGA2 (Alomone Labs) and 1:1,000 for anti-acetylated tubulin (Sigma–Aldrich).

Pulldown Assay

GST-PrBP/δ was expressed and purified as described previously (Zhang et al., 2004). Olfactory tissue from three WT mice was homogenized by brief sonication in 1 ml PBS buffer with 1mM DTT and 10 µl protease inhibitor cocktail (Roche). The insoluble debris was removed by centrifugation at 8,000 g for 10 minutes. Pulldown assays were performed as previously described (Zhang et al., 2011). Western blots were probed with polyclonal anti- $G\gamma_{13}$ (1:150; sc-26782, Santa Cruz Biotechnology). The signal was visualized by ECL (enhanced chemiluminescence) kit (Perkin Elmer).

Results

Altered Behavioral Responses to Odorants in *Pde6d*$^{-/-}$ and *Unc119*$^{-/-}$ Mice

We first investigated olfactory function in *Pde6d*$^{-/-}$ and *Unc119*$^{-/-}$ mice using an odor habituation behavioral paradigm. In experiments involving three repeated exposures to an odorant, the animals are expected to habituate and spend less time investigating the odor source with each presentation. When a novel second odorant is presented on the fourth trial, the time that the animals spend investigating the source should increase if they can detect a difference from the first odorant. Using R-carvone as the first odorant, WT and mutant groups showed relatively normal habituation (Fig. B.1). However, *Pde6d*$^{-/-}$ mice

exhibited significantly shorter investigation times than WT mice for the first ($p = 0.047$) and second ($p = 0.04$) odor presentations (indicated by *), suggesting reduced odor sensitivity. Even though the *Unc119*$^{-/-}$ mice habituated to R-carvone, they had significantly longer investigation time than WT at the third presentation (indicated by #, $p = 0.024$). The increased investigation times by WT and both sets of mutant mice in response to odorant 2 (S-carvone) compared to Trial 3 showed that all groups could identify odorant 2 as novel.

Olfactory Function Is Reduced in Mice Lacking PrBP/δ, but not in Mice Lacking UNC119

Olfactory function was also assessed at the level of the olfactory epithelium (OE) using EOG recordings, which measure the electrical field potential responses of OSNs to odor stimuli [for review see (Scott and Scott-Johnson, 2002)]. Three different odorants (2-heptanone, n-amyl acetate, and (-)-menthone) together with water as a control were tested on OE from litter-mate or age matched WT, *Pde6d*$^{-/-}$, and *Unc119*$^{-/-}$ mice. The *Pde6d*$^{-/-}$ mice had significantly reduced EOG amplitudes that were 21–25% of the average WT responses (Fig. B.2, *A* and *C* Student's *t*-test; $p < 0.01$), while *Unc119*$^{-/-}$ EOG responses resembled WT responses (Fig. B.2*B*; $p > 0.05$). Collectively, these results indicate that *Pde6d*$^{-/-}$ mice have impaired peripheral olfactory function and are dysosmic.

Localization of PrBP/δ, $G\gamma_{13}$ and $G\alpha_{olf}$ in WT and Mutant Olfactory Cilia

PrBP/δ is a soluble protein that forms diffusable complexes with lipidated proteins (Zhang et al., 2011; Zhang et al., 2004). In WT OSNs, PrBP/δ is present in dendritic knobs, dendrites and the cell bodies (somata) (Fig. B.3, *A* and *B*, left panels), but is undetectable in *Pde6d*$^{-/-}$ OSNs (Fig. B.3, *A* and *B*, right panels). Colabeling with Ac-tubulin antibody reveals strong colocalization in cilia, and weaker colocalization in dendrites, dendritic knobs and soma of WT mice (Fig. B.3*B*, left panel). This distribution is distinct to that seen in rod photoreceptors where PrBP/δ is present in inner segments and the outer nuclear layer, but not the photosensitive cilia (the outer segments) (Ishiba et al., 2007; Zhang et al., 2007).

We next investigated the localization of G_{olf} subunits in WT and *Pde6d*$^{-/-}$ by immunocytochemistry (Fig. B.3, *C* and *D*). Both prenylated $G\gamma_{13}$ and acylated $G\alpha_{olf}$ are prominently localized to WT OSN cilia (Fig. B.3, *C* and *D*, left panels). In *Pde6d*$^{-/-}$ OE, in contrast, prenylated $G\gamma_{13}$ and acylated $G\alpha_{olf}$ were essentially undetectable (Fig. B.3, *C* and *D* middle panels). Reduction of G_{olf} levels in *Pde6d*$^{-/-}$ olfactory cilia predicts decreased olfactory responses, in agreement with habituation and EOG experiments (Figs. B.1 and C.2). In *Unc119*$^{-/-}$ OSNs, $G\alpha_{olf}$ and $G\gamma_{13}$ levels were very similar to WT (Fig. B.3, *C* and *D*, right panels) again consistent with normal EOG results (Fig. B.2*B*). Interestingly, PrBP/δ deletion in mouse did not affect the localization of the prenylated transducin γ-subunit (Tγ) in retinal photoreceptors (Zhang et al., 2007), but deletion of UNC119 affected

transport of Tα in rods after light induced translocation (Zhang et al., 2011). The reasons for these differential specificities are unclear.

The results in Fig. B.3, *A*–*D*, predict a strong interaction of PrBP/δ with $G\gamma_{13}$ at the level of biosynthesis, or a role of PrBP/δ as a chaperone in $G\gamma_{13}$ trafficking to the olfactory cilia (see discussion). To test the interaction of PrBP/δ with $G\gamma_{13}$, we used the glutathione S-transferase (GST) pulldown technique with GST-PrBP/δ as a bait. The result indicated that GST- PrBP/δ, but not a GST control, could pulldown $G\gamma_{13}$ suggesting that interaction between PrBP/δ and G_{olf} is mediated by the geranylgeranyl group attached to the C-terminus of $G\gamma_{13}$ (Fig. B.3*E*). Pulldowns of $G\alpha_{olf}$ with GST-UNC119 were negative.

The *Pde6d*$^{-/-}$ Olfactory Transduction Pathway Is Functional Downstream of G_{olf}

To test the functionality of the olfactory transduction pathway downstream of G_{olf} in *Pde6d*$^{-/-}$ mice, EOGs were recorded using forskolin to bypass the ORs and directly activate ACIII. The results show that *Pde6d*$^{-/-}$ mice had similar EOGs in response to forskolin compared to WT (Fig. B.4, *A* and *B*; $n = 4$; $p > 0.05$), consistent with the notion that the defect in olfactory function in *Pde6d*$^{-/-}$ mice is upstream of ACIII. To test for normal presence of downstream components ACIII and CNGA2, we specifically labeled cilia of WT and *Pde6d*$^{-/-}$ OSNs with anti-acetylated α-tubulin (red, Fig. B.5, middle panels) and double labeled with antibodies against either ACIII or CNGA2 (green, Fig. B.5, left panels). As expected, immunostaining showed that in contrast to the absence of targeting of $G\alpha_{olf}$ and $G\gamma_{13}$ to *Pde6d*$^{-/-}$ olfactory cilia (Fig. B.3, *A*–*D*), the downstream effector

proteins ACIII and CNGA2 showed normal colocalization with acetylated α-tubulin (Fig. B.5, *A*–*D*, right panels). These results indicate that the olfactory deficits that we observed in *Pde6d*$^{-/-}$ mice are a consequence of defective transport of G-proteins to OSN cilia.

Discussion

In this communication we investigated trafficking of G_{olf} in *Pde6d*$^{-/-}$ and *Unc119*$^{-/-}$ olfactory cilia. Behavioral and EOG recordings revealed that the *Pde6d*$^{-/-}$ mouse is dysosmic, suggesting mistrafficking of G_{olf}, the only lipidated peripheral membrane protein in the olfactory cascade. Our main findings are 1) the odorant investigation times and the peak amplitudes of odorant stimulated EOGs recorded from nasal turbinates are reduced in *Pde6d*$^{-/-}$ mice compared with age-matched or littermate controls; 2) G_{olf} subunits traffic normally to the cilia in *Unc119*$^{-/-}$ OSNs, while trafficking of $G\alpha_{olf}$ and $G\gamma_{13}$ to the cilia is impeded in *Pde6d*$^{-/-}$ OSNs; 3) GST-PrBP/δ pulls down $G\gamma_{13}$ in a GST binding assay; 4) EOG responses evoked by forskolin, bypassing olfactory receptors/G_{olf} and directly activating ACIII, were unaffected in *Pde6d*$^{-/-}$ mice consistent with a defect upstream of ACIII; 5) consistent with (4), the labeling of OSN cilia in WT and *Pde6d*$^{-/-}$ with antibodies against either ACIII or CNGA2 showed normal localization of these downstream transduction components of G_{olf}.

Mechanisms regarding trafficking and ciliary targeting of heterotrimeric G proteins in sensory neurons are largely unknown. Most of the details concerning G protein trafficking and assembly of GPCR-signaling complexes for trafficking to the plasma membrane (PM) are based on transfection of recombinant constructs

in tissue culture (HEK293 cells, yeast) [for review, see (Marrari et al., 2007)]. In the canonical model, Gα subunits carrying the myristoylation consensus sequence [Fig. B.6*A* and (Farazi et al., 2001)] are cotranslationally acylated, and Gβ and Gγ subunits combine following biosynthesis and prenylation of Gγ. Gβγ then dock to the ER for processing. At the ER, the prenylated C-termini of Gγ (prenyl-CAAX) are modified by removal of the three penultimate amino acids (AAX) and carboxymethylation of the C-terminal Cys (Hannoush and Sun, 2010). There is general agreement that Gαβγ heterotrimer formation is essential for PM targeting (Marrari et al., 2007). It is unclear, however, where in the cell Gα and Gβγ interact and how the complex traffics to the PM or to cilia in polarized neurons. When $G\alpha_s$ and Gβγ were overexpressed in HEK cells, they targeted to the PM independent of the Golgi. However, when a GPCR was co-expressed, PM targeting was Golgi dependent, and both GPCR and G protein followed the classic secretory pathway (Dupre and Hebert, 2006). In olfactory sensory neurons, G_{olf} is predicted to cotransport with ORs following the secretory pathway. Little is known about assembly of ACIII with G_{olf} and OR receptors. There is evidence that transmembrane AC dimers and GPCR dimers are the basic structural units that are assembled at the ER level (Cooper and Crossthwaite, 2006; Palczewski, 2010). Apparently, entire signaling complexes including GPCRs, G protein, and target enzyme are assembled during biosynthesis and prior to PM targeting (Dupre et al., 2009; Dupre et al., 2007). One role of PrBP/δ may be involvement in assembly of the signaling complex consisting of ORs, G_{olf}, and ACIII (Fig. B.6, *A* and *B*).

Mistrafficking of $G\alpha_{olf}$ in *Pde6d*$^{-/-}$ OSNs is in contrast to the effect of PrBP/δ deletion in photoreceptors, where trafficking of Tγ and Tα subunits proceeds mostly normally. The main differences between G_{olf} and transducin heterotrimers lie in the γ-subunits. $G\gamma_{13}$ is widely expressed in the olfactory and taste epithelia, olfactory bulb, brain (Huang et al., 1999), On-bipolar cells (Ghosh et al., 2004), and mouse ovaries (Fujino et al., 2007). Rod and cone Tγ subunits are farnesylated (C15), whereas $G\gamma_{13}$ is geranylgeranylated (C20); both have limited (25%) sequence similarity to $G\gamma_{13}$. Farnesyl moieties are more tightly associated with PrBP/δ than geranylgeranyl chains (K_D of 0.7 μM and 19 μM, respectively) (Zhang et al., 2004). Despite this 27-fold difference in favor of farnesyl, geranylgeranylated $G\gamma_{13}$ is pulled down by GST-PrBP/δ, and its trafficking is affected in *Pde6d*$^{-/-}$ OSNs, while rod Tγ is not pulled down and trafficking is largely unaffected. As the C-terminal ten residues of the γ-subunits are very similar (Fig. B.6*C*), other domains located on $G\gamma_{13}$ may contribute to strengthen the interaction between $G\gamma_{13}$ and PrBP/δ.

Absence of a G_{olf} trafficking defect in Unc119$^{-/-}$ OSNs was unexpected as $G\alpha_{olf}$ is predicted to be N-myristoylated (C14 chain) at glycine 2 (G2), the site of interaction Gα subunits with UNC119 (Zhang et al., 2011). However, it has recently been observed that $G\alpha_s$, which is closely related to $G\alpha_{olf}$ and with which it shares an identical N-terminal sequence (MGCLGNSSKT), is N-palmitoylated (C16 side chain) (Kleuss and Krause, 2003). Thus it is likely that $G\alpha_{olf}$ may be N-palmitoylated as well and that a C16 chain may be too bulky to fit into the hydrophobic cavity of UNC119, providing an explanation for pulldown failure.

The *Pde6d*$^{-/-}$ OSN phenotype essentially resembles a G_{olf} knockdown. Consistent with a knockdown, we observed that *Pde6d*$^{-/-}$ EOG responses to odorants were significantly reduced, with peak amplitudes of the odorant responses approximately ranging from 21% to 25% of age-matched WT mice. Similarly, in rod photoreceptors, genetic deletion of rod Tγ led to a major downregulation of Tβ and Tα, yet low levels of Tα present in mutant outer segments were sufficient to support phototransduction at reduced sensitivity (Lobanova et al., 2008). The relatively mild phenotype of dysosmia seen in *Pde6d*$^{-/-}$ mice contrasts with that in adult $G\alpha_{olf}$ knockouts, where EOG amplitudes in response to a variety of odors were essentially zero consistent with anosmia and failure to thrive (Belluscio et al., 1998). The few $G\alpha_{olf}$ knockout mice that do survive have reduced body weight and suffer competitive disadvantages for feeding. The phenotype of reduced body weight in *Pde6d*$^{-/-}$ mice is much less dramatic, and the mutant mouse eventually recovers a normal body weight by >1 month of age (Zhang et al., 2007). It is conceivable that *Pde6d*$^{-/-}$ mice have taste deficiencies (hypogeusia or dysgeusia) or are unable to taste sweet and bitter substances, as gustducin and G_{olf} share the $G\gamma_{13}$ subunit, further contributing to the low body weight phenotype (Huang et al., 1999).

Human diseases associated with olfactory and visual defects include some forms of Leber Congenital Amaurosis (LCA) and Bardet-Biedl syndrome (BBS) (den Hollander et al., 2006; Harville et al., 2010; Jin and Nachury, 2009). An in-frame deletion in CEP290 (NPHP5), a protein localized to the centrosome and cilia, is associated with LCA, a type of severe retinal degeneration

characterized by visual impairment from birth (den Hollander et al., 2006; den Hollander et al., 2008). This mutation has also been linked to abnormal olfactory function in both humans and mice due to disrupted trafficking of olfactory signal transduction G-proteins to the cilia (McEwen et al., 2007). BBS proteins that are mutated in Bardet-Biedl syndrome are associated with basal bodies, centromeres, and microtubule transport (May-Simera et al., 2009; Ross et al., 2005). BBS1, BBS4, and BBS8 knock-out mice have reduced responses to odorants caused by impaired protein trafficking, including $G\gamma_{13}$ and ACIII as well as disrupted cilia structure (Kulaga et al., 2004; Tadenev et al., 2011). Although the human *PDE6D* gene has not yet been associated with a human olfactory or retinal dysfunction, our data suggest that patients lacking the *PDE6D* gene may be dysosmic, hypogeusic, and may develop a recessive cone-rod dystrophy.

Acknowledgements

This work was supported by National Institute of Health grants EY08123, EY019298 (WB), EY014800-039003 (NEI core grant to the University of Utah), by NIH DC002994 supplement (MI,MS), DC002994, and NIA 1K07AG028403 (ML), by a grant of the Foundation Fighting Blindness, Inc. (WB), and unrestricted grants to the Departments of Ophthalmology at the University of Utah from Research to Prevent Blindness (RPB; New York). WB is a recipient of a Research to Prevent Blindness Senior Investigator Award.

Reference List

1. **Ache BW, Young JM**. Olfaction: diverse species, conserved principles. *Neuron* 48: 417–430, 2005.

2. **Bakalyar HA, Reed RR**. Identification of a specialized adenylyl cyclase that may mediate odorant detection. *Science* 250: 1403–1406, 1990.

3. **Belluscio L, Gold GH, Nemes A, Axel R**. Mice deficient in G(olf) are anosmic. *Neuron* 20: 69–81, 1998.

4. **Ben-Chaim Y, Cheng MM, Yau KW**. Unitary response of mouse olfactory receptor neurons. *Proc Natl Acad Sci USA* 108: 822–827, 2011.

5. **Bonigk W, Bradley J, Muller F, Sesti F, Boekhoff I, Ronnett GV, Kaupp UB, Frings S**. The native rat olfactory cyclic nucleotide-gated channel is composed of three distinct subunits. *J Neurosci* 19: 5332–5347, 1999.

6. **Brunet LJ, Gold GH, Ngai J**. General anosmia caused by a targeted disruption of the mouse olfactory cyclic nucleotide-gated cation channel. *Neuron* 17: 681–693, 1996.

7. **Buck L, Axel R**. A novel multigene family may encode odorant receptors: a molecular basis for odor recognition. *Cell* 65: 175–187, 1991.

8. **Cooper DM, Crossthwaite AJ**. Higher-order organization and regulation of adenylyl cyclases. *Trends Pharmacol Sci* 27: 426–431, 2006.

9. **den Hollander AI, Koenekoop RK, Yzer S, Lopez I, Arends ML, Voesenek KE, Zonneveld MN, Strom TM, Meitinger T, Brunner HG, Hoyng CB, Van den Born LI, Rohrschneider K, Cremers FP**. Mutations in the CEP290 (NPHP6) gene are a frequent cause of Leber congenital amaurosis. *Am J Hum Genet* 79: 556–561, 2006.

10. **den Hollander AI, Roepman R, Koenekoop RK, Cremers FP**. Leber congenital amaurosis: genes, proteins and disease mechanisms. *Prog Retin Eye Res* 27: 391–419, 2008.

11. **Dupre DJ, Baragli A, Rebois RV, Ethier N, Hebert TE**. Signalling complexes associated with adenylyl cyclase II are assembled during their biosynthesis. *Cell Signal* 19: 481–489, 2007.

12. **Dupre DJ, Hebert TE**. Biosynthesis and trafficking of seven transmembrane receptor signalling complexes. *Cell Signal* 18: 1549–1559, 2006.

13. **Dupre DJ, Robitaille M, Rebois RV, Hebert TE**. The role of Gbetagamma subunits in the organization, assembly, and function of GPCR signaling complexes. *Annu Rev Pharmacol Toxicol* 49: 31–56, 2009.

14. **Farazi TA, Waksman G, Gordon JI**. The biology and enzymology of protein N-myristoylation. *J Biol Chem* 276: 39501–39504, 2001.

15. **Fujino A, Pieretti-Vanmarcke R, Wong A, Donahoe PK, Arango NA**. Sexual dimorphism of G-protein subunit Gng13 expression in the cortical region of the developing mouse ovary. *Dev Dyn* 236: 1991–1996, 2007.

16. **Ghosh KK, Bujan S, Haverkamp S, Feigenspan A, Wassle H**. Types of bipolar cells in the mouse retina. *J Comp Neurol* 469: 70–82, 2004.

17. **Hannoush RN, Sun J**. The chemical toolbox for monitoring protein fatty acylation and prenylation. *Nat Chem Biol* 6: 498–506, 2010.

18. **Hanzal-Bayer M, Renault L, Roversi P, Wittinghofer A, Hillig RC**. The complex of Arl2-GTP and PDE delta: from structure to function. *EMBO J* 21: 2095–2106, 2002.

19. **Harville HM, Held S, Diaz-Font A, Davis EE, Diplas BH, Lewis RA, Borochowitz ZU, Zhou W, Chaki M, Macdonald J, Kayserili H, Beales PL, Katsanis N, Otto E, Hildebrandt F**. Identification of 11 novel mutations in eight BBS genes by high-resolution homozygosity mapping. *J Med Genet* 47: 262–267, 2010.

20. **Huang L, Shanker YG, Dubauskaite J, Zheng JZ, Yan W, Rosenzweig S, Spielman AI, Max M, Margolskee RF**. Ggamma13 colocalizes with gustducin in taste receptor cells and mediates IP3 responses to bitter denatonium. *Nat Neurosci* 2: 1055–1062, 1999.

21. **Ishiba Y, Higashide T, Mori N, Kobayashi A, Kubota S, McLaren MJ, Satoh H, Wong F, Inana G**. Targeted inactivation of synaptic HRG4 (UNC119) causes dysfunction in the distal photoreceptor and slow retinal degeneration, revealing a new function. *Exp Eye Research* 84: 473–485, 2007.

22. **Jenkins PM, McEwen DP, Martens JR**. Olfactory cilia: linking sensory cilia function and human disease. *Chem Senses* 34: 451–464, 2009.

23. **Jin H, Nachury MV**. The BBSome. *Curr Biol* 19: R472–R473, 2009.

24. **Jones DT, Reed RR**. Golf: an olfactory neuron specific-G protein involved in odorant signal transduction. *Science* 244: 790–795, 1989.

25. **Kaupp UB**. Olfactory signalling in vertebrates and insects: differences and commonalities. *Nat Rev Neurosci* 11: 188–200, 2010.

26. **Kerr DS, Von Dannecker LE, Davalos M, Michaloski JS, Malnic B**. Ric-8B interacts with G alpha olf and G gamma 13 and co-localizes with G alpha olf, G beta 1 and G gamma 13 in the cilia of olfactory sensory neurons. *Mol Cell Neurosci* 38: 341–348, 2008.

27. **Kizhatil K, Baker SA, Arshavsky VY, Bennett V**. Ankyrin-G promotes cyclic nucleotide-gated channel transport to rod photoreceptor sensory cilia. *Science* 323: 1614–1617, 2009.

28. **Kleuss C, Krause E**. Galpha(s) is palmitoylated at the N-terminal glycine. *EMBO J* 22: 826–832, 2003.

29. **Kulaga HM, Leitch CC, Eichers ER, Badano JL, Lesemann A, Hoskins BE, Lupski JR, Beales PL, Reed RR, Katsanis N**. Loss of BBS proteins causes anosmia in humans and defects in olfactory cilia structure and function in the mouse. *Nat Genet* 36: 994–998, 2004.

30. **Linder ME, Deschenes RJ**. Palmitoylation: policing protein stability and traffic. *Nat Rev Mol Cell Biol* 8: 74–84, 2007.

31. **Lobanova ES, Finkelstein S, Herrmann R, Chen YM, Kessler C, Michaud NA, Trieu LH, Strissel KJ, Burns ME, Arshavsky VY**. Transducin gamma-subunit sets expression levels of alpha- and beta-subunits and is crucial for rod viability. *J Neurosci* 28: 3510–3520, 2008.

32. **Maduro M, Pilgrim D**. Identification and cloning of unc-119, a gene expressed in the Caenorhabditis elegans nervous system. *Genetics* 141: 977–988, 1995.

33. **Magee T, Seabra MC**. Fatty acylation and prenylation of proteins: what's hot in fat. *Curr Opin Cell Biol* 17: 190–196, 2005.

34. **Marrari Y, Crouthamel M, Irannejad R, Wedegaertner PB**. Assembly and trafficking of heterotrimeric G proteins. *Biochemistry* 46: 7665–7677, 2007.

35. **Marzesco AM, Dunia I, Pandjaitan R, Recouvreur M, Dauzonne D, Benedetti EL, Louvard D, Zahraoui A**. The small GTPase Rab13 regulates assembly of functional tight junctions in epithelial cells. *Mol Biol Cell* 13: 1819–1831, 2002.

36. **Marzesco AM, Galli T, Louvard D, Zahraoui A**. The rod cGMP phosphodiesterase delta subunit dissociates the small GTPase Rab13 from membranes. *J Biol Chem* 273: 22340–22345, 1998.

37. **May-Simera HL, Ross A, Rix S, Forge A, Beales PL, Jagger DJ**. Patterns of expression of Bardet-Biedl syndrome proteins in the mammalian cochlea suggest noncentrosomal functions. *J Comp Neurol* 514: 174–188, 2009.

38. **McEwen DP, Koenekoop RK, Khanna H, Jenkins PM, Lopez I, Swaroop A, Martens JR**. Hypomorphic CEP290/NPHP6 mutations result in anosmia caused by the selective loss of G proteins in cilia of olfactory sensory neurons. *Proc Natl Acad Sci USA* 104: 15917–15922, 2007.

39. **Munger SD, Leinders-Zufall T, Zufall F**. Subsystem organization of the mammalian sense of smell. *Annu Rev Physiol* 71: 115–140, 2009.

40. **Nancy V, Callebaut I, El Marjou A, de Gunzburg J**. The delta subunit of retinal rod cGMP phosphodiesterase regulates the membrane association of Ras and Rap GTPases. *J Biol Chem* 277: 15076–15084, 2002.

41. **Norton AW, Hosier S, Terew JM, Li N, Dhingra A, Vardi N, Baehr W, Cote RH**. Evaluation of the 17-kDa prenyl-binding protein as a regulatory protein for phototransduction in retinal photoreceptors. *J Biol Chem* 280: 1248–1256, 2005.

42. **Palczewski K**. Oligomeric forms of G protein-coupled receptors (GPCRs). *Trends Biochem Sci* 35: 595–600, 2010.

43. **Reed RR**. Signaling pathways in odorant detection. *Neuron* 8: 205–209, 1992.

44. **Ronnett GV, Moon C**. G proteins and olfactory signal transduction. *Annu Rev Physiol* 64: 189–222, 2002.

45. **Ross AJ, May-Simera H, Eichers ER, Kai M, Hill J, Jagger DJ, Leitch CC, Chapple JP, Munro PM, Fisher S, Tan PL, Phillips HM, Leroux MR, Henderson DJ, Murdoch JN, Copp AJ, Eliot MM, Lupski JR, Kemp DT, Dollfus H, Tada M, Katsanis N, Forge A, Beales PL**. Disruption of Bardet-Biedl syndrome ciliary proteins perturbs planar cell polarity in vertebrates. *Nat Genet* 37: 1135–1140, 2005.

46. **Schwindinger WF, Robishaw JD**. Heterotrimeric G-protein betagamma-dimers in growth and differentiation. *Oncogene* 20: 1653–1660, 2001.

47. **Scott JW, Scott-Johnson PE**. The electroolfactogram: a review of its history and uses. *Microsc Res Tech* 58: 152–160, 2002.

48. **Tadenev AL, Kulaga HM, May-Simera HL, Kelley MW, Katsanis N, Reed RR**. Loss of Bardet-Biedl syndrome protein-8 (BBS8) perturbs olfactory function, protein localization, and axon targeting. *Proc Natl Acad Sci USA* 2011.

49. **Zhang H, Constantine R, Vorobiev V, Chen Y, Seetharaman J, Huang YJ, Xie G, Montelione GT, Gerstner CD, Davis MW, Inana G, Whitby FG, Jorgensen EM, Hill CP, Tong L, Baehr W**. UNC119 regulates G protein trafficking in sensory neurons. *Nature Neuroscience* 14: 874–880, 2011.

50. **Zhang H, Li S, Doan T, Rieke F, Detwiler PB, Frederick JM, Baehr W**. Deletion of PrBP/{delta} impedes transport of GRK1 and PDE6 catalytic subunits to photoreceptor outer segments. *Proc Natl Acad Sci USA* 104: 8857–8862, 2007.

51. **Zhang H, Liu XH, Zhang K, Chen CK, Frederick JM, Prestwich GD, Baehr W**. Photoreceptor cGMP phosphodiesterase delta subunit (PDEdelta) functions as a prenyl-binding protein. *J Biol Chem* 279: 407–413, 2004.

52. **Zufall F, Munger SD**. From odor and pheromone transduction to the organization of the sense of smell. *Trends Neurosci* 24: 191–193, 2001.

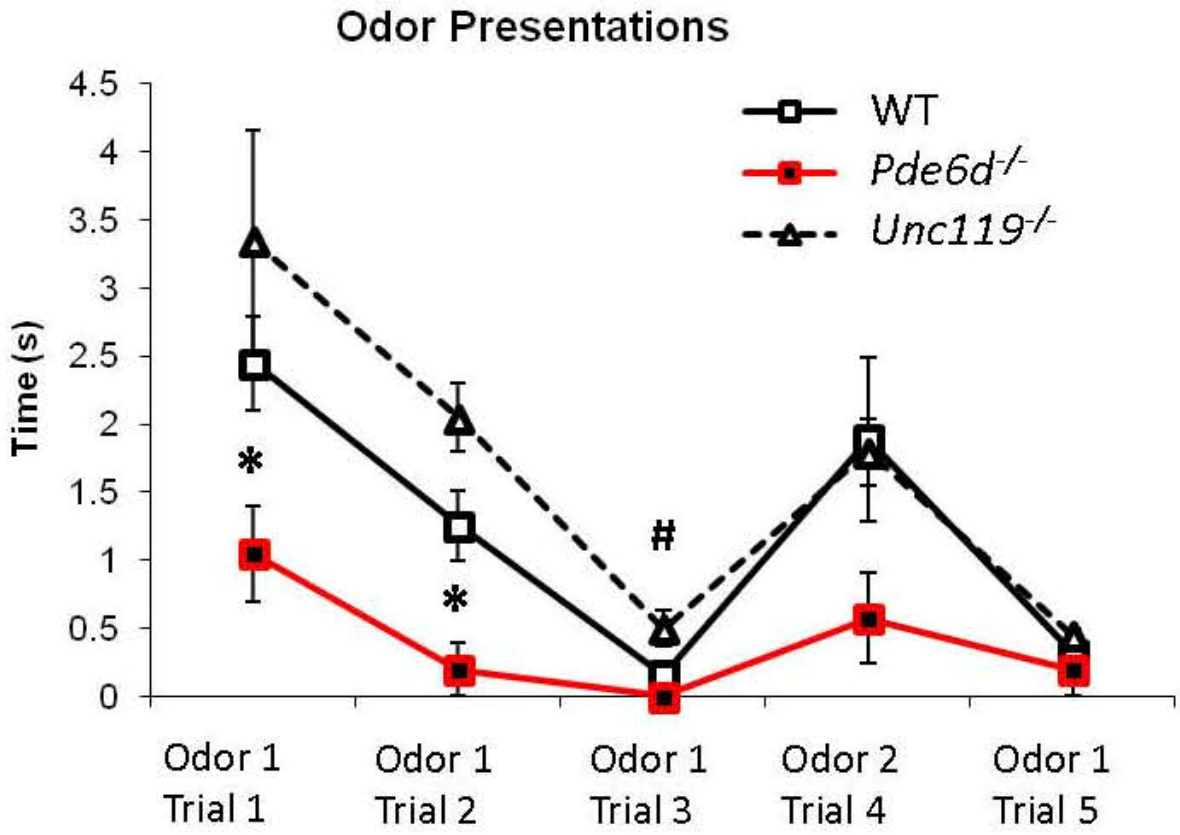

Fig. B.1: Odor presentations to WT, *Pde6d*$^{-/-}$, and *Unc119*$^{-/-}$ mice in a habituation behavioral paradigm. Odor 1, R-carvone; odor 2, S-carvone. All groups showed normal habituation to R-carvone. *Pde6d*$^{-/-}$ mice have significantly shorter investigation times than WT mice; the *Unc119*$^{-/-}$ mice had significantly longer investigation time than WT. WT and both mutant mice identified odorant 2 as novel. Significance was determined by unpaired Student's *t*-tests; * indicates significance at $P \leq 0.05$; # indicates significance at $P \leq 0.03$. The results show that *Pde6d*$^{-/-}$ mice are dysosmic and retain some olfactory function.

Fig. B.2: EOG responses to various odorants (2-heptanone, n-amyl acetate, (-)-menthone) in WT and mutant mice. (*A*) representative EOG traces from WT and *Pde6d*$^{-/-}$ mice in response to a water control and the odorants indicated. (*B*) representative EOG traces from WT and Unc119$^{-/-}$ mice. *Pde6d*$^{-/-}$ mice are dysosmic while *Unc119*$^{-/-}$ mice have normal olfaction. Prolonged responses in the (-)-menthone traces (green) were occasionally observed in both WT and *Pde6d*$^{-/-}$ and are likely due to the longer 1-sec pulse used to generate a similar response amplitude to other odorants (see Methods). (*C*) average peak EOG responses to the three odorants and water controls are shown for both WT (open bars) and *Pde6d*$^{-/-}$ mice (solid bars). For each odorant, Student's *t*-tests were performed on the averaged peak EOG responses in knockouts compared to the averaged WT responses. * indicates significance at $P \leq 0.01$; $n = 3$.

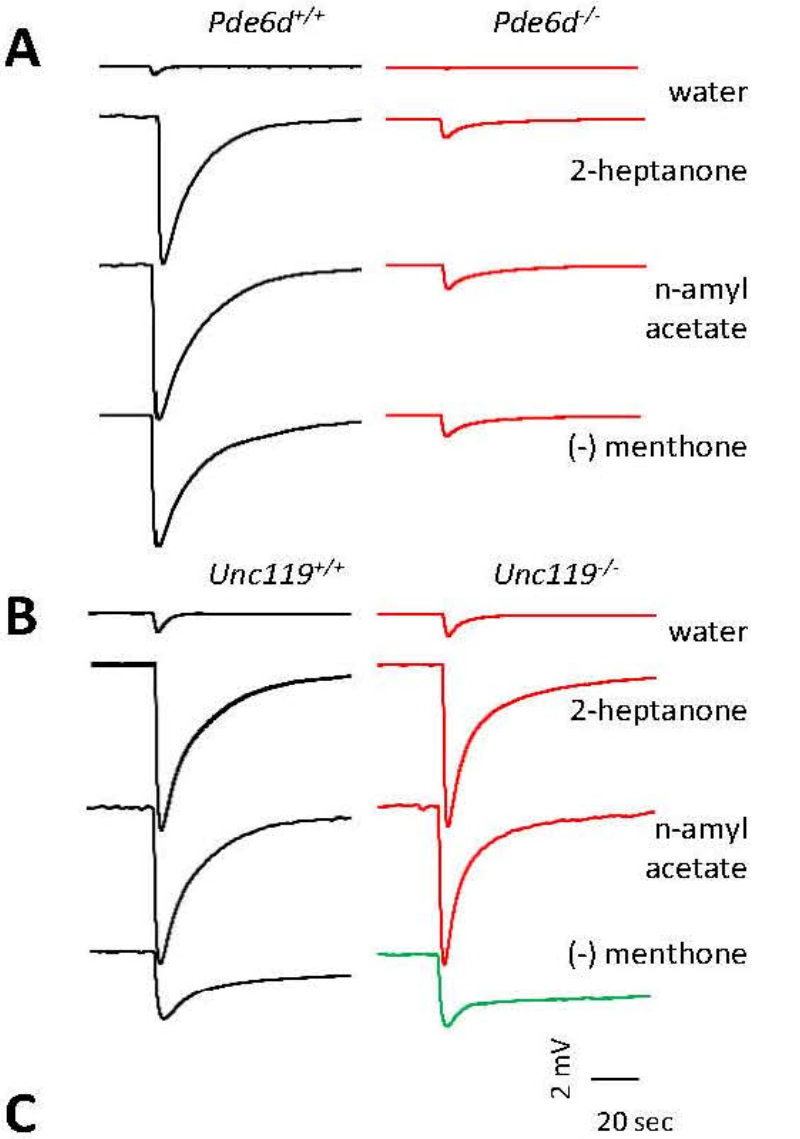
A
Pde6d+/+
Pde6d-/-
water
2-heptanone
n-amyl
acetate
(-) menthone
B
Unc119+/+
Unc119-/-
water
2-heptanone
n-amyl
acetate
(-) menthone
2 mV
20 sec

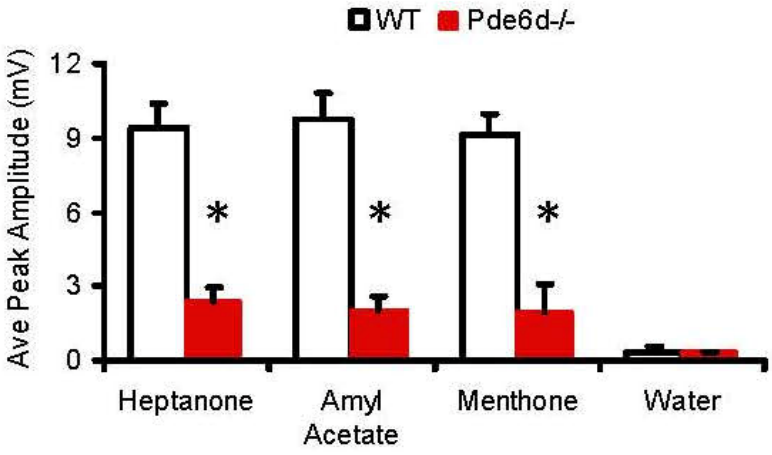
C
WT
Pde6d-/-
Ave Peak Amplitude (mV)
12
9
6
3
0
*
*
*
Heptanone
Amyl
Acetate
Menthone
Water

Fig. B.3: Localization of PrBP/δ, $G\gamma_{13}$ and $G\alpha_{olf}$ in WT and mutant olfactory epithelia. (*A*) WT and *Pde6d*$^{-/-}$ olfactory epithelium (OE) cryosections were probed with anti-PrBP/δ (green) antibody. PrBP/δ is present in dendrites and cell bodies of WT mice, but is essentially undetectable in the *Pde6d*$^{-/-}$ OSNs. (*B*) PrBP/δ colocalizes with acetylated tubulin (AcTub, red) in olfactory cilia. (*C, D*) WT, *Pde6d*$^{-/-}$, and *Unc119*$^{-/-}$ OE cryosections probed with polyclonal anti-$G\gamma_{13}$ and anti-$G\alpha_{olf}$ antibody. $G_{\gamma 13}$ is localized to cilia in WT and *Unc119*$^{-/-}$OSNs but is undetectable in *Pde6d*$^{-/-}$ cilia (*C*). $G\alpha_{olf}$ is localized to the cilia in WT and *Unc119*$^{-/-}$ mice, but is essentially absent from cilia of *Pde6d*$^{-/-}$ mice (*D*). (*E*) direct interaction between PrBP/δ, the protein encoded by the *Pde6d* gene, and $G\gamma_{13}$. Mouse olfactory extract pulldowns with GST-PrBP/δ and GST as a control were identified with anti-$G\gamma_{13}$ antibody. Input, olfactory crude extract. Pulldown, proteins bound to glutathione beads.

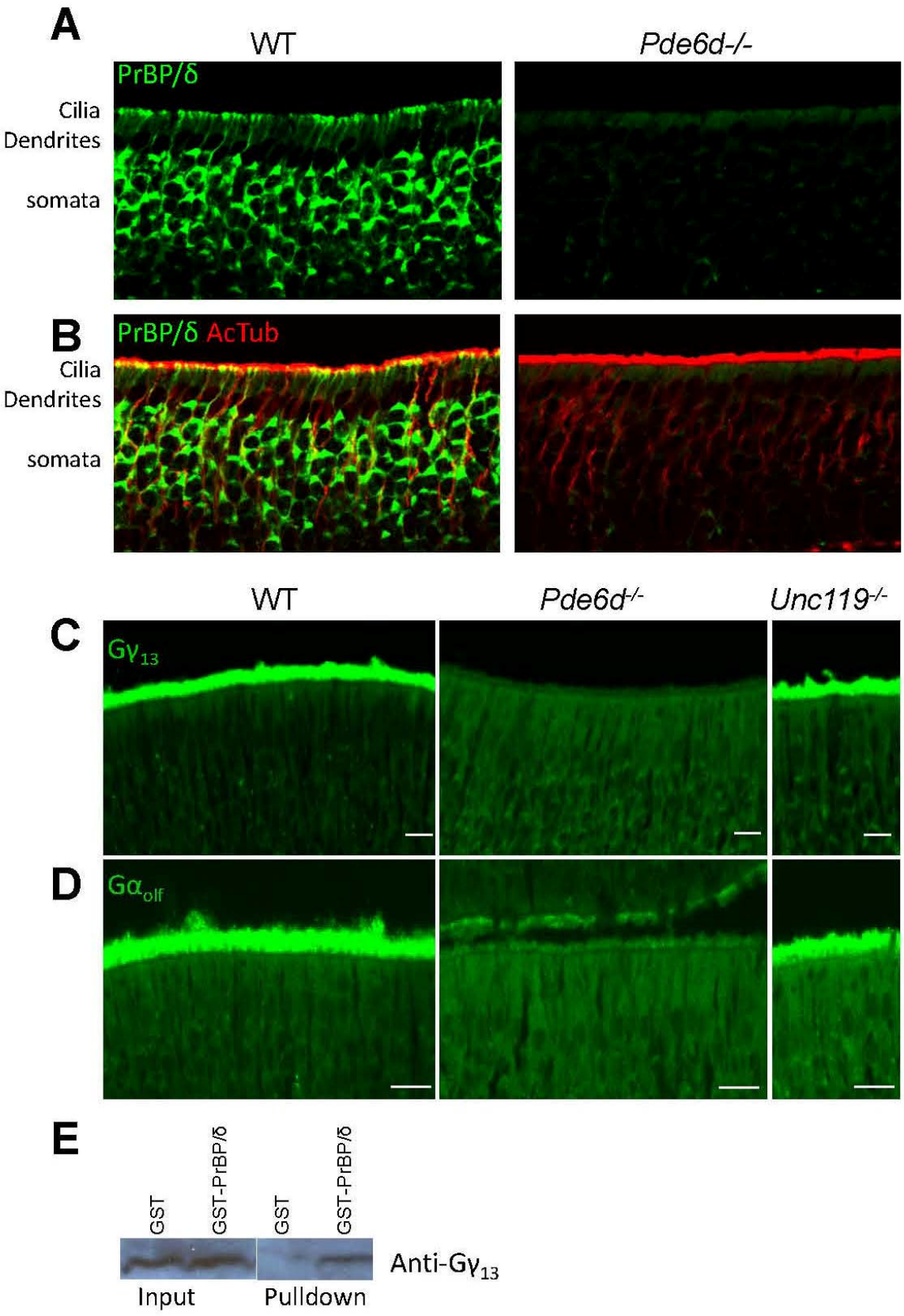
A
WT
Pde6d-/-
PrBP/δ
Cilia
Dendrites
somata
B
PrBP/δ AcTub
Cilia
Dendrites
somata
WT
Pde6d-/-
Unc119-/-
C
Gγ13
D
Gαolf
E
GST
GST-PrBP/δ
GST
GST-PrBP/δ
Anti-Gγ13
Input
Pulldown

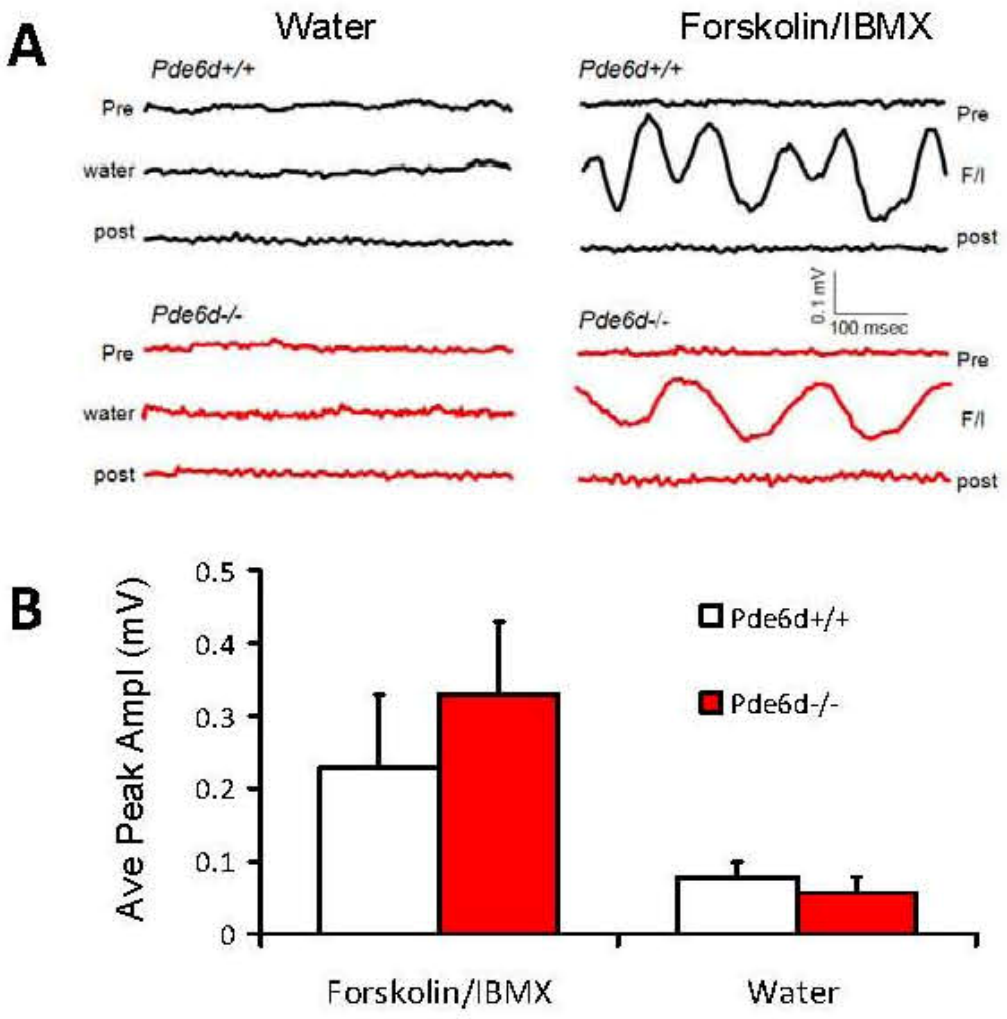

Fig. B.4: Forskolin stimulation of ACIII. (*A*) representative EOG traces before, during, and after H_2O control, and 100 µM Forskolin + 1 mM IBMX (F/I) are shown for WT and *Pde6d*$^{-/-}$ mice. (*B*) Average peak EOG responses to F/I and H_2O control were not significantly different using a Student's *t*-test p = 0.3; n = 3 WT, 3 Pde6d$^{-/-}$. The results show that the cAMP signal transduction pathway is functional downstream of the olfactory G-proteins in *Pde6d*$^{-/-}$ mice.

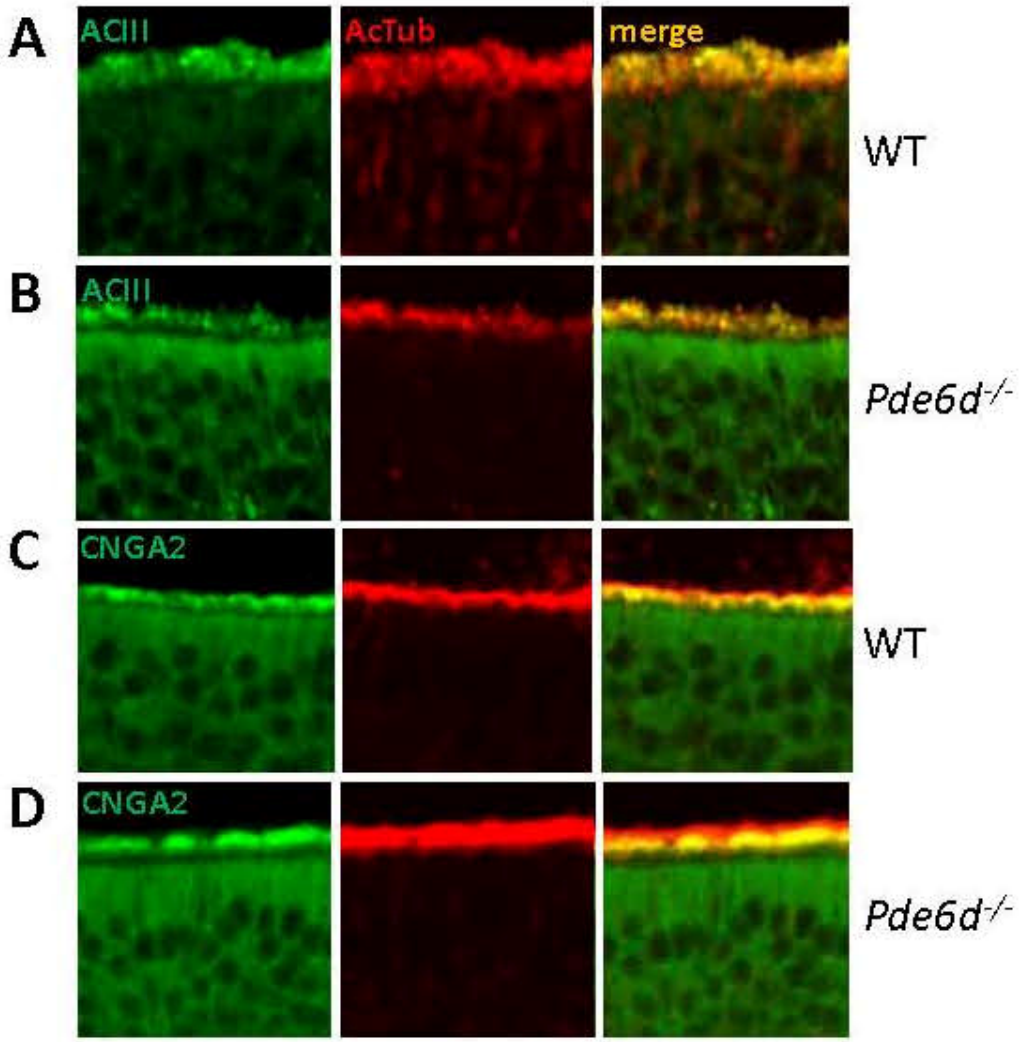

Fig. B.5: ACIII and CNGA2 in OSNs show proper targeting to OSN cilia. (*A, C*) Confocal images of immunostainted (WT) and (*B, D*) (*Pde6d*$^{-/-}$) olfactory epithelium cryosections. Cilia are identified by the acetylated α-tubulin immunoreactivity (red). ACIII and CNGA2 (green) are located in cilia and colocalize with acetylated tubulin in both WT (*A, C*) and *Pde6d*$^{-/-}$ mice (*B, D*).

Fig. B.6: Cartoon of G_{olf} trafficking in OSNs. (*A*) Normal trafficking of membrane proteins. Following biosynthesis, prenylated $G\gamma_{13}$ and acylated $G\alpha_{olf}$ dock at the endoplasmic reticulum (ER) and form a soluble complex with the help of lipid binding protein(s). Transmembrane proteins (ORs, ACIII, olfactory channel subunits CNG_{olf}) are synthesized at the ER, exit the ER, and combine with G_{olf} to form a signaling complex to be trafficked to the olfactory cilia. (*B*) Trafficking in the absence of PrBP/δ. In the absence of PrBP/δ, $G\beta_1\gamma_{13}$ and $G\alpha_{olf}$ remain bound to the ER and are likely degraded. The signaling complex lacking G_{olf} subunits, but containing ORs, ACIII, and CNG subunits traffics normally. (*C*) The C-terminal regions of rod, cone, and olfactory Gγ subunits. The last 21 residues of rod Tγ, cone Tγ, and $G\gamma_{13}$ are shown. The penultimate 10 residues are highly conserved, yet only $G\gamma_{13}$ is pulled down by GST-PrBP/δ (GST-PrBP/δ could not pulldown Tγ from WT mouse retina lysates.)

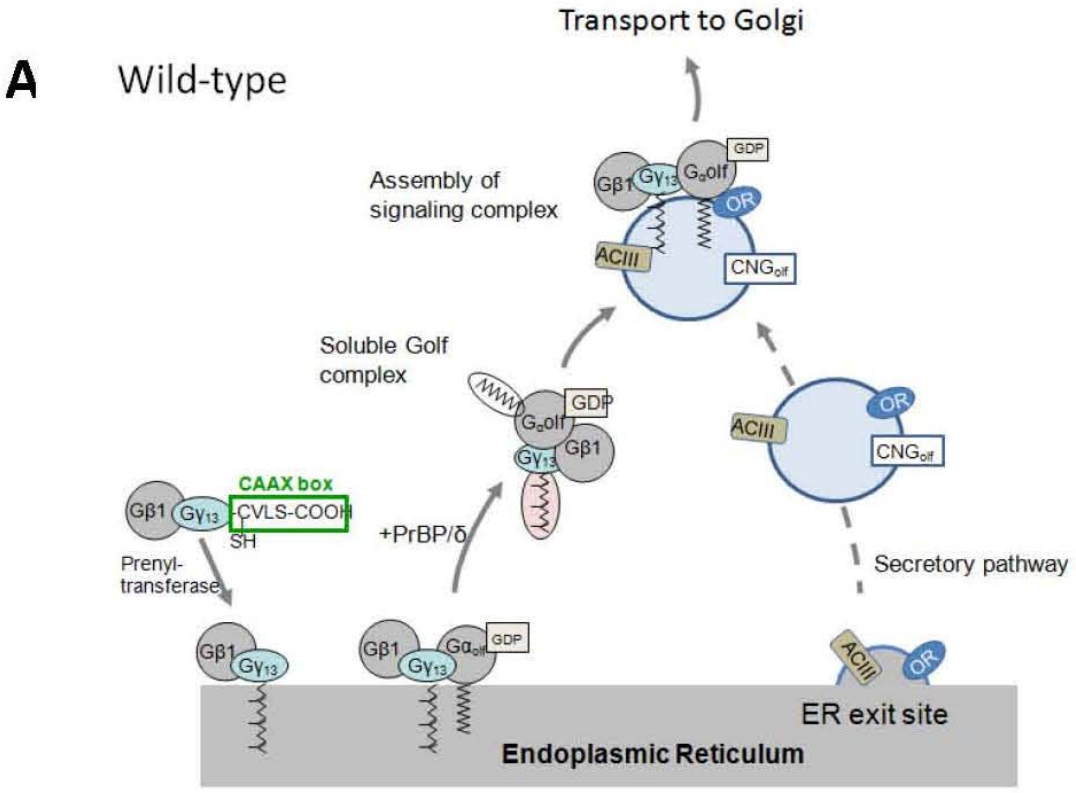

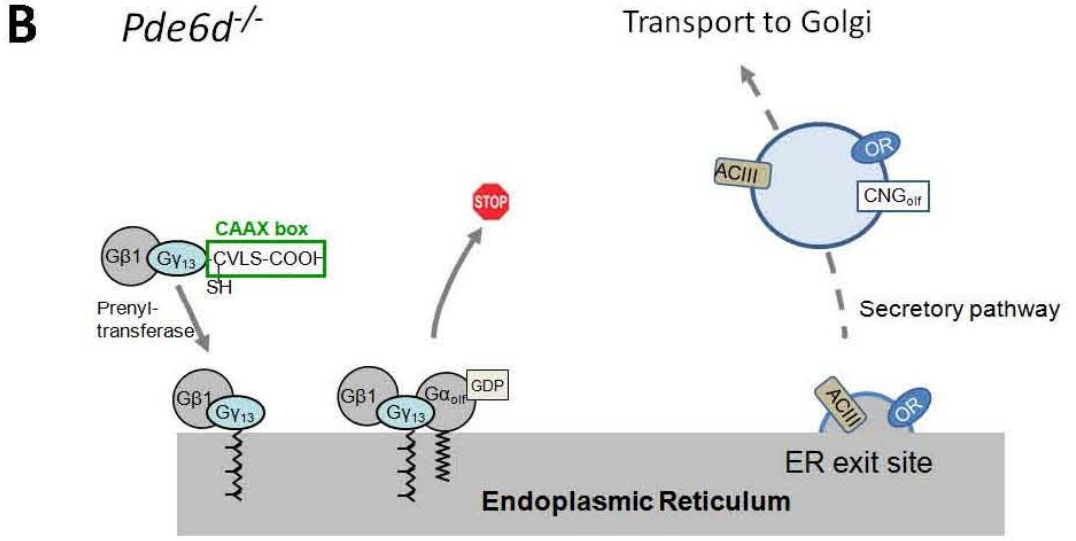

C

```
53 LVKGIPEDKNPFKELKGGC-farnesyl (CaaX box CVIS)rod Tγ  (Gngt1)
49 FLKGIPEDKNPFKE-KGGC-farnesyl (CaaX box CVIS)cone Tγ (Gngt2)
47 FLNPDLMKNNPWVE-KGKC-ger-ger  (CaaX box CTIL)Gγ13    (Gng13)
```

APPENDIX C

METHODS AND TECHNIQUES

Introduction

I wrote this appendix to give people more details on the methods and techniques used to obtain the data. I feel that the amount of information about the methods in the journal articles (Chapter 2, 3, and 4) is not enough for another person to successfully repeat my work without the following suggestions, which may be helpful in terms of producing ideas and possibly saving time and resources.

For the tissue slices used in Chapters 2 and 3, there is an art to prepare, transport, position in chamber, maintain the solution flow through chamber, and image a great spot. It took me a few years to develop my skills to achieve my standards for healthy slices, especially olfactory bulb ones.

The challenge I had for Chapter 4 was to get reliable, strong EOG responses for a full hour without the tissue getting wet or dry. The application of dissolved IMBX/FSX was also tweaked to obtain the most reliable data.

Chapter 2: Preparing Live Acute OB Slices

First week neonatal mice pups were used both for their adaptability to a relatively simple acute live slicing method and for study of PACAP effects during

early maturation. The slightest physical trauma to a live OB acute slice often significantly decreases the vitality of the slice (personal observations). I speculated that the low success rate of acute live brain slices in older animals is why some researchers only collect acute live slices from mouse or rat embryos up to 24 hours postnatal (personal conversations). I, however, developed tricks that sometimes gave slices with good vitality from P2 to P5 neonatal pups. Minimizing the steps between the live animal and recording from slices helped increase the viability of the acute slice. One step-saver was to use the skull as a natural embedding material instead of embedding the OB in a foreign material such as the typical agarose, gel, or carrots. For pups older than P6, when the skull becomes calcified and difficult to slice through, an approach I would like to try is cutting off the skull at the eye sockets, but keeping the lower part of skull as a way to hold the OB in place. There will be an age when it would be better to remove the OB from the skull. As the animals mature, meninges enclose the OB, and one has to peel these off the OB in order to make good adult OB slices (personal observations).

Chapter 2: Permeant Ca^{2+} Sensitive Dyes

Experiments on the same slice often last about 4 hours. When imaging the same tissue for prolonged amounts of time, the bleaching of fluorescent labels on the tissues is a common problem. When I did experiments on sustentacular cells (Chapter 3), I was able to incubate the slices in Fluo-4 AM for about 15 minutes at 37ºC and complete the experiment within an hour after incubation. This is because I had no need to wash out the treatments for over 60

minutes after each application as I did for PACAP, which has a long response duration. When I worked with PACAP, each slice was imaged for about 4 hours. Thus, it was necessary to load the slices with Fluo-4 AM for nearly an hour at 37ºC and use them within an hour. Fluo-4 then lasts throughout the experiment with small adjustments for the loss of fluorescent dye near the end.

In Chapter 2, we showed data for GAD65-dtTomato transgenic mice and we wished we could look at GAD67 labeled transgenic mice. Unfortunately, we did not have a GAD67-dtTomato transgenic mouse colony. However, we did have access to a GAD67-GFP transgenic mouse colony, and we put in the effort to use the mice. We have showed that using Rhod-3 as an alternative permeant Ca^{2+} sensitive dye would work, but Rhod-3 has the problem of loading in the dendrites more than the soma. Figure C.1 shows the double loading of both Rhod-3 (Fig. C.1*A*) and Fluo-4 (Fig. C.1*B*) on an olfactory bulb (OB) live slice of a wildtype (WT) mouse. Figure C.2 shows a x2 magnification of where the Rhod-3 and Fluo-4 dyes are loaded. Figure C.3 shows how Rhod-3 looks in the GAD67-GFP transgenic mouse OB. Rhod-3 rarely overlaps with the GAD67-GFP label found mainly on the soma, proving the dye to be useless for recording Ca^{2+} activation of somas but potentially useful for imaging Ca^{2+} in dendrites.

<u>Chapter 2: dtTomato Fluorescent Bleaching</u>

For the mice expressing the fluorescent dtTomatomarker, the confocal imaging bleaching unfortunately happened quicker compared to mice expressing GFP fluorescence. To minimize the exposure to background light, I built a black box to place over the microscope. The box has a removable door on the front so

the experimenter can look into the eyepiece (Fig. C.4, *A* and *B*). The side shown in Fig. C.4 has a large opening toward the back for accessing the stage shifters. I used the box when I needed to image the red fluorescent of the dtTomato throughout experiments lasting as long as 4 hours.

Chapters 2 and 3: Perfusion System

For Chapters 2 and 3 calcium imaging of live slices, a perfusion system was used to manage a constant, slow flow of 1–2 mL per minute from the bottles containing the physiologic solutions. A vacuum pump was used at the opposite side of the chamber from the incoming flow. The vacuum pump got clogged from time to time, mainly due to air bubbles or loose pieces of tissue. When the pump is not working, the chamber can overflow and solutions drip over the stage onto the air table, making a mess. Furthermore, the chamber where the slices were placed has its challenges. When the chamber bath is too high, the loop injected solution often flows along the sides and very little hits the tissue. When the chamber bath is too low, the static from the chamber walls draws the solution away from the center where the slice is being held. Here, I want to share my ideas to make the experiments more pleasurable to do.

The key thing to look at is the chamber itself. Figure C.5 shows the chamber I used for calcium imaging live slices. The whole chamber size was 24 x 60 mm, and the width of the chamber bath was 14 mm. I discovered that this width is more effective than wider chambers. However, the disadvantage was the limited range of areas to take pictures of during perfusion due to the need for avoiding close connection with the side walls of chamber. The incoming solution

comes in on the right side and the pipe opening fit into the chamber should be horizontal and perpendicular to the chamber bottom geometry (Fig. C.5*A*). The chamber walls are made from plexiglass (Fig. C.5*B*) with a separable, replaceable thick coverslip glass bottom (Fig. C.5*C*). Vacuum grease was used to seal the edges between chamber wall and coverslip bottom, which was stuck together using vacuum grease. The wire running between the chamber wall and coverslip bottom is a very thin stainless steel wire. This wire is used for holding slices in place during experiments with minimum perfusion flow displacement. The pipe on the left side is the vacuuming end, where solution is being drawn out of the chamber (Fig. C.5*D*).

To maintain a reliable, constant perfusion flow throughout the experiments, I found that keeping the chamber bath level low is the most promising approach. We want the experimental drugs, especially those applied through loop injection, to run smoothly directly over the slice and effectively get washed out. What I did was to put films of silicone coating (Sigmacote, from Sigma Chemicals) on the surface and interior walls of the chamber plexiglass and along the edges of the glass coverslip bottom. Sigmacote makes the surfaces water repellant and once it is applied, the film can last a long time. The glass coverslip bottom has a narrow silicone-free lane down the length of the middle so the solution tends to flow along the center, where the slice is positioned, instead of detouring along the sides of the chamber bath. A small piece of kimwipe (2 x 3 cm square, folded twice in one-thirds to make a 1 x 2 piece) is placed 4–6 mm from the slice to draw solution away from the whole

diameter of the slice (8 mm diameter for mouse pup noses). The vacuum is connected to surface of the kimwipe, pulling off the solution at a steady rate.

Chapter 4 and Appendix C: Electro-olfactogram Setup

Figure C.6 shows the setup of the electro-olfactogram system. Humidity is kept at moderate levels. If the humidity is too high, the olfactory epithelium (OE) surface becomes watery and does not perform as well. To keep the humidity from soaking the tissue, I used a lamp light as a drying agent (Fig. C.6; below yellow arrow). When the humidity is low, the plastic sheet helps keep the moisture in the work space (Fig. C.6*A*). The small water bath under the plastic sheet (Fig. C.6*B*) aids in increasing the warm moisture. (A humidifier may supply moisture, but it is often too chilly for the tissue.) Not pictured was the heated (34ºC) water bath source for the low-pressure moisture vapor, which is supplied through the white vaporizing-tube (Fig. C.6; above green arrow).

Odorants are applied using a picospritzer (not pictured), which makes the odorants air-bound through the side of the vaporizing-tube, about 3 inches from the opening (Fig. C.6; red arrow). The odorant is loaded onto the filter of pipette tips (the tips were autoclaved to make the filter pores bigger) and snapped onto the holder (Fig. C.6; white arrow). The opening of the vaporing-tube is placed 2.5–3.0 cm from the surface of OE. The glass funnel sucks away the odorants, clearing the smell out of the work space, especially when covering the space with plastic sheet (Fig. C.6; blue arrow).

Other parts included the perfusion system for loop injecting solution-bound drugs (e.g., IBMX/FSK) for testing the function of downstream mechanisms (Fig. C.6*C*) and the electrode holder (Fig. C.6*D*).

Chapter 4 and Appendix C: Animals Used

The biggest challenge I encountered was keeping the OE tissue at a constant humidity throughout the experiments. I am very confident with the data I collected because the wild type data results were consistent for seven different odorants tested between 2009 and 2013. However, a strictly controlled environment with accurate humidity and temperature would undoubtedly improve recordings. Over the years of EOG recordings, I observed that the wild type mice in animal facility A had an overall 30% smaller response to odors than the wild type mice in animal facility B. Could it be the long-term humidity? Population density? Cleanliness of cages? We can only speculate because the animal facility environments were supposed to be the same. For this reason, I stress the importance of using animals from just one animal facility.

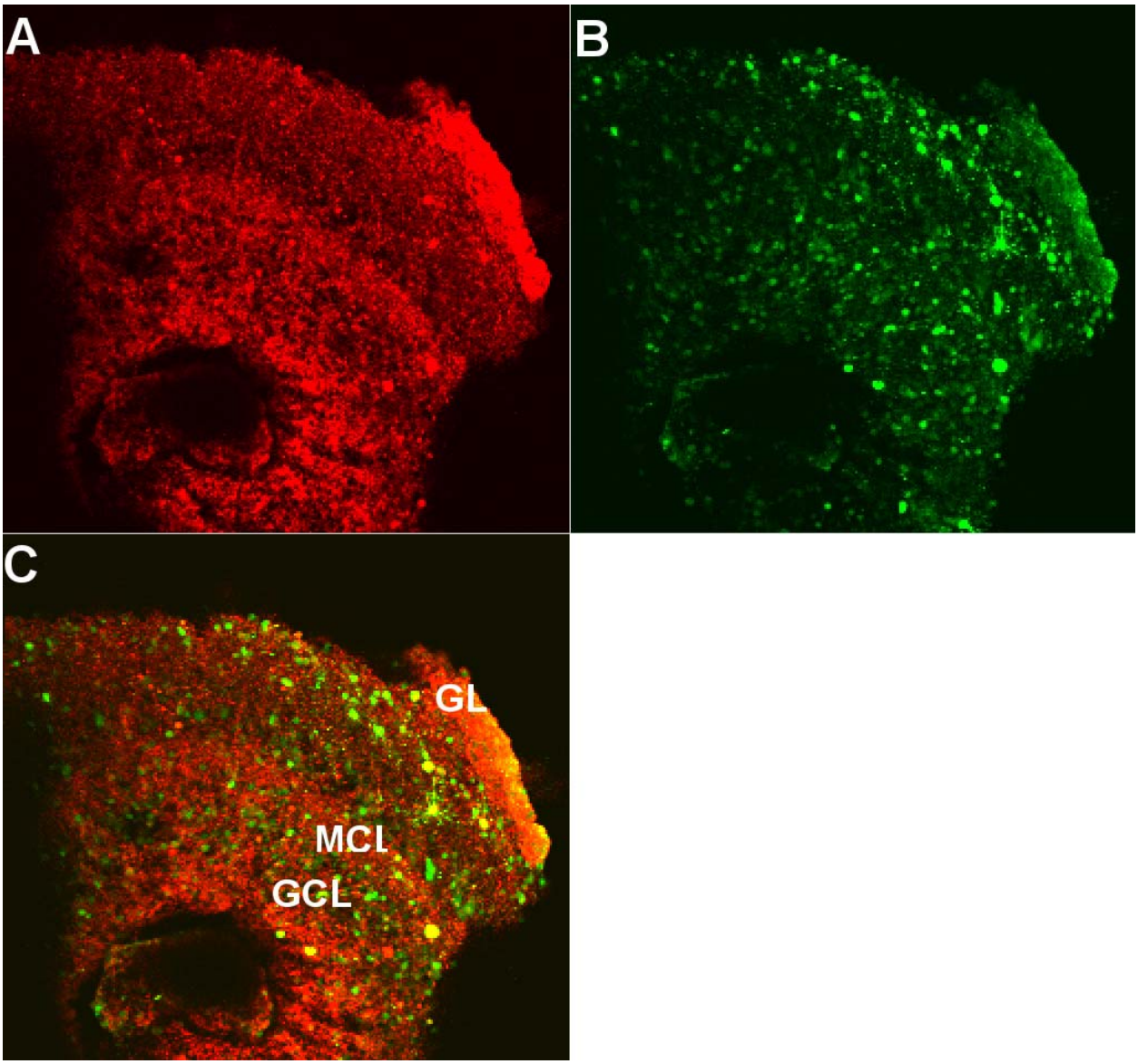

Fig. C.1: Projection of all layers of live olfactory blub slice in wildtype mice. (*A*) Rhod-3 labels mainly the dendrites and a few soma (most of the somas were observed to be dead cells). (*B*) Fluo-4 loads into the soma more effectively than Rhod-3. (*C*) Combination of *A* and *B*, showing the labeling of layers [glomerular layer (GL), mitral cell layer (MCL), granule cell layer (GCL)]. The glomeruli balls of dendrites from tufted cells and mitral cells are where the Ca^{2+} activity is best reported for Rhod-3. Scale bar at 100 µm.

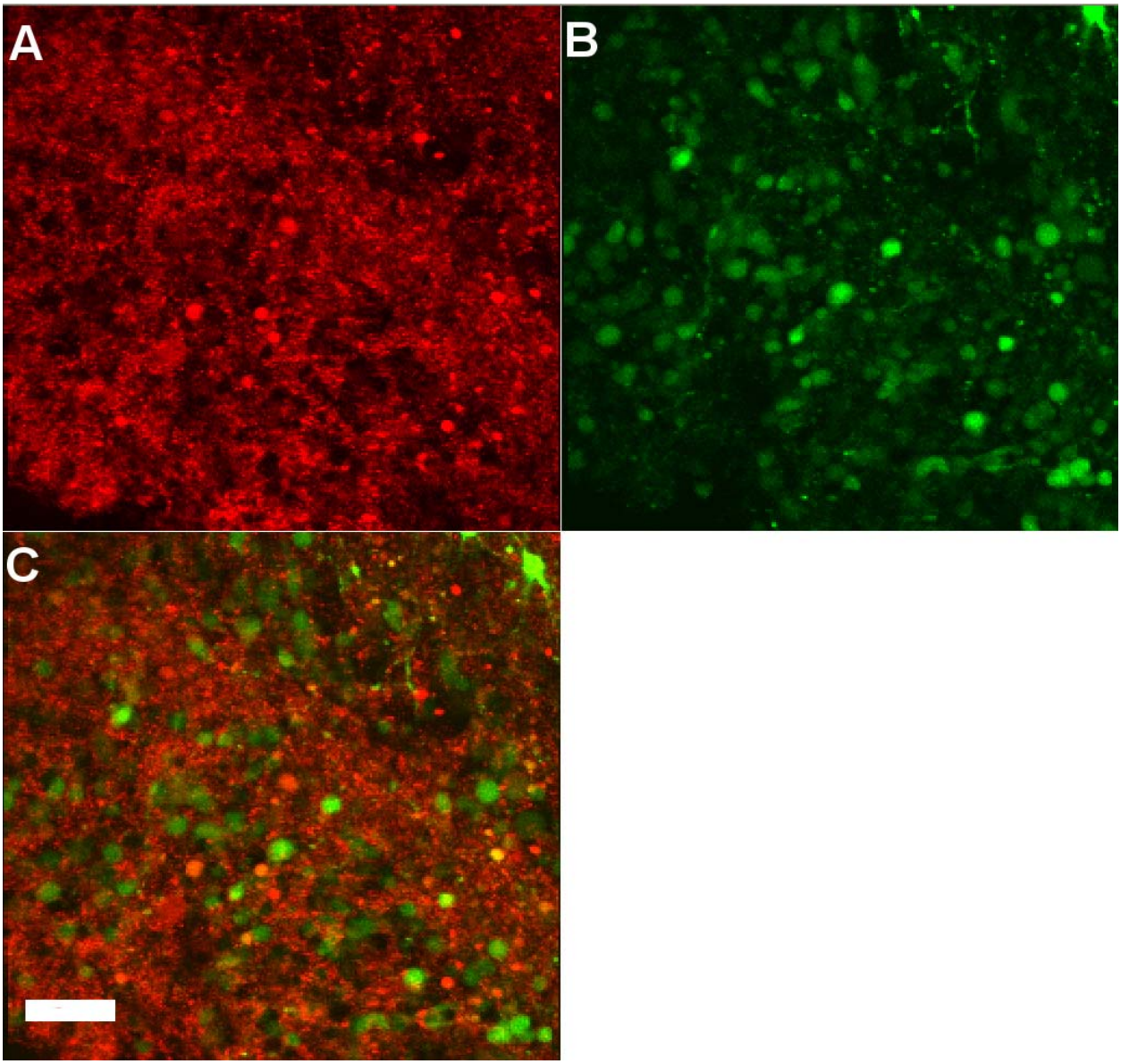

Fig. C.2: Close up projection of granule cell layer in live olfactory blub slice of wildtype mouse. (*A*) Rhod-3 labels mainly the dendrites and a few soma (most of the somas that are labeled with Rhod-3 were observed to be dead cells). (*B*) Fluo-4 loads into the soma more effectively than Rhod-3. (*C*) Combination of *A* and *B*. Scale bar at 50 µm.

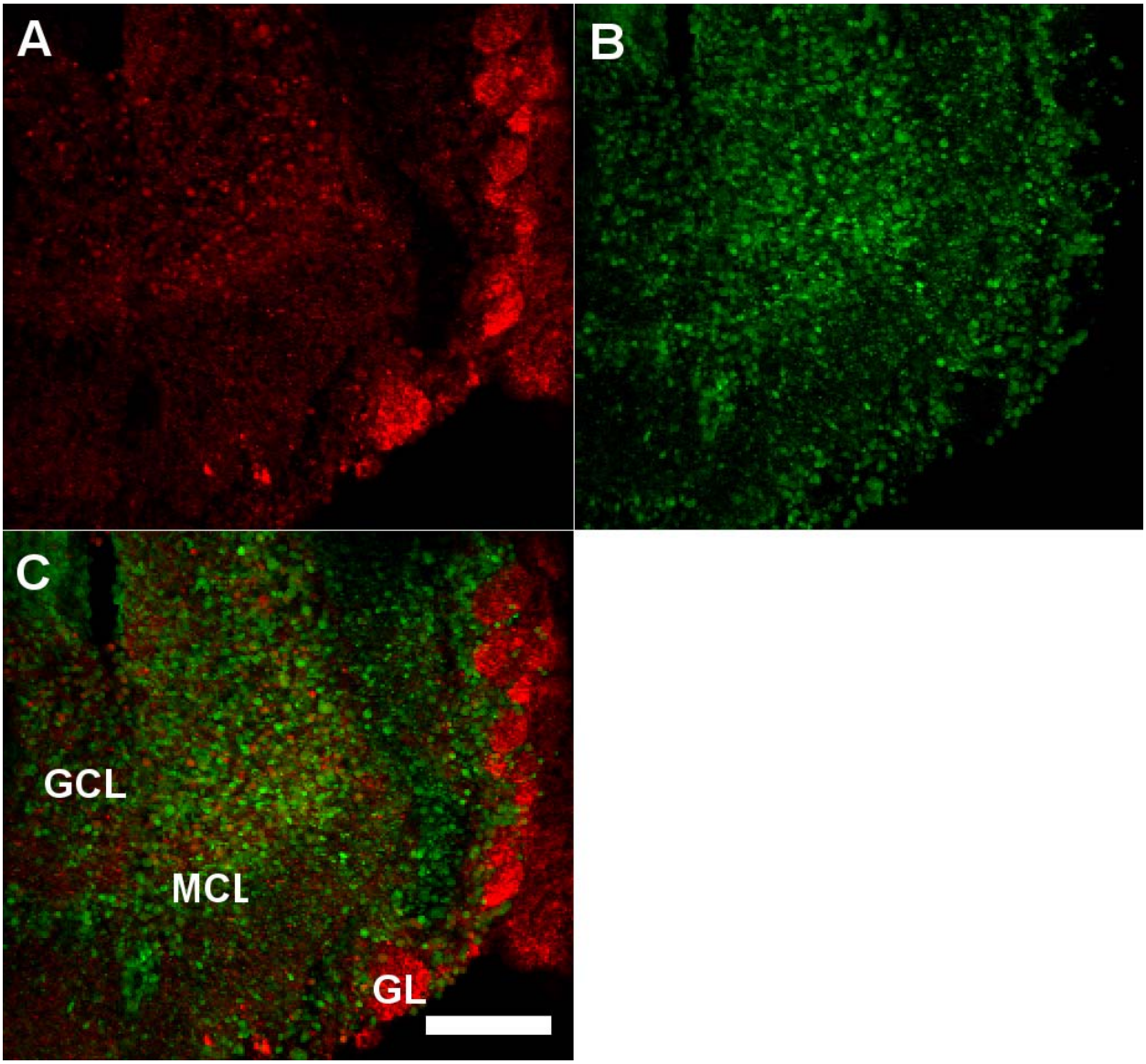

Fig. C.3: Projection of all layers of live olfactory blub slice in GPF-GAD67 mice. (*A*) Rhod-3 rarely loads into the soma of the GPF-GAD67 label (*B*). (*C*) Combination of *A* and *B*, showing the label of layers [glomerular layer (GL), mitral cell layer (MCL), granule cell layer (GCL)]. The glomeruli balls of dendrites from tufted cells and mitral cells are where the Ca^{2+} activity is best reported for Rhod-3. Scale bar at 100 µm.

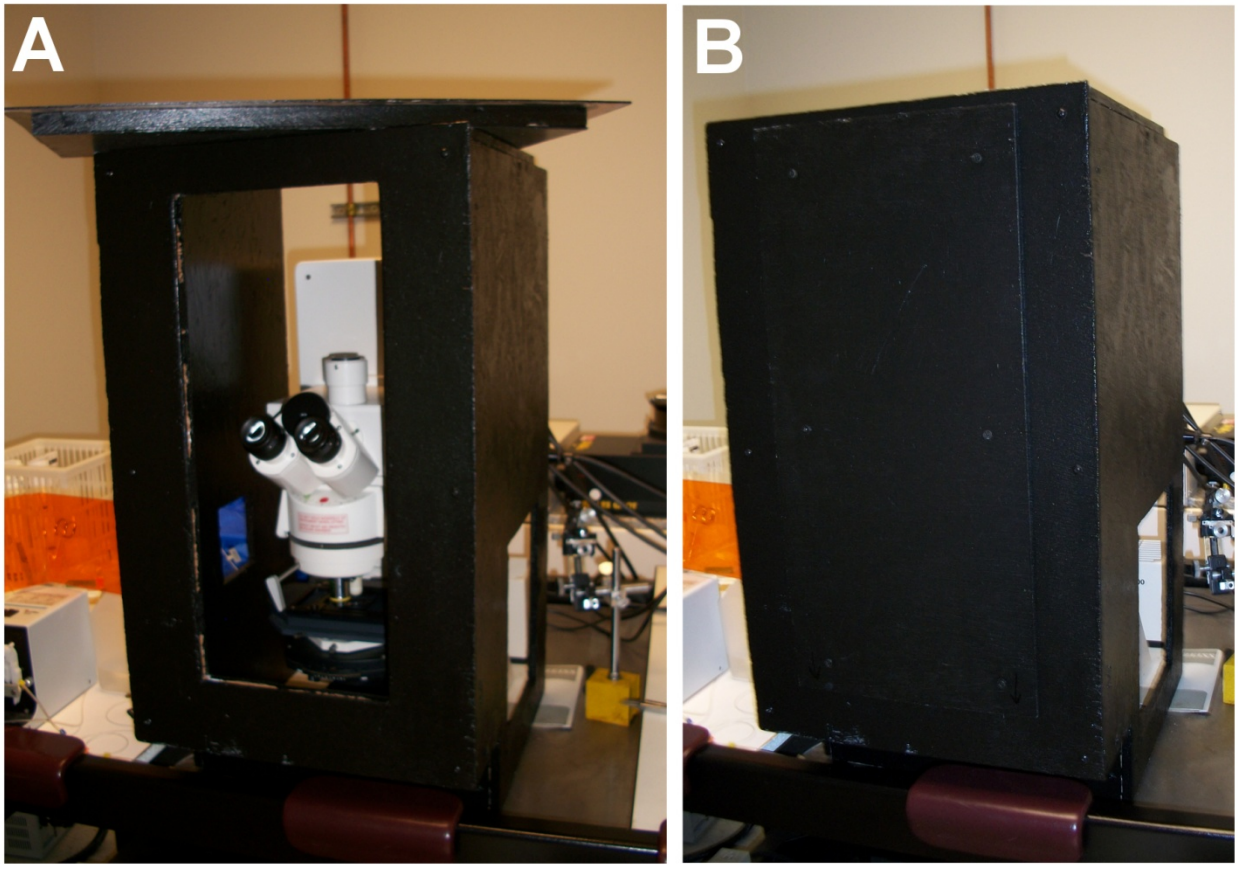

Fig. C.4: Black box designed for minimizing light exposure to dtTomato fluorescent in experiments taking hours to complete. (*A*) The box has a removable door on the front so the investigator can look into the eyepiece. (*B*) The removable door is sealed into the box when there is no need to look into the eyepiece. The large opening toward the backside is for accessing the stage shifters.

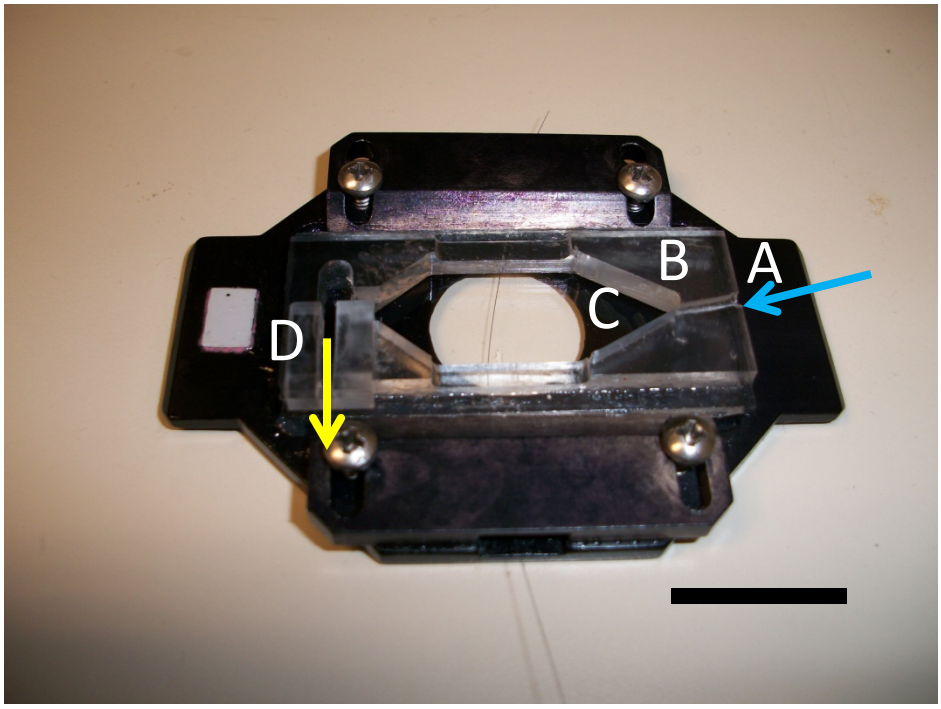

Fig. C.5: The chamber used with the perfusion system for live slice experiments. (*A*) Incoming solution side, the stainless metal pipe is fitted into the hole (blue arrow). (*B*) Chamber walls made from plexiglass. (*C*) Thick coverslip glass bottom. (*D*) Vacuuming end, another stainless metal pipe is sandwiched between the split in the plexiglass (yellow arrow). Scale bar is at 20 mm.

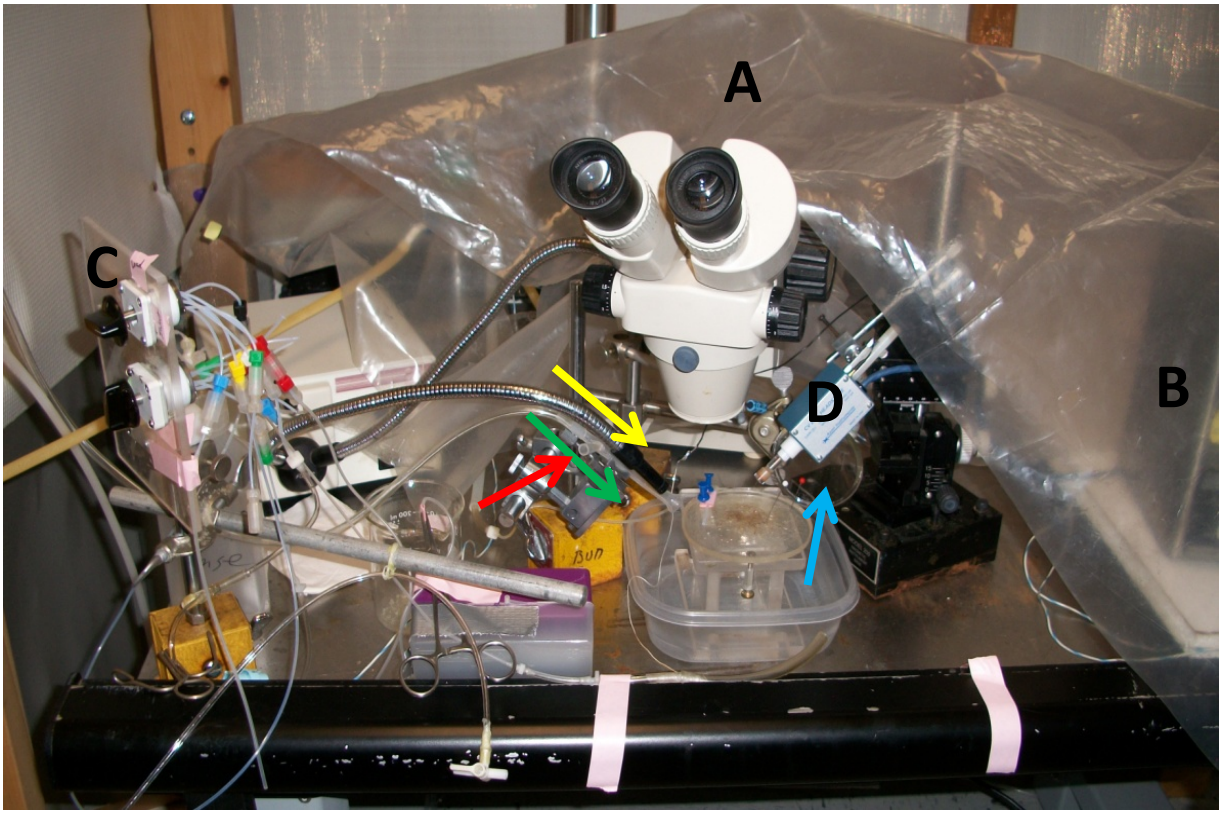

Fig. C.6: Electro-olfactogram setup. (*A*) Plastic sheet for keeping moist within the work space (cover entire system when not looking into scope). (*B*) Small water bath as humidifier. (*C*) Perfusion system for solution-bound drug application. (*D*) Electrode holder and headstage, which is plugged to axopatch. **Yellow arrow:** Lamp. **Green arrow:** Vaporing-tube. **Red arrow:** Air-bound odorant input on side of vaporing-tube. **White arrow:** Odorant-loaded pipette tip holder. **Blue arrow:** Glass funnel, which is hooked to vacuum for sucking away odorants.